University of Strathclyde

Department of Mechanical & Aerospace Engineering

Crack Growth Modelling from Stress Concentrations under Cyclic Loading Histories

Ross Beesley

Submitted to the Department of Mechanical and Aerospace Engineering in Fulfillment of the degree of

Doctor of Engineering (EngD) In Nuclear Engineering

2017

Declaration of author's rights

This thesis is the result of the author's original research. It has been composed by the author and has not been previously submitted for examination which has led to the award of a degree.

Ross Beesley

May 29, 2017

Acknowledgements

I would like to acknowledge the people who played important roles throughout this project and who provided continual help, support and encouragement

First and foremost, I would like to thank my supervisors Dr Haofeng Chen and Dr Martin Hughes, without whose support, this project would not have been possible. Dr Chen, my academic supervisor has been the lead supervisor during my time at the University of Strathclyde and he has provided continual support and was always available to help guide me through this project. My colleagues in the Structural Integrity and Life Assessment Research Group (SILA), and other fellow PhD students have also offered technical support and encouragement and they have become close friends. Dr Martin Hughes has also provided ongoing support during the entire project and as my lead supervisor during my secondment at Siemens, he helped me to integrate well into the company at Lincoln and Finspång. He and the entire SI team provided a great deal of support throughout my placement, and as a result, I really enjoyed and valued my time at the company. I would also like to thank Andrew Mills, the Materials Testing Team Leader at Siemens who offered his experience and support during the experimental aspects of this project.

A great deal of thanks also goes to Dr David Stanley and the EngD Centre, for making the EngD scheme possible. This is a fantastic programme and one that I really value. The skills that this scheme has provided me with have already helped to shape me and my career and I have no doubt that they will continue to do so in the future. I will be eternally grateful for this opportunity and the nurturing support that the EngD Centre offers.

I would also like to thank Dr Alex Galloway for his role and assistance as my IMechE MPDS mentor, helping me work towards attaining Chartered Engineer status.

Finally, but just as importantly, I would like to express my gratitude to my family and close friends, who all offered a great deal of indirect support and encouragement during the course of this project. They all helped to make my time at the University of Strathclyde enjoyable and unforgettable.

Abstract

Structural integrity is a vitally important field of engineering with fracture and fatigue causing the vast majority of mechanical failures. This is of particular importance within the power industry where the consequences of failure can be severe. Power plant components may contain complex geometries and critical features which can introduce stress concentrations, and are often subject to complex cyclic loading histories. Consequently, fatigue is a dominant failure mechanism which can limit the component life.

This research is targeted towards industrial gas turbines, with a specific application to nozzle guide vanes, in which, the extreme temperatures involved induce great thermal loading, compromising their integrity. To this end, extensive development is continually performed to carefully balance their thermal and structural requirements. However, there is still a need to improve understanding of these complex stress distributions.

Conventional fatigue life assessment methods can be overly simplistic and tend to offer a one-size-fits-all approach, potentially providing overly conservative values of fatigue life. More realistic methods with improved levels of accuracy are therefore needed. This highlights the requirement for more bespoke techniques that can offer a greater understanding of the stress distributions in these complex components and high specification materials. During the development of such bespoke methods, it is important that they are readily accessible for routine use within engineering, by providing a user-friendly step-by-step approach. This industrial sponsored research aims to address these issues and provide a turn-key solution.

Included in this procedure, are two novel methodologies which have been developed during the course of this work. These are the Reversed Plasticity Domain Method for the determination of the critical loads to cause low cycle fatigue failure, and the Modified Monotonic Loading Concept for the calculation of the cyclic J-integral.

Publications & Conferences

Conferences Attended

2014 ASME Pressure Vessels & Piping Division Conference

Anaheim, California, USA

20th-24th July 2014

Research Presentation Day Mini Conferences

This one day conference held annually at the University of Strathclyde celebrates the University's research achievements and provides an opportunity for interdisciplinary sharing and collaboration for academic and industrial partners.

Research Presentation Day 2014

25th June 2014

Research Presentation Day 2015

24th June 2015

Research Presentation Day 2016

22nd June 2016

Peer Reviewed Publications

A novel simulation for the design of a low cycle fatigue experimental testing programme[1]

Beesley, R, Chen, H & Hughes, M 2017, 'A novel simulation for the design of a low cycle fatigue experimental testing programme' Computers and Structures, vol 178, pp. 105-118. DOI: 10.1016/j.compstruc.2016.09.004

On the Modified Monotonic Loading Concept for the Calculation of the Cyclic J-Integral[2]

Beesley, R, Chen, H & Hughes, M 2015, 'On the modified monotonic loading concept for the calculation of the cyclic j-integral' Journal of Pressure Vessel Technology, vol 137, no. 5, 051406., 10.1115/1.4029959

On the cyclic J-integral of a 3D semi elliptical surface crack[3]

Beesley, R, Chen, H & Hughes, M 2014, 'On the cyclic J-integral of a 3D semi elliptical surface crack' Paper presented at ASME Pressure Vessels and Piping Conference 2014, Anaheim, United States, 20/07/14 - 24/07/14.

Honours and Awards

At the ASME PVP Conference 2014 in Anaheim, California, USA, the work of Paper [3] above was awarded a certificate of recognition by the Senate of the Pressure Vessel and Piping Division of the American Society of Mechanical Engineers (ASME) at the Student Paper Competition, shown in Figure 1. In addition, Second Runner-Up prize in the PhD category was awarded in the Final Paper Competition, shown in Figure 2.

ASME

SETTING THE STANDARD

CERTIFICATE OF RECOGNITION

This Certificate is Awarded by
the Senate of the Pressure Vessels & Piping Division to

Ross M. Beesley

The University of Strathclyde, Scotland, United Kingdom

In Recognition for being a Finalist
(PhD Category) in the

Rudy Scavuzzo 22nd Annual Student Paper Competition
at the 2014 ASME Pressure Vessels & Piping Conference
and presenting a paper entitled

On the Cyclic J-Integral of a 3D Semi-Elliptical Surface Crack

July 23, 2014

Young W. Kwon
President, PVPD Senate

Douglas A. Scarth
Chair, PVPD Honors & Awards Committee

Figure 1: Student Paper Competition Finalist Certificate

ASME

SETTING THE STANDARD

CERTIFICATE OF RECOGNITION

This Certificate is Awarded by
the Senate of the Pressure Vessels & Piping Division to

Ross M. Beesley

The University of Strathclyde, United Kingdom

In Recognition for being the Second Runner-Up
(Ph.D. Category) in the

Rudy Scavuzzo 22nd Annual Student Paper Competition
at the 2014 ASME Pressure Vessels & Piping Conference
and presenting a paper entitled

On the Cyclic J-Integral of a 3D Semi Elliptical Surface Crack

July 23, 2014

Young W. Kwon
President, PVPD Senate

Douglas A. Scarth
Chair, PVPD Honors & Awards Committee

Figure 2: Second Runner-Up in Final Student Paper Competition Certificate

Contents

List of figures

List of tables

Nomenclature

α	Coefficient of thermal expansion
α_0	Ramberg-Osgood parameter
α_p	Prandtl creep law parameter
β	Ramberg-Osgood parameter
β_d	Dorn law parameter
γ	Hyperbolic sine law material constant
γ_g	Garofalo law parameter
Γ	Contour path surrounding crack tip
Γ_c^0	Two-dimensional propagating crack surface
$\frac{\Delta\varepsilon_p}{2}$	Plastic strain amplitude
$\Delta\varepsilon_{ij}^c$	Strain increment
ε	Strain
ε_e	Elastic strain
ε_c	Creep strain
$\bar{\varepsilon}_f$	Creep ductility
ε_p	Plastic strain
ε_T	Total strain

$\dot{\varepsilon}_c$	Creep strain rate
$\dot{\varepsilon}^c_{ij}$	Incompressible strain rate history
$\bar{\dot{\varepsilon}}$	Effective strain rate
ε_{ref}	Reference strain
ε^p_{ref}	Uni-axial plastic strain at the reference stress
ε'_f	Fatigue ductility coefficient
η_e	Elastic component of geometry dependent constant for calculation of J
η_p	Plastic component of geometry dependent constant for calculation of J
θ	Thermal load
λ	Load multiplier
λ_{UB}	Upper bound load multiplier
λ_{LB}	Lower bound load multiplier
λ_s	Shakedown limit multiplier
ν	Poisson's ratio
ρ^r_{ij}	Residual stress
σ	Stress
σ_{cr}	Creep stress relaxation
σ_{ref}	Reference stress
σ_{th}	Thermal stress
σ_y	Yield stress
ϕ_c	Creep damage
ϕ_f	Fatigue damage

ϕ	XFEM enriched function
ψ	XFEM Enrichment term
ω_c	Creep damage per cycle
ω_f	Fatigue damage per cycle
ω_T	Total damage per cycle
a	Crack length
A	Crack surface area
A_c	Creep crack growth rate material parameter
A_R	Ramberg Osgood parameter
A_n	Norton Bailey creep law parameter
A_g	Garofalo creep law parameter
b_b	Bailey creep law parameter
B	Body thickness
B_f	Friction stress law parameter
B_n	Norton Bailey creep law parameter
B_t	Time fraction rule parameter
c	Fatigue ductility exponent
C^*	R5 C^* creep crack propagation parameter
C	Paris Law material constant
C_D	Miner's rule damage fraction
C'	Dowling & Begley Law material constant
C_p	Pradntl creep law parameter

d_c	Creep damage
D	Damage factor
D_d	Dorn creep law parameter
E	Young's modulus
E'	Modified Young's modulus
$\bar{E}$	Multi-axial Young's modulus
G	Energy release rate
G_C	Critical energy release rate
H	Heaviside term
J	J-integral
ΔJ	Cyclic J-integral
J_1	J-integral at load point 1
J_2	J-integral at load point 2
J_e	Elastic component of J-integral
ΔJ_e	Elastic component of cyclic J-integral
J_p	Plastic component of J-integral
ΔJ_p	Plastic component of cyclic J-integral
k_t	Time fraction rule parameter
K	Stress intensity factor
K_{IC}	Critical stress intensity factor
K_1	Stress intensity factor at load point 1
K_2	Stress intensity factor at load point 2

K_{max}	Stress intensity factor at maximum load
K_{min}	Stress intensity factor at minimum load
K_I	Stress intensity factor
m'	Dowling & Begley Law material constant
m	Paris Law material constant
m_b	Bailey law parameter
m_g	Hyperbolic sine law material constant
m_n	Norton-Bailey creep law material constant
N	Number of cycles
n	Strain hardening parameter
n_f	Friction law parameter
n_g	Garofalo law parameter
n_n	Norton Bailey parameter
N_I	Shape function of a standard finite element
P	Load
ΔP	Load range
P_L	Limit load
q_c	Creep crack growth rate material parameter
q_j	Degrees of freedom at original element node
R	R ratio
R'	Characteristic length
s	Arc along Γ

S	3D body boundary
t	Time
Δt	Cycle time period
$t*$	Time fraction rule
t_h	Hold time
t_f	Creep rupture time
T	Temperature
T'	Traction vector
u	Displacement vector
U	Potential energy
u_I	Standard degree of freedom at the element node
V	Volume
V_f	Work done during fracture
w	Un-cracked ligament
W	Strain energy density
Z	Elastic follow-up factor

Acronyms

AGR	Advanced Gas-Cooled Reactor
ASME	American Society of Mechanical Engineers
BPVC	Boiler Pressure Vessel Code
CCGT	Combined Cycle Gas Turbine
CNC	Computerised numerical control
DCA	Direct Cyclic Analysis
DSCA	Direct Steady Cyclic Analysis
DE	Ductility Exhaustion Method
DPI	Dye penetrant inspection
eDSCA	Extended Direct Steady Cyclic Analysis
EDM	Electrical discharge machining
EPFM	Elastic plastic fracture mechanics
EPP	Elastic perfectly plastic
FE	Finite element
FEA	Finite element analysis
FEM	Finite element method
FFS	Fitness for service

GUI Graphical user interface

HCF High cycle fatigue

IR Infra-red

LCF Low cycle fatigue

LEFM Linear elastic fracture mechanics

LMM Linear Matching Method

LSM Level set method

MML Modified Monotonic Loading

MPI Magnetic particle inspection

NDE Non destructive examination

NGV Nozzle guide vane

PWR Pressurised water reactor

RO Ramberg Osgood

RPDM Reversed Plasticity Domain Method

RSM Reference stress method

SBS Step-by-step

SIF Stress Intensity Factor

SEM Scanning electron microscope

TAGSI Technical Advisory Group on the Structural Integrity of High Integrity Plant

TF Time-fraction rule

TMF Thermo-mechanical fatigue

UT Ultrasonic testing

UTS Ultimate tensile strength

VCCT Virtual crack closure technique

XFEM eXtended finite element method

Thesis Structure

This thesis comprises 2 distinct parts, the foundation research and the core research. Part I introduces the background theory and numerical techniques that form a foundation of this project. Part II describe the core analyses and the development of techniques for the industrial research application. All specialised terms are defined in the Glossary.

Part I

Foundation Research

Chapter 1

Introduction

1.1 Introduction

Structural integrity assessments form a core part of product development across a wide range of engineering disciplines. In such applications, safety critical and high value components must be designed to exacting standards. To achieve this requires a thorough understanding of material and component behaviour over the range of temperatures and structural loads experienced in service and the effects of cyclic loading on its potential failure mechanism. The continual refinement of component designs and the development of more advanced analysis tools, combined with rapidly developing computational ability are driving the need to better understand the failure mechanism through improved modelling techniques. Crack growth modelling of complex design features under cyclic loading histories can give rise to localised stress concentrations and hence this is an important field for further development and as such is closely aligned with the needs of industrial research.

1.2 Nature of the Project

The nature of the Engineering Doctorate (EngD) programme is to provide an industrial focussed doctoral project with a consideration of the associated business challenges. This is incorporated through working directly with an industrial sponsor and in conjunction with a Post Graduate Diploma in Enterprise Management from the University

of Manchester Alliance Business School. These additional arms augment the doctorate with relevant business acumen which are directly applicable to large scale, industrial and commercial engineering.

To address the industrial aspects of this project, it is sponsored by and run in collaboration with Siemens Industrial Turbomachinery Ltd. This relationship provides an industrial and commercial focus for the research and development work undertaken during the project. This research concerns industrial gas turbines, and although not exclusive to this field, the work presented here is targeted towards this technology.

The Manchester University courses have provided relevant business skills which have helped approach the technical requirements of the project, with an appreciation of the financial constraints and commercial challenges of the real world. This has provided a broad understanding of the commercial aspects of modern engineering and highlighted the requirements for this research project. The industrial link provides context for this research in real life applications and current industrial challenges, which have been particularly relevant in this project with Siemens. Some of the work in this thesis has already been applied to industrial applications at Siemens, and following company approval, the final deliverable methodologies are ready for adoption within the business.

1.3 Technical Background

This research is targeted towards industrial gas turbines, with a specific application to the nozzle guide vanes (NGVs), the precisely designed components which direct hot gases onto the turbine blades. The extreme gas temperatures involved induce great thermal loading on the NGVs, compromising their thermal and structural integrity. To counteract this, they are designed with through thickness cooling holes, enabling the material to withstand these harsh conditions. However, these cooling holes are inherently small, and whilst they ensure thermal integrity, they introduce very localised stress concentrations which can adversely affect the integrity of the structure. Extensive development is continually performed to carefully balance the thermal and structural requirements of these components. Since these cooling holes are fundamental to the design, the stress concentrations cannot be entirely removed, and these components must be designed to work in the presence of extreme and highly localised stresses.

There is therefore a requirement for enhanced understanding of these highly complex stress distributions. As a result, fracture and fatigue life assessment are performed during the design, development and operation of these components.

Finite element analysis forms a major part of regular integrity assessment of components and can provide a detailed prediction of the stress-strain responses under given loading conditions. However, there are issues concerning the accurate and realistic prediction of fatigue life due to difficulties with crack growth modelling. A number of pioneering developments have been made in recent years, however, continued work is still required to ensure the integrity of components and to maintain the highest levels of safety.

Conventional fatigue life assessment methods can be overly simplistic and tend to offer a one-size-fits-all approach, potentially providing overly conservative values of fatigue life. More realistic methods with improved levels of accuracy are therefore needed. This is particularly important with the current drive for continually improving efficiency. This can be achieved through weight reduction of components and with the use of highly specialised materials such as superalloys. With such complex geometries and high cost materials, these generalised fatigue life assessment methods are becoming less appropriate. This highlights the requirement for more bespoke techniques that can offer a greater understanding of the stress distributions in these complex components and high specification materials. During the development of such bespoke methods, it is important that they are readily accessible for routine use within engineering, by providing a user-friendly step-by-step procedurised approach.

This thesis presents novel fracture mechanics and fatigue assessment techniques that are applicable to highly complex industrial test specimens. While the particular focus lies within industrial gas turbines, the techniques developed are applicable to any structural integrity assessment across a range of engineering disciplines, making it very powerful for use within industrial applications.

These individual techniques are incorporated into a sequential procedure for complete crack growth modelling and fatigue life assessment, from initiation through propagation, to ultimate failure. The procedure comprises a number of independent steps, offering a great deal of power and flexibility to the user, allowing them to run the

complete analysis as established in this thesis, or to tailor individual steps to specific applications and conditions, without the need to fully understand the individual aspects and theoretical concepts of the method. This addresses the requirement for an accessible, user-friendly approach for routine fatigue life assessment.

Due to the nature of the EngD and industrial application, the emphasis of the work is on the application of theoretical concepts to real life industrial components with an appreciation of the commercial constraints. This worked comprises three main strands:

- The design of a bespoke industrial test specimen which represents the highly localised stress concentrations found in the nozzle guide vanes.
- The design of an experimental testing programme to induce low cycle fatigue failure in this specimen, providing information of the failure modes of the NGVs. This test programme is designed using the Reversed Plasticity Domain Method (RPDM) which is developed in this thesis.
- The development of a method for the calculation of the cyclic J-integral, providing details of the crack propagation rate and growth path. This is performed using the Modified Monotonic Loading (MML) concept which is developed in this thesis.

1.4 Research Background

High temperature components in nuclear and other power plant applications undergo cyclic loading due primarily to start-up and shut-down transitions and hence the justification of component life under these conditions is critical. Existing methods have been incorporated into design codes [4] and conventionally these are based on material life data generated using plain specimen fatigue tests together with plasticity and creep models.

To date, most testing and modelling work has focused on the characterisation of material response in isothermal standard tests, i.e. creep, tensile and low cycle fatigue (LCF) tests. This approach produces acceptable component life predictions in many cases, however, long-term exposure at high temperature can affect the material in different ways.

Consequently, thermo-mechanical cyclic testing is now carried out to provide more accurate information on the cyclic behaviour of these materials and also to present design curves that can be used with greater confidence for this type of load cycling [5]. An understanding of the type of phasing of the stress and temperature cycles is also important for accurate life prediction.

Crack initiation in standard fatigue tests is typically defined as a given percentage load drop towards the end of the test. This may correspond to a crack depth of 0.5mm or more. This definition of initiation may have a significant impact on life predictions when dealing with stress concentrations. In reality, microcracks may form relatively early in life. For a stress concentration region, this can mean that for much of the cyclic life, a growing crack may develop in a stress field characterised by high stress gradients, plasticity and creep effects at the surface and complex residual stress fields. These effects are a major contributor to widely recognised notch sensitivity effects.

The failure process modelling therefore needs to be supplemented with a crack growth assessment. At the design analysis stage, the majority of fatigue crack growth assessments are made using standard stress intensity factor solutions and the un-cracked body stress field. Explicit modelling of cracks in finite element analysis is usually carried out only under special circumstances due to both the lengthy modelling process and the need for a validated method, even though the finite element method has previously been used to solve fracture mechanics problems.

Today, leading codes such as ABAQUS [6] have extensive crack tip parameter solution capability. Recently, this capability has been enhanced by the introduction of the eXtended Finite Element Method (XFEM). This has the advantage over conventional finite element modelling of cracks in that the model geometry does not have to conform to the crack, leading to significant simplifications, especially with regard to crack propagation simulation. In other words, with XFEM, cracks can propagate in any direction across a mesh, even through existing elements. Conventional finite element based crack analysis requires time-consuming crack modelling and updating to simulate a growing crack. Specialist software packages exist which can help the process of modelling cracks using the conventional finite element method including Zencrack [7] and Franc3D [8] and these have been shown to be capable of modelling crack development under a

number of different conditions. The XFEM capability now offers another route, which although limited due to the early stage of implementation, does open up the possibility of more accurate modelling of component failure processes such as thermo-mechanical fatigue (TMF) crack initiation and crack growth at complex component features.

1.5 Aims and Objectives

The primary aim of this project is to develop a method of life prediction for complex structural features containing highly localised stress concentrations. Building on existing knowledge of crack behaviour and fatigue life models, this will include crack propagation modelling, with particular emphasis on early growth out of the local stress field. Careful consideration is required for the effects of high stress gradients and the evolution of the initial stress fields prior to crack development.

The measurable objectives for this project are:

1. Develop a new understanding of the crack initiation and propagation processes, the influence of local high gradient stress fields and the evolution of this due to cyclic creep and plasticity.

2. Compare crack modelling methods with respect to accuracy of the solution and practical modelling limitations for both single step analysis and fatigue crack growth modelling.

3. Assess the theoretical limitations of different crack modelling methods and their applicability to high temperature problems in turbines, particularly XFEM.

4. Review the definition of crack initiation (or first detectable indications) and the implications for crack size.

5. Develop a new industrial test specimen for use within Siemens which offers suitable representations of real gas turbine components.

6. Define new tests to validate new crack growth modelling methods.

7. Perform crack propagation modelling of complex geometries under the influence of cyclic plasticity.

8. Compile developed techniques into a step-by-step procedure, allowing a complete crack growth assessment in a user-friendly and ergonomic manner.

9. Disseminate the outputs to the UK research community and industrial partners.

1.6 Research Justification

Currently, fatigue life assessment of stress concentration features is limited by the effects of high stress gradients and local inelastic material behaviour. This can result in overly conservative predictions of the component life. This is compounded by the difficulty of accurate crack behaviour modelling in these regions. It is estimated that the cost of premature retirement of components which may be capable of many more hours of operation, is considerable, possibly up to £500,000 per year across Siemens [9]. Therefore, improved methods of life prediction with increased levels of accuracy are vitally important. This project aims to address this by the development of novel techniques with the potential to provide greater accuracy of results.

1.7 Research Significance and Importance of Life Extension

This project has a specific industrial focus on gas turbines, however, the research works are not exclusive to this industry and are applicable to a number of different fields in the power and aerospace industries since both of these involve elevated temperatures, high stresses and extended hold times. This work is also applicable to the nuclear industry and other traditional fossil fuel power plants, as well as renewable energy sources such as wind and marine turbines. This work is of particular importance and relevance within the nuclear industry since the current UK fleet of nuclear reactors is approaching the end of the intended working life. However, due to the fact that very few new reactors have been commissioned, the UK is now in a position that it has no choice but to extend the life of these aging reactors. Nuclear currently contributes approximately 21% of the UK's electricity demand, however, up to half of this capacity is due to be retired by 2025. The next generation of reactors are not estimated to come

online until 2025 with more entering service in 2030.

This does not allow significant contingency for delays in the manufacturing and commissioning process and if for some reason, these reactors are unable to generate power by 2025 and 2030, this would put extensive pressure on the electricity generation industry. With potentially half of the current fleet retiring in the coming decade, this would mean a 10% deficit in UK electricity. The use of renewable energy sources does play its part in UK, and worldwide electricity generation, and there have been major advancements in recent years. However, despite this, the aging and retiring fleet of nuclear reactors poses a major challenge for the UK electricity generation industry. Due to consumer habits and a society that expects a reliable constant electricity resource, it is unlikely that a significant reduction in electricity supply could be tolerated. For this reason, there is growing importance for renewing the UK's nuclear reactor fleet, and until these are operational, it is clearly vital that the current capability is extended as much as possible and other power sources are utilised where possible to make up this electricity shortfall. Due to the highly inhospitable environment to which power plant components are subjected, mechanical failures such as fatigue and fracture will become increasingly likely as the plants approach the end of their intended life. To ensure the highest levels of safety are maintained, continual inspection of components is performed and, if possible, parts are replaced as necessary. However, there are a number of components that due to a variety of reasons such as their size, position or condition, may not be possible to replace. Such an example is the reactor pressure vessel in a Pressurised Water Reactor (PWR). This contains the entire reactor and so its replacement would require the creation of a new reactor which is not a viable option. When these components were first manufactured, they were issued with a recommended life which predicted them to be safe to use up to a certain number of hours (or cycles) of operation. These were defined many years ago based on structural integrity understanding at the time and so it is entirely possible that these were overly conservative and with modern advances in understanding, modelling and inspection techniques and fatigue life prediction, that these components are in fact safe to use for longer than was originally believed. In order to gain a better understanding and be able to predict more accurate values of component life time, extensive study is routinely performed

into structural integrity, crack initiation and propagation modelling, fatigue cracking, creep rupture and creep fatigue. This has been a widely investigated area of engineering for many decades, however, due to the reasons explained above, it is arguably more important now than it has ever been before. This is not only applicable to the nuclear industry, but is true across all energy sources and power generation industries. This study is also vitally important and directly applicable to other industries such as transport, including rail and aviation, space technologies and civil engineering. Hence, extensive funding is provided, both in academia and industry, for the study of structural integrity, as advancements in this field directly influence the standard of living and public safety of societies around the world.

1.8 The Power Industry

As discussed above, the primary driving factors for the research and development of the field of fatigue and fracture are safety related and originated in the aerospace and power industries, where the consequences of failure are potentially catastrophic. More recently, a secondary area of interest has arisen which is more commercially and socially driven to ensure the maximum return on investment, whilst minimising environmental impact. A more accurate prediction of component lifetime would optimise the use of valuable resources and expensive materials, and obviate the need to retire components prematurely, thus extending their useful working life.

1.9 Industrial Gas Turbines

Currently, the field of fatigue and fracture is applied across a broad spectrum of industries but the particular application of this investigation is to industrial gas turbines.

A gas turbine is a type of internal combustion engine. They are very similar to aeroplane engines and the only difference is their intended use; aeroplane engines generate thrust, whereas gas turbines are used for either mechanical drive or electricity generation.

The basic principal of a gas turbine is commonly represented by the simple phrase, *"suck, squeeze, bang, blow."* This describes the four distinct stages of a gas turbine.

Initially, air is drawn into the engine which is then compressed in the compressor. This air is then drawn into the combustion chambers, where fuel is injected, and subsequently ignited, causing an explosive reaction. The exhaust gases are then expelled which pass across the power turbine, generating rotational motion. The power turbine is connected to the compressor turbine and so rotation of the shaft causes the compressor turbine to also rotate, drawing in more air and continuing the process. The rotating shaft can then either be connected to a gear box for mechanical drive, or to an electrical generator. This process is illustrated in Figure 1.1, and Figure 1.2 [10] demonstrates how this process relates to a real turbine.

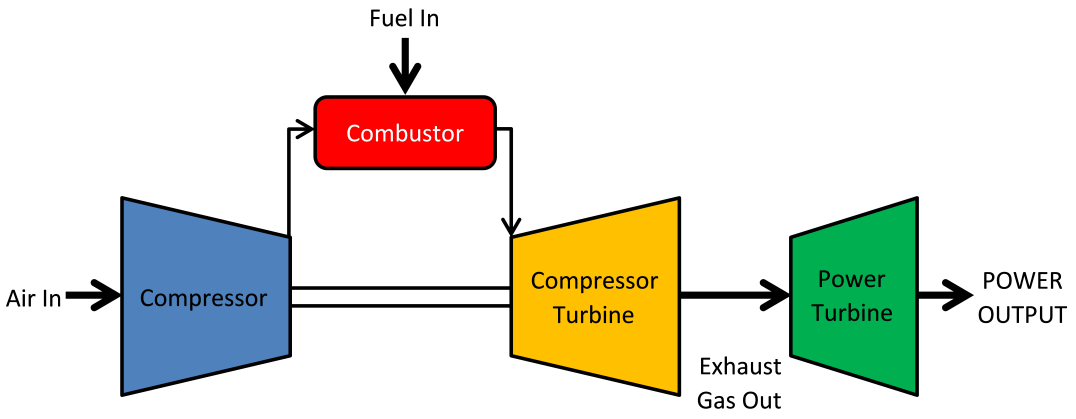

Figure 1.1: Schematic diagram illustrating the gas turbine process

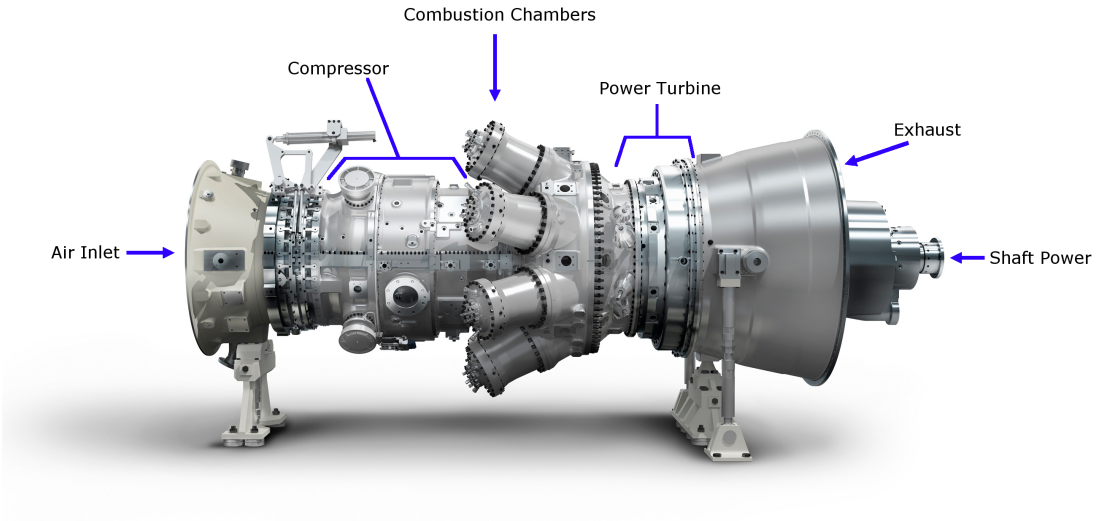

Figure 1.2: Components of the gas turbine engine [10]

Gas turbines operate on the principal of the Brayton Cycle. This is a thermodynamic cycle that consists of 4 individual processes as illustrated in Figure 1.3. The cycle begins in the inlet and compressor with an adiabatic compression, meaning no heat is gained or lost by the system (1-2). The fuel and air mixture is then combusted at a constant pressure (2-3). The gas then undergoes adiabatic expansion in the turbine and exhaust nozzle (3-4). In this stage, work is taken out of the system to drive the compressor and for power output in the form of electrical generation or mechanical drive. The gas is then cooled at a constant pressure to its original condition (4-1) where the cycle repeats.

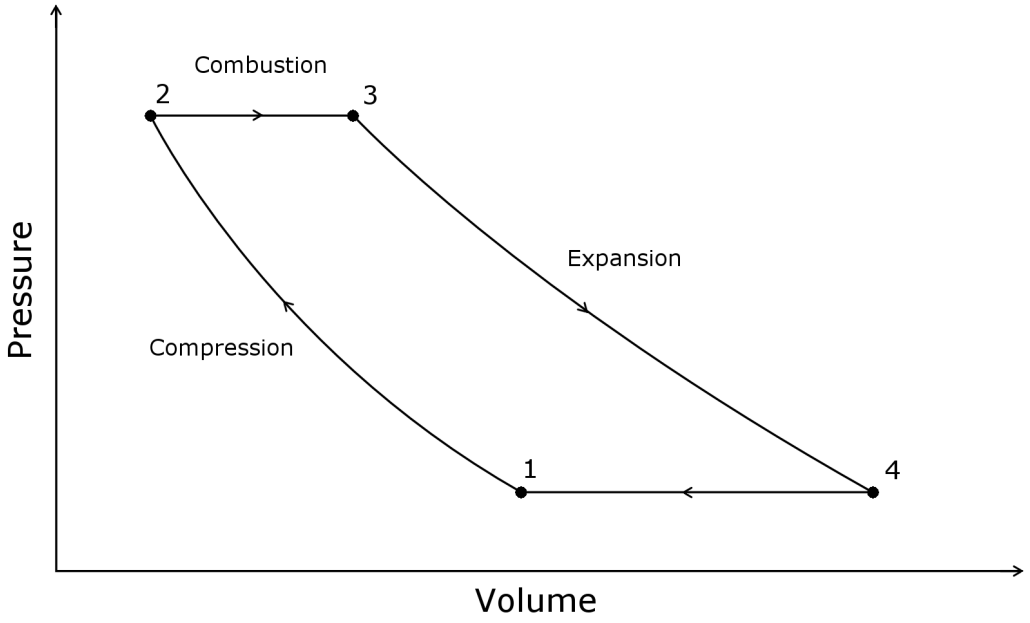

Figure 1.3: Schematic showing the Brayton cycle

Gas turbines typically operate with a thermal efficiency of 35-40% in a single cycle format. However, they can also be used in a combined cycle, where, in addition to the standard operation, a heat recovery system captures the thermal energy of the exhaust gases to create steam, which is then used to drive a steam turbine, generating additional electricity. This system is referred to as a Combined Cycle Gas Turbine (CCGT). This clearly requires additional infrastructure and greater investment. However this system makes use of otherwise wasted thermal energy in the exhaust gases which has allowed the overall efficiency of CCGT plants to exceed 60%.

1.9.1 Gas Turbine Usage

Gas turbines are very compact in size compared to other energy generation methods such as coal and nuclear and their high levels of power generation result in a very high energy density. For this reason, they are commonly used in isolated systems which are not connected to a networked electricity supply, such as oil platforms, for local electricity generation and for powering pumps for extracting oil and natural gas.

They are also used in developing and emerging countries for small scale, local electricity generation due to their relatively low cost compared to coal and oil fired power plants and ease of implementation and operation. Their small, off-the-shelf format also means that they can be delivered by a single, heavy goods vehicle, reducing delivery and installation costs.

An additional advantage of gas turbines is their rapid start-up time, being able to go from cold to full power in a matter of minutes. This makes them ideal for an emergency electricity supply in the event of power failure in places such as hospitals, where backup electricity could be required at a moment's notice. However, this rapid start-up process can put excessive mechanical and thermal stresses on the components, meaning that fatigue and fracture can have significant effects on the integrity of the structure. For this reason, extensive work is routinely performed in the design and structural assessment of gas turbine components. This gives rise to the requirement for advanced crack growth modelling assessments for use within gas turbines and the power industry as a whole.

1.10 Novel Features of the Project

The main objective of the research presented in this thesis contributes to the development of a complete crack growth modelling and assessment procedure. Due to the industrial bias of this project, the research presented in this thesis aims to bridge the gap between academia and industry. As such, the main novelties lie in the application of theoretical concepts to real life, highly complex components such as those found in gas turbines, thus providing state of the art methodologies that are suitable for routine use within Siemens Industrial Turbomachinery as well other industrial applications.

The key novel aspects of this project are:

1. The design and creation of a bespoke industrial test specimen to act as a benchmark for subsequent analyses (Chapter 4).

2. Development of a user-friendly and efficient technique for the calculation of low cycle fatigue life through a novel application of the Linear Matching Method, suitable for highly complex components under extreme loading conditions [1]. (Chapter 5)

3. Creation of the Modified Monotonic Loading Concept (Chapter 6), a user-friendly finite element approach for the accurate calculation of cyclic J-integral values for crack growth modelling calculations, that is applicable to highly complex crack geometries and engineering structures.

4. Implementation of the MML concept through demonstration on a complex notched specimen, offering a complete cyclic J-integral analysis of a semi-elliptical surface crack, considering three-dimensional variation and likely crack propagation direction.

5. Proposal of a complete crack growth modelling procedure (Chapter 7), incorporating the novel developments presented in this thesis, into a single methodology, providing a complete assessment of crack initiation and growth, propagation direction and fatigue life of complex industrial components.

1.11 Thesis Overview

This thesis is structured as follows:

Chapter 2 introduces this research project by providing the theoretical background of the field. This includes an overview of fracture mechanics and fatigue and introduces the fundamental theories. A brief history of the field is included for general interest and a number of well known case studies are presented which highlight the importance of the continued study of this area. This chapter provides a foundation understanding, forming the basis of the subsequent chapters.

Chapter 3 expands the basic theory defined in Chapter 2 and introduces some advanced and highly technical fracture mechanics and fatigue methodologies. A thorough review is performed and their limitations are identified. This highlights the requirement for further study, investigating the development of the new techniques introduced in the subsequent chapters.

Chapter 4 proposes the design of a bespoke and highly complex test specimen. The requirement for a new test specimen is explained with reference to industrial gas turbine components and the rationale and justification of the proposed design is discussed. A rigorous investigation is performed allowing optimisation of the design to allow it to meet the required strict specifications. Appropriate machining techniques are considered and the manufacturing process is evaluated through an experimental investigation. This component offers a representative specimen which provides a benchmark for the subsequent analyses.

Chapter 5 proposes a novel technique for the design of an experimental testing programme suitable for causing low cycle fatigue crack initiation in the bespoke and highly complex industrial test specimen designed in Chapter 4. A thorough investigation is performed which identifies a range of suitable applied loads which are sufficient for causing crack initiation and for each load within this range, a low cycle fatigue analysis is conducted. This investigation demonstrates the capabilities of this novel technique for calculating experimental testing design loads for highly complex industrial test specimens.

Chapter 6 introduces the Modified Monotonic Loading concept as a novel technique for the calculation of the cyclic J-integral. This proposed method is tested on a complex industrial specimen in order to calculate the cyclic J-integral, ΔJ, along a 3D semi-elliptical surface crack under a range of loading conditions, aiding in the prediction of crack growth rate and direction.

Chapter 7 proposes a procedure for a complete crack modelling assessment. This method is based on the preceding chapters and is capable of calculating the fatigue life to crack initiation and likely crack location, as well as total propagation fatigue life and crack growth direction. An extension to the theory established in

Chapter 5 is also made to include a creep dwell in the cyclic loading history to assess the effect of the creep and fatigue interaction on the structural integrity of a component. This is the key deliverable of the project and provides a user friendly tool that can be used in industrial applications for the complete analysis of fatigue and creep fracture.

Chapter 8 presents the conclusions of the study and offers recommendations for further research.

Chapter 2

Theoretical Background

Chapter Overview

This chapter presents an introduction to the field of fracture mechanics, fatigue and creep. The basic principles are explained and the history that led to the development of these fields is included for general interest. These core principles provide a foundation for the subsequent chapters. A number of fatigue failure case studies are presented, which highlight the importance of understanding fatigue and fracture. Through learning from these events, future developments in the field can be made and help to prevent such incidents from occurring again in the future. A number of methods for the assessment of fatigue failure are explained which demonstrate their use in industrial applications.

2.1 Fracture Mechanics

2.1.1 Overview of Fracture Mechanics

Fracture mechanics is the study of the initiation and propagation of cracks within a structure and aims to provide an understanding of how materials fail. This knowledge of how, where, and when a structure will fail allows precautionary measures to be taken to prevent failure, through maintenance or replacement of the critical components. The impact of material fracture varies depending on the specific application but the results can be catastrophic. Therefore, gaining an understanding of fracture and the ability to predict when a crack will initiate and propagate must be understood to ensure the safe design and utilisation of structural components. Fracture mechanics provides generalised techniques that are widely applied to a number of different industries and applications, and for this reason, this field of study attracts a large number of researchers [11–16].

To address the need to understand the failure behaviour, fracture mechanics aims to answer three main questions:

1. *Where* - the location of crack initiation and the direction of crack growth
2. *When* - after how many cycles will the crack initiate and how many additional cycles can be endured before the crack grows to a critical length at which point, instantaneous collapse occurs
3. *How* - the precise load at which crack initiation will occur

The field of fracture mechanics has undergone extensive investigation in recent decades and as a result, the ability to predict and prevent failures through fracture has increased considerably. It is a vitally important field of engineering but despite the recent advances, further understanding is still required to help ensure the highest levels of safety of engineering structures for years to come.

This section introduces the basic theory of fracture mechanics and provides a foundation for the subsequent chapters.

2.1.2 History of Fracture Mechanics

Fracture mechanics is a relatively new engineering discipline which has only really come into mainstream existence since World War II. Before this, there was awareness of the presence of cracks in structures, but they were considered insignificant and unlikely to pose any threat to the structural integrity of engineering components. However, as is now known, this was not the case, with fracture and fatigue being the cause of the vast majority of structural failures, and it was not until a series of disasters occurred in the mid-1900s that engineers realised the impact that fracture can have on components. Examples of these are presented in this chapter, highlighting the severe consequences of this failure mechanism and the vital importance of gaining a thorough understanding in order to prevent such incidents from occurring again in the future. The following sections briefly summarise the development of the field of fracture mechanics.

Alan A. Griffith

Alan Arnold Griffith was an English engineer who lived from 1893 to 1963 and was a pioneer in the field of metal fatigue and stress fracture. His most famous work was on the theory of brittle fracture [12] but later in life he also worked on the theoretical design of gas turbines. Griffith's interest in fracture concerned the relationship between the predicted and actual strengths of materials, observing that components had a greatly reduced strength compared to their predicted strength. He postulated that this difference was due to the presence of micro-cracks and other flaws within the lattice of the material which reduced their overall strength by acting as a stress concentration, which could ultimately cause rupture of the component. The effect that the presence of cracks and sharp corners has on the induced stresses in a structure had previously been studied by Inglis [17] which provided a basis for Griffith's hypothesis, however, prior to this, the presence of internal micro-cracks had not been considered and consequently, the strength of engineering components had been greatly over-estimated. All subsequent fracture mechanics investigations were based on his theory and as a result, Griffith is considered by many to be one of the founding engineers of this field [18]. Following this investigation, and with the work of Inglis, Griffith developed his own theory of brittle fracture by considering the first law of thermodynamics, which states that the

energy of an isolated system is constant and so energy cannot be created or destroyed. He applied this theory to fracture in an attempt to explain crack propagation with reference to the energy balance. He proposed that if the strain energy that is released when a crack grows in size by a set increment, is greater than the surface energy of the material, then any contained flaws in the material will become unstable and thus fracture will occur. It can be argued that this work in the 1920s provided a foundation for modern theories of fracture mechanics. Griffith paved the way for modern fracture mechanics, and although his work revolutionised structural integrity, his method had a number of limitations. His approach was relatively generalised and theoretical, and difficulties were encountered when applying his methodologies to real components. The two main limitations of Griffith's theory were that (1) the surface energy was a global concept and difficulties arose when applying this to finite geometries and (2) that it was only really applicable for very brittle materials.

George Irwin

George Irwin, an American scientist who lived from 1907 to 1998 extended Griffith's work to make it more generally applicable to real life components. He developed Griffith's theory of brittle fracture by replacing the surface energy with the specific effective fracture surface energy, incorporating plastic deformation at the crack tip during growth [19]. This modification greatly improved its usefulness as a solution for engineering problems and became known as the energy release rate concept. Soon after, Irwin became aware of the work of Westergaard, a Danish engineer, who in the 1930s, had developed a technique for the analysis of stresses and displacements ahead of a crack [20]. Irwin took this methodology and demonstrated that these stresses and displacements in the region of the crack tip could be related to the energy release rate through an additional parameter, which became known as the stress intensity factor (SIF). Irwin's work in this field led to the development of the principles of linear elastic fracture mechanics (LEFM) and for this reason, Irwin is often referred to as the father of fracture mechanics.

2.2 Background Theory of Fracture Mechanics

As Griffith found, structures contain many small imperfections and microcracks. A structure may be able to sustain a number of small cracks, however, as they grow under loading, they may reach a critical size, at which point the load can no longer be sustained and the crack propagates throughout the structure. Fracture mechanics aims to understand the point at which the crack changes from a stable to unstable state.

Fracture mechanics can be broadly split into two main categories depending on a material's fracture behaviour and its stress-strain response to a given applied load. These are linear elastic fracture mechanics (LEFM) and elastic-plastic fracture mechanics (EPFM). These categories exhibit different behaviours and occur either side of the yield point of a material, which is the load where a material begins to deform plastically. Below this load, LEFM occurs, whilst above, the material undergoes EPFM. From observing a material's stress-strain curve, these different classifications of fracture mechanics can easily be visualised and are explained in the following sections.

Linear Elastic Fracture Mechanics

The most simplistic case is linear elastic fracture mechanics in which a material is assumed to behave linearly and elastically when the applied load is below the yield stress of a material, denoted by σ_y. In this case, the relationship between stress and strain is linear and provided that the yield is not exceeded, the material can be loaded and unloaded repeatedly with no accumulation of damage. A prime example of this is an elastic band, which can be pulled and released, and as long as the load is always below the material's yield point, the band will return to its original shape and no deformation or damage will occur.

Non-Linear Elastic Fracture Mechanics

It is possible for some materials to behave in a non-linear elastic manner. In this case, after an initial linear behaviour, with increasing load, the relationship between stress and strain becomes non-linear, despite still being below the yield point. As in LEFM, when the applied load is removed, the accumulated strain is relieved and no damage occurs.

Elastic Plastic Fracture Mechanics

The other main category of fracture mechanics is elastic plastic behaviour. This occurs when the applied load is above that of the yield point of the material. Here the relationship between stress and strain becomes non linear and any applied load that is above the yield will cause permanent deformation. Initially the damage will be small, however, if the load is maintained, then damage will accumulate and the material will ultimately fracture. A prime example of this is a paper clip. If it is bent very slightly with an applied load below the yield, it will behave elastically and return to its original position once the load is removed. However, if a larger load that is above the yield point is applied, then the paper clip deforms plastically and will not return to its original position. In this case, plastic damage has occurred. These different behaviours can be visualised on a stress-strain curve as shown in Figure 2.1.

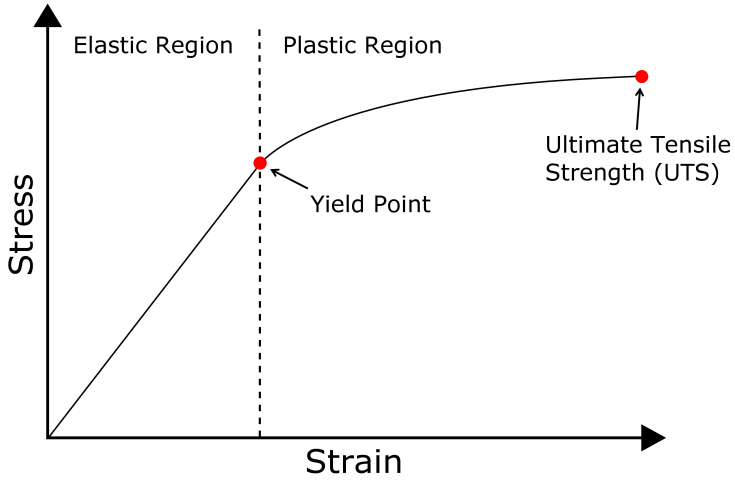

Figure 2.1: Generic stress-strain curve showing yield point and elastic and plastic regions

2.3 Strain Hardening

When the yield stress is exceeded and plastic deformation occurs, the material behaviour changes greatly. In metallic structures, at stresses above the yield point, strain hardening can occur, which is a strengthening of the metal caused by inter-granular movement within the crystal structure.

From observing the stress-strain response, within the plastic region when strain or

work hardening occurs, the stress in the material increases, thus raising its strength and its ability to withstand loads. However, with this, the strain also increases, thus causing additional plastic deformation, reducing its fatigue life. Work hardening in this way, can provide enhanced strength to a material if applied correctly and to an acceptable degree.

The way in which the strain hardening occurs can vary widely in different materials and different relationships have been developed that describe the way the material behaves post yield. A number of material strain hardening laws exist, but arguably one of the most commonly used is the Ramberg-Osgood relationship [21]. This describes the non-linear stress-strain relationship of a material at and above its yield point. The Ramberg-Osgood relationship states:

$$\varepsilon = \frac{\sigma}{E} + \alpha_0 \left(\frac{\sigma}{E}\right)^n \tag{2.1}$$

where ε is strain, σ is stress, E is the Young's Modulus and α_0 and n are material constants. The first half of the equation describes the linear elastic region, whilst the second half describes the strain hardening relationship, providing a full description of the material's stress-strain behaviour.

It is sometimes appropriate to ignore material hardening when performing engineering analyses for ease of simulation. In such cases, an elastic perfectly plastic (EPP) material model can be employed. This is a simplified relationship which offers an approximation of material properties with a lack of material hardening. It assumes that with increasing levels of strain, the stress will never exceed the yield stress. This is an idealistic case and in reality will never occur since some hardening will always take place. However, within finite element analysis (FEA), this allows plasticity to be modelled in a simplified manner to approximate the post yield behaviour of the material. Due to these simplifications, the accuracy of solutions obtained is compromised, however, its ease of implementation and the computing effort is significantly reduced compared to that of more complex hardening models. A generic stress-strain plot showing material hardening and EPP models is illustrated in Figure 2.2.

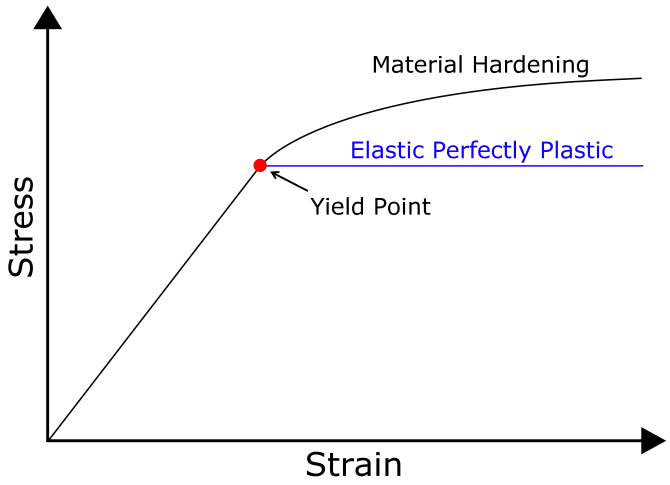

Figure 2.2: Generic stress-strain curve showing material hardening

2.4 Ultimate Fracture

If a sufficiently high load is maintained then fracture will ultimately occur. Different materials exhibit varying stress-strain responses and different fracture characteristics which impact on the manner in which they fail. Some materials, such as ceramics and glasses, undergo brittle fracture, in which very little plastic deformation occurs before fracture. The crack will propagate very rapidly and little or no perceivable damage will occur prior to failure. The fracture surfaces of this type of failure tend to be very smooth.

Other materials undergo a different type of fracture, known as ductile fracture. In this case, considerable plastic deformation can occur prior to fracture. Many metals behave in this way. In the case of a tensile test, a specimen will begin to stretch and narrow, known as necking, before ultimately failing. This type of fracture tends to occur more slowly than brittle fracture and as a result, the fracture surfaces are markedly different. They are much less smooth and often display a characteristic shape known as cup-and-cone in which one end is concave in shape, and the other is convex where they were previously attached. These two types of fracture exhibit very different stress-strain responses as illustrated in Figure 2.3.

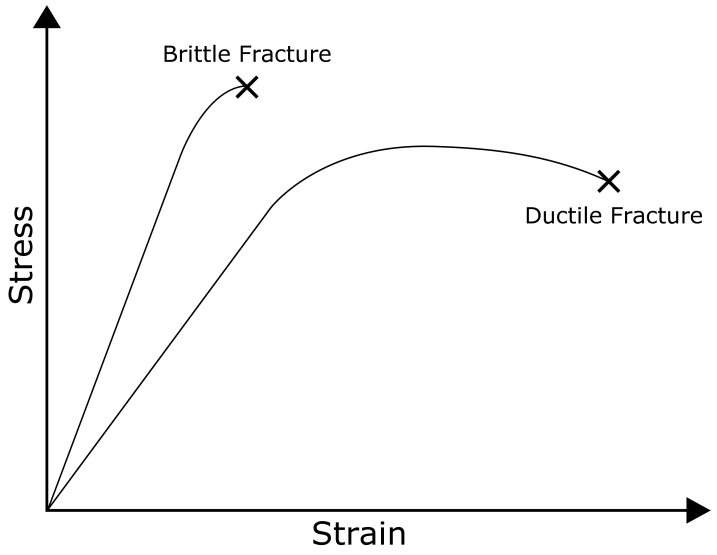

Figure 2.3: Generic stress-strain responses of ductile and brittle fracture

However, fracture behaviour does not always fit exactly into either of these categories and different materials can occupy a range of positions on a spectrum between the two. Temperature can also influence a material's fracture behaviour. There exists a critical temperature, known as the ductile-brittle transition temperature, at which point, the fracture behaviour changes. Below this temperature, brittle fracture will take place, whilst above it, ductile fracture occurs.

These different types of fracture and the stress-strain responses of materials greatly affect a material's properties and its behaviour, and so must be thoroughly understood when considering the design and material selection of engineering components.

2.4.1 Modes of Fracture

The manner in which a material fractures is commonly split into three distinct categories known as the modes of fracture. These explain the way in which a crack propagates through a component and relates to the type of loading. Mode I is an opening mode as a result of tensile loading, Mode II is in-plane shear and Mode III is out of plane shear. These are illustrated in Figure 2.4.

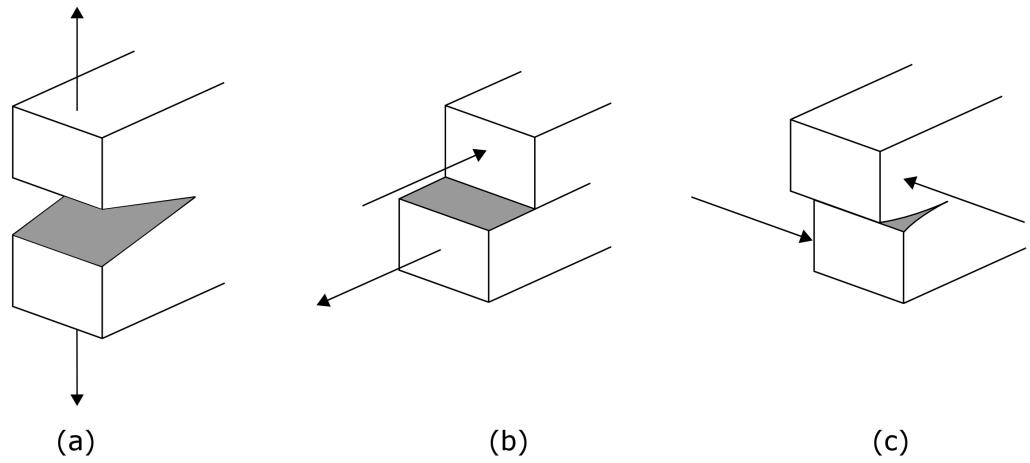

Figure 2.4: Modes of Fracture showing (a) Mode I: Opening, (b) Mode II: In-plane Shear, (c) Mode III: Out-of-plane Shear

2.5 Strain Energy Release Rate

Griffith's and Irwin's work gave rise to the strain energy release rate, which, for a linear elastic material, is defined as the rate of change of potential energy per unit crack surface area,

$$G = -\frac{\partial(U - V_f)}{\partial A} \tag{2.2}$$

where U is the potential energy, V_f is the work done during fracture, and A is the crack surface area. When fracture occurs, $G = G_c$, where G_c is the critical energy release rate [16](p.13). The energy release rate, G, acts as the driving force for fracture whilst the critical energy release rate, G_c is a material's resistance to fracture.

2.6 Stress Intensity Factor

The geometry of a component greatly influences its structural integrity. Design features such as notches or sharp corners, and even minor defects such as scratches and areas of corrosion can act as stress raisers and limit a structure's ability to resist fracture by reducing the limit load, which is the point at which fracture occurs.

The stress intensity factor (SIF), proposed by George Irwin, as mentioned in Section 2.1.2 offers a measure of a stress raising feature such as a crack and the extent of its influence on the stress in a component. It is used as a fracture parameter that relates the stresses in the crack tip region to the energy release rate. In a purely elastic material, the SIF can completely characterise the conditions at the crack tip.

The stress intensity factor, denoted K_I is a function of the stress within a component and the size of the crack, and is defined as:

$$K_I = Y\sigma\sqrt{\pi a} \tag{2.3}$$

Where K_I is the stress intensity factor, σ is the remotely applied stress, a is half of the crack length and Y is a geometrical factor. When K_I reaches a critical value known as the fracture toughness of a material, denoted by K_{IC}, fracture will occur and thus K_{IC} is a measure of a material's fracture resistance.

Since the stress intensity factor is geometry specific, for a known geometrical factor, K can be calculated analytically. Extensive experimental testing has permitted the development of a set of standardised equations for calculating the stress intensity factor for a number of different crack and model geometries, and these are openly published in stress intensity factor handbooks e.g. British Energy Handbook [22]. This allows the SIF of a wide range of specimen geometries to be calculated with relative ease. However, these lists are not exhaustive and so may not be able to provide solutions for highly complex and bespoke geometries. For such cases, K can be calculated numerically and modern computational analysis tools can perform this with ease. Complete crack simulation such as this is vitally important and there are a number of methods of using fracture mechanics to evaluate fracture and fatigue life including the R5 and R6 procedures [4, 23] and stress intensity factor analysis which is discussed in the following sections.

2.6.1 Relating the Strain Energy Release Rate to the SIF

It is possible to relate the SIF to the strain energy release rate, G:

$$G = \frac{K_I^2}{E'} \tag{2.4}$$

where E' is the Modified Young's Modulus and $E' = E$ for plane stress and $E' = \frac{E}{1-\nu}$ for plane strain conditions, and ν is the Poisson's ratio. This relationship also holds for the fracture toughness and so the critical strain energy release rate can be given by:

$$G_c = \frac{K_{IC}^2}{E'} \tag{2.5}$$

For purely linear elastic material behaviour, these two relationships are equivalent.

2.6.2 The J-Integral as a Fracture Parameter

The stress intensity factor only applies for purely linear elastic material behaviour and with increasing levels of plasticity, the SIF becomes less accurate and so an alternative parameter is required. The J-integral offers such an alternative that can more accurately represent increasing levels of plasticity.

The J-Integral was first proposed by Jim Rice in 1968[13] and allows characterisation of the crack tip area without directly focusing on the crack tip itself[24]. This parameter depends on the stress-strain field near the crack tip. It has a path independent nature, meaning that its value can be calculated using an integration path that is sufficiently far from the crack tip. The J-Integral can be considered as a potential energy difference between identical bodies with slightly different crack lengths, thus simulating the change in potential energy as a crack grows. Analytical calculations of the J-Integral have proven to have a good degree of accuracy and it can also be calculated experimentally through consideration of the load displacement data. Under LEFM, the J-Integral is equivalent to the strain energy release rate so that:

$$J = G = \frac{K^2}{E'} \tag{2.6}$$

From this relationship, it can be assumed that for small scale yielding where the plasticity is localised to the crack tip, the behaviour in the global structure is predominantly elastic and by ignoring the crack tip conditions and considering the SIF away from the singularity, the J-integral can be given by:

$$J = \frac{(K')^2}{E'} \tag{2.7}$$

where K' is the stress intensity factor away from the crack tip. However, when the plasticity becomes more significant and widespread, the value of the J-integral exceeds these values and different methods of calculation are required. The use of the J-Integral allows fracture mechanics concepts to be extended to allow for the inclusion of plasticity, and in essence, provides an alternative to the SIF when considering elastic-plastic fracture mechanics.

J was initially defined by Rice for two-dimensional problems as:

$$J = \int_{\Gamma} \left(W dy - T' \left(\frac{\partial u}{\partial x} \right) ds \right) \tag{2.8}$$

where Γ is the contour path surrounding the crack tip, starting from the lower flat crack surface and continuing along the path to the upper flat surface, as illustrated in Figure 2.5. W is the strain energy density, T' is the traction vector defined according to the outward normal along Γ, u is the displacement vector and ds is an element of arc length along Γ [13].

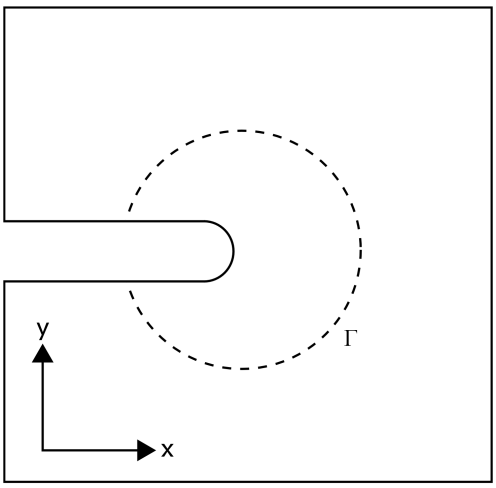

Figure 2.5: Image showing a contour, Γ surrounding a crack tip

Since J is related to the energy released during fracture, it can also be approximated experimentally in relation to the load-history data. Integrating the load displacement curve calculates the total energy released and this is proportional to the J-integral. This is illustrated in Figure 2.6, where A is the crack, and A' is the crack at a later time period once some propagation has occurred and dU is the potential energy released

during crack opening.

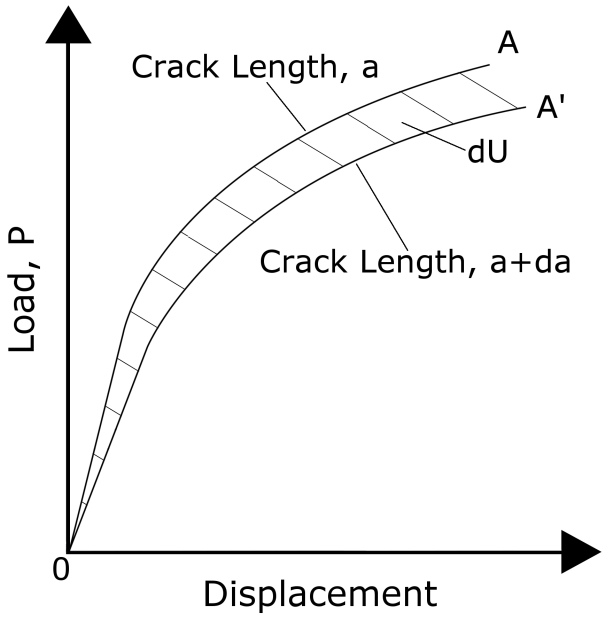

Figure 2.6: Load displacement curve showing energy released during fracture

Once the energy released during crack opening has been determined, the J-integral can be calculated as follows[25]:

$$J = -\frac{1}{B}\frac{dU}{da} \tag{2.9}$$

where B is the body thickness, a is the crack length and U is the potential energy illustrated by the area underneath the load displacement curve. However, since this relationship is proportional to a single body thickness parameter, it is only applicable for constant thickness bodies such as standard compact tension specimens or holed plates, and as such may not be suitable for highly complex, bespoke geometries.

Sumpter and Turner[26] expanded the concept of the J-Integral and separated the J-Integral into both elastic and plastic components so that,

$$J = J_e + J_p \tag{2.10}$$

where, J_e and J_p represent the elastic and plastic components of the J-Integral respectively. With consideration of Equation 2.9, they developed an energy form of the J

integral[27]:

$$J = \frac{\eta_e U_e}{B(w-a)} + \frac{\eta_p U_p}{B(w-a)} \tag{2.11}$$

where U_e and U_p are the elastic and plastic components of the energy released during fracture, η_e and η_p are geometry dependent constants, w is the uncracked ligament and a is the crack length.

At low levels of plasticity, J is dominated by the elastic component and so the linear elastic based strain energy release rate, as discussed above, is sufficient for calculating J. However, when the effect of the plastic zone becomes more substantial, this linear elastic approximate is no longer valid, highlighting the importance of this parameter.

The development of commercial and bespoke finite element software packages has made the J-Integral a more promising technique and as a result, its use in fracture mechanics has increased in recent years[28–30].

2.7 Fatigue

Fatigue is a failure mechanism in which gradual damage occurs as a component undergoes cyclic loading. Due to this repeated loading, failure can occur at induced stress levels significantly lower than the ultimate tensile stress and yield stress limits. For this reason, fatigue is potentially very dangerous since even small loads over a large number of cycles can cause catastrophic damage. Structural fatigue is a prominent failure mechanism in engineering components and it is estimated to be the cause of up to 90% of all mechanical failures in metals [31, 32] and is also the cause of failure for many polymers and ceramics. The fatigue life of a component is expressed as the number of cycles that a component can undergo before critical cracking occurs. Fatigue damage occurs in three distinct stages; initiation, propagation and failure. The first stage is crack initiation when small micro-cracks begin to form. While these may be sustainable up to a certain point, when a crack reaches a critical size, immediate and rapid crack extension occurs throughout the specimen, potentially causing catastrophic failure. Since fatigue accounts for so many mechanical failures, the study of fatigue has attracted many researchers for a number of years [33–38] and is still widely investigated today [39–48] .

2.7.1 Fatigue & Fracture Failure Case Studies

A number of well-known examples of the impact of fatigue failure exist which highlight the importance of studying this type of failure. It is vitally important for engineers to study such cases as learning from these incidents can assist in refining engineering design, hence minimising the risk of future disasters. There are many examples of where the fatigue mechanism has caused failure in a structure and three of the most commonly cited ones are described below.

World War II Liberty Ships

The Liberty ships were a class of warship built by the United States Maritime Comission in World War II. They were designed for rapid construction, when ships were required urgently. To increase the speed of production, their components were pre-fabricated and welded together. This allowed the ship to be constructed very rapidly with the

average construction time being 42 days and the fastest taking only four and a half days. A feature that enabled this rapid construction was that many of the rivets were replaced with welds. At the time, welding on this scale was a relatively new technique and so the workers were inexperienced and there was very little documentation available to offer guidance. Many Liberty ships were affected by deck and hull cracks with approximately 1200 of the entire fleet of 2710 suffering cracks, resulting in the complete loss of 200 ships. There were a small number of extreme cases, where the ships suddenly split entirely in two, as can be seen in Figure 2.7 [49]. A number of factors are believed to have led to these disasters. It was discovered that the grade of steel used to make the Liberty ships had low fracture toughness and suffered from embrittlement. This material became even more brittle in lower temperatures and it was found that the temperature of the cold waters of the North Atlantic Ocean was below the ductile to brittle transition temperature and so the failure mechanisms of these steels changed from ductile to brittle. Fatigue also was a factor in the failures of these ships. In calm waters, the structural integrity of the ships could have been sufficient, however, in open seas when conditions were choppier, the motion of the waves caused the hull and deck of the ships to flex and bend. This cyclic motion of the waves caused repetitive fatigue loading on the structure. This combination of the brittle material and fatigue loading caused nucleation of cracks in the welded joints which acted as stress concentrations. As the hull continued to be flexed and bent, this caused the cracks to propagate [50]. Since the joints were welded rather than riveted, the cracks could propagate across very large distances with no features present to arrest the crack. Riveted joints could have prevented this happening on this scale as a crack could not propagate so far and so fast. Each of these factors played a role in the failures. The impact of an individual factor may not have been so severe, however the combination of the factors had catastrophic results and caused one of the greatest recorded maritime disasters in the 20th Century. These disasters prompted a great interest in fracture mechanics and they can be attributed to the beginning of this engineering discipline.

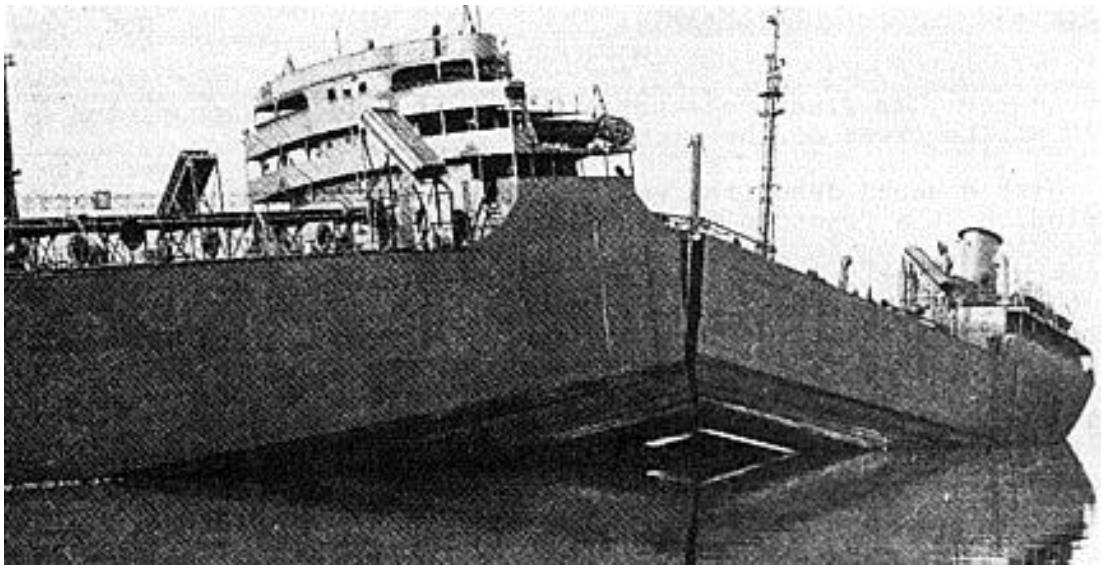

Figure 2.7: Image showing a Liberty ship that had cracked in two [49]

De Havilland Comet

The de Havilland Comet was the first production commercial jet-powered airliner, manufactured by the British aviation company, de Havilland Aircraft Company Limited. Its first flight was in 1949 and its official launch was in 1952. Unfortunately, the Comet had a fundamental design flaw which resulted in 3 catastrophic fatigue failures in 1954, just over one year after entering commercial service. At the time, the fatigue failure and stress concentrations were not well understood and a fundamental design flaw was overlooked in that the windows and hatches in the plane were square with sharp corners. The body around the windows was fixed with rivets, rather than the adhesive bonding that was used elsewhere in the aircraft. These sharp corners and rivets acted as stress concentrations, drastically increasing the localised stresses in the proximity of these features. In the design stage of the aircraft, these stress concentrations had been overlooked and instead global estimates were made based over a large area. This resulted in the fracture and fatigue life calculations being performed with values of stress that were much lower than those that occurred in reality. For the optimum efficiency of the operation of the engines, the Comet had a cruising altitude of 40,000 feet. Although modern planes regularly cruise at this altitude, at the time of the Comet, this was the first time that a pressurised aircraft of this size which contained windows

had been flown at this altitude. To compensate for the low pressure environment, the cabin was pressurised to an equivalent pressure of 8,000 feet, which induced a pressure differential across the fuselage wall of 56kPa [32]. This pressure gradient was double what had previously been experienced by commercial aircraft, inducing great stresses in the structure. For each flight, an aircraft cabin is pressurised before take-off and depressurised after landing. This induces a cyclic internal pressure loading on the body of the aircraft and over the operational life of the plane, this cycle is repeated thousands of times, causing gradual fatigue damage to the structure. In the case of the Comet, this fatigue loading of a substantially increased load range, severely compromised the integrity of the structure, causing cracks to initiate from the sharp corners of the windows and hatches. As the plane continued to operate, this cyclic loading was repeated until ultimate failure occurred, resulting in the loss of three aircraft. Cracking emanating from the sharp corners of the square windows is shown in Figure 2.8 [51, 52]. These disasters brought awareness of stress concentrations in engineering structures and highlighted the importance of design for the minimisation of stress and elimination of such concentrations. This revolutionised aircraft design with round windows to minimise the stress concentrations.

Figure 2.8: Image showing cracking initiating at window corners of the de Havilland Comet [51,52]

Aloha Airlines Flight 243

On 28th April 1988, a Boeing 737 operated by Aloha Airlines was subject to an explosive decompression, resulting in a large section of the fuselage fracturing and separating, as shown in Figure 2.9 [53]. This plane was operated on an short haul service between

the Hawaiian islands. The nature of this service was short distance, high frequency, shuttle flights, resulting in a very high number of flight cycles for a comparatively low number of flight hours. Although Aloha Flight 243 had only 35,496 flight hours, this was accumulated over 89,680 flight cycles, which is defined as take-off and landing. Current Federal Aviation Administration (FAA) regulations state that an airframe must be permanently withdrawn from service after 34,000 flight cycles or 34,000 hours, whichever comes first. Therefore, by current standards, this plane had greatly exceeded its safe working life. This cycling of pressurising and depressurising of the aircraft induced substantial stresses in the structure. An additional factor was the location of the flight routes. Since it was flying in an ocean environment, high levels of salt in the atmosphere had caused corrosion cracking in the aircraft. After the event, it was even reported that on entering the plane, a passenger had noticed a substantial crack in the airplane fuselage, however, this was never reported to staff. The mechanical failure was determined to be due to cracking that had originated from a rivet joint which acted as a stress raiser, which was perhaps further exacerbated by corrosion cracking [54]. Signs of this failure would have been apparent prior to the incident, however, the Aloha Airlines maintenance program had failed to detect the presence of this significant fatigue damage.

Figure 2.9: Image showing fuselage damage caused to Aloha Airlines flight 243 as a result of fatigue failure [53]

2.7.2 Mechanism of Fatigue

The examination of fatigue failure case studies, highlights the importance of a rigorous understanding of fatigue failure and stress. Continued investigation into such failures can hopefully prevent similar incidents from happening again in the future. Real-life cases such as the ones described above, together with the experimental testing that has been performed over the years has allowed a much greater understanding of fatigue failure to be gained through extensive investigation with the result that the mechanism of fatigue is now much better defined and categorised.

Fatigue is characterised by three main stages, crack initiation, crack propagation and failure. However it is important to note that fatigue can take place without the component necessarily failing.

Crack Initiation

During crack initiation, small micro-cracks will form and begin to grow. These cracks may be sustainable up to a certain point, but if the loading is maintained the micro-cracks may reach a critical length.

Crack Propagation

If the micro-cracks reach their critical length, immediate and rapid crack extension occurs throughout the specimen. This is the point at which the crack changes from a stable to an unstable state.

Failure

If the loading is maintained, the propagating crack will continue throughout the entire specimen, causing catastrophic failure.

2.7.3 Fatigue Analysis

Analysing the fracture surface of a component that has undergone fatigue failure can clearly show the three stages of the mechanism. Figure 2.10 shows a scanning electron microscope (SEM) image of a fractured rectangular wire [55]. The point of crack initiation can clearly be seen as a point defect, identified by the large red arrow in

the image. This crack can be seen to propagate away from the initiation point. Once the crack propagation is established, striations in the material can be seen as bands radiating away from the initiation point. These striations are referred to as 'beach marks' since they resemble the pattern that an ebbing tide leaves on a sandy beach. These different bands occur as a result of the cyclic loading that occurs when the crack surface is repeatedly opened and closed. This continues and the crack propagates up to a critical point at which the material can no longer sustain the crack. Whereupon the beach marks cease, as identified by the smaller red arrows, and complete and rapid fracture occurs. At this point, a single load fractures the specimen and so no beach marks are produced and the pattern can be seen as homogeneous. This type of analysis assists in the determination of a degradation mechanism that has occurred. If the reason for failure is unknown, the fracture surface can be analysed in this way and the failure mechanism determined, thus allowing future improvements to be made to prevent or delay fatigue from re-occurring.

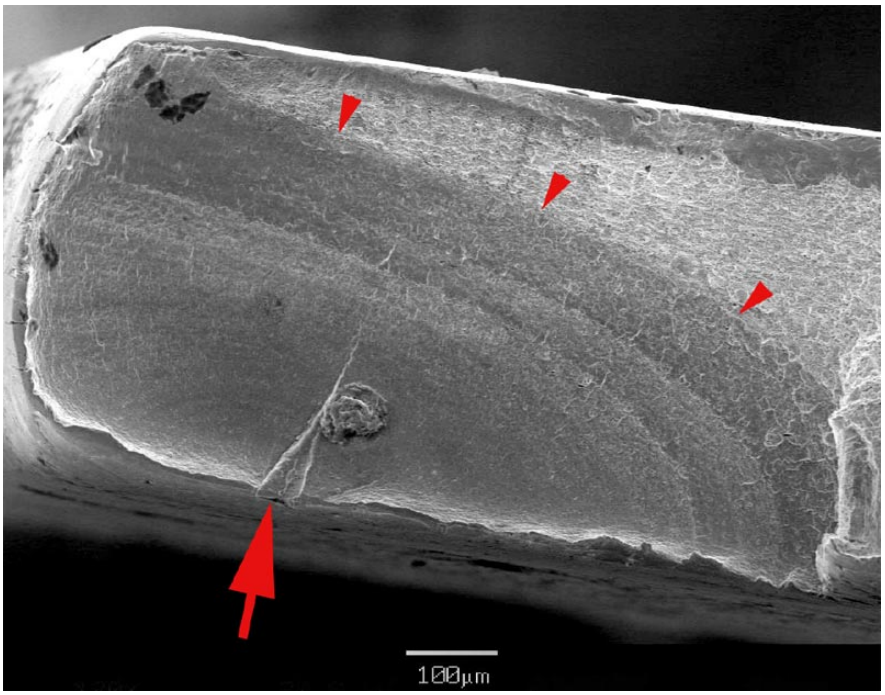

Figure 2.10: Fatigue Fracture Surface [55]

2.7.4 Fatigue Classification

Fatigue is characterised by two different categories, high cycle and low cycle fatigue. High cycle fatigue (HCF) involves low stresses in which the deformation is primarily elastic and typically requires more than 10^4 cycles before failure occurs. Under HCF, induced fatigue damage is due to local plasticity around a stress raiser such as a crack tip. Low cycle fatigue (LCF) occurs when the stress is close to, or at the yield limit of a material and is thus large enough to induce plastic deformation, resulting in a greatly reduced lifetime, with failure occurring in less than 10^4 cycles. Under LCF, fatigue failure can occur either by local plasticity or by global plasticity throughout the entire specimen. This is characterised by the Coffin-Manson relation [56, 57] whereby the total number of cycles to failure is proportional to the plastic strain, so that:

$$\frac{\Delta\varepsilon_p}{2} = \varepsilon'_f(2N)^c \tag{2.12}$$

where $\frac{\Delta\varepsilon_p}{2}$ is the plastic strain amplitude, ε'_f is an empirical constant referred to as the fatigue ductility coefficient, $2N$ is the number of reversals to failure and c is the fatigue ductility exponent, a material constant. This offers an efficient method of calculating the low cycle fatigue life of a structure based on the strain range history data and is widely used in industrial applications.

Fatigue data can be determined experimentally and is commonly characterised using an S-N curve [58], where the number of cycles to failure (N) is plotted against applied stress (S), as shown in Figure 2.11.

It can be seen that for low stresses, the total number of cycles to failure is very high. As the stress increases, the number of cycles to failure decreases. This relationship is derived from extensive experimental results. For a given material and an applied cyclic stress, a fatigue limit can be defined, below which, failure will never occur.

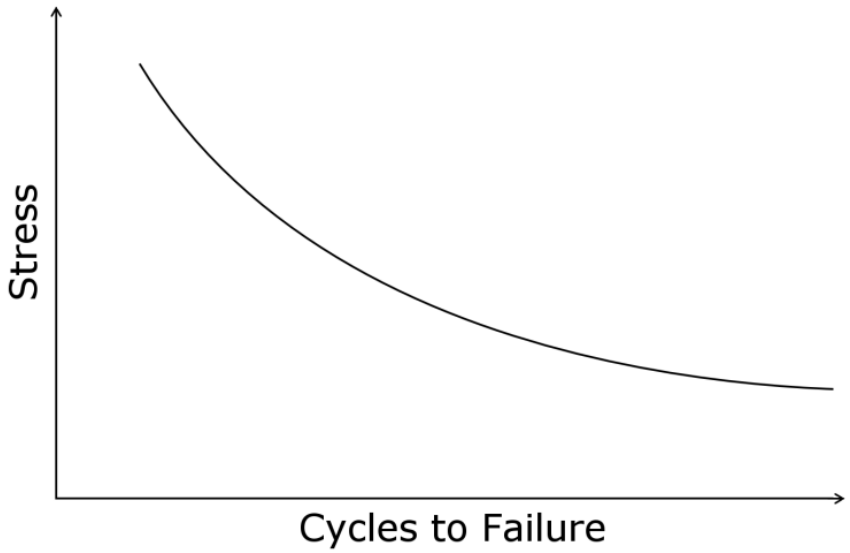

Figure 2.11: Generalised S-N Curve

2.7.5 Types of Fatigue

Mechanical

The most common form of fatigue is mechanical and occurs when a specimen is subjected to a cyclic variation of structural loading. This can be between tensile and compressive forces as found in any rotational system or a variation between maximum and minimum uni-directional forces. This variation in cyclic loading is referred to as the R-ratio which defines the ratio of minimum peak stress to maximum peak stress, $R = \frac{\sigma_{min}}{\sigma_{max}}$.

The mechanical fatigue resistance of a material is generally proportional to its yield strength, and so materials with a high yield strength will tend to be more resistant to mechanical fatigue.

Thermal

Thermal stresses arise when varying temperature conditions are applied to a specimen causing the component to expand and contract, thus inducing internal stresses. Thermal fatigue occurs due to the variation in thermal stress concentrations that are induced through cyclic thermal loading conditions.

The thermal stress of a material is proportional to the thermal expansion coefficient and temperature range, such that:

$$\sigma_{th} = E\alpha\Delta T \tag{2.13}$$

where, σ_{th} is the thermal stress, E is Young's Modulus, α is the coefficient of thermal expansion and ΔT is the temperature range.

It can therefore be seen that the higher the thermal expansion coefficient, the higher the stress, and the more the material is susceptible to thermal fatigue.

Thermo-mechanical

Thermo-mechanical fatigue (TMF), as the name suggests, is the combination of both mechanical and thermal fatigue and occurs when a specimen is subjected to cyclic structural and thermal loading conditions. The two mechanisms work cumulatively to further increase crack initiation and propagation rates, thus greatly affecting the fatigue life. This is commonly found in high temperature, rotational applications such as gas and steam turbines.

The phase lag between the mechanical and thermal loads can have varying affects on the stresses induced in the structure. In phase TMF occurs when the mechanical and thermal load are cycled at exactly the same rate and so maximum mechanical and thermal loading occur simultaneously. Conversely, out of phase TMF occurs when a phase lag exists between the two loads so that maximum and minimum values occur at different times. If the two loads are separated by a 180°phase lag, then the maximum of one load and the minimum of the other load occur simultaneously. This is referred to as completely out of phase TMF. These different categories of TMF are illustrated in Figures 2.12 to 2.14

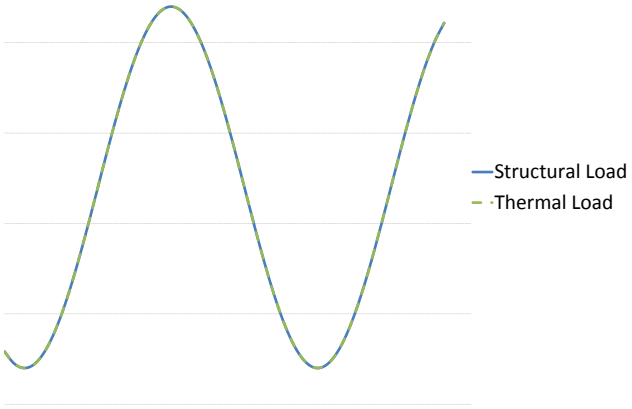

Figure 2.12: In Phase TMF

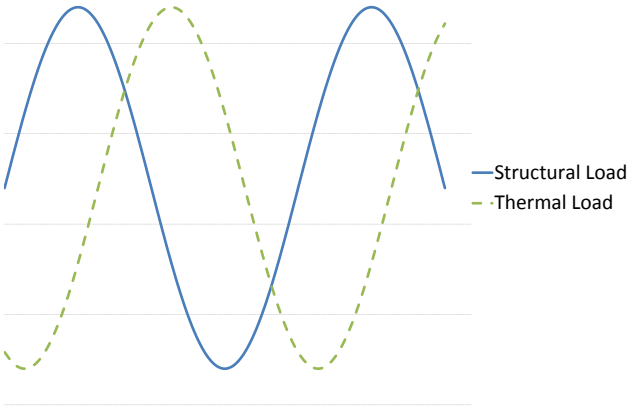

Figure 2.13: Out of Phase TMF

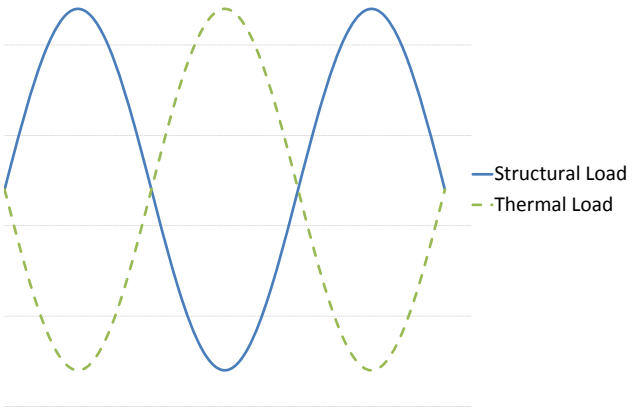

Figure 2.14: Completely Out of Phase TMF

Corrosion Fatigue

The presence of a corrosive environment can exacerbate fatigue. Corrosion can cause pitting and other surface damage, introducing stress raisers, as well as increasing the crack growth rate, thus further limiting the fatigue life of the component. Plotting corrosion fatigue failure data on the S-N curve clearly demonstrates the drastic effect that corrosion has on fatigue and this is illustrated in Figure 2.15. The presence of corrosion dramatically reduces the stress required to cause fatigue failure and thus the number of cycles to failure is also significantly reduced.

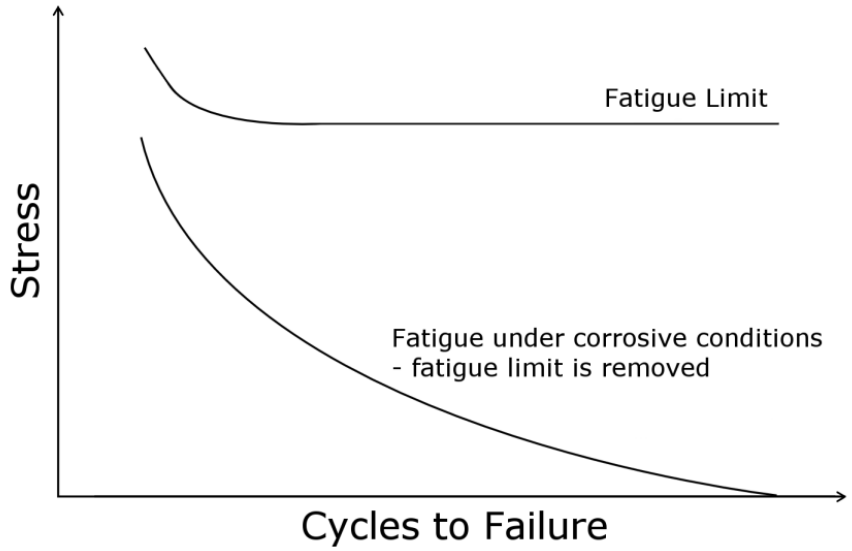

Figure 2.15: Generalised S-N curve with corrosion data

The corrosion fatigue resistance of a material, depends highly on the surface finish of the material. Smooth, un-notched surfaces will have a greater resistance to fatigue than those with surface damage such as pitting. This is true of all types of fatigue, but is of particular importance in corrosion fatigue resistance.

2.7.6 Fatigue Life

Due to the potential consequences of failure, it is clearly vitally important to be able to predict the fatigue life of a component. A number of different methods for calculating the fatigue life of a component are described in Section 2.8.

Complete fatigue life comprises two separate components, crack initiation and crack

propagation. Crack initiation life describes the number of cycles undergone by the specimen before any notable cracking occurs; the extent of cracking is defined by a critical crack length, often denoted, a_c. Crack initiation is said to have occurred once the crack reaches the critical length, a_c. Crack propagation life describes the number of additional cycles that can be sustained before the crack grows to the length where ultimate fracture occurs, or it reaches an additional defined critical crack length. The critical crack length can be user defined depending on the application and the associated safety margins.

2.7.7 Factors Affecting Fatigue Life

There are a number of factors that can limit the fatigue life of a component. Crack initiation will occur at locations where the stress is higher than surrounding regions, known as a stress raiser. Design features such as notches or sharp corners, and even minor defects such as scratches and corrosion can introduce stress raisers, reducing the critical stress at which crack initiation can occur, thus requiring a reduced load or fewer loading cycles for failure to occur.

Material microstructure can also affect the fatigue life; microscopic anomalies such as impurities, atomic dislocations or slip planes reduce the force required to cause cracking, thus greatly increasing the likelihood of failure. These imperfections can arise from impurities in the crystallographic structure or as a result of the manufacturing process such as work hardening or residual stresses from heat treatment or welding.

The loading pattern during normal component operation can also have a significant impact on the fatigue life. If minimum and maximum stress values are both in either tension or compression, the fatigue life will be longer than for a situation where minimum loading is compressive and maximum loading is tensile which will induce greater stresses in the component and thus shorten the fatigue life.

2.8 Fatigue Life Assessment Methods

The ability to predict a component's fatigue life is clearly vitally important and a number of assessment methods have been developed which offer efficient methods of estimating the number of cycles to failure of engineering components which are routinely

used in industry. Different methods are suited to specific applications and must be used appropriately to ensure the highest level of accuracy is achieved.

There are three sets of life assessment methods, those that calculate the number of cycles to initiation, those that calculate the crack growth rate per cycle of a propagating crack and others, called total life approaches, that separate the model into each stage of the fatigue process to determine the complete life through initiation and propagation to ultimate failure. Total life approaches have been found to provide a more accurate representation of the complete fatigue process. Some of these methods are discussed in greater detail in the following sections.

2.8.1 The Paris Law

In the study of Linear Elastic Fracture Mechanics, the fatigue life of a material is commonly represented by Paris' Law, which relates the stress intensity factor range to the critical crack growth. Paris stated that the crack grown rate $\frac{da}{dN}$ is proportional to the stress intensity factor range and two material constants by the following relationship [33].

$$\frac{da}{dN} = C\Delta K^m \tag{2.14}$$

where a is the crack length, N is the number of load cycles, $\Delta K = K_{max} - K_{min}$ is the stress intensity factor range and C and m are constants. The stress intensity factor range is the difference between the stress intensity factor at maximum and minimum loading.

General fatigue crack growth behaviour can be illustrated schematically on a log-log plot of ΔK against the crack growth rate, $\frac{da}{dN}$, as shown in Figure 2.16. This relationship can be broadly split into three separate regions, region 1 where the loading is below the threshold for fatigue to occur, region 2 where fatigue occurs and region 3 where fracture and failure occurs. The Paris Law is a simplified model which provides a representation of the fatigue behaviour in region 2, which is assumed to be linear on a log-log relationship.

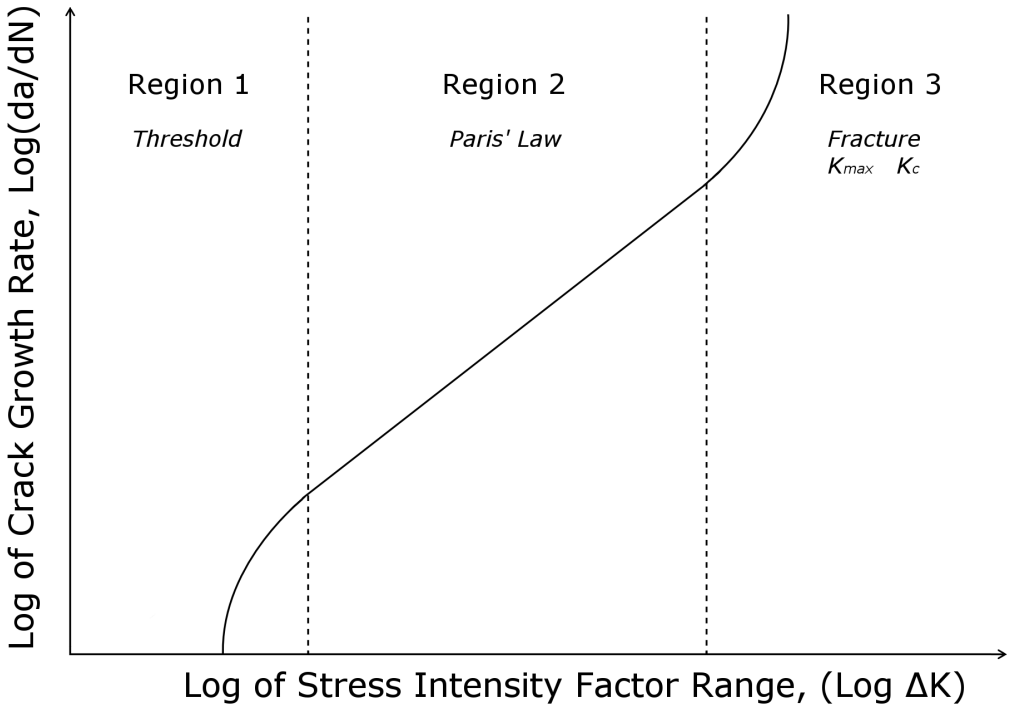

Figure 2.16: Generalised fatigue crack growth behaviour showing the Paris' Law Relationship

2.8.2 The Neuber Correction Method

The Neuber Correction Method [59–63] is one of the most well known methods and is widely used in industry for fatigue life assessment [64, 65]. This is a strain-based life assessment method that is approximated from a purely elastic solution. A linear elastic analysis is performed and the induced behaviour at a stress concentration is calculated. The strain life method requires true stresses and strains and so a correction factor is applied to adjust the elastic solution for local plasticity, to allow the approximate deformation to be determined. The stress range and strain range can then be predicted from this modified solution. Since this method is based on the stress concentration and the induced strain range, it is sensitive to the material properties under investigation. This method is also very conservative, but is especially relevant in highly technical industries such as the power industry, where a high degree of conservatism is often required due to the safety implications.

2.8.3 The Cyclic J-Integral as a Fatigue Parameter

The SIF models purely elastic behaviour, and so beyond the limit of LEFM, when significant plasticity occurs, it no longer offers a satisfactory measure of fatigue life, rendering the Paris Law less accurate for fatigue life assessment. The use of the LEFM concept to calculate a component's fatigue life can yield inaccurate, under-conservative results for cracks growing within a plastic zone. For this reason, an elastic-plastic fracture mechanics approach is required which can more reliably assess the effect of the plastic zone. To this end, a different parameter is needed for the accurate prediction of the fatigue life during plastic deformation.

The cyclic J-integral, denoted ΔJ, offers such an alternative, which in essence is an EPFM equivalent to the stress intensity factor. To address the requirement for a fatigue life assessment method during plastic deformation, Dowling and Begley[66] developed an extension to the Paris law which incorporates this cyclic loading version of Rice's J-integral fracture parameter, ΔJ. They proposed a similar power law behaviour for fatigue life when levels of plasticity are significant. Just as the stress intensity factor range is used to calculate linear elastic fatigue life, they proposed that the elastic-plastic fatigue crack growth rate is a function of the J-integral range, ΔJ, and two material constants, and is given by:

$$\frac{da}{dN} = C'(\Delta J)^{m'} \tag{2.15}$$

where $\frac{da}{dN}$ is the crack growth per cycle and C' and m' are material constants.

Unfortunately, a number of issues are encountered when calculating the cyclic J-integral. Unlike the stress intensity factor, which for cyclic loading is simply equal to $K_{max} - K_{min}$, the cyclic J-Integral, is a function of the stress and strain range, $\Delta\sigma$ and $\Delta\varepsilon$ and as a result, is not simply equal to $J_{max} - J_{min}$. For this reason, calculating the cyclic J-Integral is inherently more difficult than for monotonic loading and no standard techniques have yet been developed to determine ΔJ. In order to allow its inclusion in the Dowling & Begley law for the calculation of the EPFM fatigue life, the J-Integral must be reliably extended to allow for cyclic loading conditions, much like the SIF range is used in LEFM cyclic fatigue.

The cyclic J-Integral is a measure of the elastic and plastic work performed for crack growth to occur when subjected to a cyclic loading history. As a result, from Sumpter and Turner's theory[67], that the J-integral comprises its elastic and plastic components, as in Equation 2.10, it can be assumed that the cyclic J-integral also comprises its elastic and plastic components, so that

$$\Delta J = \Delta J_e + \Delta J_p \tag{2.16}$$

At low levels of plasticity, ΔJ is dominated by the elastic component and so the linear-elastic based strain energy release rate is sufficient for calculating ΔJ. However, when the effect of the plastic zone becomes more substantial, this linear elastic approximation is no longer valid and thus a reliable method of its calculation is vitally important.

One approximate method of calculating the ΔJ is the energy method. In a similar manner as for monotonic loading in Section 2.6.2, the cyclic J-integral, ΔJ is also related to the energy released during fracture, meaning it can be calculated experimentally from load-history data. Considering the entire load history including loading and unloading, ΔJ can be approximated experimentally by integrating the load displacement curve between the minimum load, P_{min}, and maximum load, P_{max} to calculate the total energy released during fracture. This is illustrated in Figure 2.17.

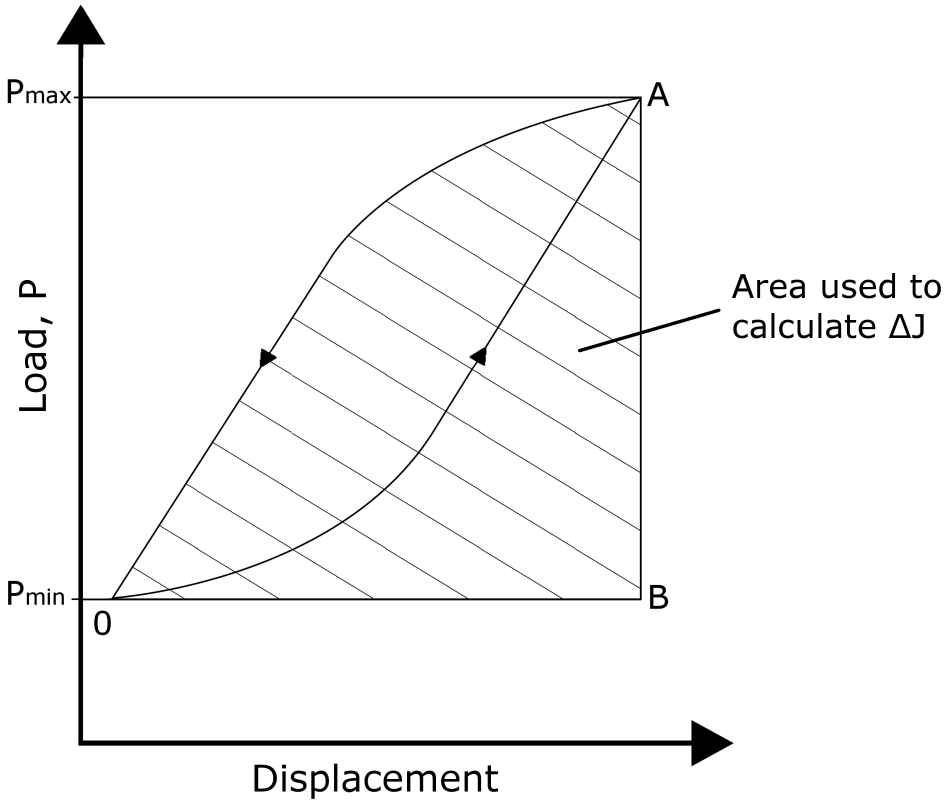

Figure 2.17: Load displacement curve showing energy released during fracture under a cyclic loading history

Once the potential energy released during fracture is known, the cyclic J-integral can be approximated in a similar way as proposed by Sumpter and Turner for monotonic loading (Equation 2.11), through the following relationship as proposed by Webster and Ainsworth[68](p.193-194):

$$\Delta J = \frac{\eta_p dU}{Bb} \tag{2.17}$$

where $dU = AreaOAB$ is the potential energy released during fracture, η_p is a geometrical factor, B is the body thickness, and $b = w - a$ is the un-cracked ligament where w is the total body width and a is the crack length.

However, as with the monotonic case, this is only applicable to bodies of constant thickness, and due to the presence of the geometrical factor, the relationship is geometry specific and only suitable for a small number of specimens.

Predefined geometrical factors exist in the literature [68](p.194) only for compact tension specimens, tension specimens and bend specimens. For compact tension specimens $\eta_p = 2 + 0.52\frac{b}{w}$, for bend specimens $\eta_p = 2.0$ and for tension specimens, $\eta_p = 1.0$. However, for any other geometries, the geometrical factors would need to be determined using other means, adding additional complications in the calculation of the cyclic J-integral.

For these reasons, this method of calculating the cyclic J-integral is not suitable for complex and bespoke specimens. This poses a significant issue for the calculation of the cyclic J-integral and a more widely applicable and reliable method of calculating ΔJ is clearly required. This is the topic of investigation in Chapters 3 and 6.

2.9 Testing and Monitoring of Fatigue

Fatigue life assessment methods are not solely sufficient for a complete understanding and prediction of a component's lifetime and in addition, extensive fatigue monitoring and testing is performed in all the life stages of a component, from design, through operation and retrospective inspection after retirement.

There are a number of different methods of monitoring fatigue fracture, with some methods causing partial or destructive damage to the material. Whilst such methods clearly cannot be used during operation of a component, they can give valuable insights into retired components once operation has completed and the component removed. However, it is also vital to be able to monitor components whilst they are in operation and different techniques must be used in order to achieve this without causing any damage. A valuable range of techniques exist which are non destructive and are referred to as non-destructive examination (NDE).

Although these methods are outside the scope of this project, they are worth considering here since they offer vitally important engineering tools which are used routinely in industry. These techniques can aid the validation and monitoring of fatigue life and a brief introduction to some of these methods is provided in the following section.

2.9.1 Non-Destructive Examination

Non-Destructive Examination (NDE) is the process of detecting properties of a material without damaging or altering a component in any way. This group of analysis techniques can be used to detect flaws and cracks in a material, helping to determine the fatigue and fracture properties. NDE plays an important part in structural health monitoring for assessing integrity and predicting remaining working life.

Visual inspection

The most fundamental method of NDE is visual inspection. This is merely the naked eye observation of a component surface to monitor any abnormalities that may be present including leaks and cracks. This technique does not probe the surface and so cannot detect anything inside the material. Cameras can be used to monitor inaccessible or hazardous areas, however, all detection is conducted by the operator. It is the least sophisticated method of NDE and depends entirely upon an individual's detection ability.

Dye Penetrant

Dye penetrant inspection (DPI) is an extension of the scope of visual inspection. A dye is applied to a surface of a component which then penetrates into any cracks or imperfections on the surface of the material. The excess dye is removed with a developing agent that draws the penetrant from the cracks. The dye then clearly shows the locations of any cracks that are present on the surface. Ultra-violet (UV) light may be used to assist in the detection of the dye. This technique is only capable of detecting surface imperfections and is once again dependent on the operator's detection ability.

Ultrasonic inspection

Ultrasonic Inspection (UT) is a more advanced technique than visual inspection. It uses short wavelength ultrasonic signals to detect any imperfections inside a material. It works in the same manner as radar systems in submarines and ultrasound methods in the medical industry for viewing inside the human body. A signal is transmitted

from a probe onto the surface of the component, which then travels through the material and reflects off any surfaces that it encounters. By monitoring the detection of reflected signals, any internal features can be detected. This technique offers little information regarding the type of feature detected and it relies on the individual inspector's experience and ability to identify internal features. It is a highly manual and laborious technique, undertaken in arduous working conditions for the technician, thus impacting on the operator's ability to detect flaws. The possibility of human error must be factored in and appropriate action taken to ensure that operators are able to work at their optimal ability and that multiple measurements are taken to increase the reliability of readings.

Infra-Red Testing

Infra-red (IR) testing, uses infra-red imaging to detect any heat variation in a component. Such a variation can indicate cracks or holes in a component where thermal energy is lost and detected by the IR imaging device. An example of where this technique may be used is monitoring pipework containing a high temperature fluid. If the pipe is well insulated, any points of high thermal radiation could indicate a crack in the pipe or a region of thinner pipe wall. This technique can be very easy to perform, it does not require any cladding, cover or insulation to be removed and can be performed simply with an IR camera.

Magnetic Particle Inspection

In magnetic particle inspection (MPI) a magnetic field is first applied to the component and then the surface is covered in ferrous iron particles. The magnetic field will be affected by the presence of cracks in such a way that the iron particles will be attracted to and concentrate around any surface defects. This allows imperfections to be easily visible, however this technique is only applicable to magnetic materials such as ferritic steels.

Eddy Current Testing

In eddy current testing, electromagnetism is applied to a component and the resulting magnetic field is monitored. Any imperfections or cracks in the specimen will impede the magnetic flux and thus affect the magnetic field. Monitoring the field with a receiver can identify the location of defects. This technique is only applicable to magnetic materials and the conductivity of the material will dictate the depth into the material that this technique can detect.

Radiography Testing

Cracks and imperfections can be detected with the use of X-Ray and gamma radiation. Defects have different radiation absorption rates compared to solid material and thus their location and any other material variation can be detected.

Acoustic Emission (AE) Testing

Acoustic Emission testing is a method of fatigue crack growth monitoring through analysis of sound waves and acoustic excitation that are generated during propagation [69]. Sensors are positioned on a specimen that can detect cracks by "listening" for noises caused during movement of a crack. This technique can provide a great level of detail of crack growth in complex geometrical specimens and by mapping the detected signals, the crack growth progression and development can be determined.

Leak Test

Leak testing can be used to detect cracks in pressure containment components such as pressure vessels and piping, by pumping liquid or gas penetrants into the component at high pressure. Tests can then be performed to detect the penetrant gas. Typical examples are helium or radioactive isotopes of xenon. Helium is inert and is therefore a safe option which can be detected by a mass spectrometer. Xenon isotopes are radioactive and so may not be suitable for some applications, however, the radiation, and therefore the location of the crack can easily be detected. As a low cost method, soapy water can also be used since the presence of a gas leak will produce bubbles on the component surface, which are easily visible.

Choice of NDE Test

It can be seen that there are numerous different NDE tests which vary widely in cost and sophistication. The optimal test to use depends on the specific application in question. Highly technical and high risk applications such as in the nuclear industry require highly sophisticated techniques with less concern for the associated cost. For low-technology applications, a much less sophisticated and cheaper technique may be deemed sufficient.

2.9.2 Fitness for Service Assessment

Fitness for service (FFS) assessments offer a method of evaluation of the structural integrity of components. FFS assessments consider crack geometry, material properties and loading conditions in order to offer a quantitative measure of the structural behaviour of a component. This is used to determine the consequences of failure, safety classification, tolerable likelihood of failure and safety of operation. These standards offer guidelines on how to assess a structure through its design, manufacture, operation and life extension, ensuring maximum levels of safety. A number of different procedures exist which are widely used in the heavily regulated power industries, in particular the nuclear industry. These include R5[4] & R6[23] and ASME Boiler & Pressure Vessel Code (BPVC) Section III[70]. These assessment guidelines aid the evaluation of fatigue in nuclear power plant components and help to minimise the risk of failure to verify safe operation. This is achieved through strict guidelines for optimal design and manufacture as well as extensive and regular monitoring and inspection routines.

R5 and R6 Procedures

The R5 procedure, developed by British Energy, is a UK standard for the assessment of the integrity of structures at high temperature. This is used primarily in the nuclear industry for the assessment of the structural integrity of Advanced Gas-Cool Reactors (AGRs). The R6 procedure is used for the assessment of structures containing defects and together with the R5, provides the foundation of the UK's integrity assessment of the AGR fleet.

The R5 procedure uses a simplified approach based on elastic stress analysis to assess

a number of different damage mechanisms including excessive plastic deformation, creep rupture, cyclic ratchetting, creep deformation, crack initiation and crack growth.

In cases which do not relate completely to the damage mechanisms listed above, more advanced options are available, leading to less restrictive results. For highly complex cases, advice is provided to ensure accurate results using a complete, fully cyclic inelastic computational analysis. This allows a balance to be made between the simplified and less accurate elastic based analysis and computationally expensive and time consuming cyclic analysis.

ASME BPVC Section III

The ASME Boiler Pressure Vessel Code Section III is an American standard that offers a similar procedure to R5 and R6 for the evaluation of fatigue of nuclear power plant components. It is based upon empirical data obtained from extensive experimental testing to assess the fatigue endurance of austenitic steel structures in air environments. Fatigue failure is defined as the number of cycles that is required to cause a 3mm deep crack in the cylindrical specimens that were used in the tests. This poses an issue when applying the code to different geometries, materials or in different environments. However, this definition of fatigue failure is widely adopted and is ratified by the UK Technical Advisory Group on the Structural Integrity of High Integrity Plant (TAGSI). The results obtained are conservative estimates that have been shown to be highly reliable. However, due to the nature of the tests on which the fatigue estimates are based, the procedure has been found to be more restrictive than the R5 and R6 procedures.

2.9.3 Predicting Component Lifetime

Fatigue cracking and impending failure can be inherently difficult to detect but as has been seen, the consequences if not detected can be severe. Therefore, in order to reduce the impact of a failure, the fatigue life of a component must be determined during its design stage. Whilst the component is in operation, adequate safety margins must be employed. In addition, condition monitoring of the component can be performed to provide early indication of impending failure. For example, the “leak before break”

condition, where detection of leakage indicates the onset of failure, allows appropriate actions to be taken before serious consequences ensue.

2.10 Creep

The final damage mechanism that is presented in this thesis is creep. Creep is a failure mechanism in which gradual deformation occurs over extended periods of time at elevated temperatures. Creep generally takes effect at between a third and half of the melting temperature of the material, and when subjected to continuous loading for extended periods of time, inter-granular cavitation damage occurs, causing the material to plastically deform and elongate. However, the extent and rate of deformation is dependent on the material, temperature, applied structural load and dwell time. Since creep deformation occurs when components at elevated temperatures are exposed to structural loads for extended time periods, this failure mechanism is particularly prevalent in the power industry.

Figure 2.18 illustrates a typical material response subjected to an extended time constant stress load. This type of deformation can be categorised into four distinct stages. Initially elastic strain occurs immediately upon loading, primary creep then begins shortly after the load is applied and during this stage, material hardening occurs, causing the strain rate to decrease with time. Next, secondary creep occurs, at which point the deformation reaches a steady state and the creep rate becomes constant. The final stage is tertiary creep, in which the creep strain rate accelerates. During this damage phase, slip occurs along the grain boundaries of the material, causing the nucleation of voids. When these voids coalesce, creep rupture occurs and the material fails.

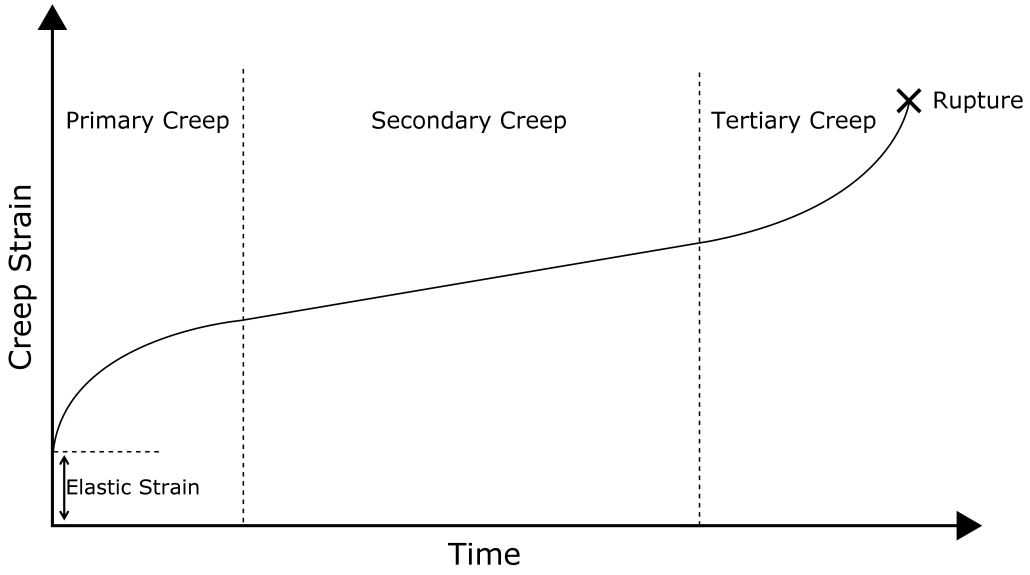

Figure 2.18: Generic creep curve showing the three stages of creep followed by rupture

2.10.1 Creep Laws

Describing the evolution of creep is very complex, however, a number of different constitutive relationships exist that have been proposed to describe each stage of the creep behaviour of a material. Different materials will follow different creep relationships for each stage and so there exist a large number of creep laws that a material may follow. The creep strain is commonly separated into its elastic and inelastic components so that,

$$\varepsilon = \varepsilon_E + \varepsilon_C \tag{2.18}$$

While the elastic strain can be determined with ease, the creep strain poses additional complications, but a number of relationships have been developed in an attempt to model the creep behaviour of materials. The creep strain can be written as a function of stress, σ, time, t and temperature T, so that,

$$\varepsilon_C = f(\sigma, t, T) \tag{2.19}$$

This can be further separated into functions of each component, i.e. stress, $f_1(\sigma)$, time, $f_2(t)$, and temperature, $f_3(T)$, such that,

$$\varepsilon_C = f_1(\sigma) f_2(t) f_3(T) \tag{2.20}$$

For the stress component, some of the proposed constitutive relationships include the Norton, Prandtl, Dorn, Garofalo and Friction Stress laws [71](p.12-13):
The Norton law:

$$f_1(\sigma) = B_n \sigma^{n_n} \tag{2.21}$$

The Prandtl law:

$$f_1(\sigma) = C_p \sinh(\alpha_p \sigma) \tag{2.22}$$

The Dorn law:

$$f_1(\sigma) = D_d exp(\beta_d \sigma) \tag{2.23}$$

The Garofalo law:

$$f_1(\sigma) = A_g [\sinh(\gamma_g \sigma)]^{n_g} \tag{2.24}$$

The friction stress law:

$$f_1(\sigma) = B_f (\sigma - \sigma)^{n_f} \tag{2.25}$$

Where, B_n, n_n, C_p, α_p, D_d, β_d, A_g, γ_g, n_g and B_f are material constants specific to each respective creep law and σ is stress.

For the time dependence component, the proposed constitutive relationships include the Secondary creep, Bailey, Andrade, and Graham and Walles laws:
The secondary creep law:

$$f_2(t) = t \tag{2.26}$$

The Bailey law:

$$f_2(t) = b_b t^{m_b} \tag{2.27}$$

The Andrade law:

$$f_2(t) = (1 + b_a t^{1/3}) e^{k_a t} \tag{2.28}$$

where b_b, m_b, b_a and k_a are material constants specific to each respective time depen-

dence creep law and t is time.

As can be seen, a number of different creep-fatigue relationships exist for both the stress and time dependence and a complete creep law can be obtained through the combination of each of these relationships. Different materials will follow different relationships and there is no single creep-fatigue law that can be applied to all materials. As such, these different relationships have been developed in an attempt to describe standardised creep curves exhibited by a range of different materials.

2.11 Creep-Fatigue Interaction

When a component is subject to a cyclic loading history, the number of cycles to failure will decrease if an extended hold time is introduced in the loading cycle and this is known as the creep-fatigue interaction. Creep and fatigue are complex mechanisms that exhibit different damage processes. Fatigue induces transgranular crack propagation, whilst creep causes intergranular cavitation damage. The combination of the two mechanisms and the accumulation of creep damage accelerates the crack growth rate.

Creep-fatigue is a prominent failure mechanism in applications that include elevated temperatures and high stresses, such as those experienced in power plant applications and is of particular importance in industrial gas turbines. For this reason, the study of this failure mechanism and the ability to model the interaction of creep and fatigue is vitally important in the design of turbine components. This is discussed further in Chapter 7.

2.12 Chapter Summary

This chapter has introduced the fundamental theories of structural integrity providing a foundation for the subsequent chapters and the rationale for this project. An overview of fracture mechanics has been provided including the background theory and a brief history illustrating the development of the field. Some basic fracture mechanics principals have been explained, including the modes of fracture, material response and stress-strain curves, as well as fracture parameters such as the strain energy release rate, stress intensity factor and the J-integral. Next, the fatigue mechanism was ex-

plained and a number of case studies were given highlighting the dangers associated with fatigue and the importance of understanding this mechanism. The fatigue process was explained and a number of different classifications were introduced. The fatigue life was discussed and a number of different methods of fatigue life assessment were introduced. This led onto the testing and monitoring of fatigue and the importance of fitness for service assessment procedures such as the R5 and ASME BPVC within industrial applications. Finally, the creep mechanism was introduced, covering the definition of a number of creep laws and the explanation of creep-fatigue.

Chapter 3

Advanced Fracture Mechanics Methodologies

Chapter Overview

This chapter extends the basic principles introduced in the previous chapter and describes more advanced fracture mechanics methodologies. A number of novel techniques are presented that make up some of the latest developments in the field of structural integrity.

Initially the traditional finite element method is explained, demonstrating how this technique is used within engineering for structural integrity and lifetime assessment. Next, a number of techniques for the calculation of the J-integral and cyclic J-integral that are used in industry are introduced. The eXtended Finite Element Method is then presented as an extension of the traditional FEM. This relatively new, and revolutionary technique is explained, highlighting its potential in routine structural integrity assessment for highly complex crack propagation analysis. The core principals are introduced and some computational examples are included to demonstrate the power of this technique. Finally, the Linear Matching Method is introduced as a highly efficient numerical tool for the assessment of structural responses to cyclic loading histories.

3.1 Traditional Finite Element Analysis for Fracture Mechanics

The Finite Element Method (FEM) is an analysis tool that provides a numerical solution to complex engineering problems including structural mechanics and fracture mechanics, stress, thermal, vibrational and dynamic analysis.

In the FEM technique, mathematical models are created to describe physical science and engineering phenomena. Depending on the complexity of the case, these models can be simple algebraic equations or a series of complex differential or integral relationships. Once the appropriate mathematical model is defined, it can be solved to describe the behaviour of the system under a given set of conditions. These mathematical models can be sub-categorised into two distinct types, analytical and numerical, depending on how they are solved. Analytical solutions yield a general mathematical expression which satisfies the model for all conditions, resulting in an exact solution. Due to this accuracy, these solutions can be very difficult and time consuming to solve and can even be unsolvable for certain conditions. An alternative approach is to use numerical solutions. This yields an approximate numerical solution and is not a general equation. This allows conditions to be modelled that would otherwise be unsolvable through other means. These solutions are approximate, but increasing the refinement of the analysis can result in highly accurate results and any discrepancies may be negligible.

The Finite Element Method was first proposed by Courant in 1943 [72] for problems in vibrational analysis but the technique has undergone extensive development over the intervening years and is still widely studied today with new developments continually being made to the technique.

The finite element method is implemented into computational numerical analysis software, allowing Finite Element Analysis (FEA) to be performed. FEA allows the user to model structures within a computer interface, discretising a geometry into a number of elements and nodes, as illustrated in Figure 3.1. A set of simultaneous algebraic equations are then created for the nodes and through solving each of these in turn, the process can be repeated for adjacent elements until the equations for all elements of a structure have been solved. Through repeated modelling on a micro

scale in this way in a number of small elements, large and complex structures can be modelled and their responses to a set of conditions simulated. This allows engineers to model structures and simulate different materials, then apply loads and boundary conditions and model the structural response, assessing the integrity of the component. This Finite Element Analysis procedure is demonstrated in Figure 3.2. Image (a) shows the initial model geometry, (b) shows the meshed model and (c) shows a typical stress contour result under a particular set of loading and boundary conditions.

Finite Element (FE) modelling is clearly an essential engineering tool, that allows analyses to be performed which would otherwise not be possible. Its continued development allows more complex cases to be studied, making them more akin to real life applications. Without the use of FE, engineering design and assessment would not be where it is today.

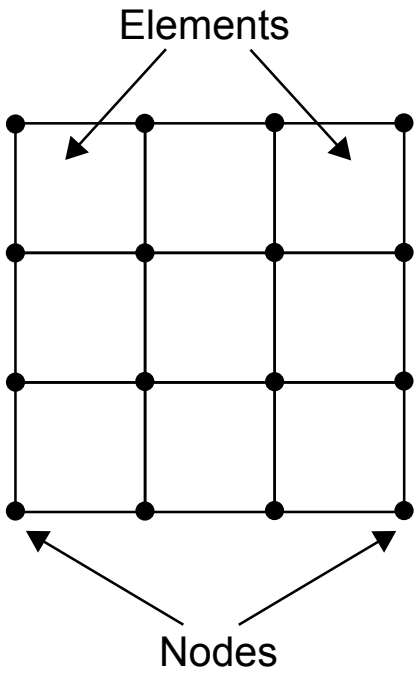

Figure 3.1: Example finite element mesh showing nodes and elements

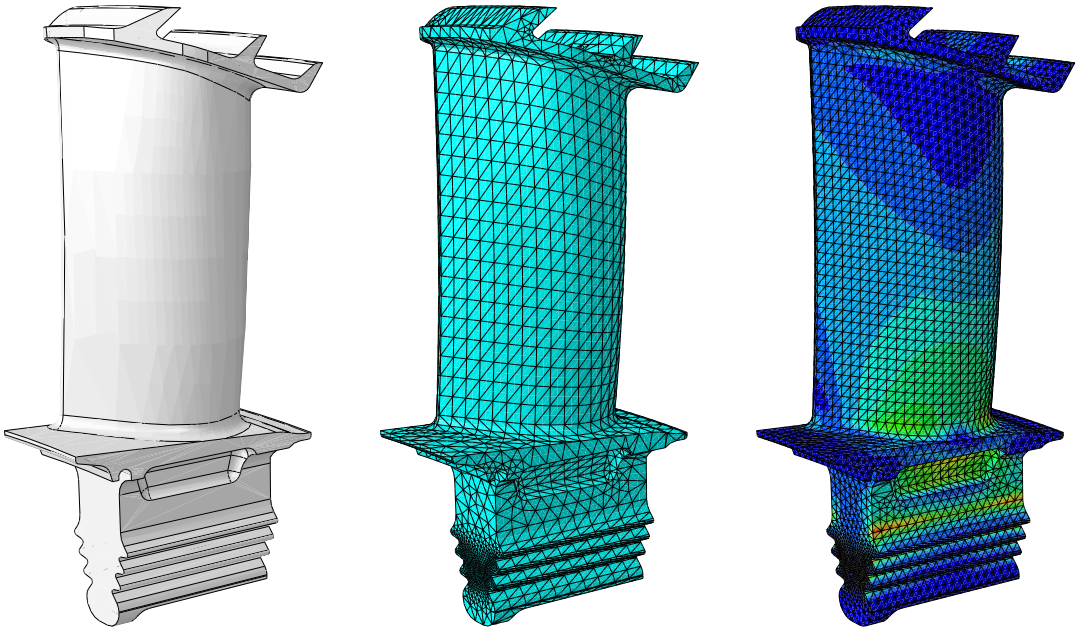

(a) (b) (c)

Figure 3.2: Turbine blade Finite Element Analysis showing (a) geometry model (b) meshed geometry and (c) stress contour results

A number of different commercially available off the shelf, as well as bespoke, finite element software packages are available, however, ABAQUS[6], is used for all computational FE analysis in this thesis.

3.1.1 Finite Element Analysis Crack Simulation

FEA allows the modelling of cracks and the calculation of their associated parameters such as SIF and J-Integral. Within FEM, this is achieved through contour integration. This allows the evaluation of integrals along paths encircling a crack front[73]. Whilst these contour integrals do not themselves directly predict how a crack will propagate, they can be used to provide valuable information and offer some indication as to how the crack may behave as well as the estimation of fatigue life.

3.2 Reference Stress Methods (RSM)

Reference stress methods (RSM) are a range of concepts that offer a means of calculating damage characteristics such as fracture, fatigue and creep, in structures subjected

to arbitrary load variations. The method suggests that the overall damage behaviour in the structure is simply related to a reference stress, which is a measure of an averaged stress state across a structure [74]. This concept offers greatly simplified methods of calculating damage characteristics of highly complex engineering structures and load cases. The Reference Stress Methods are widely adopted in industry and are used in the R5 and R6 procedures.

3.3 Calculation of the J-Integral using the RSM

The Reference Stress concept offers a viable method for the calculation of the J-integral and cyclic J-integral for fatigue analysis, and is part of the R5 procedure for fatigue crack growth calculations [4](p.4/5.A3.4). It is based on the work of Miller & Ainsworth [75], and uses the basis of the work of Sumpter & Turner [67] that separates the J-integral into elastic and plastic constituents as shown in Equation 2.10. This procedure is described for both monotonic and cyclic loading histories in the following sections.

3.3.1 J-Integral Under Monotonic Loading Conditions

It has already been established that the elastic component, J_e is proportional to the stress intensity factor and is given by:

$$J_e = \frac{K^2}{E'} \tag{3.1}$$

where, K is the stress intensity factor and E' is a modified Young's Modulus which, for plane stress conditions $E' = E$ and for plane strain conditions, $E' = \frac{E}{1-\nu^2}$ where E is the Young's Modulus and ν is the Poisson's ratio.

The plastic component of the J-integral, J_p is proportional to the reference stress, reference strain and a geometrical constant:

$$J_p = \sigma_{ref}\varepsilon^p_{ref}R' \tag{3.2}$$

Where, σ_{ref} is the reference stress, ε^p_{ref} is the uniaxial plastic strain at the reference stress, and R' is a geometrical constant, referred to as the characteristic length. These

terms are defined below: The reference stress, σ_{ref} is in essence the average stress across a geometry and is a function of the applied load, yield stress and limit load of the structure

$$\sigma_{ref} = \frac{P\sigma_y}{P_L} \tag{3.3}$$

where, P is the applied load, σ_y is the yield stress of the material, and P_L is the limit load of the specimen.

As presented in [76, 77], the uni-axial plastic strain at the reference stress can be expressed by :

$$\varepsilon^p_{ref} = 0.002\left(\frac{\sigma_{ref}}{\sigma_y}\right)^{\beta} \tag{3.4}$$

where, β is the Ramberg Osgood parameter, which is the reciprocal of the material strain hardening exponent, n:

$$\beta = 1/n \tag{3.5}$$

The characteristic length, is a constant that is dependant on the stress intensity factor and can be calculated by:

$$R' = \left(\frac{K}{\sigma_{ref}}\right)^2 \tag{3.6}$$

Therefore, combining these components, the total J-integral can be calculated using the Reference Stress Method as:

$$J = \frac{K^2}{E'} + \sigma_{ref}\varepsilon^p_{ref}R' \tag{3.7}$$

Which, in full, then becomes:

$$J = \frac{K^2}{E'} + \left(\frac{P\sigma_y}{P_L} \ * \ 0.002\left(\frac{\sigma_{ref}}{\sigma_y}\right)^{\beta} * \ \left(\frac{K}{\sigma_{ref}}\right)^2\right) \tag{3.8}$$

3.3.2 J-Integral Under Cyclic Loading Conditions

The previous section demonstrates how the Reference Stress Method is capable of calculating the J-integral under monotonic loading. It is also possible to extend this method to allow the calculation of the J-integral under cyclic loading conditions, denoted as,

ΔJ.

The cyclic stress intensity factor for cyclic loading, ΔK is given by the difference of K at maximum and minimum loading, so that:

$$\Delta K = K_2 - K_1 \tag{3.9}$$

where, K_2 is the SIF at the maximum load and K_1 is the SIF at the minimum load. As explained in Section 2.8.3, this relationship does not apply for the J-integral when there is any notable plasticity and so $\Delta J \neq J_2 - J_1$.

The cyclic J-integral, ΔJ can be calculated in a similar manner to that of the monotonic J-integral as described earlier, however, certain parameters must be modified to incorporate cyclic loading conditions. This is achieved through the inclusion of cyclic counterparts of the loading, stress intensity factor, reference stress, uniaxial plastic strain and limit load into Equation 3.7, to become:

$$\Delta J = \frac{\Delta K^2}{E'} + \left(\Delta\sigma_{ref} \Delta\varepsilon^p_{ref} R' \right) \tag{3.10}$$

where,

$$\Delta\sigma_{ref} = \frac{\Delta P \sigma_y}{\Delta P_L} \tag{3.11}$$

$$\Delta\varepsilon^p_{ref} = 0.002 \left(\frac{\Delta\sigma_{ref}}{\sigma_y} \right)^2 \tag{3.12}$$

$$\Delta R' = \left(\frac{\Delta K}{\Delta\sigma_{ref}} \right)^2 \tag{3.13}$$

Therefore, the complete equation for the calculation of the cyclic J-integral becomes:

$$\Delta J = \frac{\Delta K^2}{E'} + \left(\frac{\Delta P \sigma_y}{\Delta P_L} \ * \ 0.002 \left(\frac{\Delta\sigma_{ref}}{\sigma_y} \right)^{\beta} * \ \left(\frac{\Delta K}{\Delta\sigma_{ref}} \right)^2 \right) \tag{3.14}$$

3.3.3 Limitations of Existing Technologies

The GE/EPRI [78] and Reference Stress Method (RSM) [75] offer simplified methods of approximating the cyclic J-Integral. However, due to the nature of these methods they exhibit considerable limitations and thus produce overly conservative results. Both of these methods are based on the limit load analysis and as such do not consider the crack geometry, and are thus unable to assess three dimensional detail. Consequently, the ΔJ variation along the crack front cannot be determined and hence valuable crack propagation information is neglected. In addition, these methods are suitable for a number of documented test cases such as compact tension specimens, however, difficulties arise when applying these methods to bespoke specimens. These limitations provide great approximations in the calculation of the cyclic J-Integral, significantly reducing the accuracy of the results. For these reasons, these methods are not considered appropriate for complex 3D industrial applications. ABAQUS and other FE packages are capable of calculating the J-Integral under monotonic loading, however, they are currently unable to automatically determine the cyclic J-Integral from stress and strain histories. Manually calculating the cyclic J-Integral, would require extensive and very time consuming post processing of the analysis history data. Manually calculating in this way is therefore not feasible and so a more automated method is required if the cyclic J-Integral is to be a viable fatigue life parameter.

3.3.4 Method Summary

It can be seen that these methods offer an adequate method for the approximation of J and ΔJ. However, these calculations are based on an elastic theory by using the SIF, and so these values are only approximate and do not offer a complete analysis of the plastic behaviour. If a greater level of accuracy is required for the calculation of J and ΔJ, a different method is required that can more reliably consider the impact of the plastic zone. Such a suitable method is proposed in Chapter 6.

3.4 The Extended Finite Element Method (XFEM)

Fracture is arguably one of the most important failure modes in engineering structures and the potential consequences can be very severe as has been highlighted in the case studies of Chapter 2. Therefore, the study of fracture is a vitally important discipline and one which has been, and is still widely investigated by many researchers. In addition to fatigue life calculation to predict when a crack will initiate, it is also important to gain a thorough understanding of how a crack will behave once it has initiated. For this reason, the study of crack propagation has become critical theory in the field of fracture mechanics. The rapid increase in computing power in recent years has allowed highly complex numerical modelling to be performed. Prior to these computational advancements, such modelling would have been far too intensive and time consuming and so has not been a viable option. This has allowed the development of many bespoke computational tools designed for modelling crack initiation and propagation in complex three-dimensional components. As a result, there now exist a number of analytical and numerical methods for modelling crack propagation which can be used to aid engineering design, structural integrity calculations and condition monitoring.

Studying cracks in two-dimensions can provide useful information about their behaviour, however, in reality, cracks are usually in three-dimensions and can have a very complex geometry and propagate along arbitrary paths. Modelling uniform straight or planar cracks can be performed with relative ease in the conventional finite element method and has been carried out for a number of years. However, this assumption that the crack behaves in a linear manner is not typical of real life applications and so can dramatically compromise the accuracy of the results when comparing to actual components. For this reason, the modelling of more complex, curved cracks has become of great interest in recent decades. As a result, a number of new methods have been developed for the modelling of the crack propagation of curved cracks. Such methods include the adaptive mesh finite element method [79], nodal force release method [80, 81], element cohesive model [82] and the embedded discontinuity model [83].

A limitation of these methods as well as classical FEM is the dependence the accuracy of the solution has on the mesh refinement of the model. The mesh must conform to the geometric discontinuity that is being modelled, e.g. a crack, and any crack

growth must align along the element boundaries. This means that the accuracy of the result is heavily dependent on the quality of the mesh, and so for reliable results, a highly refined mesh is required. In addition, the crack propagation can typically only occur along a predefined path, meaning that some understanding of the crack behaviour must be obtained before finite element modelling can be performed. For these reasons, difficulties arise when modelling complex geometries, since modelling a highly refined mesh in the critical regions of a model, for example at a crack tip, can vastly increase the computational effort, both in implementation and analysis time. The limitations of these methods highlight the motivation behind the development of the eXtended Finite Element Method (XFEM), which, due to its inherent design strengths, has become a highly efficient numerical method for modelling highly complex fracture problems. The eXtended Finite Element Method is a modification to the classical finite element method (FEM) that allows mesh independent crack propagation modelling and was first developed in 1999 by Belytschko and Black [84] and Moës et al [85]. This allows a geometrical discontinuity such as a crack to be modelled where the faces do not need to align with the element boundaries, meaning that crack initiation and propagation can be modelled without adaptive re-meshing as the crack grows along an arbitrary propagation path and without the need for a prior definition of the crack. This also greatly reduces the importance of mesh refinement in the region of the crack front. This is inherently different to the finite element method, in which, the mesh must match the geometry of any internal defects such as cracks and voids. This can cause significant mesh distortion as well as the need for extensive mesh refinement in order to obtain a suitable level of accuracy. Meshing the entire model with a very fine mesh is not practical since it will be too computationally intensive. The only alternative is to create a refined mesh in the critical regions surrounding the crack tip, whilst employing a more coarse mesh in the less critical regions away from the crack. This leads to a non-uniform mesh distribution which can be very labour intensive and time consuming for an engineer to model. The strengths of XFEM mean that the mesh dependence on the accuracy of results is reduced since the mesh does not need to match the geometry of the discontinuities contained within the specimen and so arbitrary crack propagation can be modelled without adaptive re-meshing, thus significantly reducing the compu-

tational effort. XFEM is also capable of calculating crack parameters such as the SIF and J-integral. However, ABAQUS is currently only capable of calculating these for stationary cracks, thus limiting its use for industrial applications. Since its conception in 1999, the method has undergone extensive development and is becoming widely used for complex fracture mechanics investigations across a wide range of industries including materials science, aeronautical and space technologies and civil engineering. Today, there exist a number of bespoke XFEM software packages and the technique is also available in a range of commercial finite element software packages such as ABAQUS and ANSYS, allowing increased ease of use and ergonomic implementation for the user.

3.4.1 XFEM Concept

The XFEM concept is based on the partition of unity method as introduced by Melenk and Babuska in 1996 [86]. This states that the standard finite element method can be augmented by the addition of an enrichment function, $\psi(x)$

$$\psi(x) = \sum_I N_I(x)\phi(x) \tag{3.15}$$

where, $N_I(x)$ satisfies the partition of unity such that, $\Sigma_I N_I(x) = 1$ and ϕ is an enriched function. Belytschko et al [87] developed this concept in 2000 and introduced a parameter, c_I, allowing the calculation of the enrichment function.

$$\psi(x) = \sum_I N_I(x)c_I\phi(x) \tag{3.16}$$

The basic premise of the XFEM is an extension of the FEM to allow the incorporation of the discontinuity into the finite element method. This gives rise to its name as the Extended Finite Element Method.

3.4.2 Calculation of the Discontinuous Displacement Field

In order to allow this inclusion, three main conditions are required, the magnitude of the discontinuity, i.e. the displacement step change across the crack faces, the location of the discontinuity and the crack initiation and propagation criteria. The magnitude of the discontinuity can be determined using cohesive zone modelling or the virtual

crack closure technique (VCCT) in linear elastic fracture mechanics, the location is determined by the level set method (LSM) and the initiation and propagation criteria are predefined by the user. These conditions are incorporated into the XFEM technique through the inclusion of enrichment terms within the displacement field. The addition of these terms allows the accurate description of a complex displacement field such as one containing a discontinuity. The displacement function, u^h, can then be described as:

$$u^h = \sum_I N_I(x)u_I + \psi(x) \tag{3.17}$$

where, N_I is the shape function of a standard finite element, u_I is the standard degree of freedom at the element node and $\psi(x)$ is the enrichment term used to calculate the unknown and complex displacement field. Through the partition of unity as introduced by Melenk and Babuska, which states that $\Sigma_I N_I(x) = 1$, Belytschko and Black [84] further developed this to:

$$u^h = \sum_I N_I(x)u_I + \sum_J N_J(x)\phi(x)q_J \tag{3.18}$$

The term, $\Sigma_I N_I(x)u_I$ is the standard finite element approximation, and the term $\Sigma_J N_J(x)\phi(x)q_J$ is the enrichment term approximation, where q_J are the degrees of freedom at the original element node which act as a scaling factor of the enrichment term in order to achieve the most accurate approximation of the displacement field. For convenience, this term is defined as the enrichment shape function and is denoted $\psi_J(x) = N_J(x)\phi(x)$, thus further simplifying the displacement function to:

$$u^h = \sum_I N_I(x)u_I + \sum_J \psi_J(x)q_J \tag{3.19}$$

This allows the enrichment shape function to represent the discontinuity separately from the standard finite element solution, meaning that the discontinuity can be described completely independently of the element mesh. This gives the extended finite element method a unique advantage over the standard finite element method for the modelling of discontinuous problems such as cracks, voids and interfaces.

3.4.3 Heaviside Function

During crack propagation in the XFEM analysis, this enrichment shape function is further split into two sub-components, the Heaviside enrichment term and the crack tip enrichment term. The displacement function then becomes:

$$u^h = \sum_I N_I(x) \left[u_I + H(x)a_I + \sum_{\alpha=1}^{4} F_\alpha(x) b_I^\alpha \right] \tag{3.20}$$

where $H(x)a_I$ is the Heaviside term and $\Sigma_{\alpha=1}^{4} F_\alpha(x) b_I^\alpha$ is the crack tip enrichment term. This function now allows the description of all elements, including those affected by the discontinuity. As described above, the $N_I(x)u_I$ term applies to all nodes in the model, the Heaviside term, $H(x)a_I$ applies to the nodes whose shape function is split by the crack interior, and the crack tip enrichment term applies to nodes whose shape function is split by the crack tip. This allows localised enrichment around the crack and crack tip.

3.4.4 Level Set Method

The displacement functions described above allow a description of the crack, however, it does not determine the location of the crack. This is achieved with the use of the Level Set Method (LSM), which together with the displacement function, fully describe the crack propagation behaviour by defining the geometrical features of the discontinuity and the movement of the discontinuity through a fixed mesh. Two level set functions define the complete crack geometry, one defines the crack face and the other the crack front. A level set function in the spatial and time domain, $f(x(t), t)$ is used to define the discontinuity in a mesh independent manner. During the computational analysis, this function must always satisfy the zero condition for points on the crack, such that:

$$f(x(t), t) = 0 \tag{3.21}$$

A dataset, $\gamma(t)$ is then created containing the points that satisfy this condition. The nodal value of all remaining nodes is calculated and then compared to this function. Each nodal value indicates the distance of the node from the crack face, where a positive

value corresponds to one side of the crack face, a negative value to the other and a zero value at the crack face. This function can describe the crack faces, however, another level set function is required to define the moving crack tip which is defined as:

$$g(x(t), t) \tag{3.22}$$

This was defined by Stolarska et al [88] as a function of position and velocity so that:

$$g_i = (x - x_i)\frac{\nu_i}{\|\nu_i\|} \tag{3.23}$$

where x_i is a known position and ν_i is the moving velocity of the crack tip. For a straight line crack, this function will equate to zero so that $g_i = 0$. This can be illustrated pictorially as shown in Figure 3.3 for the two-dimensional propagating crack surface, Γ_c^0.

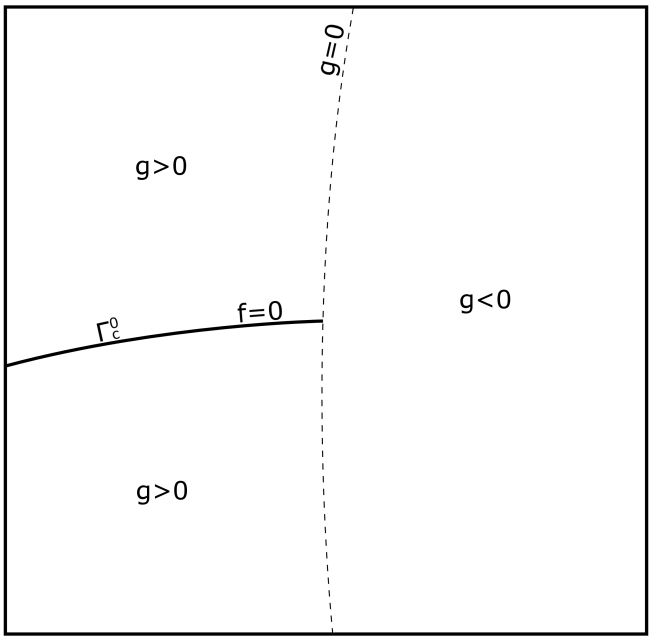

Figure 3.3: Diagram showing Level Set function values relative to a propagating crack

These level set functions can be calculated with the increasing time increment, $n + 1$, allowing a description of the propagation path of the crack, f^{n+1} and g_i^{n+1}. For example, if a crack is stationary during the time step, then,

$$f^{n+1} = f^n \tag{3.24}$$

or for a small propagation, then,

$$f^{n+1} = \pm \left\| (x - x_i) \frac{\nu_i}{\|\nu_i\|} \right\| \tag{3.25}$$

and,

$$g_i^{n+1} = g_i^n - \Delta t \|\nu_i^n\| \tag{3.26}$$

These functions then allow the precise and complete description of an evolving discontinuity and can be conducted entirely independently of the element mesh.

3.4.5 Computational Implementation

The XFEM concept is implemented into computational analysis through Hansbo and Hansbo's theory of the superimposed element formulation [89] and the method for crack propagation with the use of phantom nodes developed by Song et al [90]. This allows a convenient implementation of the XFEM technique into the traditional Finite Element framework in modern software packages such as ABAQUS and ANSYS. When a structure fractures, new crack faces are created; in order to be able to model this within the traditional FE framework, new nodes would need to be generated in order to allow the creation of new elements along the crack faces. Within computational XFEM, this is achieved with the introduction of phantom nodes. In the enriched region containing the discontinuity, these phantom nodes are implemented into the finite element mesh. Although not genuine FE nodes, this has the effect of duplicating all the nodes in the crack region, allowing new elements to be created as a crack propagates. Without this modification, the number of nodes would not be conserved during propagation. The phantom nodes are distributed evenly across the face of the discontinuity and so the original nodes on the upper face are paired with phantom nodes on the lower face, which are removed when the crack opens, in order to create a complete element. This simultaneously occurs on the other side of the crack face, where the original nodes from the lower face are paired with phantom nodes from the

top face. This allows the element to split into two whilst still maintaining its integrity. This is illustrated in Figure 3.4.

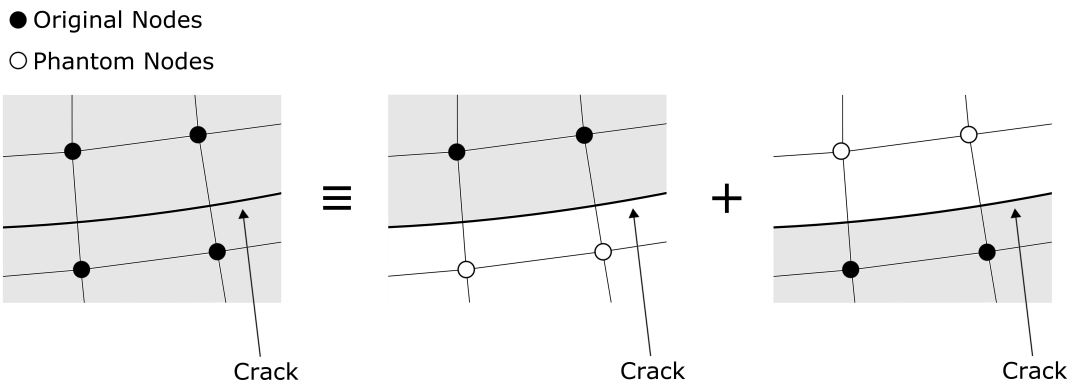

Figure 3.4: Diagram showing original and phantom nodes as a crack propagates

3.4.6 Advantages of the XFEM Technique

The key advantages of the eXtended Finite Element Method can be summarised as following:

1. XFEM is developed under the standard framework of FEM and retains all the advantages of the conventional FEM method
2. XFEM allows mesh independent modelling of a propagating crack
3. The XFEM technique allows crack initiation and propagation within the element boundaries, meaning that structured meshes can be implemented for the modelling of complex geometry cracks, significantly reducing the computational cost
4. The crack can propagate throughout the model without the need for adaptive remeshing as the simulation progresses
5. The elements containing crack faces are enriched with additional degrees of freedom, allowing the shape function to accurately calculate the stress field at the crack tip, permitting an accurate solution to be obtained even with a coarse mesh
6. XFEM has been incorporated into commercial finite element software packages

allowing very convenient implementation of the technique even for the most complex applications

3.4.7 Limitations with the XFEM Technique

Despite the strengths of the XFEM technique, the technique is still in relative infancy, having only been developed in the 1990s and it still has a number of limitations, which are summarised below:

1. The power of XFEM is its ability to predict its own crack path. However, this is less suitable for cases where crack path is determined a priori such as debonding or delamination which follows a predefined path. For such a case, other techniques such as the virtual crack closure technique (VCCT) are considered more appropriate

2. XFEM is only capable of modelling a single crack within a component. Crack branching or modelling of multiple cracks is not currently supported

3. Extensive fracture material properties are required for an accurate simulation and these are not always readily available, thus reducing its viability for use in an industrial application

4. XFEM cannot currently calculate contour integrals for propagating cracks

These limitations may make XFEM currently less suitable for an industrial application where existing and more well established methods are preferred. Despite this however, XFEM is still undergoing extensive development and successive new versions of ABAQUS, and other FE codes, often include progressive enhancements as new concepts are developed. These advancements will continue to make the XFEM technique more appropriate for extensive use for fracture mechanics within industry and academia.

3.4.8 XFEM Example

In order to better demonstrate the XFEM technique, a simple example is performed on a holed plate subject to a uniaxial tension as outlined below. Within ABAQUS CAE, a half plate of length of 100mm, width of 50mm and centre hole diameter of

20mm is modelled and subjected to a uniaxial tension at one end, whilst the opposite end is constrained as illustrated in Figure 3.5. Symmetry boundary conditions are applied to the left side edge to simulate the entire plate. A mild steel is modelled with a Youngs Modulus of 200GPa, Poissons ratio of 0.3 and yield stress of 200MPa. For the fracture analysis, a number of additional damage conditions can be set based on the induced stresses or strains. In this example, a maximum principal stress damage criteria is implemented that dictates that crack initiation will occur when the induced stress reaches the specified critical value.

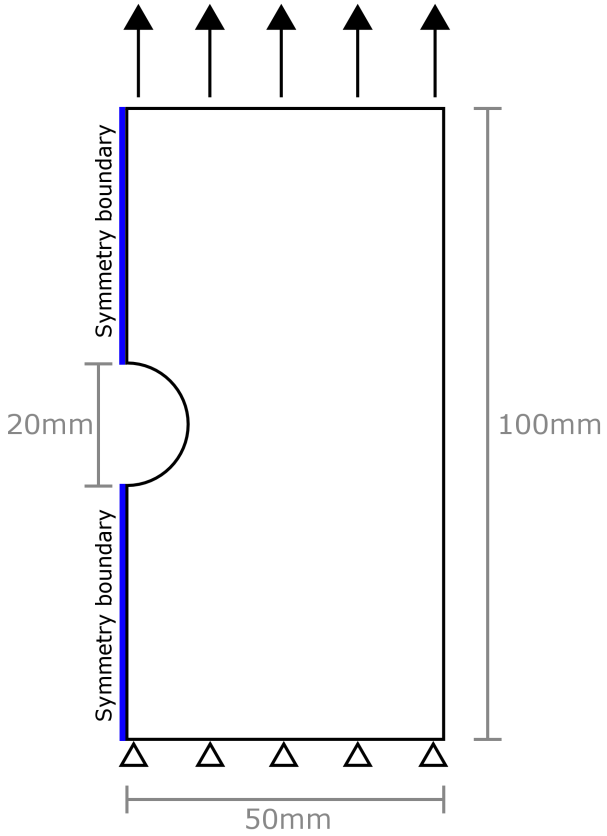

Figure 3.5: Diagram showing XFEM model geometry

During the XFEM analysis, the crack initiation and propagation are modelled according to the specified criteria. As soon as the induced stress reaches the damage criteria, the crack initiates and propagates along an arbitrary, solution dependent path throughout the specimen until ultimate fracture occurs. Figure 3.6 is a snapshot taken

during the crack propagation which clearly shows the crack does not adhere to the element boundaries and is contained within the elements. This is one of the main strengths of XFEM.

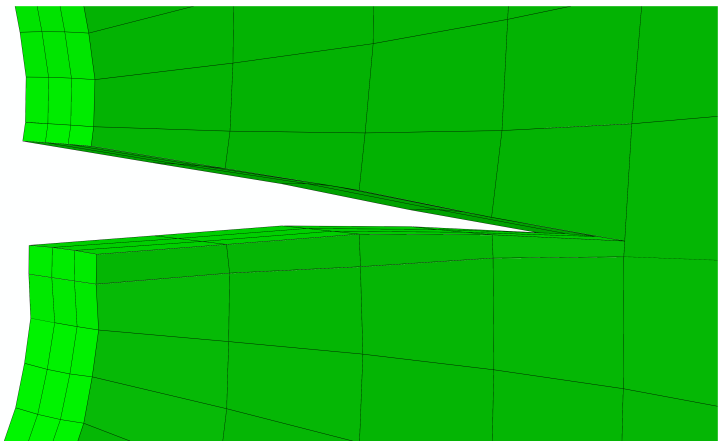

Figure 3.6: Image showing XFEM crack propagating through an element

Figure 3.7 shows a series of images that clearly demonstrate the crack propagation with increasing time, starting from crack initiation at the point of highest stress and propagating throughout the specimen.

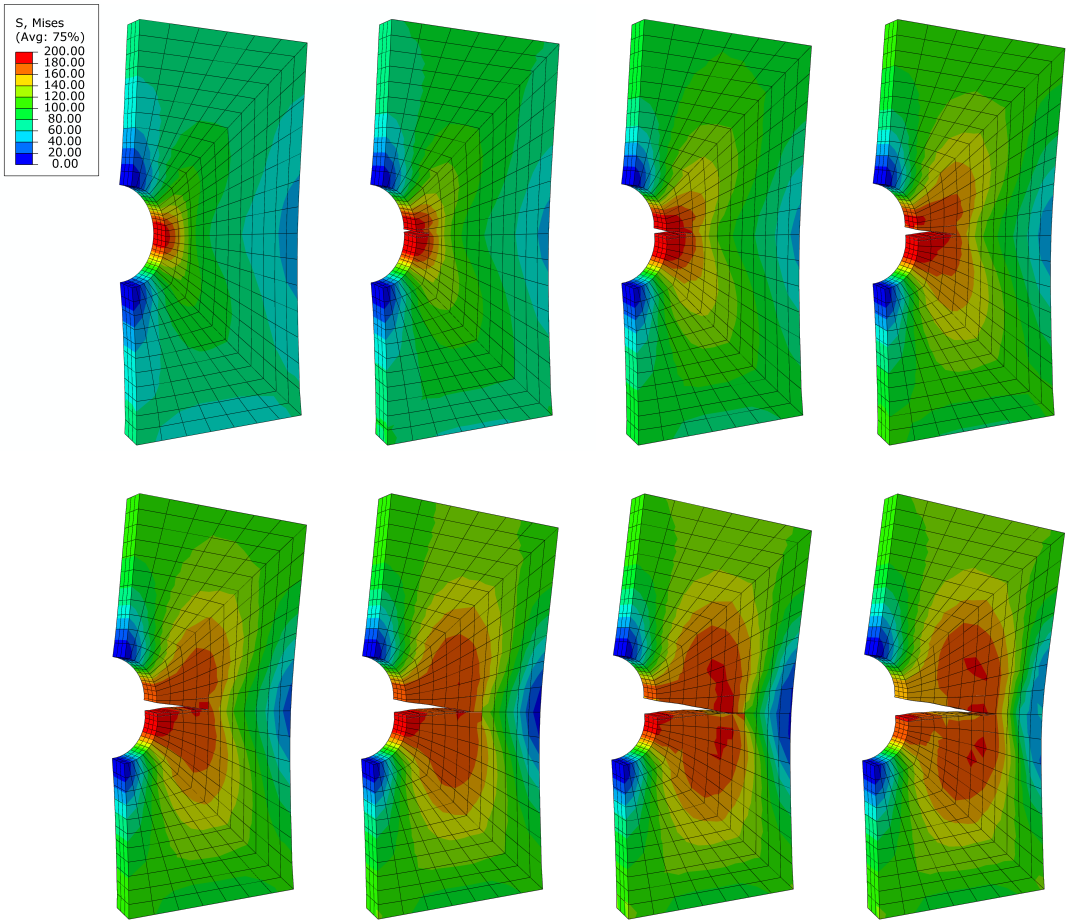

Figure 3.7: Series of images showing the propagation of the crack with increasing time

Figure 3.8 shows a contour plot of the Phi level set method surrounding the crack which identifies the location of the crack relative to the nodes of the finite element mesh. The contour shading indicates the proximity of the crack front to the mesh with orange and red meaning close proximity whilst blue means that the crack face is further from the boundary. In addition, numerical values of the PhiLSM are printed at the node locations, further indicating the proximity of the node to the crack, with values tending to 0 as the crack approaches the node. This is a valuable output which clearly displays the location of the crack faces.

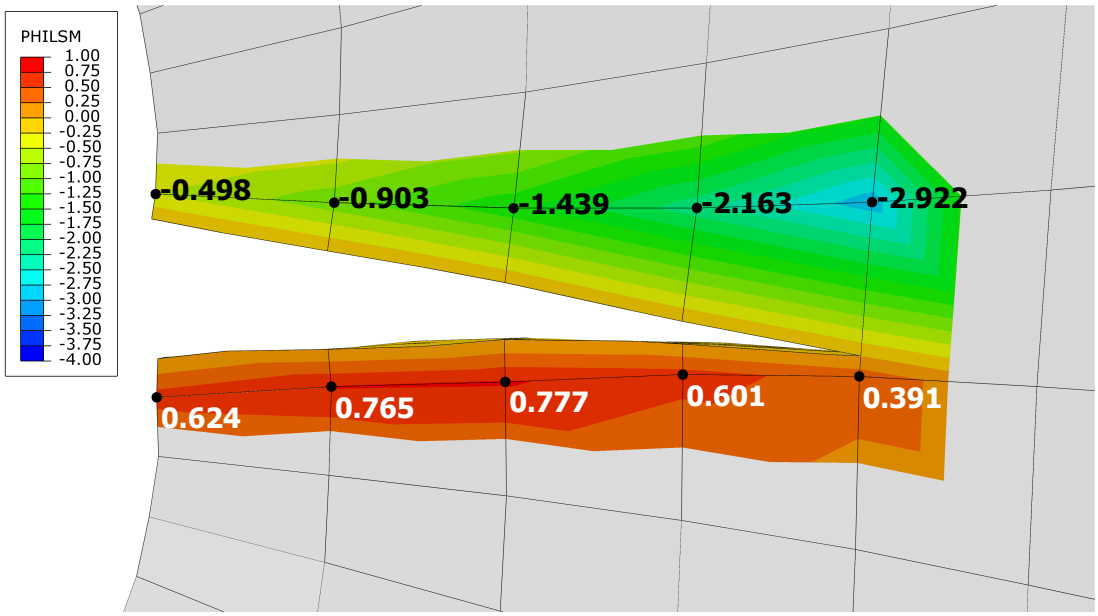

Figure 3.8: Phi Level Set Method at nodes surrounding the crack tip

3.4.9 Practical XFEM Example

Building on the successful demonstration of the XFEM technique on a simple geometry, it is important to apply the technique to a more complex application to assess its viability for use in the structural analysis of real industrial engineering components. This example demonstrates the application of XFEM to a practical application of a gas turbine blade. The complexity is greatly increased relative to the previous example of a holed plate by the presence of complex geometrical features, the inclusion of curved surfaces and the lack of specific stress raising features such as notches or pre-assigned cracks. This means that the most likely location of crack initiation is difficult to predict, unlike the previous example in which the location could more easily be predicted to occur at the edge of the centre hole. These features are more akin to those of complex industrial applications and so this case provides a more thorough benchmark test for the capabilities of the XFEM technique.

The blade is modelled using a representative nickel-based superalloy subject to centrifugal loading at 3600rpm as well as pressure forces acting on the leading edge of the blade. No advanced analysis is included here and instead, this example is used to demonstrate the model complexity that can be incorporated into the XFEM technique.

Figure 3.9 includes a series of images showing the propagation of a crack throughout the blade. The crack can be seen to initiate from the point of highest stress on the leading edge of the blade which then propagates across the width of the blade before ultimate failure occurs.

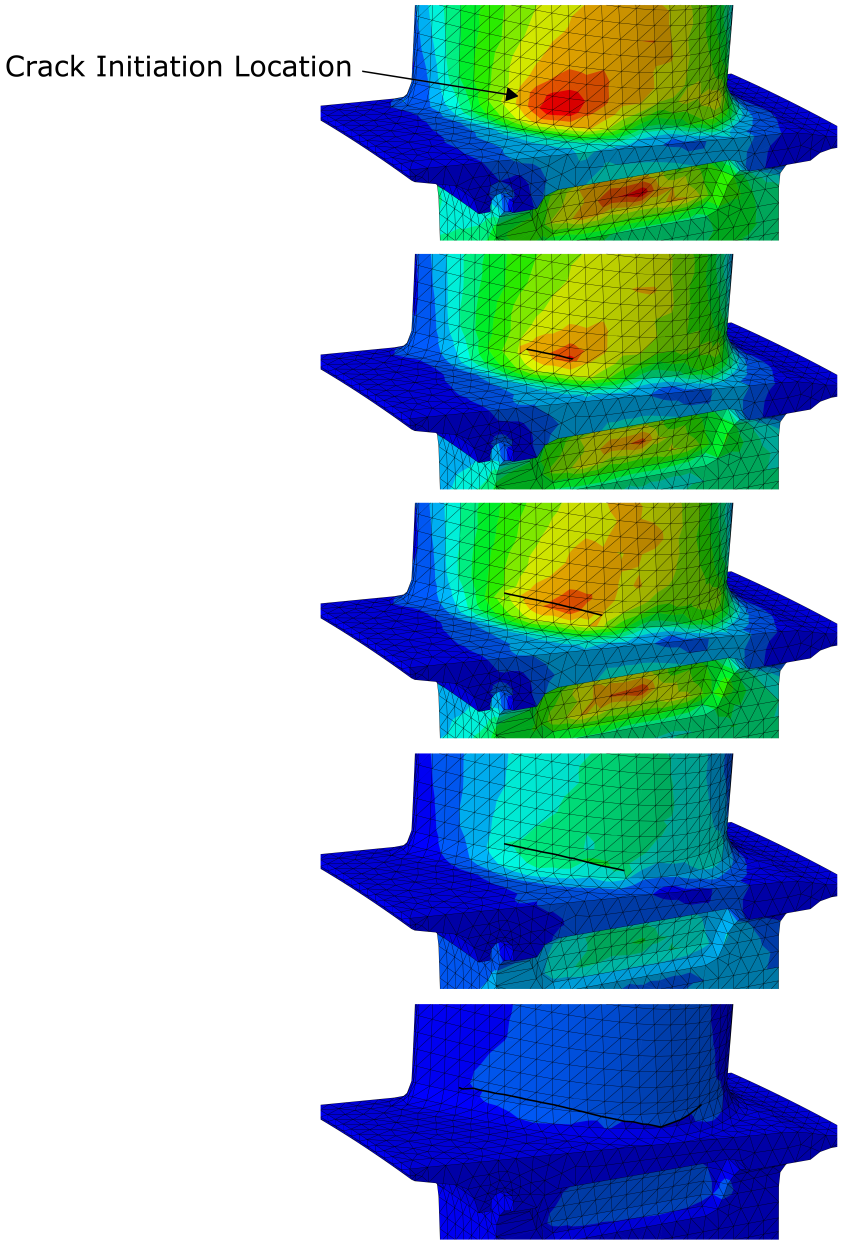

Figure 3.9: Series of images showing the propagation of the XFEM crack through a turbine blade

3.4.10 Method Summary

This example has clearly highlighted the power of XFEM for complex applications, but due to its relative infancy and the current limitations of the technique, its use in industry is not commonplace. However, the global interest in XFEM is driving its continued development and it shows a great deal of potential for regular use in the future within industry and academia for the structural integrity of complex engineering structures.

3.5 The Cyclic Response of Structures

Chapter 2 introduced the fatigue failure mechanism and the damage that can occur under a cyclic loading history. However, it is not always this simple and the situation can become much more complex, with the magnitude of the loads having a significant effect on the type of damage that occurs. It is therefore vitally important to gain a thorough understanding of each of these mechanisms and the load at which they occur.

With increasing applied loads, a material can exhibit a range of behaviours including purely elastic behaviour, elastic shakedown, reversed plasticity and low cycle fatigue, ratchetting followed by incremental collapse and ultimately, instantaneous collapse. If a cyclic load that is less than the yield limit is applied to a specimen, then the material will exhibit purely elastic behaviour and no damage will occur. If the applied load is greater than the yield limit, but less than a critical value known as the shakedown limit, then some plastic deformation occurs but after a certain number of cycles, no further damage accumulates and the response shakes down to purely elastic behaviour but in the presence of some residual stress [91]. At loads above the shakedown limit, but less than another critical value, the ratchet limit, reversed plasticity occurs in which a small amount of incremental plastic deformation occurs within the first few repeated cycles before reaching a stabilised response, at which point, the material shakes down to form a closed hysteresis loop. In this steady-state response, yielding occurs during each cycle, however, no further incremental plastic strain occurs. Crack initiation will occur when the material is subject to loads within this range and as a result, this region is associated with low cycle fatigue where the number of cycles to failure is determined by

the plastic strain range [92]. Above the ratchet limit, the plastic strain incrementally accumulates during each repeated loading cycle. This response is known as ratchetting and will lead to ultimate failure if the cycled load range is maintained [93]. Finally, instantaneous collapse will occur if the applied load is sufficiently large to cause failure in a single loading step.

These different damage mechanisms are commonly presented and visualised on the Bree Interaction Diagram [94–96]. This is an efficient tool that plots the primary and secondary stress ranges, and displays the elastic, plastic cyclic, shakedown and ratchetting behaviour regions and the boundaries between them. This was originally developed to address a very simple example problem of a thin walled cylinder, but this methodology is also applicable to more complex specimens. Each of these regions will exhibit different damage mechanisms with their own unique stress-strain responses.

Each failure mechanism can be better understood by studying the induced stress-strain response. These are illustrated within each respective region of the schematic Bree Interaction diagram as shown in Figure 3.10. This shows the typical responses that can be obtained at varying uniaxial loads, however, the precise response of different materials or specimens may vary. The x-axis represents a static load, whilst the y-axis represents a cyclic load and so different combinations of x and y coordinates demonstrate the response at different loading R-ratios.

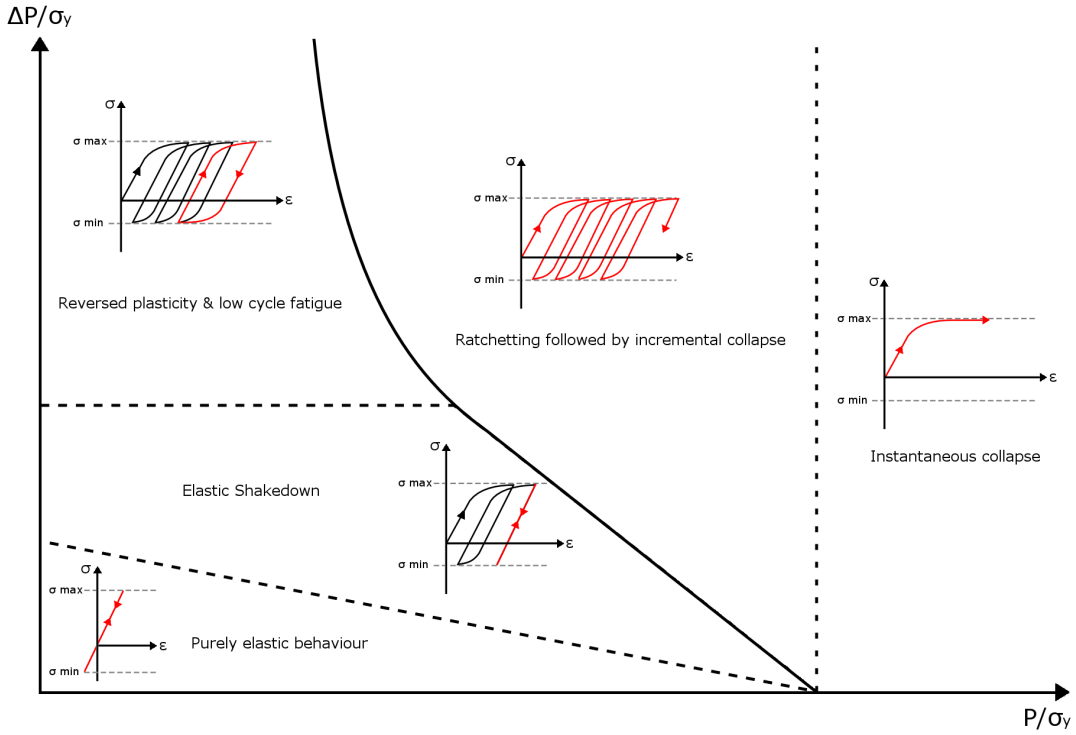

Figure 3.10: Bree interaction diagram showing typical stress-strain responses at each region

3.6 Step-by-Step Analysis

The analysis of the steady state response of engineering structures provides invaluable information about the integrity of components when subject to cyclic loading. Few analytical methods exist for this type of investigation and numerical Finite Element modelling can provide much needed information. The steady state response of a structure can be calculated with the use of extensive FE modelling in which every cycle is simulated in a separate step of the analysis and this is referred to as a step-by-step analysis. This can generate high levels of accuracy, however, in order to achieve a steady state response, a large number of cycles are required and consequently, complete modelling in this way is very computationally expensive and time consuming. Although the increase in computing power in recent years has made this type of analysis more feasible, there are significant limitations for routine use. Whilst it is possible to manually determine the limit boundaries and thus determine the structural response with the use of this technique, it cannot directly predict the location of the limit boundaries and

can only indicate the type of structural response that occurs at a given load, whether it is instantaneous collapse, ratchetting, reversed plasticity or shakedown. Therefore, since the position of the boundaries is not known, the process is entirely trial and error and is incredibly time consuming and computationally intensive. Numerous analyses would need to be run and their strain history responses monitored. The user would then need to modify the applied loading and rerun the analysis, continually refining the position of the boundaries in an iterative manner. For this reason, this is clearly not a viable option for determining the location of the limit boundaries. However, it can provide a very useful method of verification if the position of the boundary is already known. Performing a small number of step-by-step analyses above and below the limit boundary lines and monitoring their strain response can verify the accuracy of the limits.

3.7 Direct Cyclic Analysis

In the conventional step-by-step approach to model a cyclic structural response, each individual cycle is simulated until a stabilised response is achieved which is very time consuming and computationally expensive. Direct cyclic analysis (DCA) methods are quasi-static analyses that model the stabilised cyclic response directly without the requirement to model the transition period and is achieved by iteratively performing a Fourier transform of non-linear material behaviour. This can provide an alternative method of determining the steady state shakedown and ratchet response of structures.

A key advantage of these techniques over step-by-step analyses is that full details of the entire load history are not required and instead, only the most dominant loads acting on the structure are needed. This leads to significantly reduced computational expense and analysis times, whilst still maintaining a comparable level of accuracy to step-by-step FE methods [97].

A number of different direct methods exist for the calculation of shakedown limits, including the Mathematical Programming Method [98], Nonlinear Superposition Method [99] and Repeated Elastic Methods [100]. The shakedown limits can also be determined through iterative methods such as those proposed by Casciaro and Garcea [101, 102].

3.8 The Linear Matching Method

The Linear Matching Method [103, 104] is a direct method for damage assessment and provides a numerical procedure for the calculation of the shakedown and ratchet limits [105]. It creates an approximation of a highly complex, non-linear material response through the modification of a series of linear elastic analyses.

The method comprises a number of steps; it begins by performing a linear elastic analysis, the LMM then modifies the modulus at each node in the structure so that the induced stress matches the yield stress of the material. An additional linear elastic analysis is then performed using these modified values of the modulus. This causes the stresses to redistribute throughout the structure and the process repeats iteratively, continually modifying the modulus until the stress throughout the structure redistributes to match that of an elastic-plastic material response. This series of elastic analyses mimics the response of a highly complex, inelastic solution in a very efficient and computationally inexpensive manner. This process of modifying the modulus to allow stress redistribution is illustrated in Figure 3.11 [106](p.9).

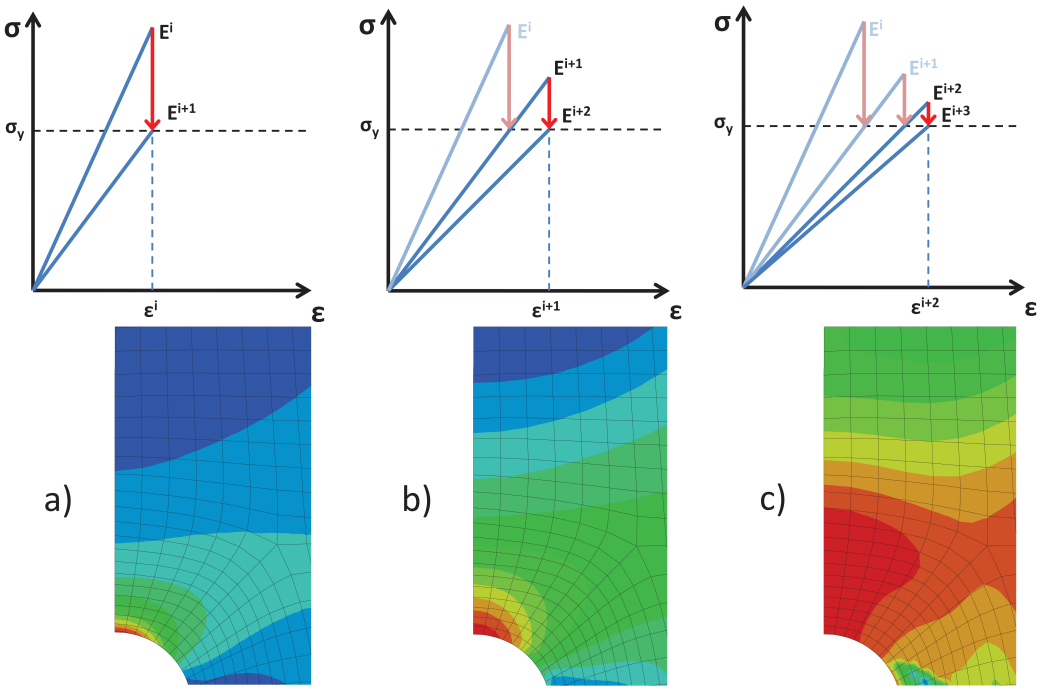

Figure 3.11: Modulus modification and stress redistribution during LMM analysis [106]

The LMM has far greater flexibility and versatility than the other currently existing methods, described above in Section 3.7 [107]. The LMM has two main unique features over other direct methods. Firstly, the equilibrium and compatibility are satisfied at each stage of the analysis and secondly, it has the capability of performing a detailed ratchet analysis [92, 108–111]. This ratchet procedure also calculates the plastic strain range, making it a viable method for the calculation of the low cycle fatigue life [112]. In addition, the LMM allows the incorporation of temperature dependent material properties and has recently been developed to allow for the inclusion of creep fatigue interaction [113]. The Linear Matching Method is operated within the commercial finite element package, ABAQUS [6], through the use of user subroutines. In recent years, the code has also been incorporated into an ABAQUS plugin with an ergonomic graphical user interface (GUI), greatly increasing the ease of use for the user [114–116]. Due to the power of the LMM, it has been part of the R5 research programme for a number of years [108, 110] and is routinely used by EDF for the structural analysis of many nuclear power plant components [117, 118]. However, despite the major advantages of the LMM, its use is not widespread and is still fairly uncommon outside of the work of EDF.

The Linear Matching Method, is capable of calculating the real stress range and strain range and is not based on an approximation as in the Neuber Correction Method. This provides a much more accurate method of life prediction. If a level of conservatism that is comparable to the Neuber Correction Method is required, a generous a safety margin can be manually applied. However, the increased accuracy in the life prediction greatly improves the efficiency and economic implications of engineering components, since a greater understanding of the fatigue life of the structure is gained.

3.9 Chapter Summary

This chapter has introduced some highly advanced computational techniques in the field of fracture mechanics. An explanation of the traditional finite element method was included and its use for modelling highly complex geometries was demonstrated through a turbine blade example. Next, the reference stress methods were introduced, their use for the calculation of the J-integral and cyclic J-integral was explained and the

limitations of the technique were highlighted. The eXtended Finite Element method was also presented, its fundamental theory was explained and its application demonstrated through two case studies. The limitations of the technique in its current state mean that it is not yet widely adopted, however this innovative technique shows a great deal of potential and with its continued development, it may become an invaluable component in routine structural integrity assessment in industrial applications in the future.

The response of structures to a cyclic loading history was then discussed and the different damage mechanisms that can occur depending on the applied load were explained. Different methods of determining these material responses were introduced, including the step-by-step analysis in which each cycle of the analysis is modelled until the system reaches a steady state. This is very computationally expensive and time consuming and cannot always conclusively determine the different mechanisms. Direct cyclic analysis methods offer a suitable alternative that model the steady state response directly, without the need to model the transition region. These methods significantly reduce the computational expense of the complete step-by-step analysis. The Linear Matching Method is such a direct method and its strengths over other existing methods clearly demonstrate its power for routine structural integrity assessment.

Part II

Core Research & Industrial Application

Chapter 4

Designing a Bespoke Industrial Test Specimen

Chapter Overview

This chapter describes the design process of a novel, bespoke industrial test specimen that was developed during a secondment at Siemens Industrial Turbomachinery Ltd. The requirement for the specimen is explained, the rationale behind the design is described and technical engineering drawings are included. The machining process for the manufacture of the test specimen is described and the encountered limitations and potential issues are discussed. A design issue resulting from these limitations in the machining process is investigated through a dimensional sensitivity study. Finally, an experimental inspection study is performed to ascertain the impact of the machining limitations. Based on the successful results and satisfactory outcomes of this study, the manufacture of the test specimen was authorised and allowed to proceed.

4.1 Introduction

The nozzle guide vanes (NGVs) of gas turbines are components of particular interest in this project. These are highly complex aerofoils in the stator component of the turbine that direct the hot gases from the combustors into the turbine, and as a result, undergo extreme thermal loading. The NGVs are often cast from nickel-based superalloys that have been specially tailored to suit such environments, with increased mechanical strength and resistance to thermal fatigue and creep deformation [119]. Despite the enhanced material properties of the superalloys used in gas turbines, the temperatures experienced during operation of the engine often exceed their melting points. In order to be able to work in these conditions without compromising their mechanical strength, cooling holes are incorporated into the design of the guide vane. These holes are critical in allowing internal airflow to cool components and prevent overheating during engine operation [120]. In addition, effective cooling improves the efficiency of the component, reducing fuel consumption and minimising the production of harmful emissions. The design and manufacture of the cooling holes must be exceedingly precise and they are considered a critical feature of the guide vane. A nozzle guide vane is shown in Figure 4.1 [121], showing the trailing edge (downstream side), with an enlarged view of the cooling holes.

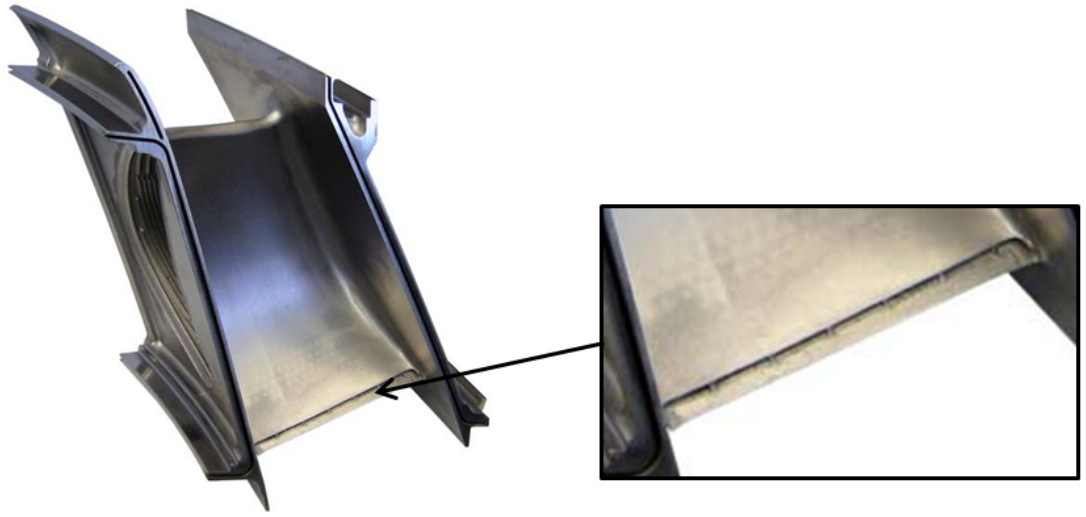

Figure 4.1: Nozzle guide vane with enlarged view of trailing edge [121]

These holes, although critical for the effective cooling of the NGV and protecting it from thermal loading, are inherently small with sharp corners, and as such introduce stress concentrations which can act as points of crack initiation.

Precise details of the geometry and complex stress distributions found in the NGVs cannot be disclosed due to the commercial sensitivity of this research at Siemens, however, a schematic diagram of such a component is shown in Figure 4.2 which illustrates the areas of stress concentrations. These can have a profound effect on the mechanical structural integrity of the component and thus must be carefully considered in the component design in order to allow a balance to be achieved between sufficient thermal and structural integrity during operation. For this reason, the design of these cooling holes is a widely investigated field and is of particular interest to Siemens Industrial Turbomachinery.

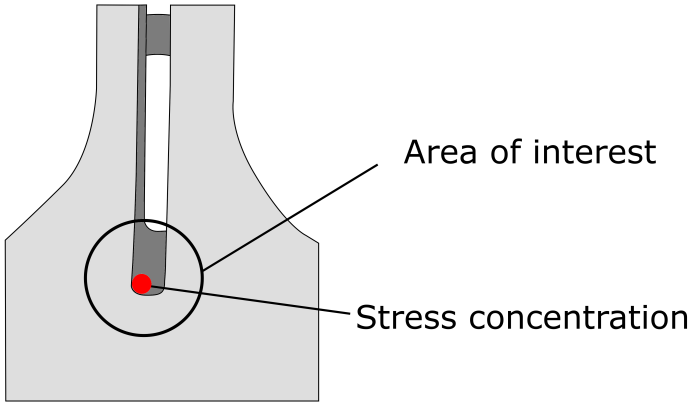

Figure 4.2: Nozzle guide vane trailing edge

4.2 Objectives

Due to the highly complex nature of the design of the cooling holes, extensive experimental testing is required in addition to finite element modelling to allow the most efficient design to be developed, optimally balancing the thermal and structural integrity requirements of the component. The nozzle guide vanes are exceedingly costly to manufacture due to the high level of precision involved, and therefore, direct experimental testing on the NGV is not viable. To this end, a test specimen is required that is representative of the nozzle guide vane trailing edge. The overarching aims

of this investigation are to gain a better understanding of the highly complex geometry of the NGV and the localised stress concentrations that are induced. This will be achieved through the design and experimental testing of a representative specimen which is sufficiently cheap and easy to manufacture for it to be a viable option.

4.3 Test Specimen Design

A complex notched specimen is designed that attempts to replicate the stress contours induced in the region of the cooling holes on the trailing edges of nozzle guide vanes, whilst still being cheap and simplistic enough to be a viable option for testing. The proposed design for this notch is a cylindrical specimen with scalloped edges and a chamfered through hole as shown in Figure 4.3.

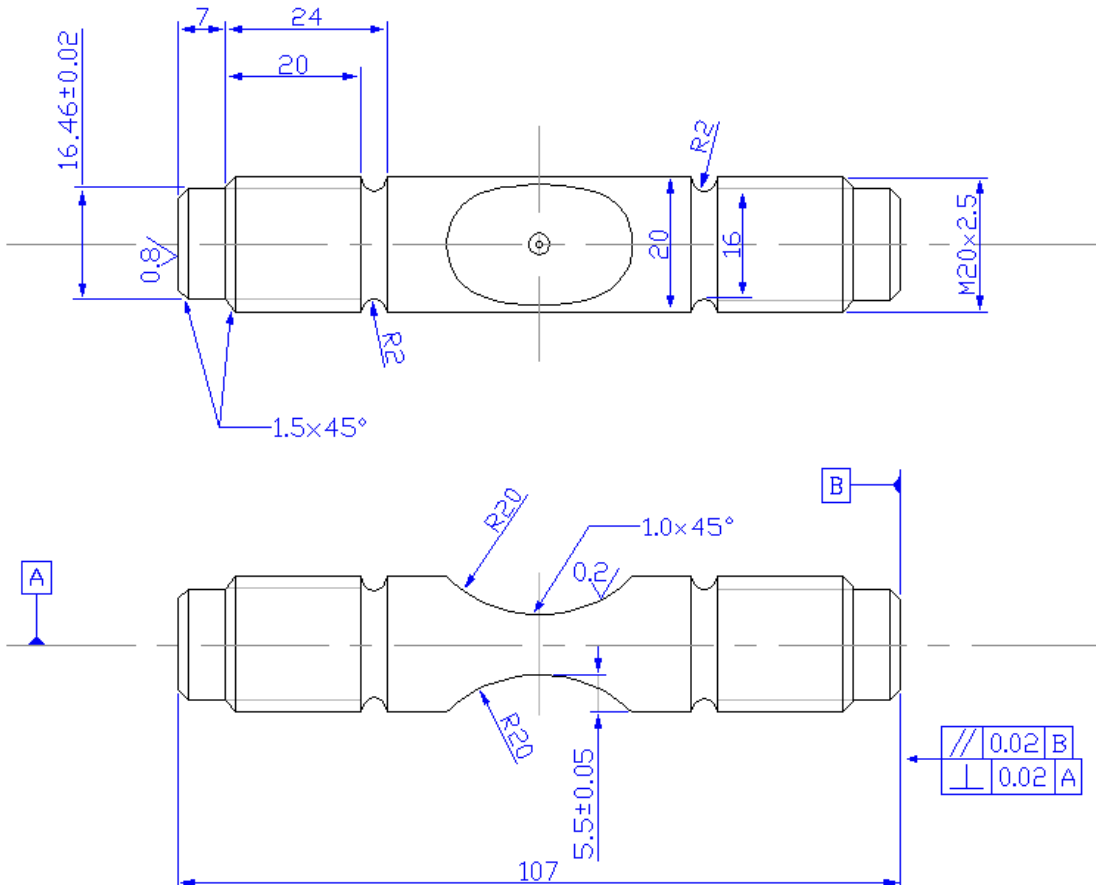

Figure 4.3: Proposed notch geometry

The specimen will be made from a suitable nickel-based superalloy, similar to those

used in industrial turbine applications. Initial finite element testing shows that the selected geometry introduces localised stress concentrations with homogeneous three-dimensional stress variation which is of a similar degree to that found in the NGVs as illustrated in Figure 4.2. The presence of the chamfer on the centre holes allows even propagation of the stresses throughout the specimen as shown in Figure 4.4. This geometry is considered to represent the trailing edge of the nozzle guide vanes as effectively as possible with such a relatively simple test specimen.

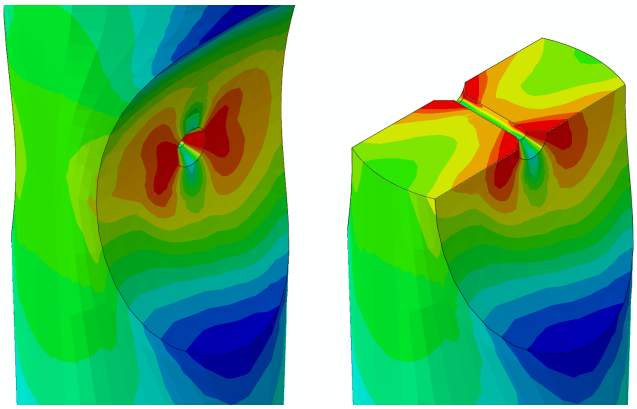

(a) (b)

Figure 4.4: Complex notch stress contours under uni-axial loading (a) complete model and (b) cross-section cut through

4.4 A Consideration of Material Properties - Nickel-Based Superalloys

Due to the extreme conditions experienced in a gas turbine, highly specialised materials must be used to ensure the components' structural integrity is maintained. Superalloys are such materials and offer suitable properties for enhanced structural integrity. Superalloys are a group of alloys that are developed to provide outstanding elevated temperature and corrosion resistance and as a result are widely used in the power, chemical and petrochemical industries.

Superalloys are commonly nickel-based, but the additional alloying elements vary widely, giving differing material characteristics. The chemical composition of nickel-based superalloys are carefully balanced with additions of a range of elements, but

principally comprise, cobalt, chromium, aluminium and titanium. The heat treatment and tempering processes used in their manufacture are also carefully controlled to ensure an optimum crystal structure for corrosion and heat resistance is obtained. This can include directional solidification or single crystal arrangements. Due to the difficulty in manufacturing processes, superalloys can be exceedingly expensive and so they are only used in the most extreme conditions where other, cheaper materials, are not suitable. Due to their enhanced properties including strength, hardness and temperature and corrosion resistance, machining such materials can pose potential problems and the use of some standard techniques for softer materials may not be possible. For this reason, advanced techniques may be required for the machining of complex geometries, further adding to the component cost.

4.5 Proposed Machining Technique

The proposed test specimen is manufactured according to the detailed engineering drawing shown in Figure 4.3. As discussed above, standard machining techniques are not suitable for precision machining of such highly complex superalloys and alternative specialist techniques are required. A commonly used technique for this level of precision machining is electrical discharge machining, EDM. This process is discussed in further detail in the following sections.

4.5.1 Electrical Discharge Machining

Electrical discharge machining (EDM) is a process in which material is cut by precisely controlled sparks between an electrode and the workpiece in the presence of a dielectric fluid. Electrical sparks are pulsed at very high frequencies, heating the workpiece to temperatures between $8000-12000\,^{\circ}\mathrm{C}$, causing the material to instantaneously vaporise at the point of spark contact. Deionised water is used as the dielectric fluid which continuously flows over the electrode, providing cooling and flushing of the removed material. This EDM process is illustrated by Jameson [122] in Figures 4.5 to 4.8.

EDM allows exceedingly fine tolerances to be achieved, providing the ability to machine highly complex shapes with a high level of precision. Since the erosion of the material is performed by the spark, the electrode and workpiece do not make contact,

eliminating the tool wear and allowing materials of any hardness to be machined by this method, provided that they are electrically conductive.

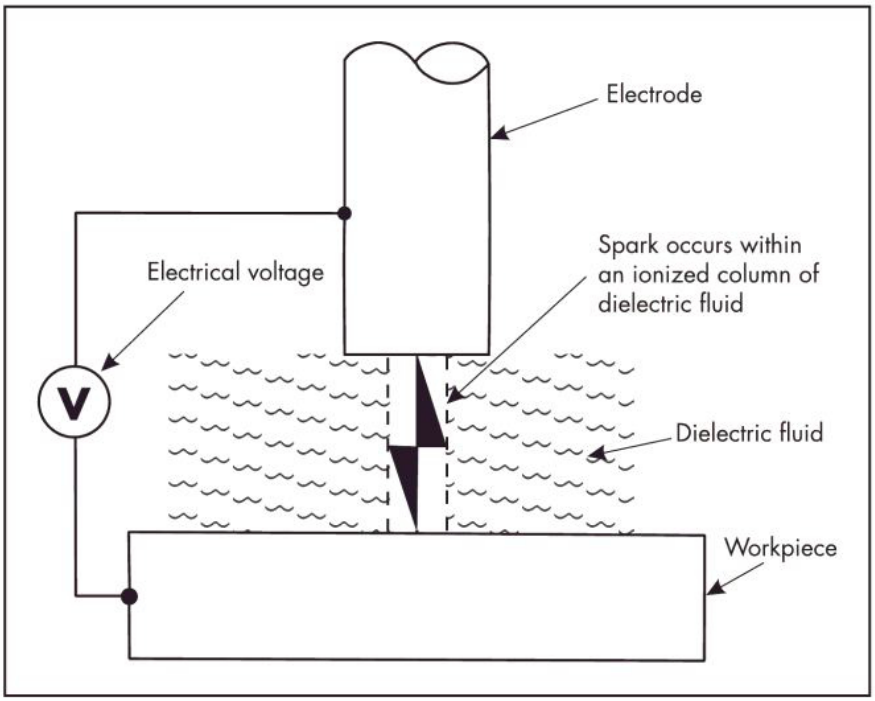

Figure 4.5: Spark occurs within a column of ionized dielectric fluid [122]

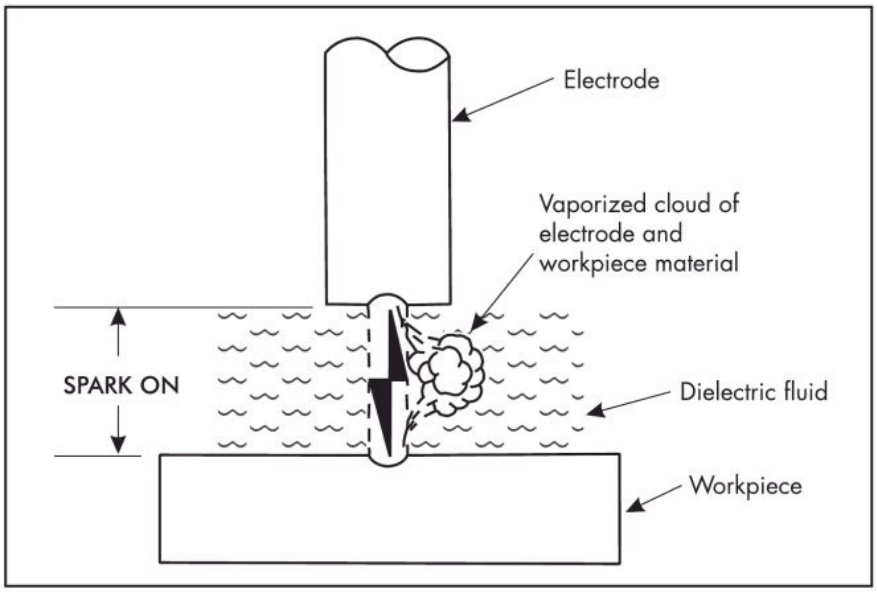

Figure 4.6: Spark ON: electrode and workpiece material vaporized [122]

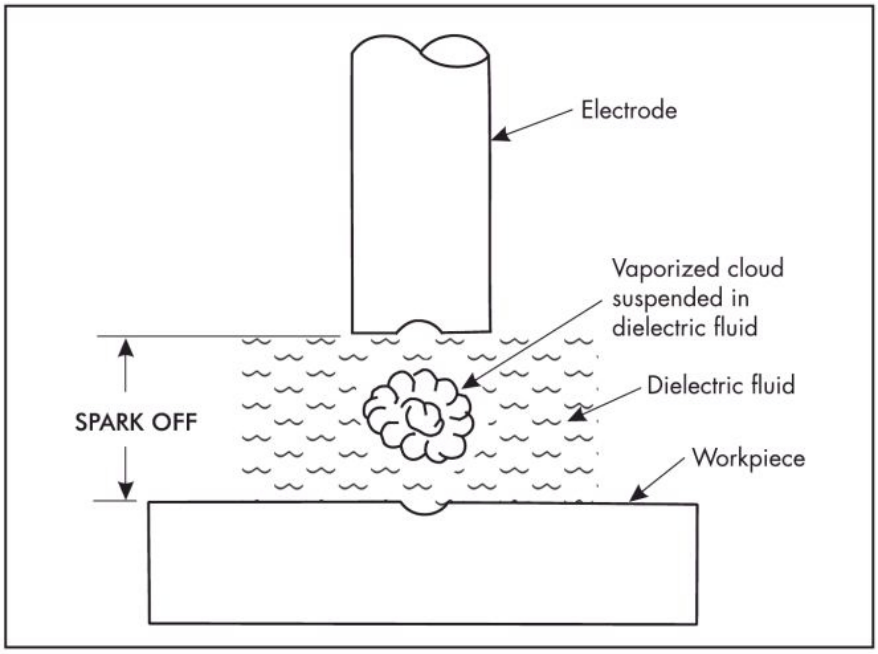

Figure 4.7: Spark OFF: vaporized cloud suspended in dielectric fluid [122]

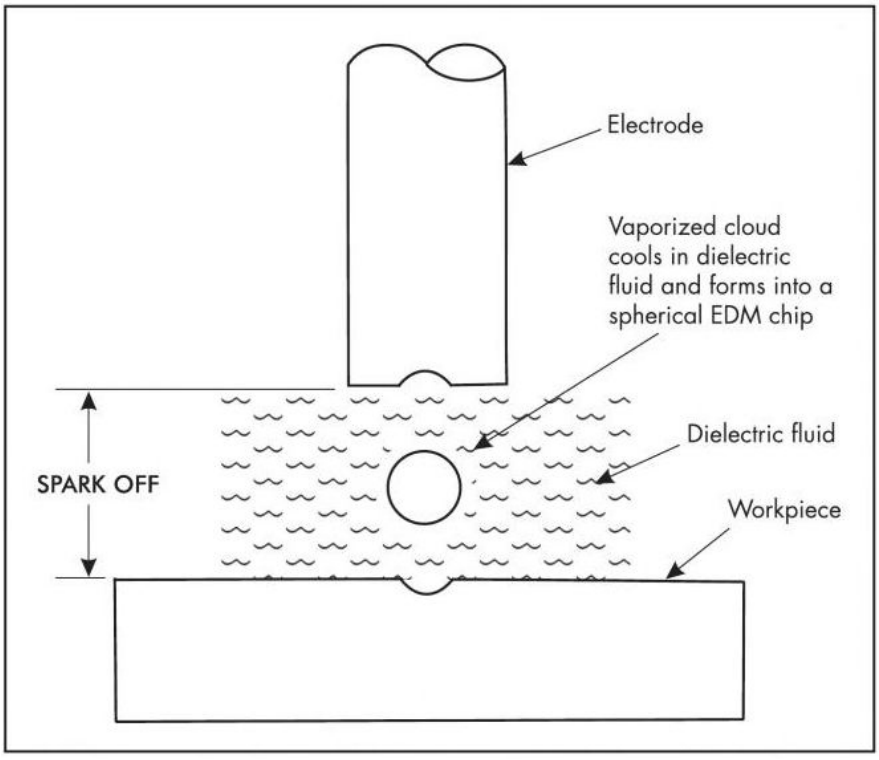

Figure 4.8: Spark OFF: vaporized cloud solidifies to form EDM chip [122]

Following electrical discharge machining, several surface layers can be observed on the material surrounding the machined regions. The top layer contains particles of expelled molten material that form spheres when they solidify and spatter the surface. These particles can be easily removed. The next layer is a recast layer where the intense heat involved in the EDM process has altered the metallurgical structure of the workpiece. This is an inevitable consequence of the process, however, it can be minimised through careful machining and by polishing the surface following machining. The next layer is a heat affected zone where the high temperature causes the metal to anneal. These layers are illustrated in Figure 4.9.

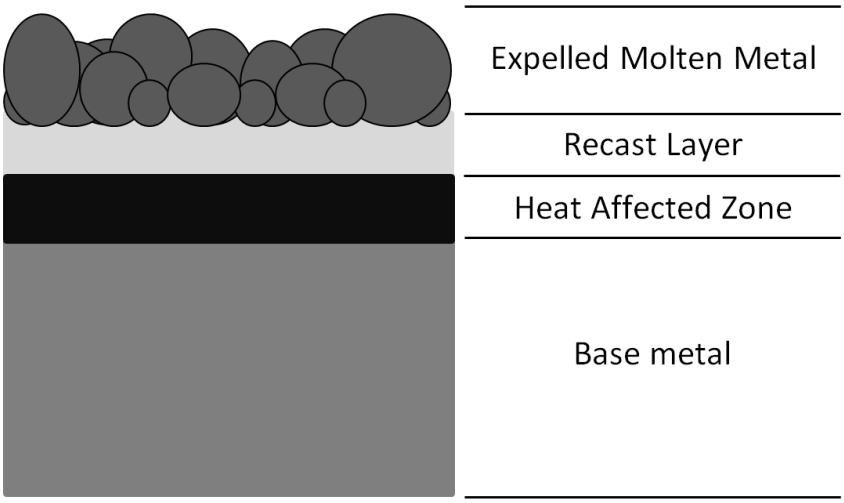

Figure 4.9: Observable surface layers formed during EDM process

The recast layer and heat affected zones can alter the mechanical properties and structural integrity of the component and so careful consideration must be made to assess whether the structural integrity has been compromised or the working fatigue life of the part has been affected.

4.6 Complex Notch Centre Hole Size Sensitivity Study

EDM is to be used as the processing technique for the production of the centre hole in the manufacture of the complex notch specimen. However, potential issues have been identified due to the small diameter of the hole. The machining process can introduce a recast layer which can alter the material properties in the critical regions

of the specimen, potentially impacting on the fatigue life and influencing the results obtained from experimental testing. The recast layer will be present to some degree in all EDM machining, however, there is a risk that since the hole diameter is so small, the recast layer thickness will be relatively very large compared to the dimensions of the hole, more greatly affecting the integrity of the component. In an attempt to address this issue, the use of a larger diameter hole is investigated. A centre hole diameter of 1mm was initially proposed as it provides similar dimensions to that of the nozzle guide vanes, which this test specimen is attempting to replicate and a larger hole may not provide such representative information. To determine whether the use of a larger hole could still accurately represent the stress concentrations of the NGV, a centre hole size sensitivity study is conducted. Finite element analyses are performed, modelling the specimen with a 1mm and 2.5mm diameter centre hole under a uniaxial tension of 300MPa. Contour plots of the induced stresses for each hole are shown in Figure 4.10 and 4.11. A front view facing the centre hole and a cross section cut through the centre line of the hole are shown in figures (a) and (b) respectively.

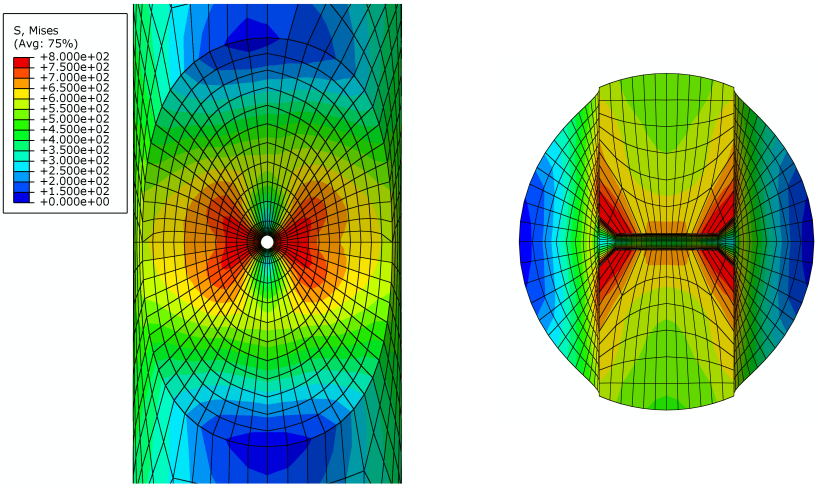

(a) (b)

Figure 4.10: Stress contour plot of specimen containing a 1mm hole (a) Front View (b) Cross Section View

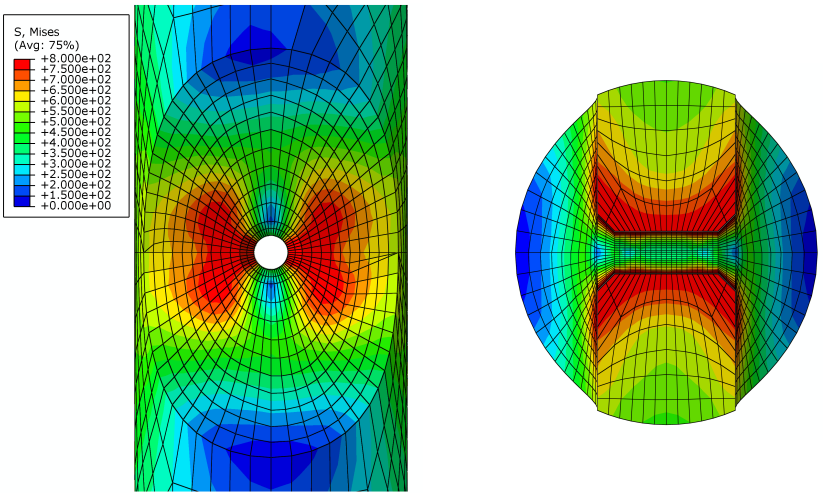

(a) (b)

Figure 4.11: Stress contour plot of specimen containing a 2.5mm hole (a) Front View (b) Cross Section View

In order to allow easier visualisation of the stress concentrations within the centre hole, contour plots are produced with a modified scale of 780-800MPa as shown in Figure 4.12. This more clearly shows the stress concentrations in the critical regions by removing all other regions of stresses less than 780MPa. In addition, the stress is plotted on a path along the through thickness direction of the hole as shown in Figure 4.13.

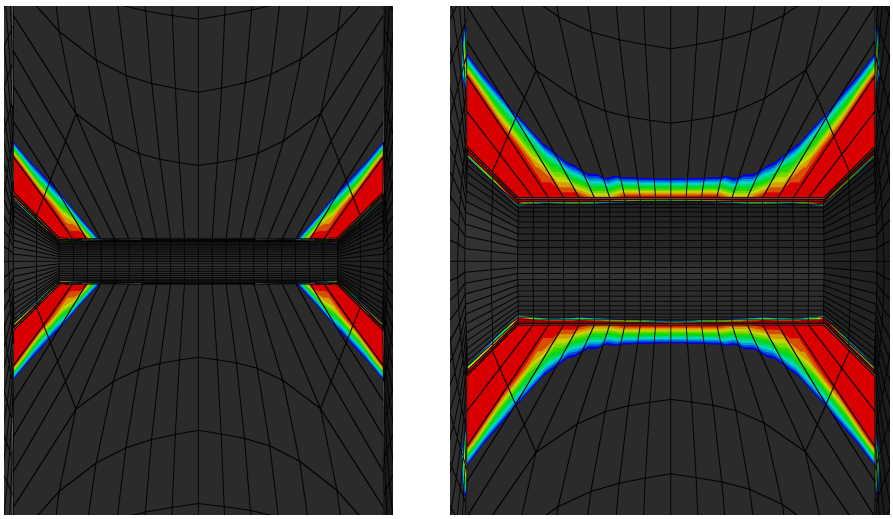

(a) (b)

Figure 4.12: 1mm & 2.5mm hole Stress Concentrations

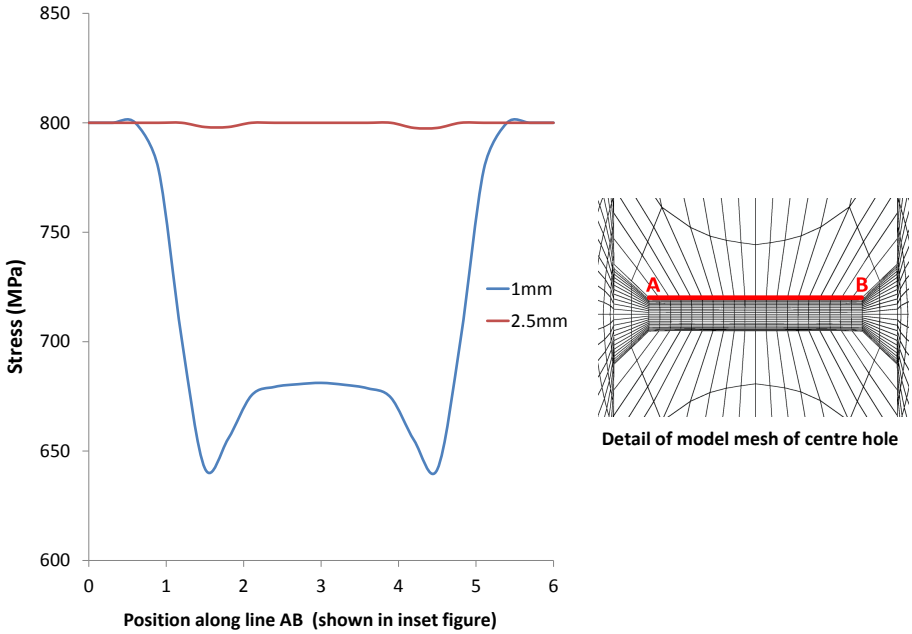

Figure 4.13: Von Mises stress distribution along through thickness direction of centre hole for 1mm and 2.5mm diameters

From these modified scale contour plots and the plot of stress distribution along the hole length, it can be seen that the 1mm hole has clear stress concentrations at the specimen faces. Whereas, with a 2.5mm hole, the stress concentrations are less localised with the peak stresses occurring along the entire length of the hole. It is apparent that increasing the size of the hole makes the stress gradient more uniform across the thickness of the specimen, removing the stress concentrations at the faces. This may less accurately represent the stress contours of the trailing edge of the nozzle guide vane. Therefore, a centre hole diameter of 1mm was chosen for the test specimen as it offered a balance between manufacturing practicality and representative stress concentrations. However, a trial specimen will be closely inspected to assess the presence and effect of any recast layer which could have significant influence on such a small hole.

4.7 Recast Layer Inspection

It has been determined that a 1mm centre hole is desirable and preferable to a larger diameter hole since it is more representative of the nozzle guide vane trailing edge cooling holes. It is understood that the recast layer induced by the electrical discharge

machining process can alter the metallurgical structure, potentially affecting the structural integrity of the component. For this reason, in order to assess the potential risk caused to the integrity of the specimen, the extent of formed recast layer must be inspected and compared to an established, in-house, company standard to determine whether the amount of recast is within tolerance. In order to assess the extent of any potential recast layer in this investigation, and to predict any effect it may have on the properties of the specimen, a trial specimen, containing two EDM machined holes of approximately 1mm diameter was manufactured, as shown in Figure 4.14. This trial specimen was closely inspected to determine whether the level of recast was within tolerance. Figure 4.15 shows projections of these holes taken using a Profile Projector, assessing the roundness of the holes.

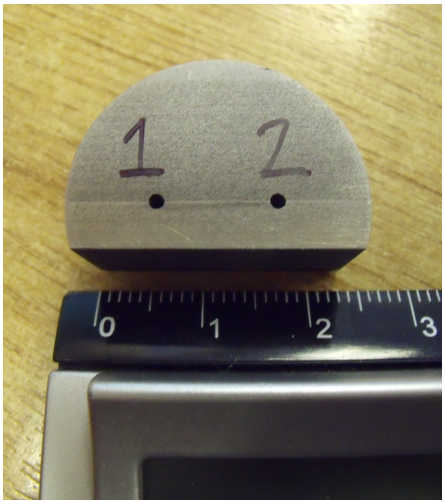

Figure 4.14: Sample Test Specimen

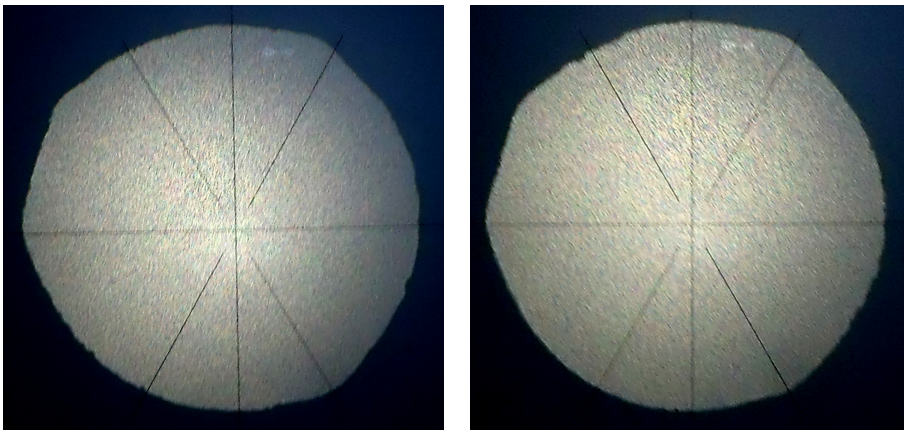

Figure 4.15: EDM Hole Profiles

4.7.1 Inspection and Results

The specimen was mounted in a plastic mould, ground and polished to 1 micron and etched in hydrofluoric acid. Etching causes corrosion to occur at the grain boundaries, making them more clearly visible in the optical inspection. The specimen was then inspected under an optical microscope to examine the presence of a recast layer. Figures 4.16, 4.17 and 4.18 show micrographs of the holes. The recast can be identified as a lighter coloured layer at the surfaces of the holes. A global image showing the entire surface of the hole with recast layer is shown in Figure 4.16. Figure 4.17 shows a point of average thickness of recast layer and locations with peak levels of recast layer are shown in Figure 4.18. These micrographs demonstrate minimal presence of the recast layer at the surfaces of the holes. A complete circumferential inspection of the holes found that the typical thickness of the recast layer varied between 0 and 5 µm with peak thicknesses in the region of 9 - 10 µm. The maximum observed thickness of recast layer was 10.99 µm.

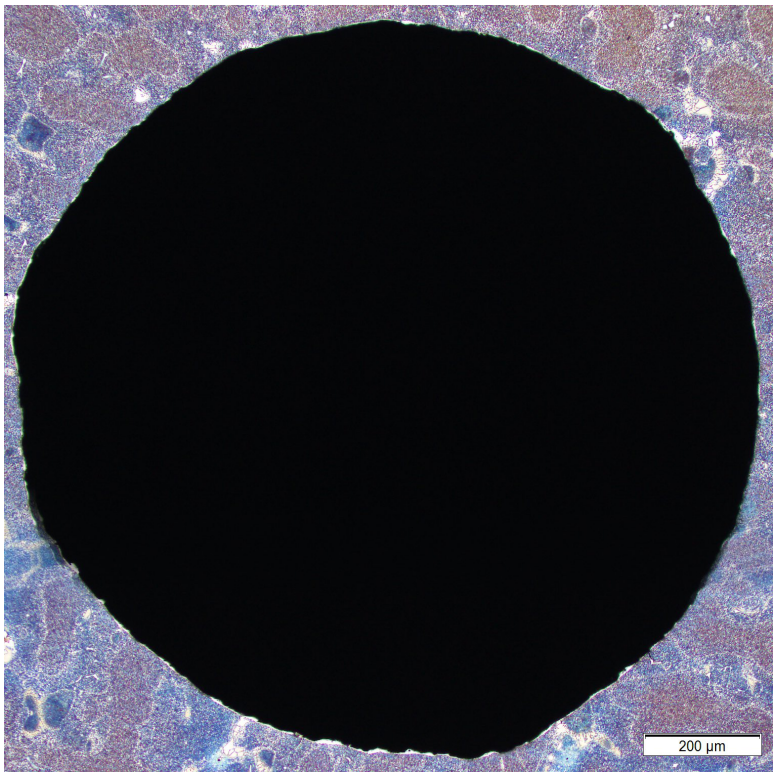

Figure 4.16: Micrograph showing global recast layer

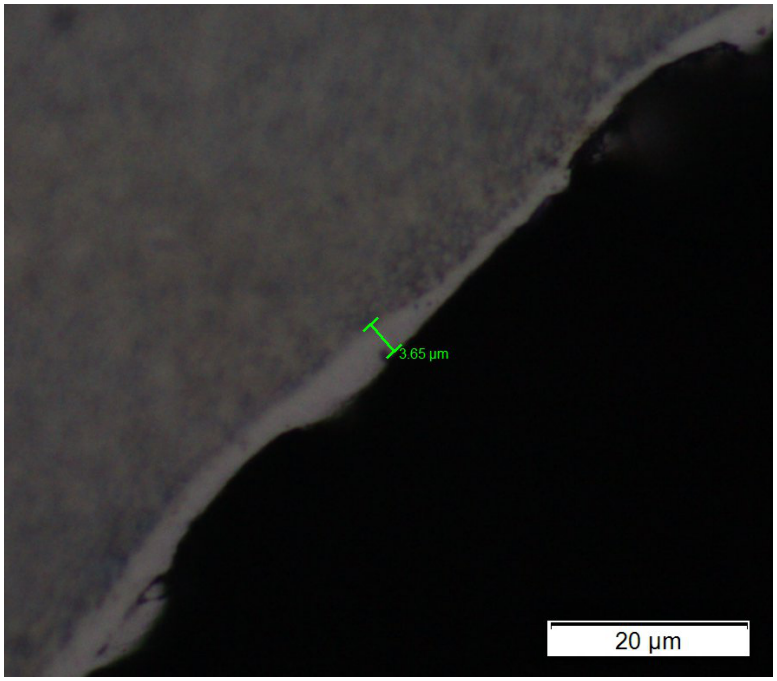

Figure 4.17: Micrograph showing typical levels of recast layer

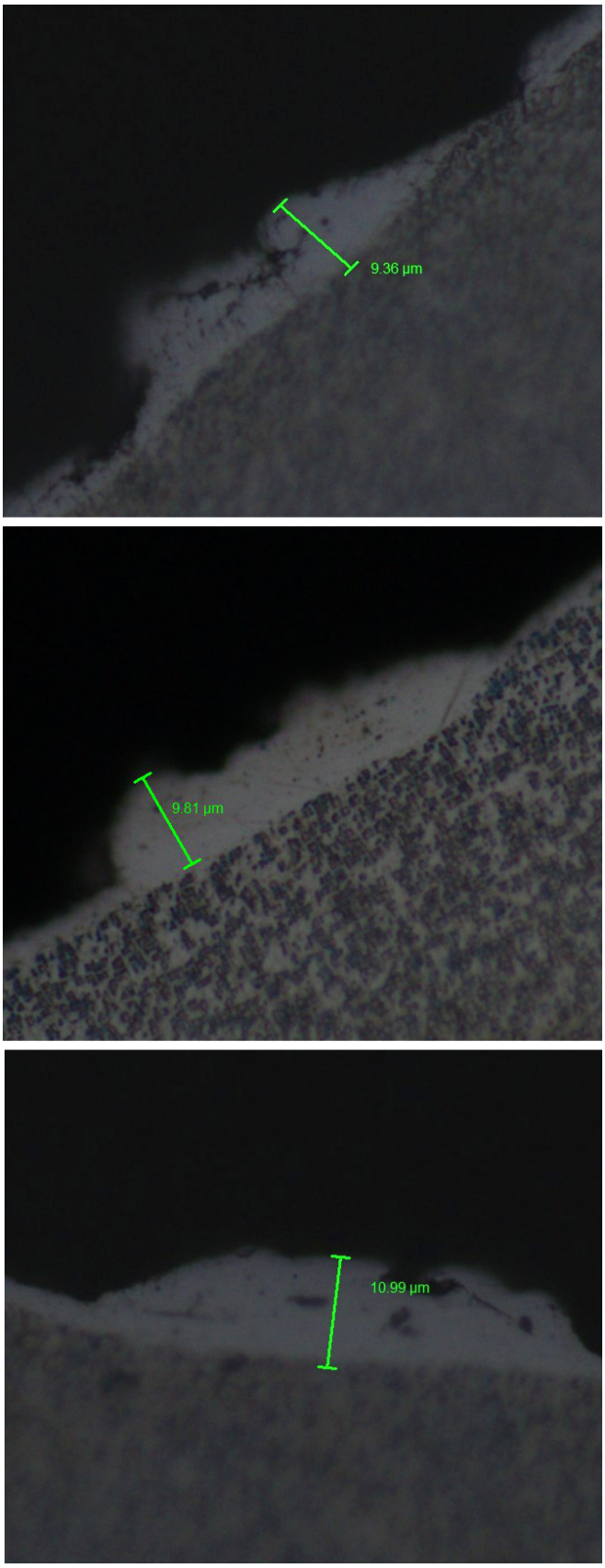

Figure 4.18: Micrographs showing maximum levels of recast layer

The levels of recast layer observed during the circumferential inspection were compared against an established Siemens company standard and were found to be far less than the maximum tolerable thickness. In addition, no cracking of the recast layers was observed. This specimen is therefore within tolerance and meets the requirements of the standard. This study has confirmed that EDM machining is a suitable manufacturing process for this specimen and is capable of producing a 1mm diameter centre hole without generating significant levels of recast layer, thus not adversely affecting the structural integrity of the component.

4.8 Test Specimen Manufacture

This work has confirmed that the original test specimen design is appropriate. The specimen was manufactured by a third party machinist using a nickel-based super alloy similar to those used in industrial gas turbines. The centre hole was machined using EDM as previously described. The scalloped edges were cut using a computerised numerical control (CNC) lathe with a single point cutter and the chamfer was machined using a centre drill following the electrical discharge machining of the centre hole. Images of the manufactured specimen are shown in Figure 4.19. Following manufacture of the specimen, the experimental testing programme could be finalised and this is the focus of the following chapter.

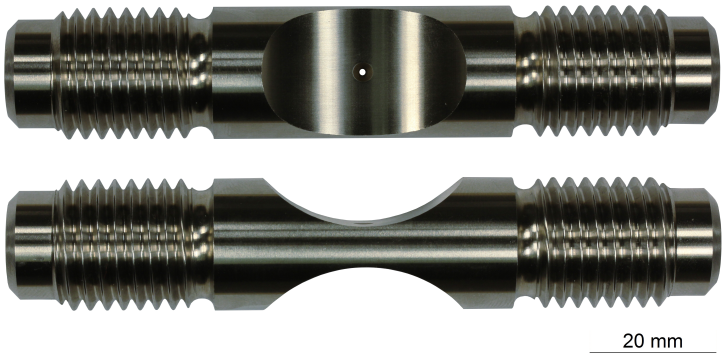

Figure 4.19: Manufactured test specimen

4.9 Chapter Summary

This investigation has described the design process of a highly complex, notched test specimen to be used by Siemens Industrial Turbomachinery Ltd that aims to represent the cooling holes of a gas turbine nozzle guide vane. Through successful design modifications based on finite element analyses, the test specimen was viewed as sufficiently representative of the NGVs, whilst being cheap and simple enough to manufacture to make it a viable option for experimental testing. Electrical discharge machining has been identified as an appropriate machining method to produce a 1mm diameter centre hole in the specimen. The induced recast layer has been highlighted as a potential issue with the EDM process and the necessary precautionary measures have been discussed. The smaller the centre hole, the greater the impact of the recast layer on the structural integrity of the component. To this end, a sensitivity study was performed on the diameter of the centre hole which determined that the larger hole was not as representative of the NGV trailing edge cooling holes and so the 1mm hole was deemed fundamental to the design. Following this, the impact of the induced recast layer was investigated through the close inspection of a sample piece that contained small diameter holes machined using EDM. The induced recast layer was closely inspected using an optical microscope and on comparison with an established company standard, was determined to be within tolerance and no cracking was found. This allowed the design of the test specimen to be authorised and subsequently manufactured.

Chapter 5

A Novel Simulation for the Design of a Low Cycle Fatigue Experimental Testing Programme

Note of publication

The work contained in the following chapter has been presented by Beesley et al in the peer reviewed Elsevier Journal of Computers and Structures [1].

Chapter Overview

This chapter proposes an innovative concept for the design of an experimental testing programme suitable for causing Low Cycle Fatigue crack initiation in a bespoke complex notched specimen. This technique is referred to as the *"Reversed Plasticity Domain Method"* and utilises a novel combination of the Linear Matching Method and the Bree Interaction diagram. This provides a method for calculating the limit boundaries and allows the necessary loading ranges required to cause a specific damage behaviour to be determined. This is the first time these techniques have been combined in this way for the calculation of the design loads in industrial components.

Initially, the background of the technique is introduced; existing methods of designing test loading programmes are described, and the capabilities of the Linear Matching Method and the way in which it can be used for calculating the limit load, shakedown and ratchet limits are explained. The proposed technique is then demonstrated on an industrial application by designing an experimental test programme for the specimen described in Chapter 4. Load ranges of between 232MPa and 387MPa are identified as sufficient for causing crack initiation. The accuracy of the Linear Matching Method for performing this type of analysis on this test specimen is verified through inspection of the strain range history from a series of step-by-step Finite Element calculations. A low cycle fatigue analysis is then performed which identified an optimum design load range of 235MPa which will cause crack initiation in approximately 650 cycles. The combination of these techniques displays their capabilities for an industrial, experimental application and demonstrates the key advantages of the technique for calculating design loads for a highly complex test specimen.

5.1 Introduction

5.1.1 Research Background

It has already been established that fatigue is a prominent failure mechanism in many industrial engineering applications, with some of the most critical being in the aerospace and power industries, due to the severe consequences of a structural failure. To this end, extensive finite element and experimental testing is routinely performed in the design

and development of engineering components for these applications and also during their subsequent operation over their normal lifetime. Chapter 2 has highlighted the importance of accurate fatigue life assessment and Chapter 3 has described the failure mechanisms that occur as a result of different loading regimes. These mechanisms have been identified as purely elastic behaviour, elastic shakedown, reversed plasticity, ratchetting and instantaneous collapse.

In addition to understanding the fatigue life, it is vitally important to be able to predict the precise load at which each of these failure mechanisms will occur in order to ensure their integrity during operational life. This is critical both in the component design stage and also during in-service condition monitoring.

Understanding the load ranges at which these conditions will occur can aid in the development of engineering components, since damaging behaviour can be avoided through careful design. Ratchetting and instantaneous collapse must be avoided for obvious reasons. However, small amounts of plasticity can be tolerated, provided that it shakes down to fully reversed plasticity or elastic shakedown since, at these loads, continued incremental plasticity and ultimate failure will not occur under repeated loading.

In order to gain a better understanding of this, extensive Finite Element (FE) modelling can be performed and these results compared with experimental test data. For this testing, it is important that the specimen is sufficiently representative of the actual plant component for the results to be applicable. For this reason, the test specimen is often designed to fail within a certain lifetime. Fracturing such a specimen during experimental testing in a safe, controlled environment provides essential information about the failure mechanisms that can occur in the final component. Its design can then be adapted if necessary to suit the operating conditions of the engineering structure. This type of testing is prominent in a number of different industries, but is of particular importance in the development of industrial gas turbines. This investigation concerns the prediction of shakedown and ratchetting failure modes within an experimental test specimen which is representative of gas turbine nozzle guide vanes.

5.1.2 The Linear Matching Method for Fatigue Life Assessment

The Linear Matching Method, introduced in Section 3.8, will be used in this investigation to assess structural response to a cyclic loading history by generating a Bree Interaction diagram through a series of shakedown and ratchet analyses.

As explained in Section 3.5, through reference with the Bree-like interaction diagram, shown in Figure 5.1, the LMM method can very efficiently determine the limit boundaries of each of these damage mechanisms by calculating the precise loads at which they occur. It also allows the assessment of intermediate loads by ascertaining what type of behaviour will occur at a given applied load. This makes it a very powerful technique for the damage assessment of engineering components.

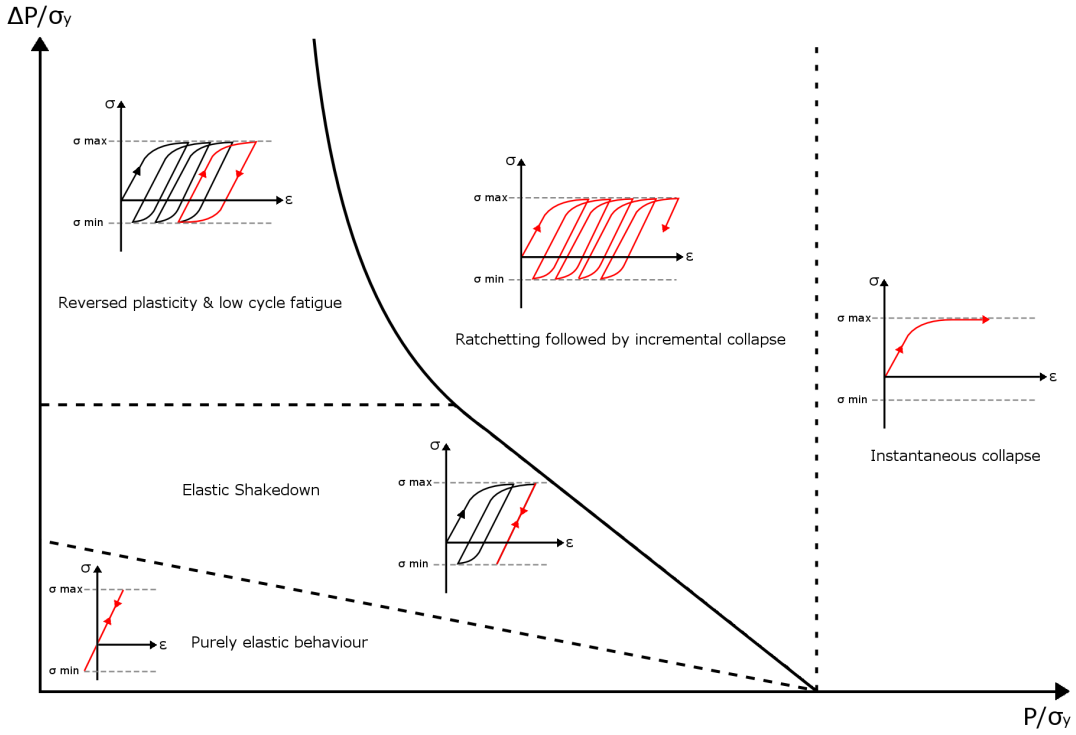

Figure 5.1: Bree interaction diagram showing stress-strain responses at each region

5.1.3 Objectives

The objective of this investigation is to design an experimental testing programme which is sufficient for causing crack initiation in a complex notched specimen. The shakedown and ratchet limits will be calculated with reference to the Bree interaction

diagram, to allow the calculation of the range of loads that will induce crack initiation. A low cycle fatigue analysis will then be performed to select an appropriate design load from this suitable range, which best satisfies the fatigue requirements of the test.

The structure of this chapter is organised as follows: Section 5.1 above has explained the rationale of this investigation, and the importance of careful design of experimental test specimens has been highlighted. In Section 5.2, a new method is proposed for the design of an experimental testing programme. In Section 5.3, a description of the problem is provided and the precise geometry of the bespoke test specimen and the material properties and loading conditions are described. A description of the finite element model that is used in the analysis is also included. Section 5.5 presents the obtained results of the shakedown and ratchet boundary limits which allows the determination of an appropriate design load range. In order to assess the accuracy of the results, the analysis convergence is investigated and the results are verified through a step-by-step analysis. Finally, in Section 5.6, a low cycle fatigue analysis is performed and an appropriate specific design load is chosen based on the obtained results in Section 5.5, with consideration of the likely location of crack initiation. The investigation concludes with a discussion of the arrangement of the experimental test that will be performed as a result of this investigation.

5.2 Numerical Procedure

5.2.1 Reversed Plasticity Domain Method

This investigation proposes a concept that utilises the Linear Matching Method and the Bree Interaction diagram in a novel combination that allows the design of an experimental testing programme for low cycle fatigue crack initiation. This is the first time these techniques have been combined in this way for the calculation of the design loads of industrial components. This method is referred to in this chapter as the *"Reversed Plasticity Domain Method"* (RPDM). It comprises a series of Linear Matching Method analyses, performed at different load points, for the precise calculation of the shakedown and ratchet limit boundaries in order to identify the reversed plasticity and low cycle fatigue region, in which crack initiation will occur. A Bree-Interaction diagram

can then be plotted for visualisation of the critical regions. Identification of this zone allows the calculation of the range of loads in which reversed plasticity and crack initiation will occur. A low cycle fatigue analysis can then be performed which calculates the number of cycles to crack initiation for any load within this range. The user may then select a single specific design load based on the fatigue life requirements of the component. The Reversed Plasticity Domain Method offers a suite of analysis tools to provide a very efficient technique that encompasses the identification of load ranges for causing specific damage mechanisms as well as the calculation of the low cycle fatigue life for crack initiation. An optional step-by-step analysis can then be performed as a means of verification if required. This investigation applies this novel technique to a complex industrial problem, clearly demonstrating its power and efficiency for the design of experimental testing programmes.

The crack initiation assessment is associated with low cycle fatigue, hence it is possible to use LCF material data to assess the lifetime from the steady state cycle strain range data. The calculation of the plastic and total strain range is performed through the first stage of the ratchet analyses of the LMM Direct Steady Cyclic Analysis (DSCA). This is a stand-alone component of the Linear Matching Method which obtains the steady cyclic stresses and strain rates for given combinations of loading through an iterative procedure which directly locates the ratchet limit [123]. This is explained further in Section 5.2.3.

It is important to note that this procedure only considers the calculation of the number of cycles to crack initiation and does not include crack propagation life. Additional analyses would need to be performed to model crack propagation. However, it is believed that for this investigation, the initiation fatigue life is sufficient for designing the experimental testing programme. The aim of this research is to calculate the appropriate cyclic load levels which induce crack initiation within a predefined number of cycles. The objective is to determine, using the proposed method, the cyclic load level that causes the crack to initiate.

5.2.2 Shakedown Theorems

The shakedown and ratchet calculations as part of the RPDM are performed by the Linear Matching Method DSCA. The precise methodology of this is thoroughly described in existing literature. The shakedown theorems are clearly explained by the work of Ponter [124] and this is briefly outlined below. It states that the shakedown limit can be described as the range of the load multiplier, $\lambda \geq \lambda_S$ for a residual stress change of zero, where λ_S is the shakedown limit and the residual stress is denoted as ρ^r_{ij}. Since the shakedown is considered a range, both upper and lower bound limits can be calculated. The LMM is capable of calculating both this upper and lower bound of the shakedown limit. The process in which the LMM performs this calculation is outlined below.

Upper Bound Theorem

The upper bound theorem is based on Koiter's theorem [125, 126], which states that "*a structure under cyclic loading would shakedown if the external work done by the loads is less than or equal to the internal work dissipated for all admissible strain rate cycles,* $\dot{\varepsilon}^c_{ij}$."

Assuming an isotropic, elastic perfectly plastic material that satisfies the Von Mises yield condition, the problem comprises a 3D body of volume, V, with a boundary, S, that experiences a cyclic mechanical loading history $\lambda P_i(x_j, t)$ on S_T and a temperature load of $\lambda\theta(x_j, t)$ within volume V, over a cycle time period Δt. λ is a load parameter and $u_i = 0$ is the displacement rate that is applied on S_U. S_T and S_U are sections of the boundary, S. The basis of the method is that the admissible and incompressible strain rate history, $\dot{\varepsilon}^c_{ij}$, is associated with a compatible strain increment, $\Delta\varepsilon^c_{ij}$ such that:

$$\int_0^{\Delta t} \dot{\varepsilon}^c_{ij} dt = \Delta\varepsilon^c_{ij} \tag{5.1}$$

where the strain increment is associated with a displacement increment field, given by:

$$\Delta\varepsilon^c_{ij} = \frac{1}{2}\left(\frac{\partial \Delta u^c_i}{\partial x_j} + \frac{\partial \Delta u^c_j}{\partial x_i}\right) \tag{5.2}$$

from the load history as above, the upper bound shakedown theorem is then given by:

$$\lambda_{UB} \int_V \int_0^{\Delta t} (\hat{\sigma}_{ij} \dot{\varepsilon}^c_{ij}) dt dV = \int_V \int_0^{\Delta t} (\sigma^c_{ij} \dot{\varepsilon}^c_{ij}) dt dV \tag{5.3}$$

where σ^c_{ij} is the stress at the yield and is associated with $\dot{\varepsilon}^c_{ij}$ and $\hat{\sigma}_{ij}$ is a linear solution associated with the given load history [108, 127]. $\lambda_{UB} \geqslant \lambda_S$ is an upper bound to the shakedown load parameter, λ_S. This can be further simplified to give:

$$\lambda_{UB} = \frac{\int_V \int_0^{\Delta t} \sigma_y \bar{\dot{\varepsilon}}(\dot{\varepsilon}^c_{ij}) dt dV}{\int_V \int_0^{\Delta t} (\hat{\sigma}_{ij} \dot{\varepsilon}^c_{ij}) dt dV} \tag{5.4}$$

where σ_y is the temperature-dependent yield stress of the material, $\dot{\varepsilon}_{ij}$ is a kinematically admissible strain rate and $\bar{\dot{\varepsilon}} = \sqrt{\frac{2}{3} \dot{\varepsilon}_{ij} \dot{\varepsilon}_{ij}}$ is the effective strain rate. This process repeats iteratively, producing a sequence of upper bound values that converge to the least upper bound.

Lower Bound Theorem

In the shakedown condition, by definition, no plastic strain will accumulate when the combination of elastic stresses and residual stress field satisfy the von Mises yield criterion. The lower bound theorem states that shakedown will occur if a time independent residual stress field exists which satisfies the equilibrium and boundary conditions and the total stress is less than the yield limit. This is based on Melan's Theorem [126, 128] which states that "*if a time constant residual stress field, $\bar{\rho}_{ij}(x)$ exists such that superposition with induced elastic stresses, $\lambda_{LB} \hat{\sigma}_{ij}(x,t)$ forms a safe state of stress everywhere in the structure, i.e.*

$$f(\lambda_{LB} \hat{\sigma}_{ij}(x,t) + \bar{\rho}_{ij}(x)) \leqslant 0 \tag{5.5}$$

then $\lambda_{LB} \leqslant \lambda_s$" where λ_{LB} is the lower bound parameter. This utilises a similar iterative process as above in which a convergent lower bound value of the shakedown limit is calculated.

5.2.3 Ratchet Theorems

The theorem for the ratchet limit analysis is based on an extension of the shakedown theorems, where the change of accumulated residual stress field, $\rho_{ij}(t_n)$ at time instance t_n, is included in the linear elastic solution. This is explained by Chen et al [110, 129].

The first step of the analysis involves the evaluation of the changing residual stress field, $\rho^r_{ij}(x,t)$ and plastic strain ranges. Within the Linear Matching Method framework, this is referred to as the Direct Steady Cycle Analysis (DSCA). This iteratively calculates the varying residual stress, $\Delta\rho^r_{ij}(x,t_n)_m$, associated with the elastic solution, $\hat{\sigma}^{\Delta}_{ij}(x,t_n)$, where n is the cycle number. This repeats iteratively from cycle $n=1$ until convergence is reached at cycle $n=M$. Using the obtained values of the residual stress history and plastic strain ranges at a time point, t_n, the second step of the analysis then performs the traditional shakedown procedure, as explained above, to assess the ratchet limit. As previously demonstrated in equations 5.1 and 5.3, the upper bound shakedown theorem can be given by:

$$\lambda_{UB}\int_V\int_0^{\Delta t}(\hat{\sigma}_{ij}\dot{\varepsilon}^c_{ij})dtdV=\int_V\int_0^{\Delta t}(\sigma^c_{ij}\dot{\varepsilon}^c_{ij})dtdV \tag{5.6}$$

where:

$$\hat{\sigma}_{ij}=\lambda\hat{\sigma}^{\bar{F}}_{ij}+\hat{\sigma}^{\Delta}_{ij}(x_k,t)+\rho^r_{ij}(x_k,t) \tag{5.7}$$

Defining the von Mises yield condition with the associated flow rule, gives the upper bound ratchet limit multiplier, λ_{UB}, subject to a cyclic load history, $\hat{\sigma}^{\Delta}_{ij}(t_n)$, and an additional applied constant load, $\hat{\sigma}^{\bar{F}}_{ij}$, as:

$$\lambda_{UB}=\frac{\int\limits_V\sum_{n=1}^N\sigma_y\bar{\varepsilon}(\Delta\varepsilon^n_{ij})dV-\int\limits_V\sum_{n=1}^N(\hat{\sigma}^{\Delta}_{ij}(t_n)+\rho_{ij}(t_n))\Delta\varepsilon^n_{ij}dV}{\int\limits_V\hat{\sigma}^{\bar{F}}_{ij}(\sum_{n=1}^N\Delta\varepsilon^n_{ij})dV} \tag{5.8}$$

where $\bar{\varepsilon}(\Delta\varepsilon^n_{ij})=\sqrt{\frac{2}{3}\Delta\varepsilon^n_{ij}\Delta\varepsilon^n_{ij}}$ and $\Delta\varepsilon^n_{ij}$ is the kinematically admissible plastic strain rate history. Based on this, the LMM then produces a sequence of monotonically reducing upper bounds and converges to the least upper bound ratchet limit [129].

The LMM algorithms iteratively compute the shear modulus, Jacobian matrix, residual stress and modified stress. This allows the user to perform a complete anal-

ysis to calculate the shakedown and ratchet limits as well as other important cyclic information such as strain range for use in LCF analysis. These theorems are embedded into the Linear Matching Method code and ABAQUS plugin[114–116]. The user-friendly environment of the plugin means that these parameters can be calculated without the need to completely understand the theoretical background. This demonstrates the power of the LMM ABAQUS plugin as an ergonomically well designed and user friendly software tool.

5.3 Numerical Application

5.3.1 Description of the Problem

The subject of this experimental test programme is the specimen designed in Chapter 4. This aims to represent gas turbine nozzle guide vanes and is shown in Figure 5.2. The test requires that crack initiation will occur in the specimen, but for time and budgetary reasons, it is essential that it occurs within a relatively low number of cycles. The Reversed Plasticity Domain Method is used to design a suitable programme.

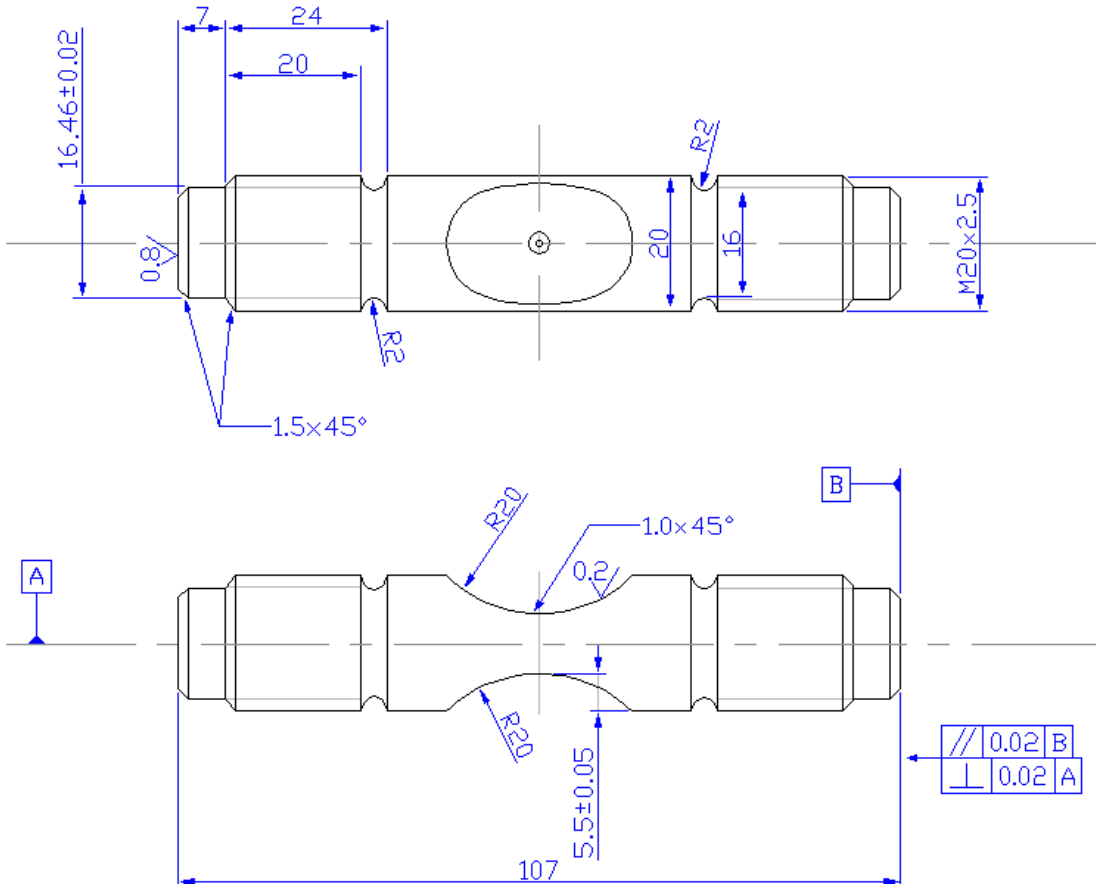

Figure 5.2: Drawing of test specimen geometry

5.3.2 Material Properties & Loading Conditions

A nickel-based superalloy, similar to those used in gas turbine applications is used in this investigation with a Young's Modulus of 178GPa and yield stress of 648MPa. The Linear Matching Method Direct Steady Cyclic Analysis procedure can accurately model elastic perfectly plastic materials. However, in addition, it is able to incorporate material hardening/softening through the inclusion of the Ramberg-Osgood formula. This matches the inclusion of hardening/softening in the R5 procedure, allowing it to work harmoniously with this procedure. This allows the LMM DSCA to be used on a wide range of material models, matching the requirements of real components very accurately if required, or on more simple cases if elastically perfectly plastic models are sufficient, which reduces the computational time. For materials that exhibit small levels of hardening, elastic perfectly plastic properties offer simplified material models

which can still provide reasonable levels of accuracy. In this investigation, both EPP and RO material models are analysed and a comparison between the two is offered. This allows the impact of material hardening on the fatigue life of a component to be demonstrated. The Ramberg-Osgood model that is adopted in this investigation follows the relationship:

$$\frac{\varepsilon_T}{2} = \frac{\Delta\sigma}{2\bar{E}} + \left(\frac{\Delta\sigma}{2A_R}\right)^{\frac{1}{\beta}} \tag{5.9}$$

where, ε_T is the total strain range, $\Delta\sigma$ is the cyclic stress range, $\bar{E}$ is the multi-axial Young's Modulus and $A_R = 1175$MPa and $\beta = 0.068$ are material constants. It is important to note that the LMM employs the RO relationship in a different form to that described in Equation 2.1 since it is based on the strain amplitude, rather than the total range.

In the LMM plugin, the user specifies an arbitrary applied reference load and loading history. The LMM then calculates the shakedown or ratchet limit multiplier as a factor of this reference load, i.e. if a reference load of 100MPa is applied and a shakedown limit multiplier of 0.5 is yielded, then the shakedown limit would be 50MPa. In this investigation, a reference load of magnitude 400MPa is applied to one end of the specimen, whilst the opposite end is pinned in position to prevent movement, as illustrated in Figure 5.3.

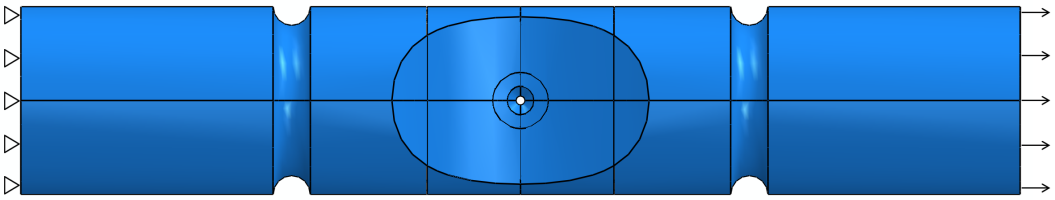

Figure 5.3: Finite element model of test specimen geometry

In Bree's original case of a thin walled cylinder, a static mechanical load and cyclic thermal loads were applied. The industrial test in this investigation is to be performed with cyclic mechanical loading under isothermal conditions. The constant temperature field means that no thermal stress concentrations will be induced, meaning that there is no primary thermal load to apply. Therefore, instead of a thermal and mechanical

load, two separate mechanical loads are applied to the test specimen. Each load will be of identical magnitude, however, one will be kept static, whilst the other is cycled. The loading history applied in this investigation is illustrated in Figure 5.4.

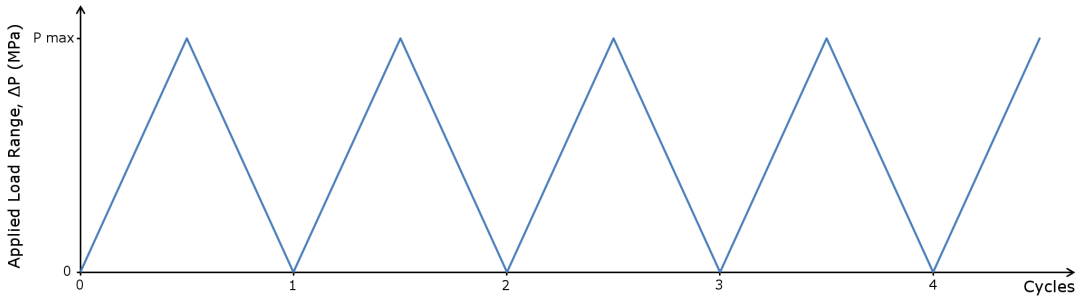

(a)

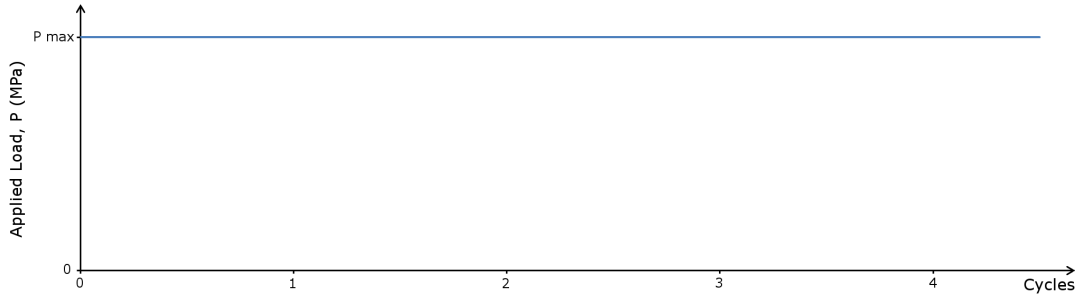

(b)

Figure 5.4: Loading history for (a) cyclic load and (b) static load

The application of independent static and cyclic mechanical loads means that the generated Bree-like interaction diagram provides information for the entire range of R-ratios since the cyclic and static loads are plotted independently on separate axes. Monitoring the response at varying values of the static load (x-axis), allows the material response at different R-ratios to be ascertained. For this investigation, an R-ratio of zero is required which corresponds to the Y-axis, at x=0.

5.4 Finite Element Model

The finite element software package, ABAQUS is used for the computational analyses performed in this investigation. Within ABAQUS, the proposed test specimen as presented in Figure 5.2 is modelled. The central region of the model containing

the chamfered centre hole is modelled using quadrilateral, hexahedral elements and the ends of the specimen are modelled with quadrilateral, tetrahedral elements. This allows the implementation of a refined mesh around the most critical regions of the specimen, whilst a more coarse mesh is used in the less critical regions, thus reducing the computational expense of the analyses. The mesh that is used in this investigation is shown in Figure 5.5 and an enlarged view of the mesh around the centre hole is shown in Figure 5.6.

The complete geometry was modelled; pinned boundary conditions were applied at one end of the specimen, and a pressure load was applied at the other. Symmetry boundary conditions could have been implemented, allowing a half, quarter or eighth model to be used rather than a full model, reducing the computational effort. However, in this particular case, due to the efficiency of the Linear Matching Method, running each analysis for the complete geometry took only a few minutes. It was therefore deemed unnecessary to invest additional modelling effort to reduce the size of model and apply symmetry boundary conditions. However, for larger and more complex models, implementing such a strategy could be beneficial.

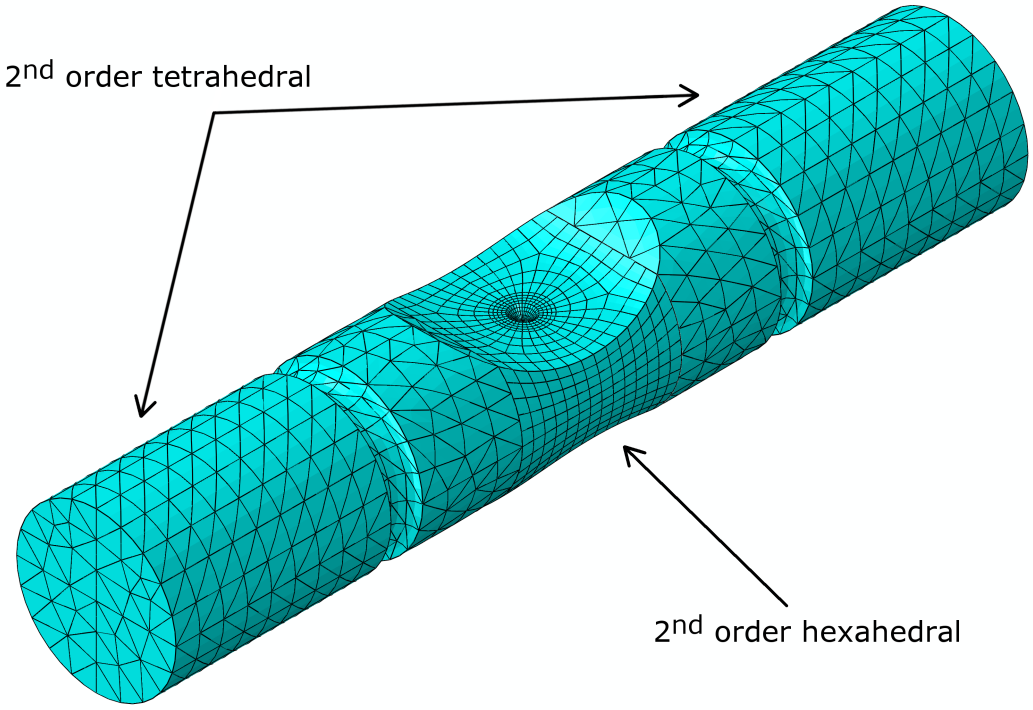

Figure 5.5: Model mesh showing different element types

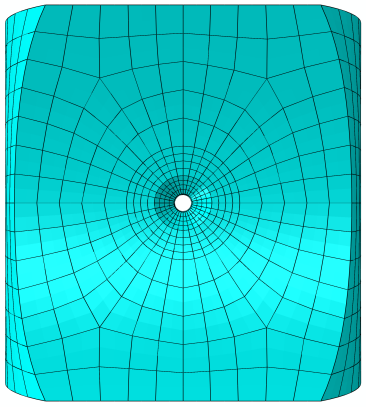

Figure 5.6: Mesh of the central region of model

5.5 Numerical Results

5.5.1 Shakedown & Ratchet Limit Boundaries

The RPDM is used to perform a number of shakedown and ratchet analyses which allows the boundary conditions of each analysis to be calculated. These results are

shown in Table 5.1 and Table 5.2; P and ΔP are the magnitudes of the static and cyclic loads respectively and P/σ_y and $\Delta P/\sigma_y$ are P and ΔP normalised with respect to the yield stress of the material.

Table 5.1: Shakedown limits calculated by the LMM

Shakedown Limits (Static Load, Cyclic Load)			
Static Load, P	Cyclic Load, ΔP	Normalised Static Load, P/σ_y	Normalised Cyclic Load, $\Delta P/\sigma_y$
0.000	231.084	0.000	0.357
23.108	231.075	0.036	0.357
46.213	231.064	0.071	0.357
69.310	231.035	0.107	0.357
92.300	230.749	0.142	0.356
115.375	230.749	0.178	0.356
145.234	242.057	0.224	0.374
387.302	0.000	0.598	0.000

Table 5.2: Ratchet limits calculated by the LMM

Ratchet Limits (Static Load, Cyclic Load)			
Static Load, P	Cyclic Load, ΔP	Normalised Static Load, P/σ_y	Normalised Cyclic Load, $\Delta P/\sigma_y$
387.379	0	0.598	0.000
347.439	40	0.536	0.062
307.330	80	0.474	0.123
267.332	120	0.413	0.185
227.312	160	0.351	0.247
187.290	200	0.289	0.309
147.260	240	0.227	0.370
107.231	280	0.165	0.432
67.197	320	0.104	0.494
27.165	360	0.042	0.556
0.000	387	0.000	0.598

The limit load is identified to be 59.8% of the yield stress of the material, which corresponds to a load of 387.3MPa. This data can be expressed graphically in the form of the Bree Interaction diagram as shown Figure 5.7. The x-axis shows the static load, P, and the y-axis shows the cycled load, ΔP, both normalised with respect to the yield stress. The letters A and B identify the locations of load points that will be used in the subsequent convergence analysis in section 5.5.2.

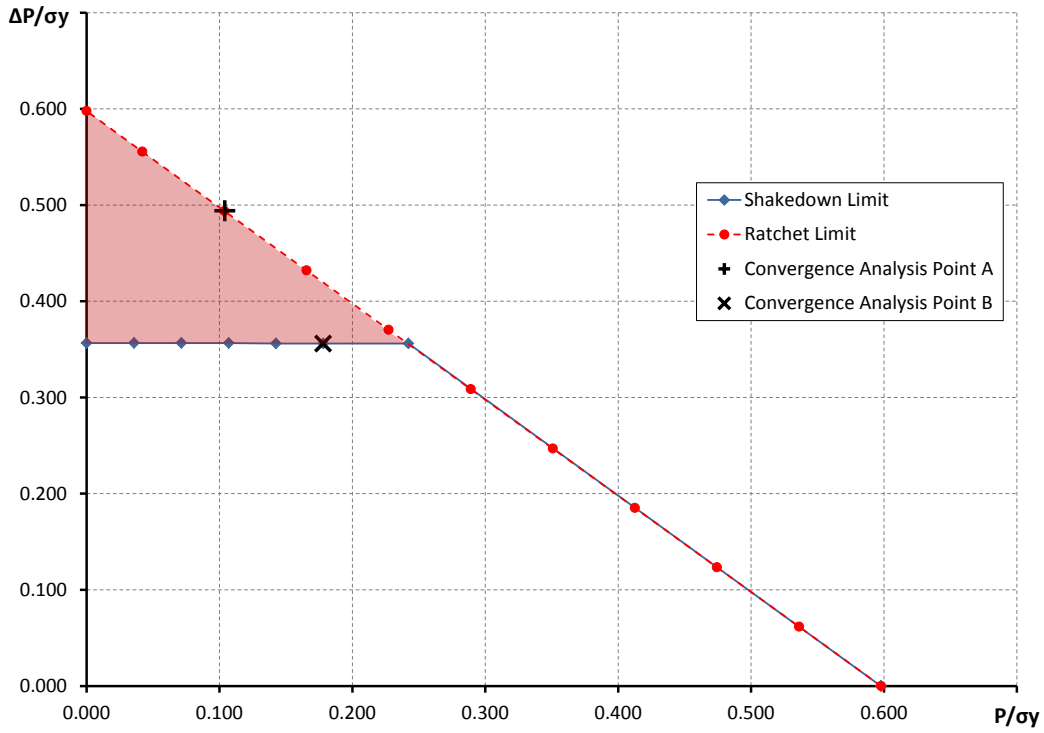

Figure 5.7: Generated Bree-interaction diagram for test specimen

Since the aim of this investigation is to determine the loads required to cause crack initiation, the area of interest on the shakedown-ratchet Interaction diagram is the reversed plasticity region, as highlighted in red in Figure 5.7, where the x-axis corresponds to the static load and the y-axis corresponds to the cyclic load. However, in the experimental test, an R-ratio of zero is required and no static load is to be applied, meaning that the only region of interest for calculating the required load range is at x=0. It can be seen that at x=0, the shakedown and ratchet limits are 0.357 and 0.598 respectively. These values are normalised with respect to the yield stress and so when corrected become 231.336MPa and 387.504MPa. Therefore, the limit loads can be summarised as given in Table 5.3. A series of step-by-step analyses are performed as a means of verification for the results generated using the RPDM and these are presented in Section 5.5.3. Due to the nature of the mechanical load and the fact that there is no thermal load, the ratchet limit coincides with the limit load and so in this particular case, there is no visible ratchetting region as any load larger than the ratchet limit load will cause instantaneous collapse.

Table 5.3: Shakedown and ratchet limit loads for the load condition of R=0

	$\Delta\ P\ /\ \sigma_y$	Load (MPa)
Shakedown Limit	0.357	231.336
Ratchet Limit	0.598	387.504

5.5.2 Convergence Investigation

In order to ascertain the accuracy of the obtained solution from the RPDM LMM analysis, it is important to consider the convergence rate. In the LMM plugin for ABAQUS CAE as part of the RPDM, the desired convergence rate can be specified as either the difference between consecutive upper bounds, or the percentage difference between upper bounds and lower bounds. As a general case, the upper bound solution converges more quickly than the lower bound [108] and so is often the preferred choice of convergence criteria. During each iteration of the analysis, the upper and lower bounds of the shakedown or ratchet load multiplier are calculated. The solution is deemed to have converged once the user-defined convergence criteria have been satisfied. In order to assess that the convergence is satisfactory, a load condition was selected from both the shakedown and ratchet regimes as indicated by the letters A and B in Figure 5.7 and the respective load multiplier is plotted at each increment as shown in Figure 5.8.

At load point A, the ratchet analysis reaches convergence fairly quickly, with the upper bound converging in approximately 20 iterations whilst the lower bound takes slightly longer, reaching convergence in approximately 47 iterations. However, at load point B, the shakedown analysis experiences a peculiar phenomenon. The upper bound reaches an initial steady state in approximately 15 iterations, however, whilst the lower bound is approaching convergence, at iteration 32, the LMM detected a change in the failure mechanism and the upper bound started to re-converge on the limit multiplier of this new failure mechanism. This caused the upper bound shakedown limit multiplier to drop below that of the lower bound multiplier. Such a situation would cause numerical errors and so in response, the LMM automatically changes the convergence criteria to be based solely on the upper bound. The analysis then continued, reaching

final convergence in approximately 55 iterations. This highlights the importance of monitoring both the upper bound and lower bound limit loads since each solution can be validated against one another, giving greater confidence in their accuracy [130]. If only one condition is used as a convergence criterion, then it could be possible to miss a failure mechanism, yielding inaccurate and incomplete results. Monitoring both lower and upper bounds that tend towards a common solution in this way is one of the major strengths of the Linear Matching Method and it makes convergence generally faster, more stable and more accurate than other methods [112].

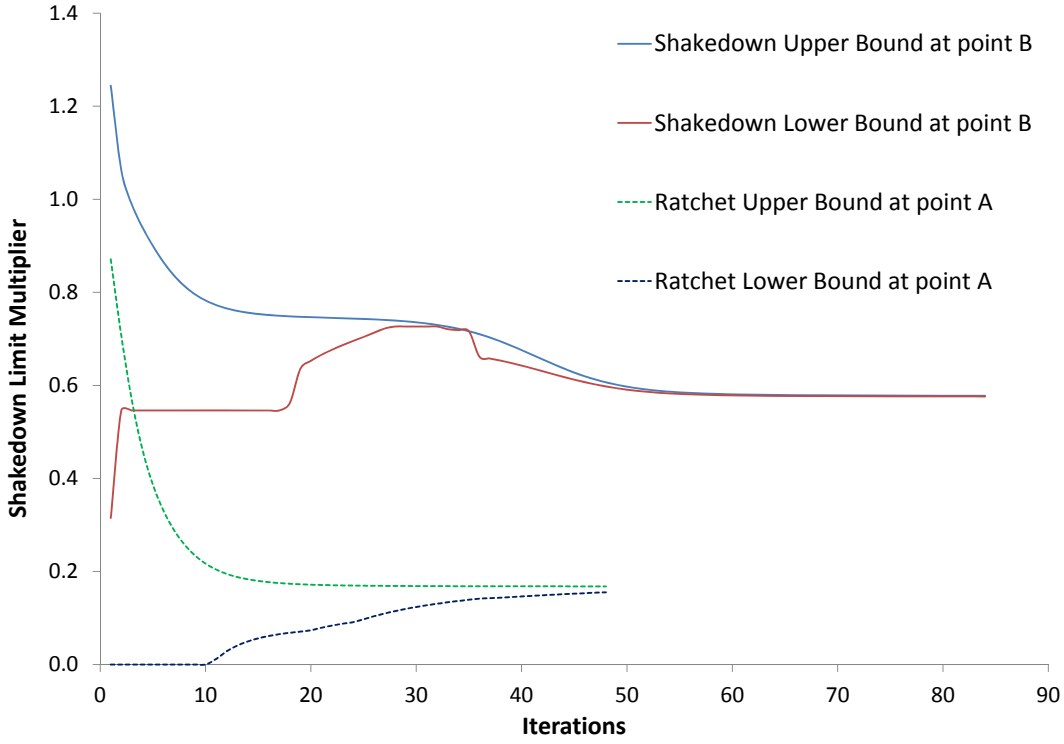

Figure 5.8: The convergence condition of iterative processes for shakedown and ratchet analysis

5.5.3 Verification of Results

The accuracy of the RPDM can be verified by performing a series of standard step-by-step analyses at different regions of the Shakedown-Ratchet Boundary diagram and monitoring the strain magnitude history data. Each type of damage behaviour exhibits a different strain response and through monitoring this, the accuracy of the location of the boundaries can be determined. For a material with elastic-perfectly plastic prop-

erties, the shakedown strain response increases linearly to a critical value, at which point it remains constant, producing a bilinear curve. Under reversed plasticity, the strain again initially increases linearly, but on reaching a critical point, oscillates about a mean value. Under ratchetting conditions, the strain continuously increases until eventual collapse occurs. These strain responses are illustrated in Figure 5.9. Observation of these responses can indicate the location of the boundaries. If at a particular load point, shakedown occurs but at a slightly increased load, reversed plasticity occurs, then it can be deduced that the limit boundary occurs between these two load points. To assess this, six analyses of 100 cycles each were performed at points above and below the shakedown and ratchet boundaries as illustrated by the crosses in Figure 5.10. This demonstrates the Shakedown-Ratchet Boundary plots with the strain magnitude response superimposed. The crosses show the load points at which step-by-step analyses were performed. It clearly demonstrates that the observed strain response accurately matches the damage behaviour, thus proving the accuracy of the RPDM results for the shakedown and ratchet boundaries.

(a)

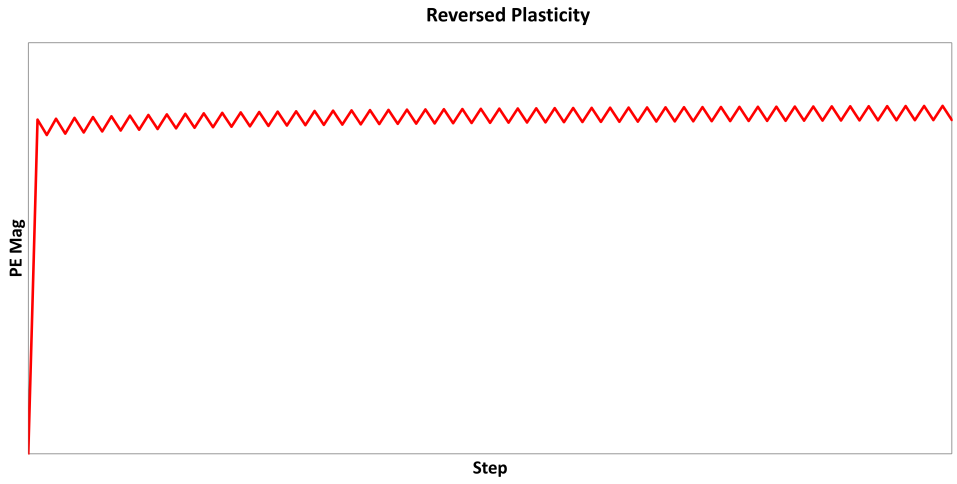

(b)

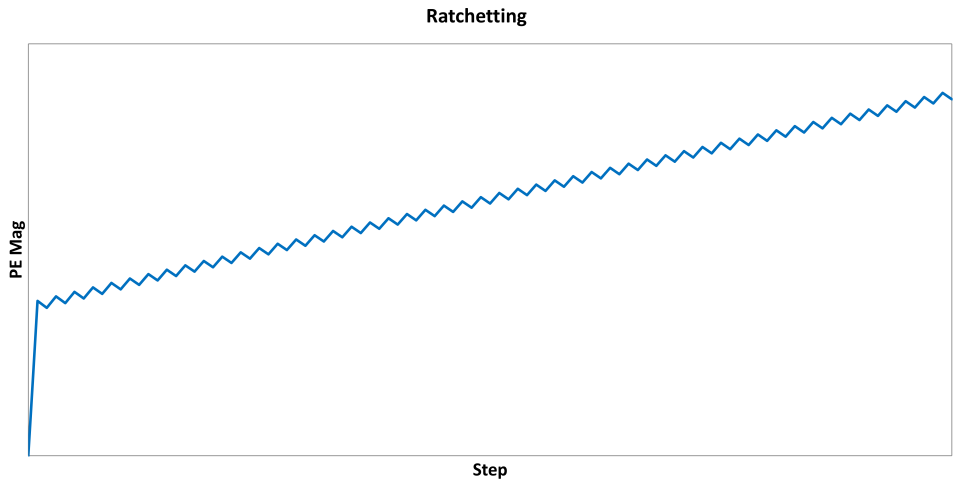

(c)

Figure 5.9: Typical strain response for (a) shakedown, (b) reversed plasticity and (c) ratchetting

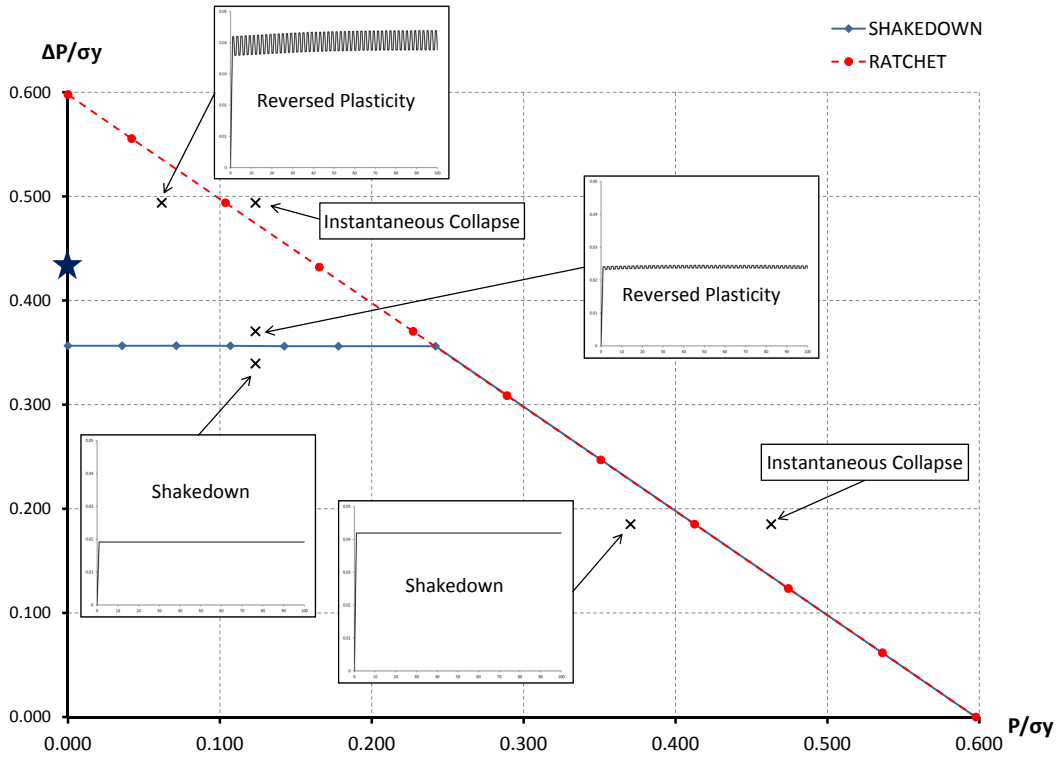

Figure 5.10: Step-by-step analysis verification of shakedown and ratchet boundaries

Following successful verification of the RPDM results by step-by-step analyses, it can be concluded that a load range of between 231MPa and 387MPa will cause crack initiation. In order to determine the most appropriate load between these ranges, a low cycle fatigue analysis is now required.

5.6 Evaluation & Discussion

5.6.1 Low Cycle Fatigue Assessment

From the Shakedown-Ratchet Boundary plot in Figure 5.7, it can be seen that the reversed plasticity region only occurs between the loads of 231MPa and 387MPa. Whilst any load between these magnitudes is sufficient for causing crack initiation, the associated number of cycles to failure will vary widely. In order to determine the most appropriate fatigue life that meets the requirements of the test, a sensitivity study is performed to calculate the number of cycles to failure for gradually increasing loads through comparison with the low cycle fatigue data that is adopted in this investigation

as shown in Table 5.4. These results are presented graphically in the form of number of cycles to failure against increasing applied load in Figure 5.11.

Table 5.4: Low cycle fatigue data

Number of Cycles to Failure	Normalised Strain Range (%)
100	1.400
500	1.016
1000	0.885
2000	0.771
4000	0.672
8000	0.585
16000	0.509
32000	0.444

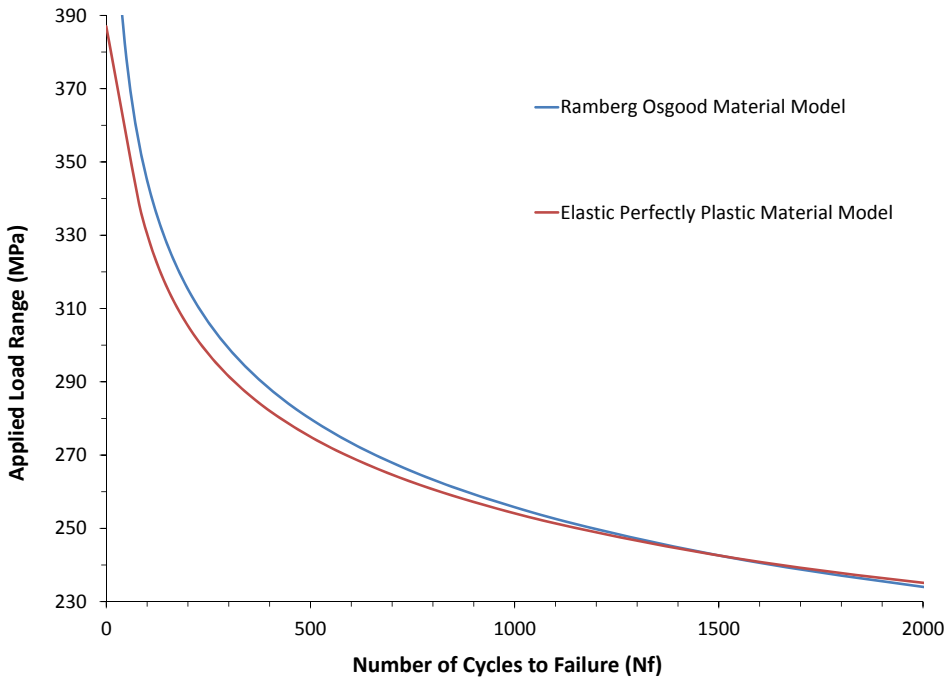

Figure 5.11: Number of cycles to failure for increasing applied cyclic load range for R-ratio of 0

The variation of LCF life to crack initiation for varying applied loads can clearly

be seen for both EPP and RO material models. As the load increases, this fatigue life decreases until the limit load is reached, where the specimen will instantaneously collapse on the first load cycle. Below the shakedown limit, the applied load is less than the low cycle fatigue limit of the specimen and so low cycle crack initiation will never occur. It can be seen that using the EPP material model, the calculated fatigue life is lower than that of the RO model, presenting a potentially overly-conservative, and unrealistic value of the total LCF life.

When performing the experimental testing in this investigation, for time and budgetary reasons, the test is required to be as short as possible. However, if the test is too short there is a possibility that critical data might be missed since the crack growth will occur too quickly. It is therefore important that the test duration is long enough to allow successful recording of all the important measurements. For this reason, a balance is required between the duration of the test and the incurred cost. To this end, a design load range of 270MPa (indicated by a dark blue star in Figure 5.10) is considered optimum since it is above the shakedown limit, ensuring that cracking occurs, yet it has a relatively long low cycle fatigue life of approximately 650 cycles to crack initiation. This will allow sufficient time to observe the necessary data that will be obtained during the test. This is summarised in Table 5.5.

Table 5.5: Stress and strain ranges calculated using both Elastic Perfectly Plastic and Ramberg-Osgood Material Models and corresponding fatigue life calculated by the RPDM

	Material Model	
	EPP	RO
Stress Range (MPa)	1296.00	1330.68
Elastic Strain Range (%)	0.7329	0.7483
Plastic Strain Range (%)	0.2436	0.2115
Total Strain Range (%)	0.9764	0.9598
LCF Life (cycles)	603	658

Both the Ramberg-Osgood and Elastic Perfectly Plastic material models are included to demonstrate the effect of material hardening on the life. It can clearly be seen that the elastic strain range for the RO model is larger than EPP, whilst the plastic strain range for the RO model is smaller than for EPP, resulting in a smaller total strain range for the RO model, yielding a longer life than for EPP. This matches the typical response that is expected for such material models, and highlights the importance of implementing realistic material models which include cyclic hardening for a thorough and accurate prediction of low cycle fatigue life. However, it can be seen that in this particular case, the absolute effect on the LCF life is relatively small.

For the chosen load of 270MPa, the steady state hysteresis loops are plotted in Figure 5.12. These confirm that the mechanism undergoes a reversed plasticity response at an applied load of this magnitude. The difference in total stress and strain ranges can also clearly be seen.

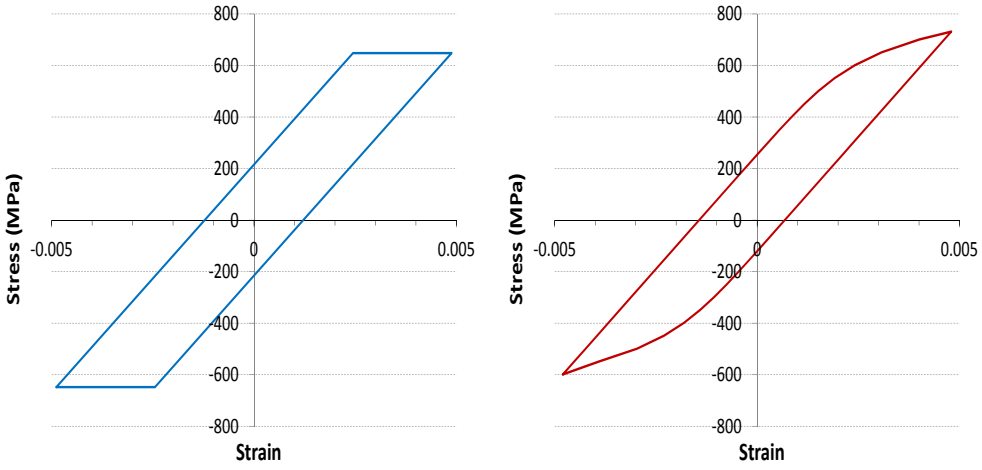

Figure 5.12: Stabilised hysteresis loop at applied load of 270MPa for (a) Elastic Perfectly Plastic Material Model and (b) Ramberg-Osgood Material Model

5.6.2 Arrangement of Experimental Test Specimen

In addition to predicting the number of cycles to failure, it is important to consider the point of crack initiation. Figure 5.13 shows the induced total strain range under loading for both EPP and RO material models. The points of maximum stress are clearly very localised at the edges of the centre hole and are likely locations of crack initiation. Due

to the symmetry of the specimen, the strain at each side of the centre hole on each face is of similar magnitude and so the exact location of initiation is unknown as it could be at one of four locations. This poses a potential issue for experimental testing and so in order to ensure that crack initiation is witnessed, each face of the specimen must be monitored.

A possible alternative would be to redesign the test specimen to create a non-symmetrical stress distribution, by for example, adding a notch on one side of the component. This would mean that the location of crack initiation could be prescribed before testing takes place, avoiding the issue of uncertainty in initiation location. However, this could also introduce asymmetrical loading and torsional effects meaning that the specimen could bend under uni-axial loading. Therefore, the geometry would have to be carefully designed to introduce an obvious stress concentration and therefore crack initiation location, whilst also ensuring even displacement in the testing rig.

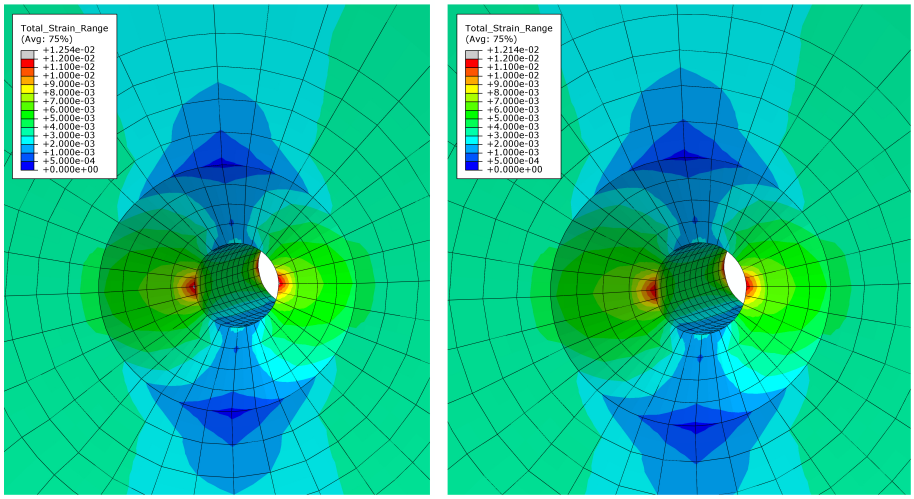

(a) (b)

Figure 5.13: Total strain range induced at stress concentration under cyclic loading for Elastic Perfectly Plastic (a) and Ramberg-Osgood (b) Material Models

It is important to note that the contour plots shown in Figure 5.13 are calculated using the nodal values, however, for the LCF analysis above, the stress and strain values are calculated at the most critical integration point in the most critical element. As a result, the values calculated by ABAQUS at the node locations are slightly higher than at the integration point. The total strain ranges calculated in the RPDM analysis using

the integration point are 0.9764% and 0.9598% for EPP and RO models respectively, as shown in Table 5.5. Whereas, the total strain range calculated at the most critical node is 1.254% and 1.214% for EPP and RO models respectively. This figure is intended for illustrative purposes to demonstrate the location of crack initiation, and not for an in depth LCF analysis.

5.6.3 Crack Propagation Analysis

In order to gain a greater understanding of the crack propagation direction prior to experimental testing, an XFEM analysis is performed. This will allow the likely crack direction to be predicted. Figure 5.14 shows a series of close up images of the centre hole, showing the progression of a propagating crack modelled using the XFEM technique. It can be seen to emanate from the points of highest stress at the edges of the centre hole at the front and back faces of the specimen. The crack then propagates through the depth of the specimen from the faces towards the centre, where both sides of the crack meet. This crack then propagates through the width of the specimen and continues to propagate, un-arrested, until complete failure occurs. This analysis provides valuable information in the preparation of the experimental testing as it allows a prediction of the crack initiation location and propagation direction.

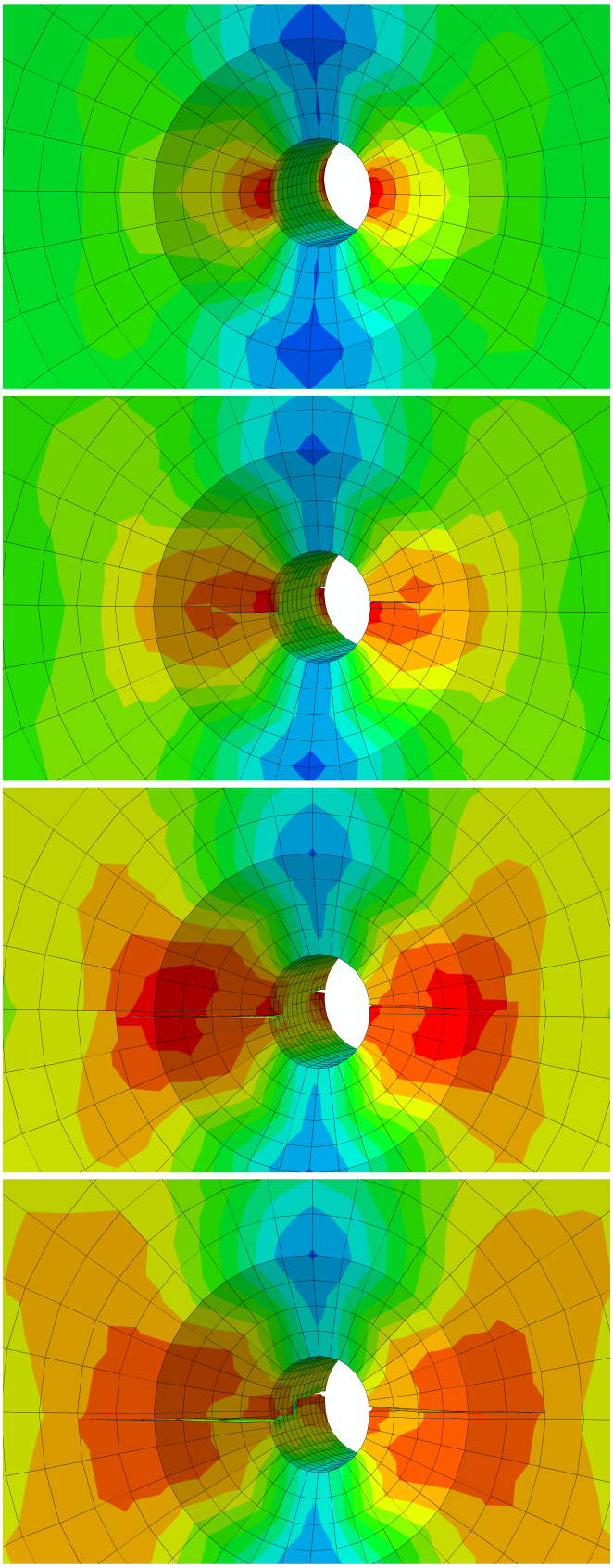

Figure 5.14: Series of images showing propagating crack using the XFEM technique

Following successful design of the experimental testing programme and calculation of the low cycle fatigue life as well as the crack initiation location and propagation path, experimental testing can now be performed. A number of test specimens, as designed in Chapter 4, have been manufactured and are shown in Figure 5.15.

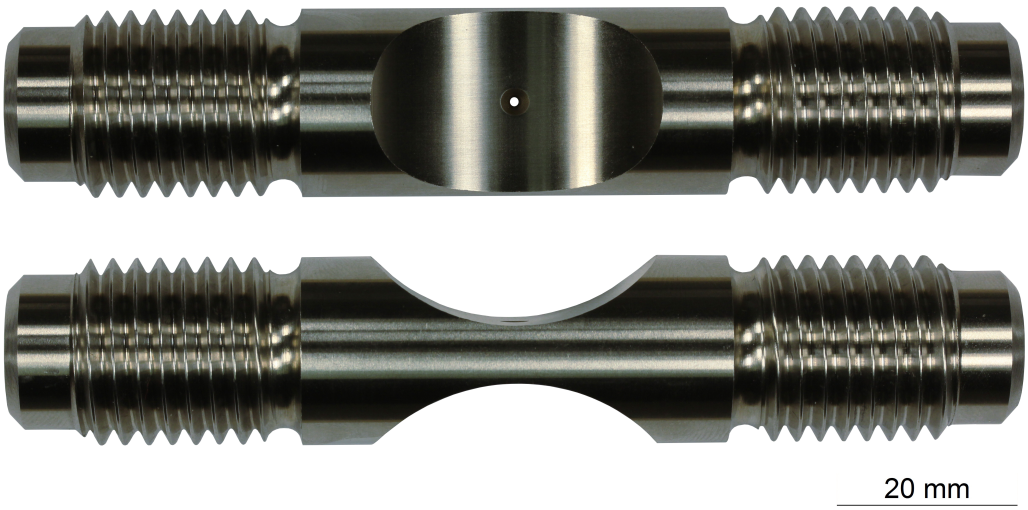

Figure 5.15: Machined industrial test specimen

The scope of the study is to perform 10 tests, comprising three series:

1. Simple fatigue cycle
2. Initial single tensile overload cycle followed by simple fatigue cycle
3. Initial single compressive overload cycle followed by simple fatigue cycle

Three specimens will be tested for each series of test conditions with the tenth specimen considered a spare, and will either be tested based on the outcome of the other 9 tests, or used as a trial run. All tests will be load-controlled and conducted at R=0 under isothermal conditions at 500°C with an applied load range of 270MPa. For the case of the overload, this is to be 25% higher than the normal fatigue cycle load, i.e. 337.5MPa. The purpose of these tensile and compressive overloads is to create a residual stress field in the notch in order to observe the effect this has on the structural integrity of the component.

During the tests, crack initiation and propagation will be measured using DC (direct current) potential drop monitoring. This is a non-destructive examination technique

that applies a constant direct current to the specimen and measures the induced resistance. Any change in the geometry through cracking will induce a change in resistance. Through correct calibration, this change in resistance can be related to crack growth [131]. To allow implementation of this technique during the testing of the specimen, measurement probes are installed either side of the central hole and a reference probe is installed away from the stress concentration for comparison purposes. This will allow the change of resistance induced in the specimen as the crack grows and its initiation and extension to be measured. These probes will be positioned outside the centre hole to avoid any impact on the test results.

In an attempt to understand the evolution of the fatigue crack, the test will also attempt to "*beach mark*" the specimen. Beach marks are visible macroscopic marks found on the fracture surface which occur when there is an interruption in the propagation of the crack. This can be performed by intermittently altering the loading cycle. In this test, a small number of cycles of R ratio of 0.5 will be performed for every 100 standard cycles, allowing the evolution of the crack front with each set of 100 cycles to be monitored.

At the time of writing, this testing had not commenced, but it is scheduled to take place over the coming years.

5.7 Chapter Summary

The Reversed Plasticity Domain Method has been proposed as a technique for the design of an experimental testing programme suitable for causing crack initiation in a complex notched specimen through the calculation of the shakedown and ratchet limits. The shakedown limit and ratchet limit loads have been identified as 231MPa and 387MPa respectively and as such, any load between these values is sufficient to cause low cycle fatigue crack initiation. The accuracy of the results obtained using the RPDM has been verified through inspection of the strain range history data of a series of step-by-step analyses. Following successful verification, a strain-based low cycle fatigue analysis was performed in order to calculate the number of cycles to crack initiation for a range of loads between the shakedown and ratchet limits. This allowed an optimum design load to be determined which meets the requirements of the test

within the imposed time constraints. Following a complete low cycle fatigue analysis, a design load of 270MPa has been selected as the optimum load for the experimental test. This load yields a fatigue life of approximately 658 cycles to crack initiation for a Ramberg-Osgood material model and 603 cycles for an Elastic Perfectly Plastic material model. The location of likely crack initiation has also been identified. Finally, the experimental procedure that will be performed as a result of this investigation has been discussed with a detailed description of each test provided.

This investigation clearly demonstrates the power and efficiency of the Reversed Plasticity Domain Method and the Linear Matching Method for the calculation of the shakedown and ratchet limits as well as the design of an experimental testing programme and LCF analysis for a highly complex industrial test specimen.

Chapter 6

The Modified Monotonic Loading Concept for the Calculation of the Cyclic J-Integral

Note of publication

The work contained in the following chapter has been presented by Beesley et al in the peer-reviewed ASME Journal of Pressure Vessel Technology [2] and at the ASME International Conference of Pressure Vessels & Piping (PVP) 2014 in Anaheim, California, USA [3].

Chapter Overview

This chapter introduces the Modified Monotonic Loading (MML) Concept as a method of calculating the cyclic J-integral. This novel approach is investigated through application to a highly complex, bespoke industrial test specimen containing a semi-elliptical surface crack. Varying loading conditions including uniaxial tension and out-of-plane shear are applied, and the relationships between the applied loads and the cyclic J-integral are established. In addition, the variations of the cyclic J-integral along the crack front are investigated, allowing the critical load that can be applied before crack propagation occurs to be determined as well as the identification of the critical crack direction once propagation does occur. These calculations demonstrate the applicability of the method to practical examples and illustrate an accurate method of estimating the cyclic J-integral.

6.1 Introduction

The focus of this chapter is the J-Integral, and how this can be extended to allow the evaluation of fatigue life. This builds the work on the foundation of elastic plastic fracture introduced in Chapter 2. The theory of the J-Integral is introduced and methods of the extension of this parameter to allow for cyclic fatigue are investigated through the application of techniques to an industrial test specimen.

6.2 Objectives

The overarching aim of this investigation is to assess the suitability of an extended monotonic analysis for approximating the cyclic J-integral (ΔJ). The limitations with current methods of determining the cyclic J-Integral have already been discussed in Chapters 2 and 3. The suitability of the proposed Modified Monotonic Loading (MML) concept is then assessed. Finally, this technique is applied to an industrial test specimen in order to calculate the cyclic J-Integral and its variation with increasing load and crack front location. This chapter is organised as follows: Section 6.3 discusses the importance of crack modelling in industrial design, Section 6.4 proposes a concept for

the calculation of the ΔJ. Section 6.5 presents the model specific to this application and the associated material and loading properties are defined. The investigation continues with Section 6.6 which presents the obtained results for the validation of the MML technique as well as the calculated cyclic J-Integral variation with increasing load and crack location.

6.3 Crack Modelling

Simulating a 3D surface crack is much more complicated than simulating a 2D crack. The variation of ΔK and ΔJ along the crack front is dependent on the type and magnitude of the applied loading and as a result will vary depending upon the location along the 3D surface crack front. Different locations will result in different values of ΔK and ΔJ and will thus affect the crack propagation direction. It is therefore vitally important to simulate the ΔJ with a high level of detail under different loading conditions in order to gain a complete understanding of the crack behaviour and thus predict its propagation.

The eXtended Finite Element Method, as introduced in Section 3.4, is capable of modelling mesh independent cracking and thus could be used in this investigation. This method is capable of calculating contour integrals such as the SIF and J-Integral, however, when a high level of geometrical detail is introduced, the accuracy of contour integration close to the crack tip is compromised. For this reason, XFEM will not be used as a technique for calculating contour integrals in this investigation and the traditional FEM is used instead.

Modelling simplified models such as infinite plates and blocks can provide valuable insight into crack behaviour. However, these large simplifications can overlook the complexities of real life applications that are found in industry. Therefore, increasing the model complexity makes computational models more akin to industrial applications and thus the results can offer more value than that of greatly simplified cases. This validates the case for modelling a complex geometry test specimen in this investigation.

6.4 Modified Monotonic Loading (MML) Concept

A concept is proposed which provides a reasonable approximation for the calculation of the cyclic J-Integral which addresses the known issues in the existing technologies. This can be achieved through modification of a monotonic loading analysis by replacing σy with $2\sigma y$ and replacing the cyclic load range with a single monotonic load equal to the range. This allows such a modified monotonic analysis to replicate the conditions of a cyclic loading analysis. This method is referred to in this chapter as the "*Modified Monotonic Loading*" (MML) concept. This follows on from the work of Chen and Chen [132]. It was discovered that in an un-cracked body subjected to variable loading conditions, the differences between this MML concept and the equivalent cyclic analysis were relatively small. Their work indicated the potential for this technique as a method of determining the cyclic J-Integral. In this investigation, this MML concept will be investigated and tested further on an industrial test specimen.

The workings of this concept can be explained in reference to the energy method of Section 2.6.2 and 2.8.3 and Figures 2.6 and 2.17. Considering a cyclic loading condition between maximum and minimum loading, and the corresponding load displacement curve, as shown in shown in Figure 6.1 (a), it can be seen that the energy released during fracture, dU, is equal to that of the MML analysis where the yield stress is doubled and a single load is applied which is equal to the load range of the cyclic loading history, shown in Figure 6.1 (b). These modifications simulate a monotonic equivalent to a cyclic loading history. Since this concept is capable of successfully replicating a cyclic loading history, the MML offers a viable method of calculating fracture parameters, such as the J-integral, for a cyclic analysis.

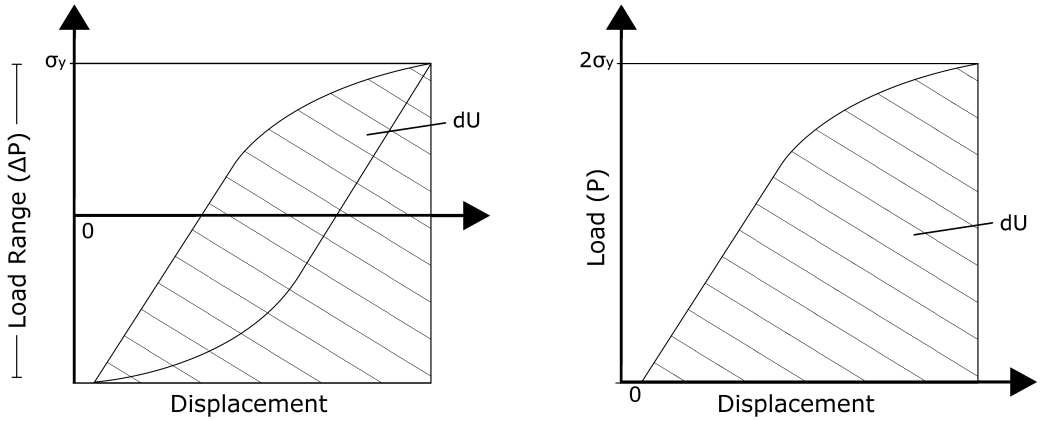

(a) (b)

Figure 6.1: Load displacement curve of (a) cyclic loading condition and (b) MML condition

As already explained in Section 2.6.2, Rice [13] originally defined the J-Integral in two dimensions as:

$$J = \int_{\Gamma} \left(W dy - T' \left(\frac{\partial u}{\partial x} \right) ds \right) \tag{6.1}$$

where T' is the traction vector, u is the displacement vector, ds is an element of arc length along the contour path, Γ, and W is the strain energy density which is given by:

$$W = \int_0^{\varepsilon} \sigma_{ij} d\varepsilon_{ij} \tag{6.2}$$

where ε is an infinitesimal strain tensor.

Tanaka [133] later extended this for cyclic loading between two states, i and j, as:

$$\Delta J_{j/i} = \int_{\Gamma} \left(\Delta W dx_2 - \Delta T' \frac{\partial \Delta u}{\partial dx_1} ds \right) \tag{6.3}$$

Altering the terminology to match Rice's original equation, allows it to be represented as:

$$\Delta J = \int_{\Gamma} \left(\Delta W dy - \Delta T' \frac{\partial \Delta u}{\partial dx} ds \right) \tag{6.4}$$

where δW is the strain energy density range between two states, i and j, which is a

function of the stress and strain range and is given by:

$$\Delta W = \int_{(\varepsilon_{mn})_i}^{(\varepsilon_{mn})_j} [\sigma_{kl} - (\sigma_{mn})_i] d\varepsilon_{kl} \tag{6.5}$$

where σ_{kl} and ε_{kl} are the stress and strain tensors respectively and σ_{mn} and ε_{mn} denote relative changes between values corresponding to the load change from one state to another. It can therefore be seen that the J-Integral is a function of stress and strain, and the cyclic J-Integral is a function of the stress range and strain range as illustrated in Equations 6.6 and 6.7. Therefore, for this concept to be viable and the hypothesis that it is capable of accurately replicating a cyclic loading analysis to hold true, then the stress and strain data from the Modified Monotonic Loading analysis must match the stress range and strain range data from a cyclic loading analysis (Equations 6.8 and 6.9). Using this assumption will then allow the determination of the cyclic J-Integral through the MML concept within ABAQUS. Following such a hypothesis, the cyclic J-Integral values under fatigue loading can be assumed to be equal to the J-Integral values from the Modified Monotonic Loading analysis (Equation 6.10). It is assumed that:

$$J = f(\sigma, \varepsilon) \tag{6.6}$$

$$\Delta J = (\Delta\sigma, \Delta\varepsilon) \tag{6.7}$$

therefore, if

$$\sigma_{MML} = \Delta\sigma_{cyclic} \tag{6.8}$$

and

$$\varepsilon_{MML} = \Delta\varepsilon_{cyclic} \tag{6.9}$$

then,

$$J_{MML} = \Delta J_{cyclic} \tag{6.10}$$

Therefore, for a cyclic loading analysis of a particular load range, the cyclic J-Integral can be approximated by performing a Modified Monotonic Loading analysis with a single load equal to the cyclic range. The computed J-Integral will depend greatly on the applied R-Ratio. In this paper, the MML concept has been demonstrated on a case

of unidirectional stress with $R = 0$. It is important to note, however, that this technique was originally devised for the case of fully reversed stress with an $R = -1$ as described by Chen and Chen [132]. It is believed that this concept performs adequately for the case of $R = -1$ if crack closure is disregarded. However, if crack closure is considered, some differences exist between the cyclic and the MML analyses and so the concept is not felt to be as accurate under these conditions.

6.5 Numerical Application

6.5.1 Finite Element Model

The finite element software package, ABAQUS is used for the computational analyses performed in this investigation. Within ABAQUS, a notched industrial test specimen as presented by Leidermark [134] and shown in Figure 6.2 is modelled employing appropriate model partitioning. A refined mesh is implemented in the most critical region of the notch, whilst a more coarse mesh is modelled in the less critical regions. Second order hexahedral elements are implemented in the model with swept elements in the crack front region, where 20 nodes are defined around the circumference, and structured elements are used elsewhere.

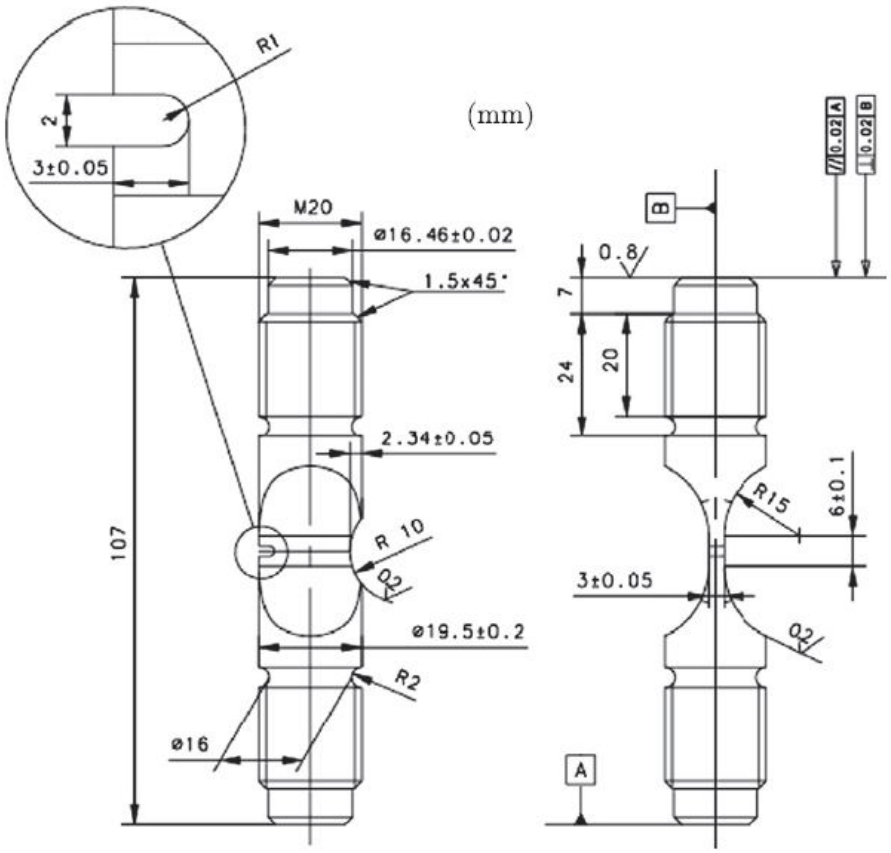

Figure 6.2: The geometry of the investigated test specimen [134]

Within the notch, a 3D semi-elliptical surface crack with a semi-major axis radius of 1mm and a semi-minor axis radius of 0.75mm is modelled with a focused mesh swept along the crack front to allow for improved accuracy. Cyclic and Modified Monotonic Loading analyses are performed and the results of each compared to assess the suitability of the method. Once validated, additional MML analyses are performed to calculate the cyclic J-Integral under uniaxial and out-of-plane shear loading. The finite element mesh of the test specimen is shown in Figure 6.3 and a close-up of the opened crack surfaces is shown in Figure 6.4.

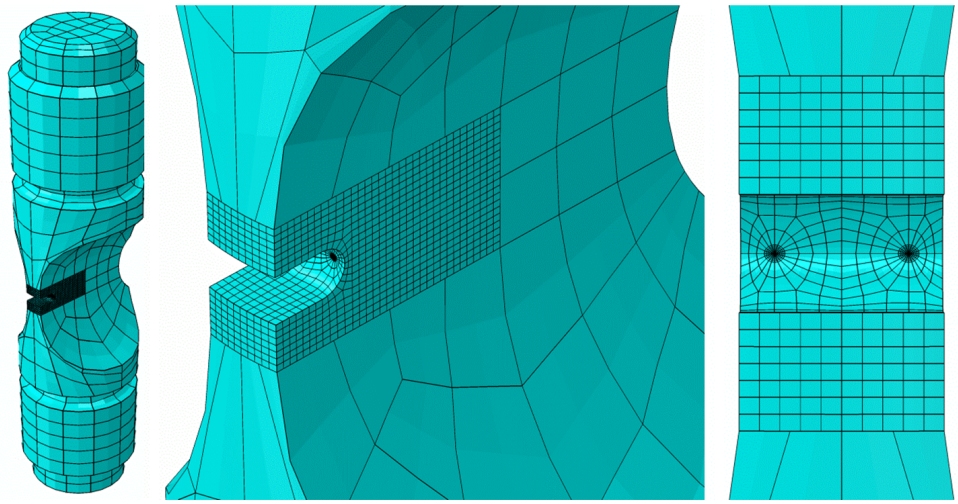

(a) (b) (c)

Figure 6.3: FE mesh of structure showing (a) entire specimen and close-up view of notch (b) and (c)

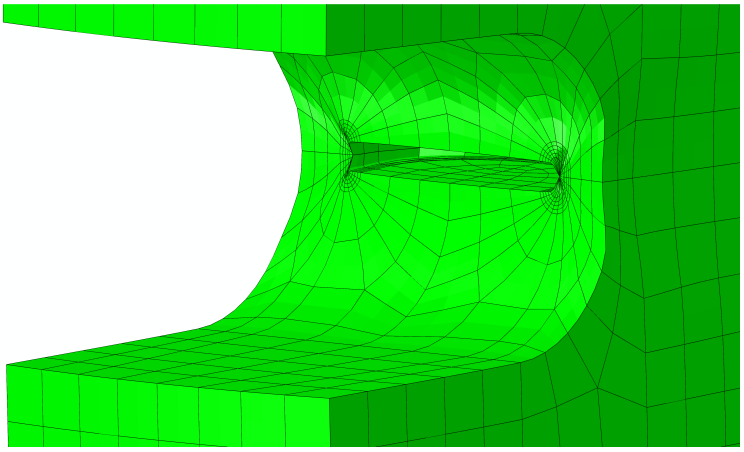

Figure 6.4: Open crack surfaces

6.5.2 Material Properties and Loading Conditions

A nickel-based superalloy similar to those in turbine applications is used in this investigation. An elastic-perfectly plastic material model is implemented with a Young's Modulus of 207GPa, Poissons' Ratio of 0.29 and Yield Stress of 1000MPa. The accuracy of the technique is tested under uniaxial tension and out-of-plane shear with both cyclic loading and Modified Monotonic Loading conditions. This allows the accuracy of the technique to be determined when applied to an industrial test specimen under

different loading conditions. Under uniaxial tension tests, pressure forces are applied to the ends of the specimen. For the cyclic loading analysis, a cyclic load range of 250MPa with a R-Ratio of zero is applied and for the equivalent Modified Monotonic Loading analysis, a monotonic pressure load of 250MPa is applied. Under out-of-plane shear loading, pressure forces are applied to the specimen above and below the notch. For the cyclic loading analysis, a cyclic load range of 600MPa with a R-Ratio of zero is applied and for the corresponding MML analysis, a monotonic pressure load of 600MPa is applied. Diagrams showing the location of the applied forces for uniaxial tension and out-of-plane shear are shown in Figure 6.5 and Figure 6.6 respectively.

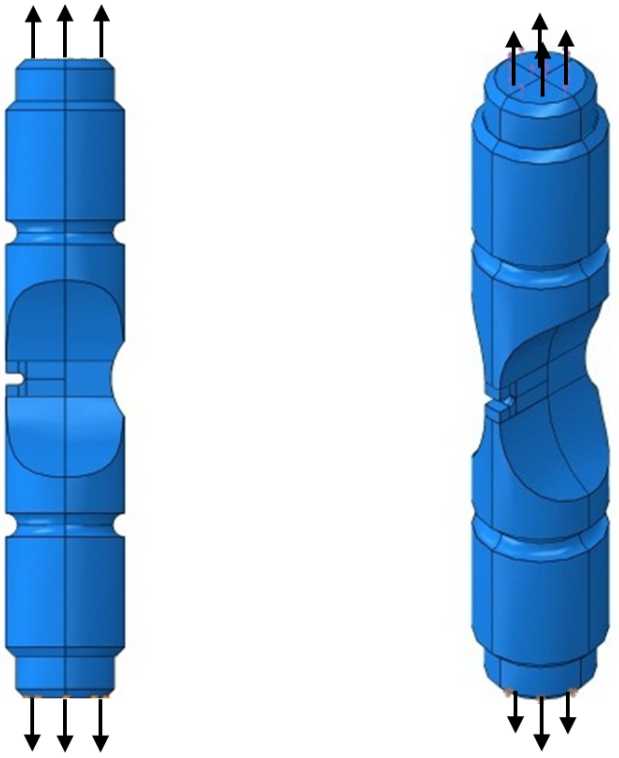

Figure 6.5: Location of applied loads under uniaxial tension conditions

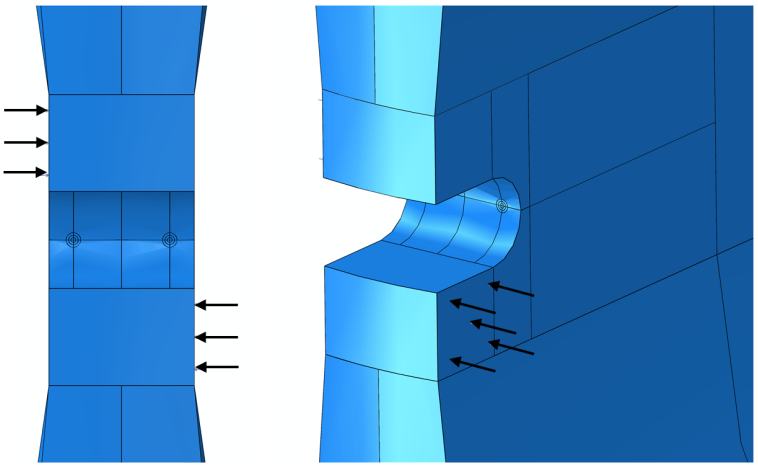

Figure 6.6: Location of applied loads under out-of-plane shear loading conditions

These analyses are merely comparative in order to visualise the differences between the cyclic loading and MML concept. Following successful validation, additional tensile tests and out-of-plane shear tests are performed in order to calculate the cyclic J-Integral using the proposed method.

6.6 Results and Discussion

6.6.1 Validation of MML Concept

The MML results are compared to the cyclic loading analysis to assess the suitability of the technique as a method of calculating the cyclic J-Integral. The stress range and strain range data from the cyclic loading analysis are compared to the stress and strain data of the MML concept. Figures 6.7 to 6.10 show Von Mises stress and Von Mises stress range and Maximum Principal strain and Maximum Principal strain range data from the MML and cyclic loading analyses for the uniaxial tension test. Figures 6.11 to 6.14 show Von Mises stress and Von Mises stress range and Maximum Principal strain and Maximum Principal strain range data from the MML and cyclic loading analyses for the out-of-plane shear test. From comparing the contour plots of the MML and cyclic analyses, it can be seen that the differences between the two are minimal as the contour plots match very closely, generally less than 3%. As is assumed in Equations 6.7 to 6.10, if the stress and strain data of the MML concept matches the stress range and strain range data of the cyclic analysis, then the MML can be assumed to offer a

reasonable approximation of the cyclic J-Integral.

From close inspection of the crack front region, it is noticed that a stress concentration exists at the first contour, where the value is greater than the yield stress. This is believed to be due to crack tip singularities and caused by numerical errors in the finite element calculation. In order to maintain the highest level of accuracy, it is important to greatly refine the mesh in the crack front region. However, due to the complexity of the geometry of the model, the degree to which the mesh can be refined is limited. The aim of this investigation is to provide a direct comparison between the stress and strain solutions of the MML concept and cyclic analyses under two different loading conditions. Since identical meshes are used in each analysis, the importance of a highly refined mesh in the critical regions is less crucial. For this reason, it is believed that this error has little to no effect on the aim of this research and so the meshing rules used in this investigation are believed to be sufficient. However, it is important to consider the effect of the mesh refinement at the crack front when performing detailed analyses for the calculation of the cyclic J-Integral.

It is important to note that a very high pressure load was deliberately applied to the specimen in this test to give a clear indication of the stress concentrations. Due to the presence of the crack, the calculated stresses in ABAQUS greatly exceed the yield. In reality this would not occur since the component would fracture before reaching such high stresses.

This technique means that a simple monotonic analysis is capable of determining the cyclic J-Integral, thus offering a quick and computationally inexpensive method of determining the ΔJ, which would otherwise be difficult and time consuming to calculate. From Equation 2.15, it can provide an invaluable method of predicting the EPFM fatigue life of a component. Some minor discrepancies exist between the contour plots of the MML and the cyclic loading analysis, however these differences are small and the differences generally occur at single node locations, likely as the result of FE numerical errors, whilst more globally, the differences are much less significant. For this reason, these results are believed to be reasonable. It is felt that the speed and ease of implementation and calculation of this technique far outweighs any potential loss in accuracy.

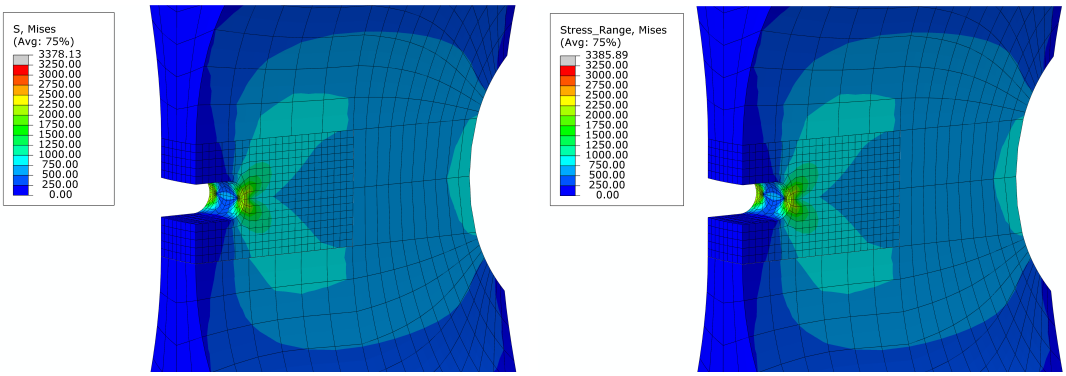

(a) (b)

Figure 6.7: Contour plots of: (a) stress from MML analysis and (b) stress range from cyclic loading analysis under uniaxial loading conditions

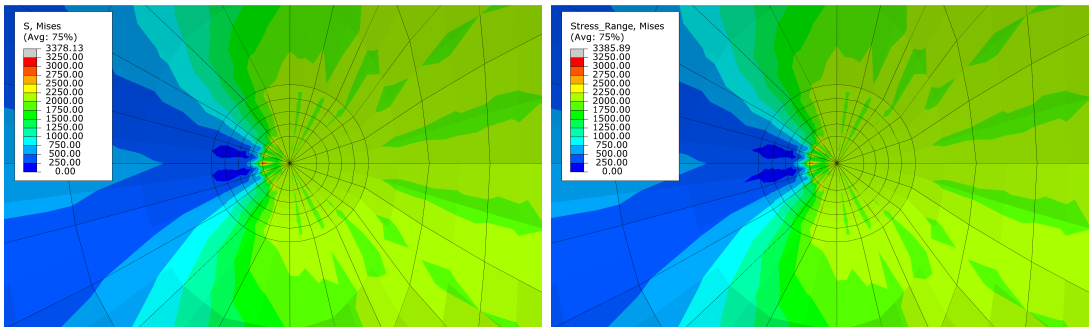

(a) (b)

Figure 6.8: Enlarged view of contour plots of crack tip of: (a) stress from MML analysis and (b) stress range from cyclic loading analysis under uniaxial loading conditions

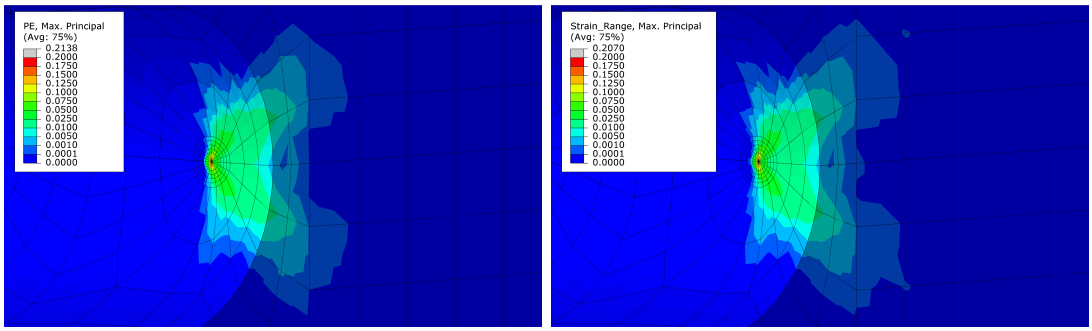

(a) (b)

Figure 6.9: Contour plots of: (a) strain from MML analysis and (b) strain range from cyclic loading analysis under uniaxial loading conditions

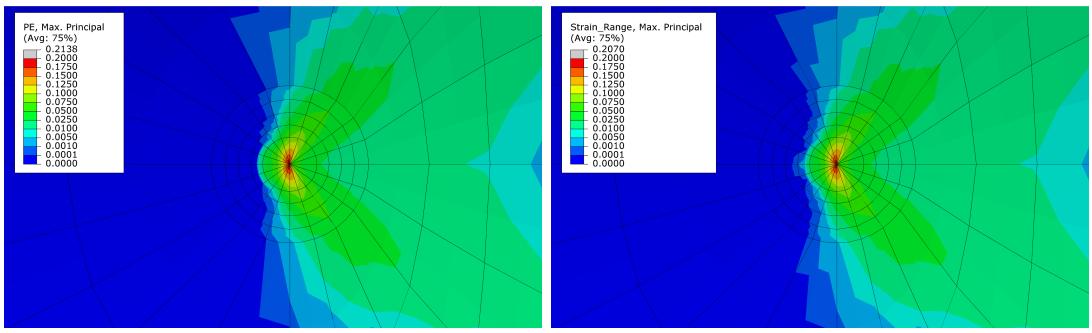

(a) (b)

Figure 6.10: Enlarged view of contour plots of crack tip of: (a) strain from MML analysis and (b) strain range from cyclic loading analysis under uniaxial loading conditions

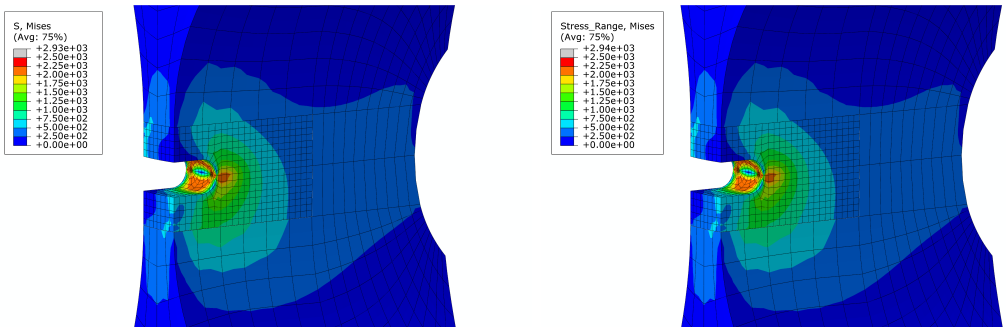

(a) (b)

Figure 6.11: Contour plots of: (a) stress from MML analysis and (b) stress range from cyclic loading analysis under out-of-plane shear loading conditions

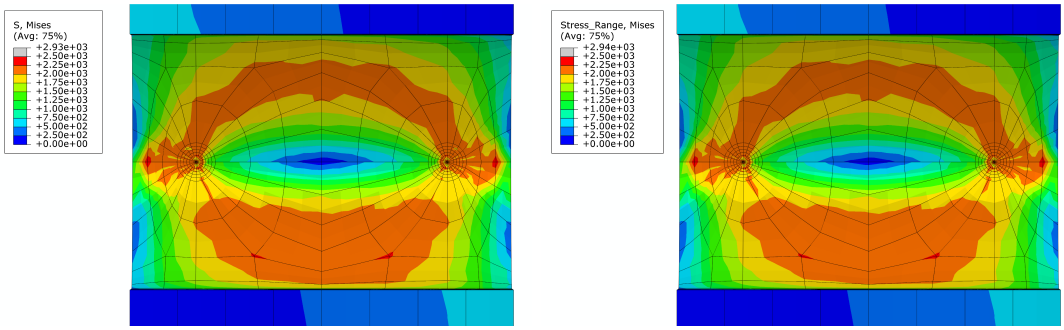

(a) (b)

Figure 6.12: Enlarged view of contour plots of crack front of: (a) stress from MML analysis and (b) stress range from cyclic loading analysis under out-of-plane shear loading conditions

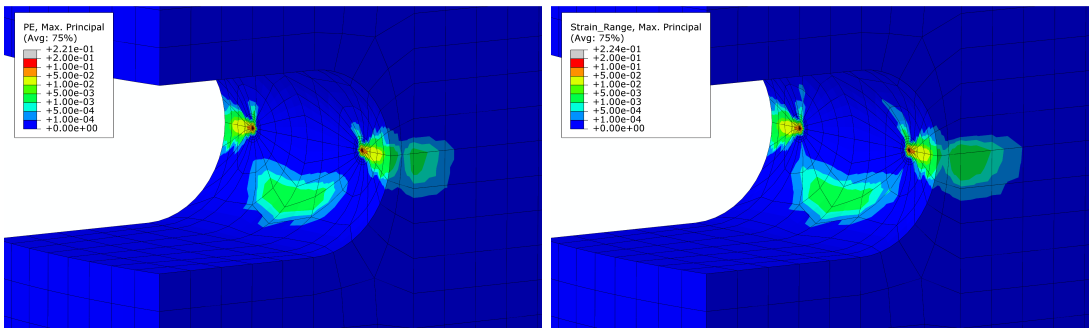

(a) (b)

Figure 6.13: Contour plots of: (a) strain from MML analysis and (b) strain range from cyclic loading analysis under out-of-plane shear loading conditions

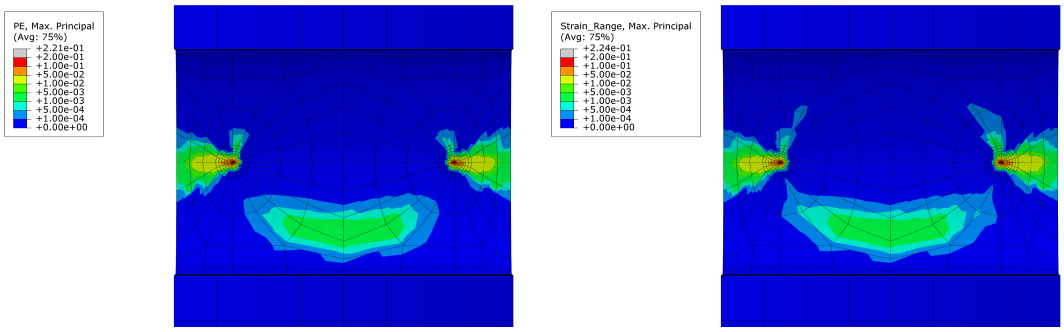

(a) (b)

Figure 6.14: Enlarged view of contour plots of crack front of: (a) strain from MML analysis and (b) strain range from cyclic loading analysis under out-of-plane shear loading conditions

6.6.2 Determination of cyclic J-Integral using the MML

An additional uniaxial tension test and out-of-plane shear test are now performed on the specimen and the induced cyclic J-Integral is recorded. The ΔJ values at different locations along the crack front are monitored in addition to the variation of ΔJ with applied load. The number of nodes that are defined along the crack front are assigned through the mesh refinement. For this investigation, the employed meshing rules implement 25 nodes along the circumference of the crack front. Figure 6.15 shows a schematic diagram of the crack front showing the node locations and numbers.

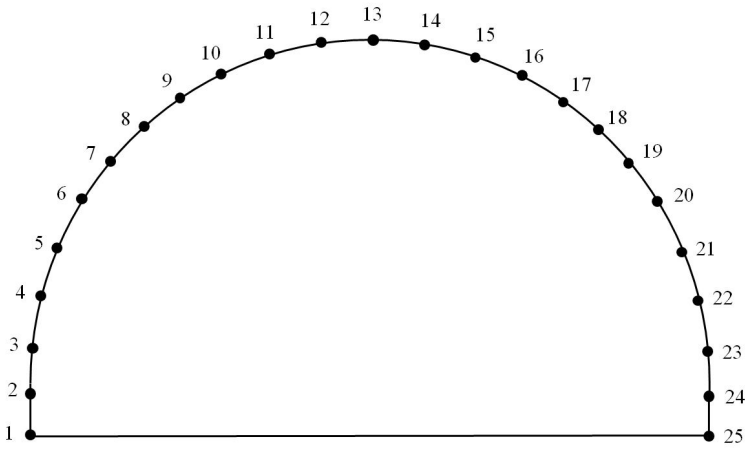

Figure 6.15: Schematic diagram showing node numbering

Node 1 is located at the far left crack edge and Node 25 is located at the far right crack edge when facing the crack opening. These node numbers are referred to in the results in Table 6.1 and 6.2, and Figures 6.19 and 6.20. For each node along the crack front, the ΔJ is calculated at 5 contours encircling the crack front. This is illustrated in Figure 6.16.

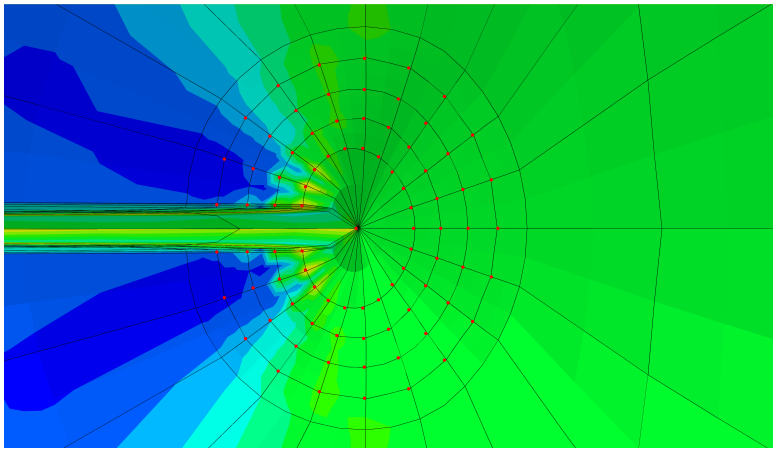

Figure 6.16: Enlarged view of crack tip showing contour paths

The 5 contours at each node are averaged to give a single mean value at each node along the crack front. This is believed to be accurate since the J-Integral is a path-independent parameter [13], meaning that the value is the same, regardless of the path along which it is calculated. Within ABAQUS, numerical errors due to crack tip singularities indicate that the values at each contour are not exactly equal, but any

differences are very small and so mean average values are believed to be sufficiently accurate. Values of the cyclic J-Integral at each contour path at each load are shown in Table 6.3 for uniaxial tension and Table 6.4 for out-of-plane shear loading. It can be seen that the first contour is slightly different to the remaining 4 contours, which have close agreement. This demonstrates the differences that occur at the crack tip due to numerical errors are very minor and so the J-Integral can be assumed to be path independent. The single values at each node are then tabulated and the average and maximum recorded, as well as far left end of crack, centre of crack and far right end of crack, shown in Table 6.1 for uniaxial tension, and Table 6.2 for out-of-plane shear. These values of the J-Integral provided here are obtained by the traditional elastic plastic fracture mechanics FEA using the MML concept. From the original hypothesis, the J integral calculated from the MML concept is assumed to be equal to the cyclic J-Integral of a cyclic loading analysis when the applied load range is equal to the magnitude of the load in the tables. Therefore these presented values can be regarded as the cyclic J-Integral.

Table 6.1: Cyclic J-integral variation with increasing uniaxial load

	J-Integral (MPa.mm)				
Load (MPa)	Average	Max	Crack Left (Node 1)	Crack Centre (Node 13)	Crack Right (Node 25)
12.5	0.0478	0.1023	0.1022	0.0276	0.1023
25	0.1912	0.4090	0.4088	0.1105	0.4090
50	0.7631	1.6015	1.6008	0.4422	1.6015
75	1.7005	3.3309	3.3298	0.9972	3.3309
100	2.9941	5.5183	5.3354	1.7783	5.3370
125	4.6408	8.3802	7.5034	2.7918	7.5046
150	6.6734	11.8929	9.8692	4.0571	9.8653
175	9.1552	16.5454	12.5029	5.6038	12.4929
200	12.1294	21.9518	15.4460	7.4913	15.4342
225	15.6357	28.1072	18.6470	9.7715	18.6323
250	19.7118	34.9707	22.1816	12.5141	22.1594

Table 6.2: Cyclic J-integral variation with increasing out-of-plane shear load

	J-Integral (MPa.mm)				
Load (MPa)	Average	Max	Crack Left (Node 1)	Crack Centre (Node 13)	Crack Right (Node 25)
30	0.0149	0.0405	0.0405	0.0048	0.0402
60	0.0596	0.1619	0.1619	0.0191	0.1609
120	0.2378	0.6376	0.6376	0.0765	0.6335
180	0.5347	1.4277	1.4277	0.1737	1.4190
240	0.9501	2.4856	2.4856	0.3133	2.4715
300	1.4805	3.7501	3.7501	0.5024	3.7321
360	2.1367	5.1968	5.1968	0.7363	5.1731
420	2.9299	6.8236	6.8236	1.0339	6.7934
480	3.8784	8.6282	8.6282	1.4173	8.5911
540	5.0106	10.6364	10.6364	1.8828	10.5925
600	6.4210	12.9883	12.9883	2.4636	12.9380

Table 6.3: The variation of the cyclic J-integral at each contour path under uniaxial tensile loading

Uni-axial Tension			
Average Cyclic J-Integral at Contours 1 to 5 (Averaged from all 25 Nodes) (MPa.mm)			
	Load (MPa)		
Contour	25	125	250
1	0.184621	4.251451	17.03563
2	0.192854	4.733544	20.19799
3	0.192909	4.740572	20.39367
4	0.192873	4.73978	20.45251
5	0.192776	4.738423	20.47896
Maximum Cyclic J-Integral at Contours 1 to 5 (Maximum of all 25 Nodes) (MPa.mm)			
	Load (MPa)		
Contour	25	125	250
1	0.392916	7.49406	29.666
2	0.414454	8.54818	35.9647
3	0.413202	8.60067	36.4048
4	0.412717	8.62294	36.4568
5	0.411896	8.63546	36.4538

Table 6.4: The variation of the cyclic J-integral at each contour path under out-of-plane shear loading

Out-of-plane Shear			
Average Cyclic J-Integral at Contours 1 to 5 (Averaged from all 25 Nodes) (MPa.mm)			
	Load (MPa)		
Contour	60	300	600
1	0.057376	1.342511	5.574633
2	0.060203	1.512485	6.611787
3	0.060199	1.51548	6.644833
4	0.060197	1.516003	6.638904
5	0.060185	1.515926	6.634665
Maximum Cyclic J-Integral at Contours 1 to 5 (Maximum of all 25 Nodes) (MPa.mm)			
	Load (MPa)		
Contour	60	300	600
1	0.152483	3.2396	10.9881
2	0.164193	3.8566	13.4225
3	0.164206	3.88042	13.5450
4	0.164372	3.88744	13.5083
5	0.164298	3.88661	13.4778

Figure 6.17 and Figure 6.18 show the cyclic J-Integral variation with increasing uniaxial and out-of-plane shear load at different locations along the crack front. Under uniaxial loading (Figure 6.17), it can be seen that the mean average, crack left and crack right agree closely due to the symmetry of the loading conditions, however, the maximum value is considerably higher and the crack centre is lower. Upon closer investigation, it was found that the variation of the ΔJ along the crack front varies widely. Figure 6.19 shows this for applied uniaxial tension monotonic loads of 250MPa and 125MPa. A maximum ΔJ value occurs slightly inside from the end of the crack, 3 nodes from each end and a minimum value occurs in the central region of the crack, where it is relatively constant. However the maximum and minimum values differ by a factor of 3. The variation of rate of change of cyclic J-Integral with increasing load

is not linear across the length of the crack. With increasing load, the maximum ΔJ values increase more rapidly and the minimum values increase more slowly relative to the values at the centre of the crack. Under out-of-plane shear loading (Figure 6.18), it can be seen that the J-Integral relationship with increasing load is very different to that of uniaxial tension. Figure 6.20 shows the variation of ΔJ along the crack front under out-of-plane shear forces of 600MPa and 300MPa. The maximum cyclic J-Integral coincides with the crack left and crack right positions with the crack centre being considerably less. This variation of ΔJ is due to the asymmetry of the loading conditions. This implies that the likeliest point of crack initiation under out-of-plane shear loading is at each side of the crack. The relationship is much more uniform than that of uniaxial tension with the maximum values occurring at the crack edge. The ΔJ steadily decreases along the crack front to a minimum at the centre with the maximum and minimum values differing by a factor of 5. The rate of change of ΔJ along the crack front is much more uniform than that of uniaxial tension.

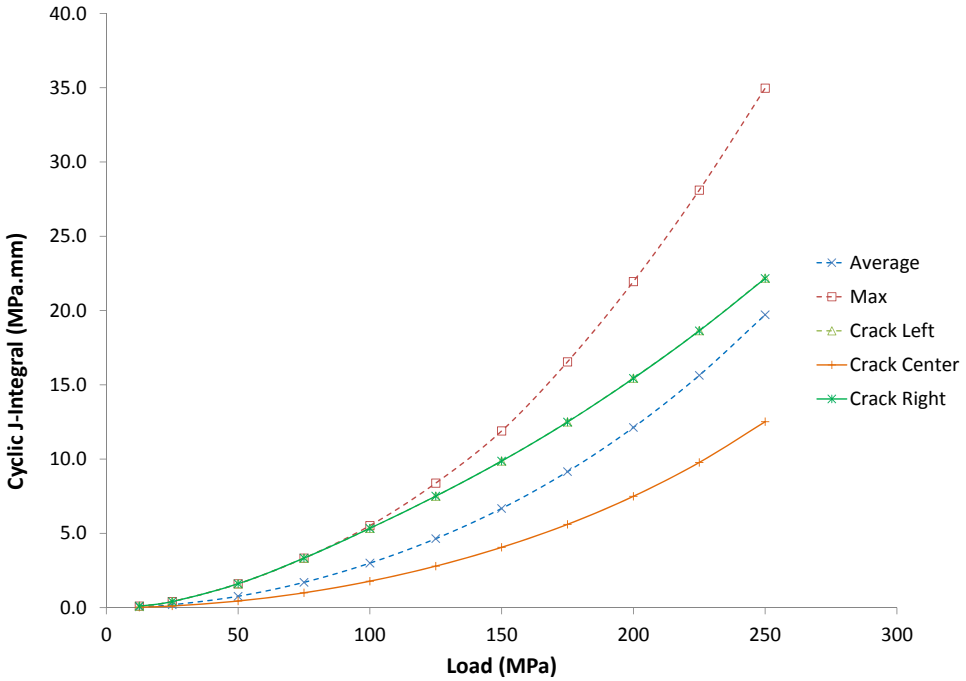

Figure 6.17: ΔJ-Integral variation with increasing uniaxial load

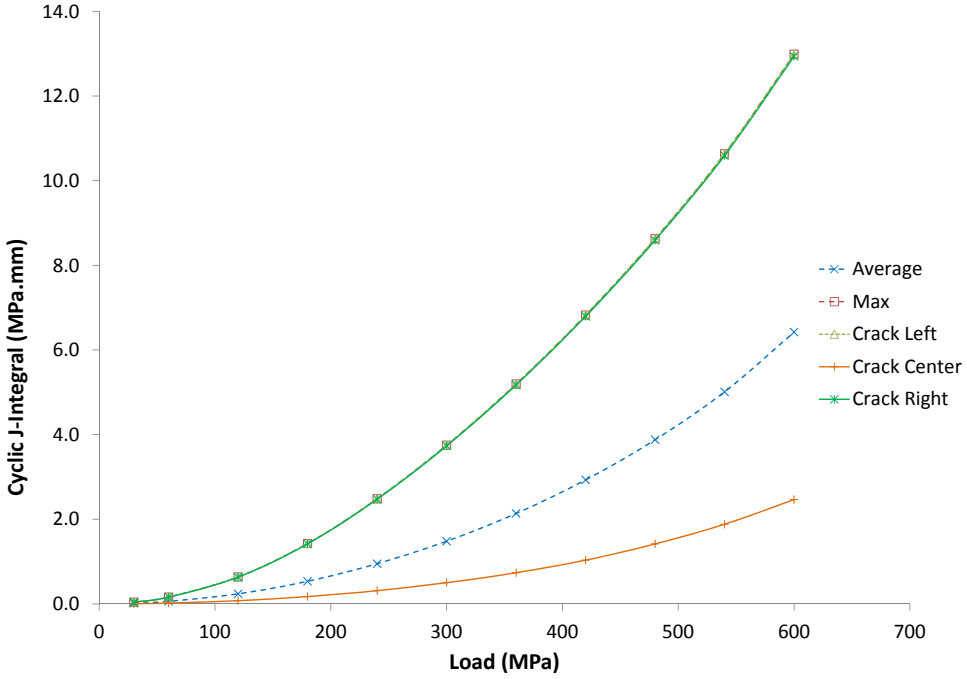

Figure 6.18: ΔJ-integral variation with increasing out-of-plane shear load

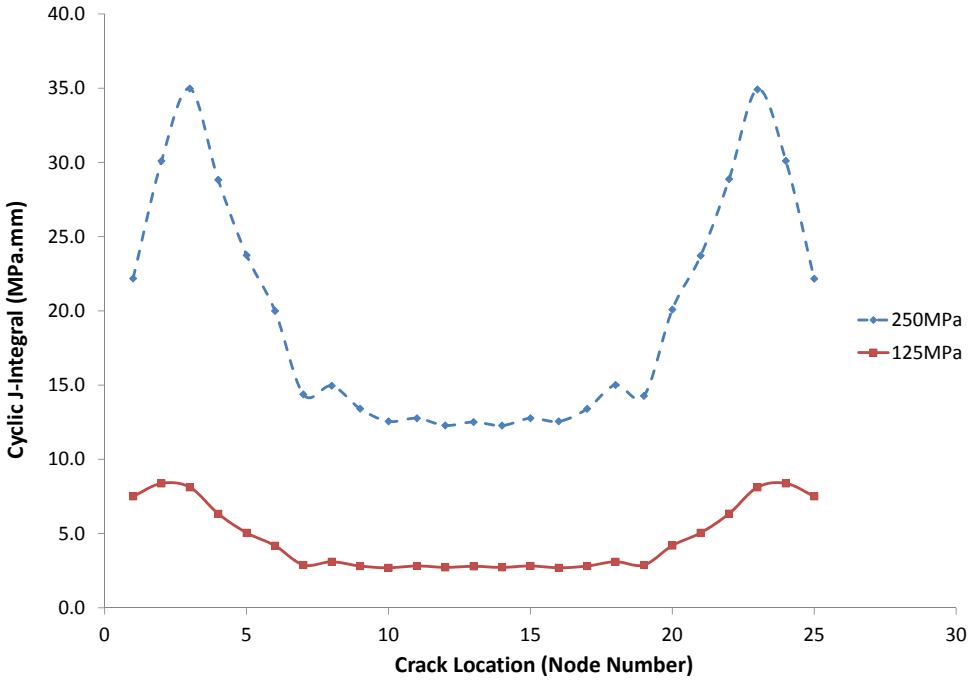

Figure 6.19: ΔJ-variation along crack front under uniaxial tension loading conditions

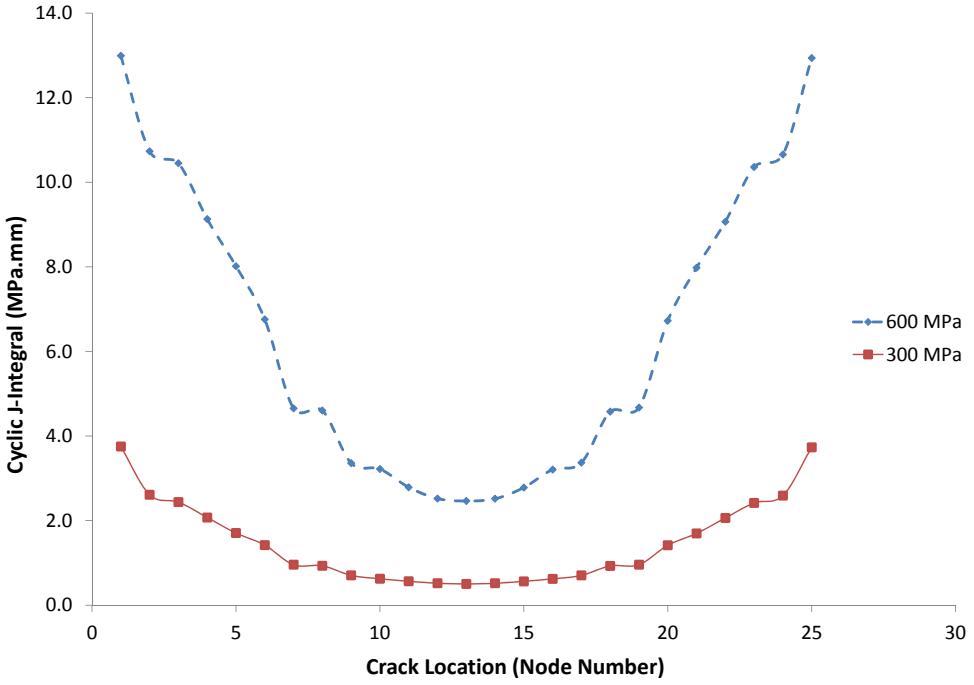

Figure 6.20: ΔJ-integral variation along crack front under out-of-plane shear loading conditions

6.7 The use of the ΔJ for the calculation of fatigue Life

Once the cyclic J-integral is known, it can be used to determine the crack growth rate and fatigue life through the Dowling & Begley Law (Equation 2.15). However, a problem arises when determining the material constants C' and m'. The standard Paris Law parameters C and m exist for a range of materials which have been determined experimentally through extensive testing. However, due to the relative infancy of the cyclic J-integral as a fatigue parameter, and the general preference of the SIF within industrial applications, such extensive testing has not yet been performed to determine the Dowling & Begley parameters C' and m'. This poses an issue when using the cyclic J-integral for fatigue analysis. Fortunately, it is possible to convert existing Paris Law parameters into their cyclic J counterparts as explained by McGlung et al. [135](p.66-67).

As explained in Chapter 2, for a monotonic loading history, the J integral can be directly related to the stress intensity factor (Equation 2.6), so that:

$$J = \frac{K^2}{E'} \tag{6.11}$$

where $E' = E$ for plane stress conditions and $\frac{E}{1-\nu^2}$ for plane strain conditions and E is the Young's Modulus. A simple extension of this relationship can be made to allow for a cyclic loading history by considering the stress intensity factor range between maximum and minimum loading, so that:

$$\Delta J = \frac{\Delta K^2}{E'} \tag{6.12}$$

Using this relationship, a convenient conversion between the standard Paris Law constants and their ΔJ equivalent can be established, allowing the Dowling and Begley relationship to offer a viable alternative to the Paris Law for fatigue life assessment under the presence of plasticity. Considering Equation 6.12 and rearranging for ΔK gives:

$$\Delta K = (\Delta J E')^{\frac{1}{2}} \tag{6.13}$$

which can be substituted into the Paris Law (Equation 2.14), so that:

$$\frac{da}{dN} = C((\Delta J E')^{\frac{1}{2}})^m \tag{6.14}$$

which by simplifying becomes:

$$\frac{da}{dN} = C{E'}^{\frac{m}{2}} \Delta J^{\frac{m}{2}} \tag{6.15}$$

therefore, letting $C{E'}^{\frac{m}{2}} = C'$ and $\frac{m}{2} = m'$, then the Paris Law becomes:

$$\frac{da}{dN} = C' \Delta J^{m'} \tag{6.16}$$

which is equal to the Dowling & Begley law and thus it can be seen that the Paris Law constants C and m can be converted to their ΔJ counterparts by:

$$C' = C\left(E'\right)^{\frac{m}{2}} \tag{6.17}$$

and

$$m' = \frac{m}{2} \tag{6.18}$$

With a conversion established, provided that sufficient material data is available, it is possible to calculate the crack propagation rate of a cracked component in the presence of plasticity using the MML method, further highlighting its importance for use in fatigue crack growth assessment.

6.8 Chapter Summary

This study has proposed and validated the Modified Monotonic Loading concept as a technique for the calculation of the cyclic J-Integral. A cyclic loading analysis was performed on an industrial test specimen under different loading conditions in order to establish a benchmark onto which the MML concept can be validated. The MML concept was then applied to the same test specimen under equivalent monotonic loading. The stress and stress range and strain and strain range data of the MML and cyclic loading analyses were compared to assess the suitability of the technique for the calculation of the cyclic J-Integral. Once validated, additional analyses were performed on the test specimen which facilitated the calculation of the cyclic J-Integral. The variation with increasing load as well as along the crack front was recorded and the following observations were made:

1. Under uniaxial tension, the maximum ΔJ occurs slightly inside from the crack edge with the minimum being at the centre.

2. Under out-of-plane shear loading, the maximum ΔJ occurs at the crack edges, with the minimum being located at the crack centre.

This technique allows the three-dimensional crack front detail of the cyclic J-Integral to be monitored and as a result it is possible to identify the likely points of crack propagation, allowing the crack growth path to be predicted. This technique can also be applied to bespoke specimens and is not limited to documented test cases such as compact tension specimens. These features are the main strengths of this concept, making it advantageous compared to other existing techniques such as the RSM and

GE/EPRI methods. This concept is inexpensive both in time and computational power and can be implemented on complex industrial specimens with great ease offering a viable and preferable method of calculating the cyclic J-Integral.

Finally, a method for the calculation of the crack propagation rate has been established through a conversion of Paris law data into their elastic plastic equivalent for use in the Dowling & Begley law.

Chapter 7

The Proposal of a Complete Crack Modelling Procedure

7.1 Introduction

This chapter combines all the computational methods that have been developed in the previous chapters and implements them into a procedure for a complete crack modelling analysis for complex industrial applications. This includes the calculation of the crack initiation fatigue life, the location of crack initiation and the loads required to cause such failure, the crack propagation fatigue life and the crack growth path, thus addressing the principal components of fracture mechanics as introduced in Section 2.1.1, providing a complete understanding of fatigue crack behaviour, by identifying the following characteristics of the crack:

1. *Where* - the location of crack initiation and the direction of crack growth
2. *When* - the number of cycles required for the crack to initiate and the number of additional cycles that can be endured before the crack grows to a critical length at which point, instantaneous collapse occurs
3. *How* - the precise load at which crack initiation will occur

The proposed procedure allows a full, in depth crack assessment to be performed, either to model predefined applied loading conditions to replicate a real component, or

to design a prospective test case. The general structure of the procedure comprises 4 steps. Step 1 identifies the likely point of crack initiation, Step 2 determines the precise loads at which crack initiation occurs and the number of cycles that can be endured before the crack initiates. Step 3 re-models the crack identified in Step 1 and performs advanced crack propagation analyses including the R5 procedure and the Modified Monotonic Loading Concept (MML) to calculate the cyclic J-Integral, ΔJ. This allows an understanding of the crack growth behaviour to be obtained and the crack growth rate to be calculated. Step 4 reviews and combines Steps 1-3 to determine the complete fatigue life and fracture behaviour. This results in the prediction of the crack location and growth direction and fatigue life to crack initiation and propagation. The outline process is illustrated in Figure 7.1 and greater detail of each step of the procedure is provided in the following section.

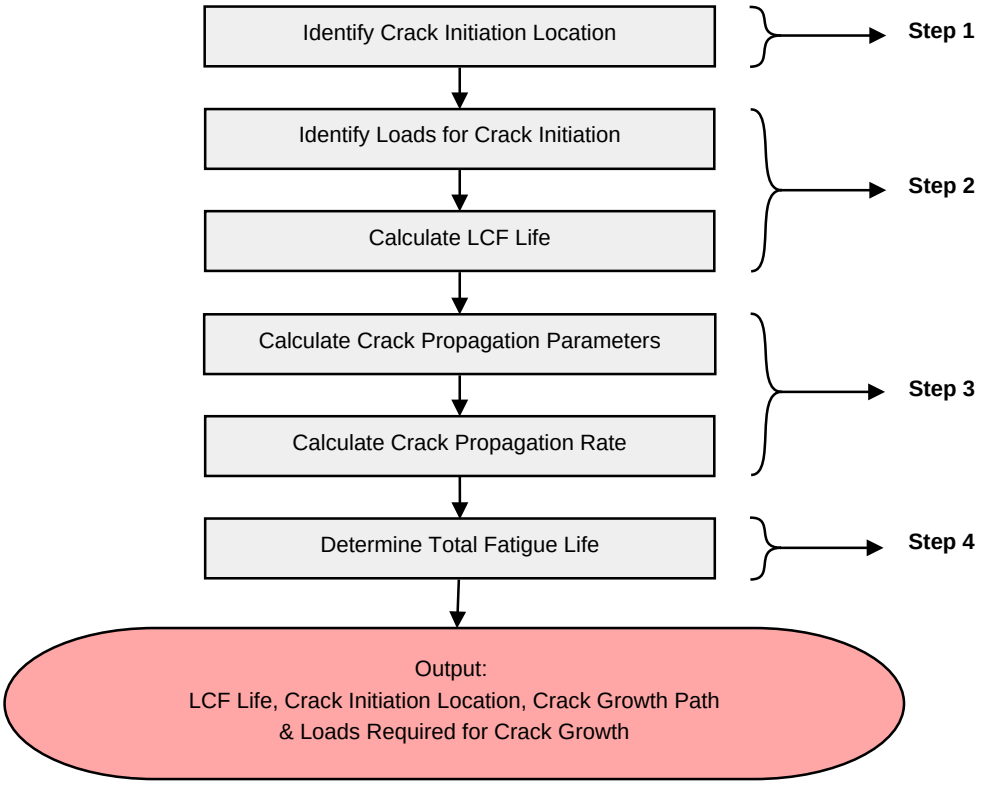

Figure 7.1: Crack assessment procedure process flow diagram

7.1.1 Input Requirements

Before commencing the crack assessment, a number of prerequisites must be established. The geometry to be analysed must be modelled and meshed to a suitable level of refinement and a number of material properties are also required. Values of the Young' Modulus, E, Poisson's ratio, ν and Yield stress, σ_y must be assigned to the model. The Paris law constants C and m (or Dowling & Begley law constants, C' and m') and strain based LCF data must also be known, however, these are not implemented in the FE model and are used for post processing purposes.

7.1.2 Step 1 - Determine Crack Initiation Location

This procedure commences with the identification of the location of crack initiation. This preliminary investigation identifies the most critical regions of the analysis, allowing the appropriate mesh refinement to be implemented in the subsequent analyses. The crack initiation location can be identified by performing an eXtended Finite Element (XFEM) Analysis. This simulates the crack growth direction, but as discussed in Chapter 3, the extent of the analysis capabilities are currently limited and so XFEM is used merely for illustrative purposes to identify the critical areas and the crack location.

It is also possible to determine the crack initiation location from a shakedown assessment for all points in the model or to perform a Neuber correction local strain based LCF analysis. These results can then be visualised in a contour plot to show the life locations.

Depending on the specimen geometry, the crack initiation location may be predicted without the use of such extensive analysis and so if the user is confident that the location of crack initiation can be accurately predicted, for example on a notched bar, this step can be skipped and the analysis can proceed directly to Step 2.

7.1.3 Step 2 - Predict Fatigue Life to Crack Initiation

In Step 2, the Reversed Plasticity Domain Method (RPDM), proposed in Chapter 5, is used to determine the loads required for crack initiation. This can then be used to design a prospective experimental test and to select a design load, or to assess actual conditions experienced by a component.

For the design of a test, as in Chapter 5, an appropriate design load can be selected from a suitable range. For modelling a real component, the load range required for causing crack initiation, calculated using the RPDM, can be compared to the actual load experienced by the component to determine whether or not it is within the range suitable for causing crack initiation. Once the design load is either chosen, or determined to be within the range for crack initiation, then a full low cycle fatigue test can be performed to calculate the number of cycles to crack initiation for the selected load. Once the design loads and fatigue life are determined, the user can proceed to step 3.

7.1.4 Step 3 - Calculate Crack Propagation Parameters & Growth Rate

Step 3 considers crack growth and involves the calculation of crack propagation parameters. There are a number of different parameters that are suitable, depending on the material properties and conditions of the component in question. This procedure can consider either the cyclic stress intensity factor, ΔK for purely elastic material models or the cyclic J-integral, ΔJ for material models that include plasticity. Once the appropriate parameter is determined, the crack growth rate can be calculated using a suitable crack growth law such as the Paris Law or Dowling & Begley Law. However, this requires suitable material crack growth behaviour and Paris law or Dowling & Begley law constants. The method of calculation of these parameters depends on the particular analysis and set of conditions. For modelling plasticity, the ΔJ is the most suitable, where as for elastic behaviour, the SIF would be appropriate. The MML concept, as proposed in Chapter 6 offers a suitable method for the calculation of the ΔJ parameter. The ΔK can be calculated using the in-built contour integral calculation capabilities of ABAQUS or from SIF handbooks, if appropriate.

However, there also exist a number of different methods of calculating these parameters including the R5 procedure, Reference Stress Method and GE-EPRI method. The choice of method again depends on the exact conditions of the analysis being performed but each can be implemented into this procedure. The crack growth rate per cycle can then be converted to the total crack propagation life.

7.1.5 Step 4 - Determine Total Fatigue Life

The final step combines the results from Steps 1-3 to perform the full crack assessment. The fatigue life to crack initiation and number of cycles for crack growth can be summed to give the total number of cycles to complete failure. The crack initiation location and crack growth path have also been determined, providing a complete analysis of the crack.

7.1.6 Procedure Overview

This procedure allows a complete fatigue crack growth assessment to be performed, providing important crack information with relative ease. The novel techniques presented in this thesis, allow the assessment to be performed for highly complex cases and materials properties, in a fast and efficient manner, whilst still maintaining a high level of accuracy. This makes this procedure more efficient, and less computationally intensive, than other currently existing techniques.

A process flow diagram illustrating each stage of the procedure as described in Sections 7.1.2 to 7.1.5 is shown in Figures 7.2 to 7.5.

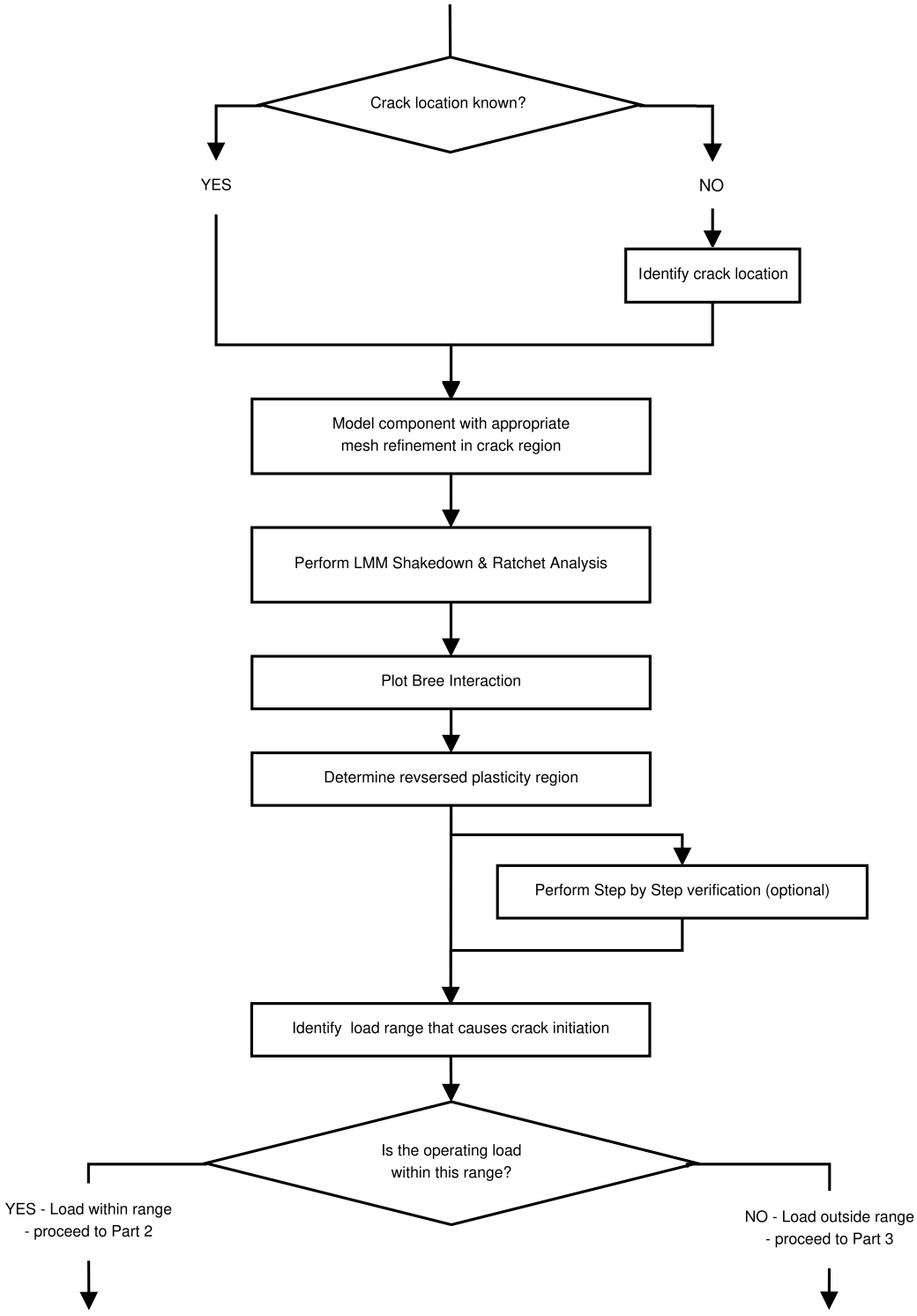

Figure 7.2: Crack Assessment Procedure Process Flow

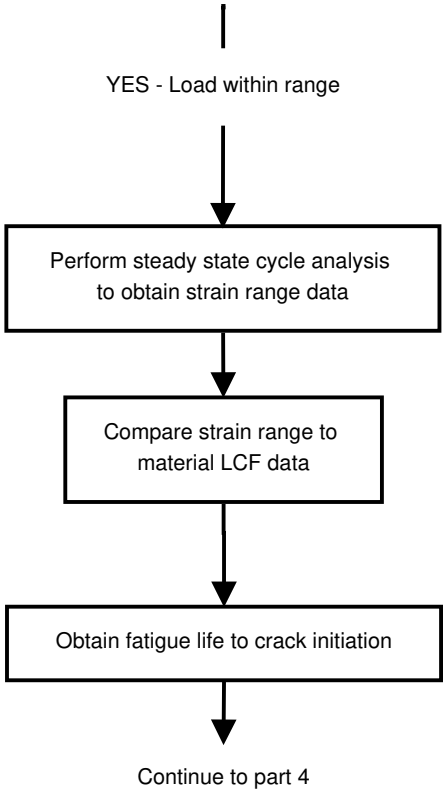

Figure 7.3: Crack Assessment Procedure Process Flow - Part 2

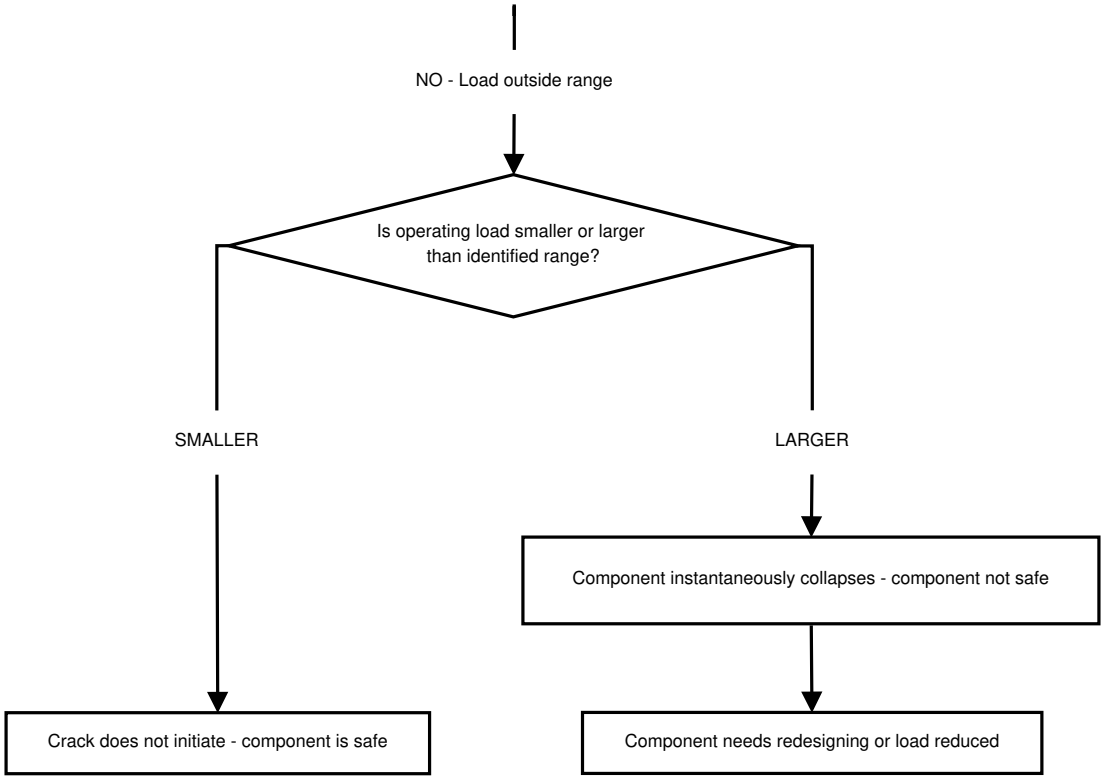

Figure 7.4: Crack Assessment Procedure Process Flow - Part 3

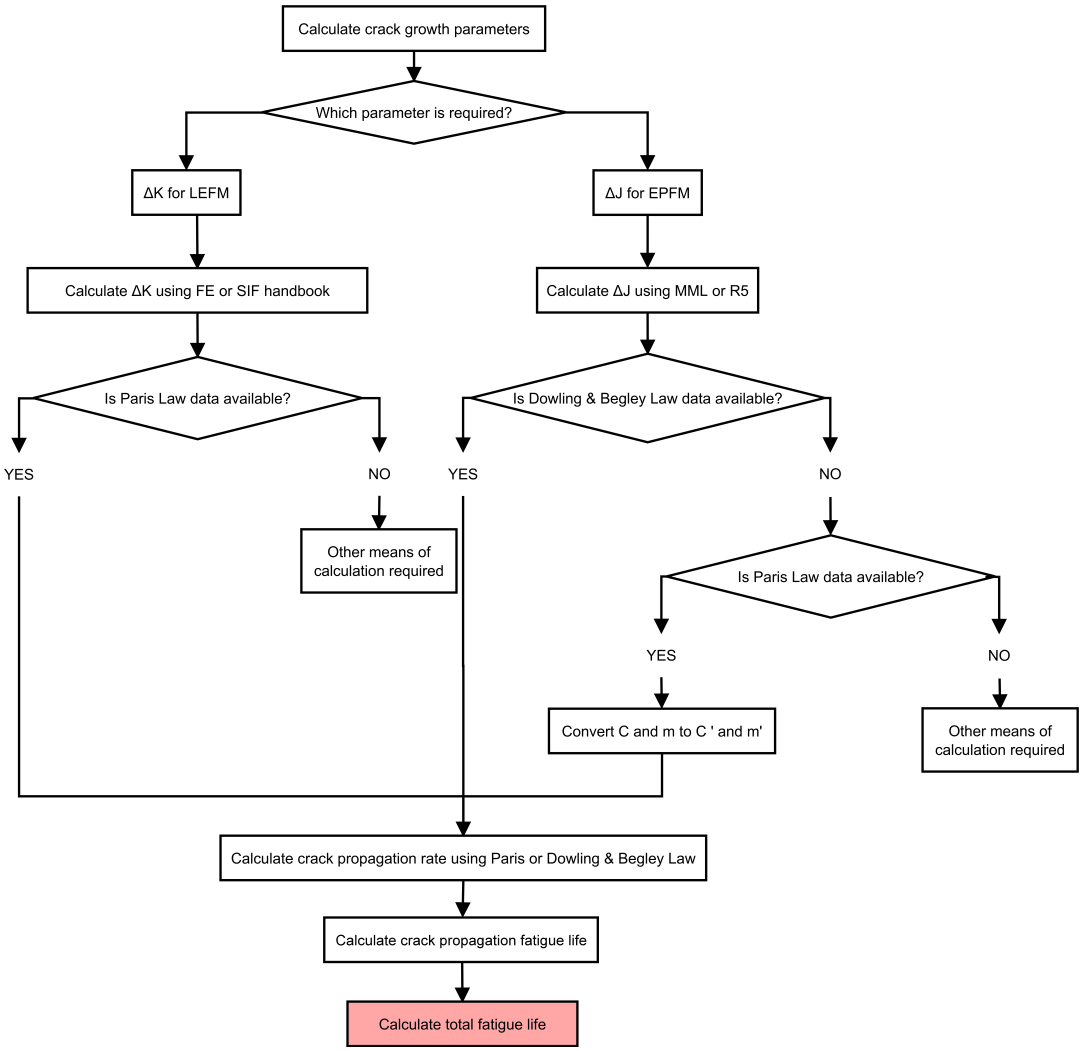

Figure 7.5: Crack Assessment Procedure Process Flow - Part 4

7.2 Implementation of Procedure

In order to demonstrate the proposed procedure, a case study is performed in which the technique is applied to a simple case of a holed plate.

Specimen Geometry & Loading Conditions

A holed square plate of side length 50mm and centre hole radius of 5mm is modelled as shown in Figure 7.6. It is made of a material with Young's Modulus of 178GPa, Poisson's ratio of 0.33 and yield stress of 648MPa. The plate is subject to a temperature load of 500 °C in the centre hole and 20 °C at the outside edges. In addition, a uniaxial

tensile load of 400MPa is applied to the top edges. Symmetry boundary conditions are applied on the left and bottom faces to simulate a complete square plate of side length 100mm as shown in Figure 7.7.

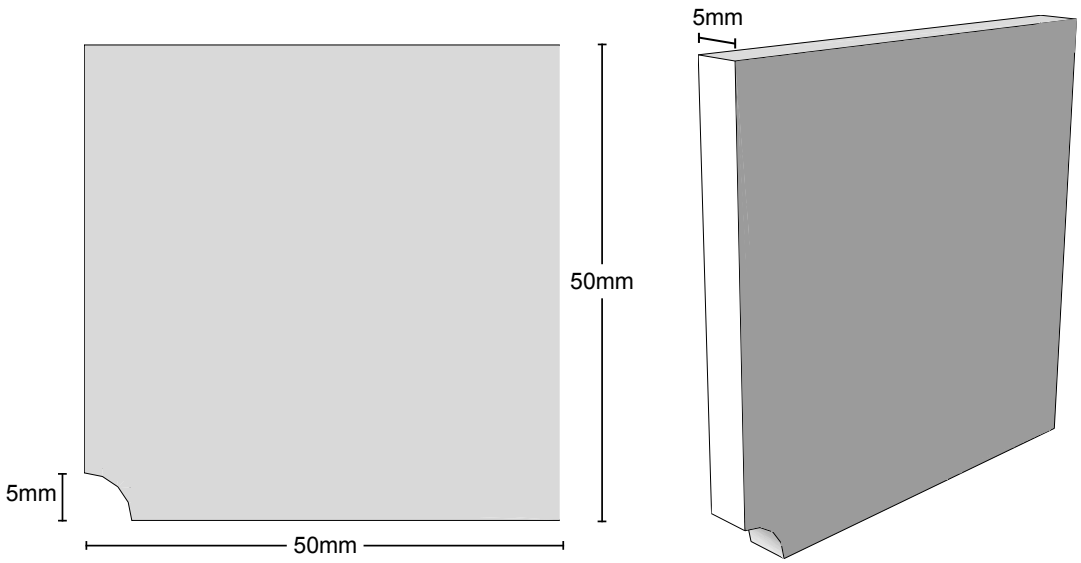

Figure 7.6: Dimensions of holed plate

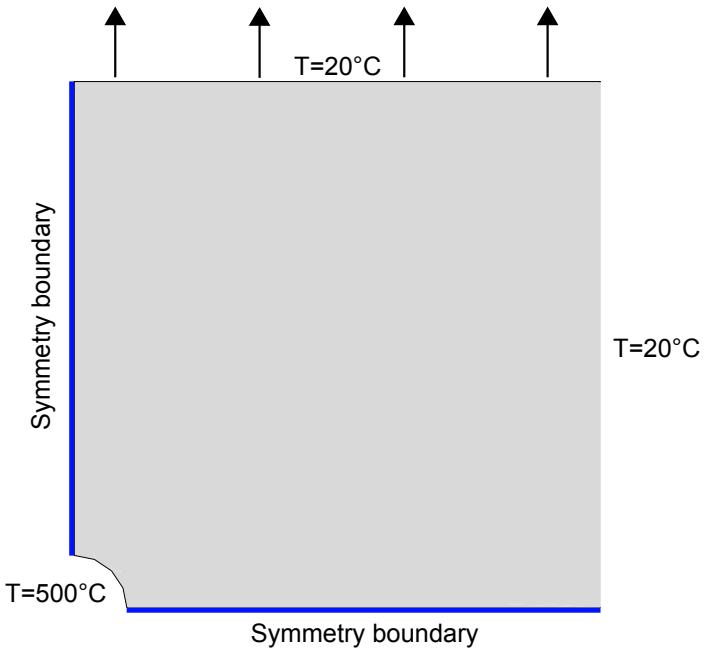

Figure 7.7: Diagram showing applied loads on holed plate

7.2.1 Step 1 - Identify Crack Initiation Location Using XFEM Analysis

The XFEM analysis is performed to identify the crack location and the results of this are given in Figure 7.8, clearly showing the crack path. Figure 7.8 (a) shows the PHI Level Set Method contour plot, which as explained in Chapter 3, illustrates the proximity to the crack front. Figure 7.8 (b) is the Status XFEM contour plot which clearly highlights the elements that are cut by the crack front by highlighting the cut elements in red. Figure 7.9 shows the stress contour of the crack path, all clearly highlighting the location of the crack path.

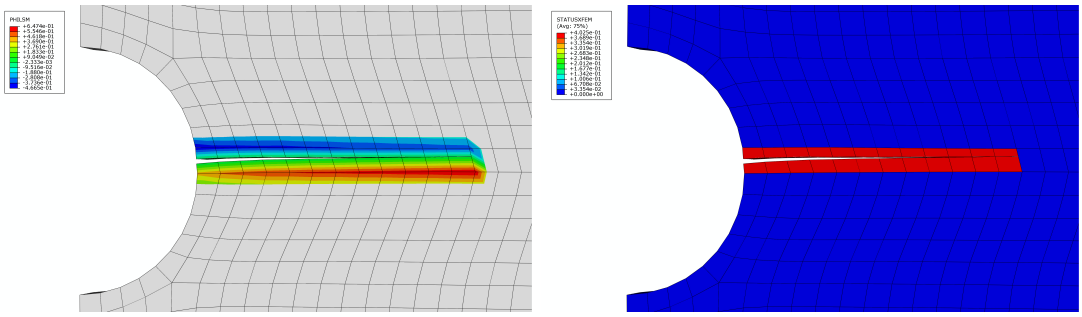

(a) (b)

Figure 7.8: XFEM Crack Growth Path showing (a) PhiLSM contour plot and (b) Status XFEM contour plot

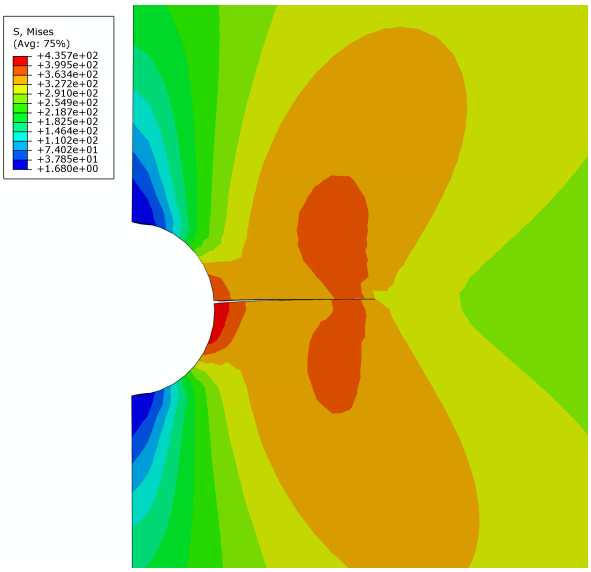

Figure 7.9: Closeup view of XFEM crack path showing von Mises stress distribution around the crack

Following the XFEM analysis, the location of the crack, and therefore the most critical region of the model, has been identified. This allows appropriate mesh refinement to be implemented in Step 2 of the procedure.

7.2.2 Step 2 - Identify Loads for Crack Initiation and LCF Life using the RPDM Analysis

In Step 2, the geometry is remodelled, implementing suitable mesh refinement in the critical regions as identified in Step 1. The RPDM analysis (Section 5.2.1) is then performed to determine the location of the shakedown and ratchet boundaries. The results are presented on the Bree-Interaction diagram in Figure 7.10

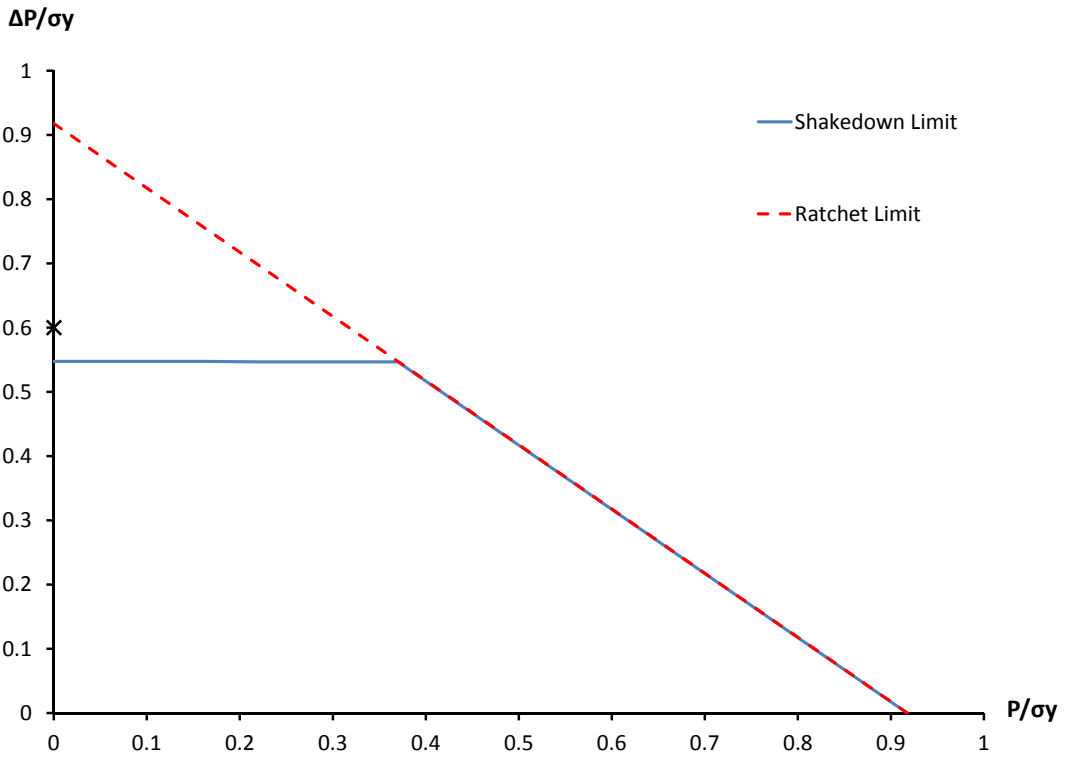

Figure 7.10: Bree interaction diagram showing shakedown and ratchet limits

It can be seen that at cyclic loads below $0.54\sigma y$ the material undergoes shakedown. However, for applied cyclic loads of greater than $0.54\sigma_y$ and less than $0.91\sigma_y$ the material exhibits reversed plasticity. Above these loads, instantaneous collapse occurs. For a R-ratio of 0, i.e. loads between 0 and P_{max}, this corresponds to the Y-axis at $x = 0$, meaning that any cyclic load between 349MPa and 589MPa will cause reversed plasticity.

Since this investigation is being performed merely to demonstrate the technique and is not replicating a specific load case, arbitrary loads within the reversed plasticity region are selected. The chosen structural load is $0.6\sigma_y$ which corresponds to a load of 388MPa, as indicated by the black cross in Figure 7.10.

Once the material response is ascertained, as per the RPDM analysis, an additional ratchet analysis is performed in order to calculate the LCF life. This is performed for both an EPP and RO material model and the hysteresis loops of each are shown in Figure 7.11.

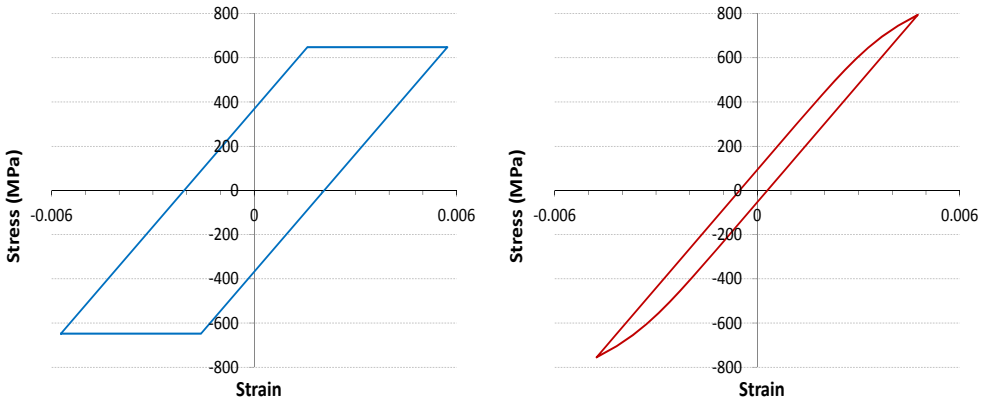

Figure 7.11: Stabilised hysteresis loop at applied mechanical load of 388MPa for (a) Elastic Perfectly Plastic Material Model and (b) Ramberg-Osgood Material Model

Through comparison with the material LCF data shown in Table 7.1, the fatigue life can be obtained and the results are shown in Table 7.2 for both EPP and RO material models.

Table 7.1: Low cycle fatigue data

Number of Cycles to Failure	Normalised Strain Range (%)
100	1.400
500	1.016
1000	0.885
2000	0.771
4000	0.672
8000	0.585
16000	0.509
32000	0.444

Table 7.2: Stress and strain ranges calculated using both Elastic Perfectly Plastic and Ramberg-Osgood Material Models and corresponding fatigue life calculated by the RPDM

	Material Model	
	EPP	RO
Stress Range (MPa)	1296.00	1549.209
Elastic Strain Range (%)	0.7303	0.8696
Plastic Strain Range (%)	0.4151	0.0823
Total Strain Range (%)	1.1454	0.9519
LCF Life (cycles)	275	697

7.2.3 Step 3 - Calculate Crack Propagation Parameters

Following calculation of the crack initiation fatigue life, Step 3 then calculates the crack propagation parameters and the crack growth rate. As has been established, there are a number of suitable techniques for the calculation of these parameters, depending on the specific application. However, in this investigation, the MML concept is used for the calculation of the cyclic J-integral.

The preliminary XFEM analysis in Step 1 has established the location of crack initiation and this is illustrated in Figure 7.12. The geometry is remodelled containing a small crack with the appropriate mesh refinement, simulating the initial stages of the crack. As is established in ASME BPVC, crack initiation failure is deemed to have occurred once the crack has reached a length of 3mm. For this reason, in this crack propagation analysis, the predefined crack length is set at 3mm. The MML procedure is then performed, allowing the calculation of the cyclic J-integral, and crack propagation rate. The results of this are shown in Table 7.3, and the variation of the cyclic J-integral along the crack front is shown in Figure 7.13.

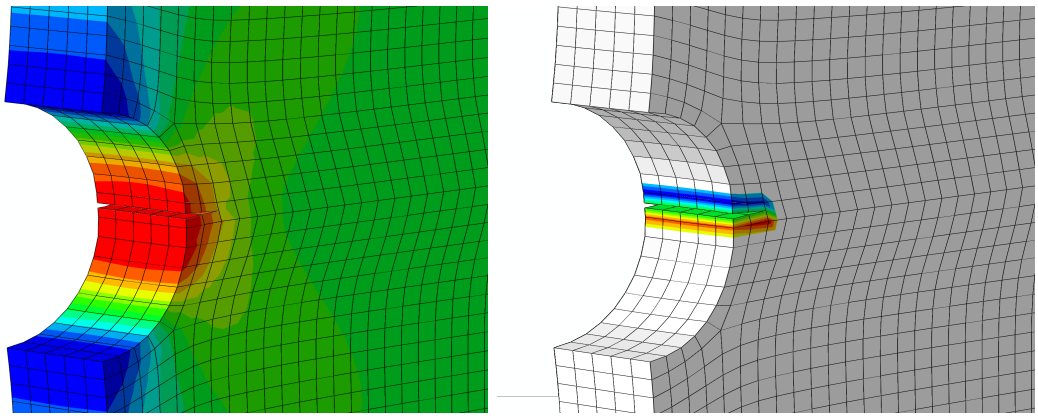

(a) (b)

Figure 7.12: XFEM Analysis showing location of crack initiation in (a) Von Mises stress contour and (b) PhiLSM contour plot

Table 7.3: Cyclic J-integral variation

	Cyclic J-Integral (MPa.mm)	
Contour	Crack Average	Maximum
1	3.0466	3.2051
2	3.2715	3.4533
3	3.2004	3.3791
4	3.1302	3.3049
5	3.0521	3.2198
Contour Average	3.1402	3.3124

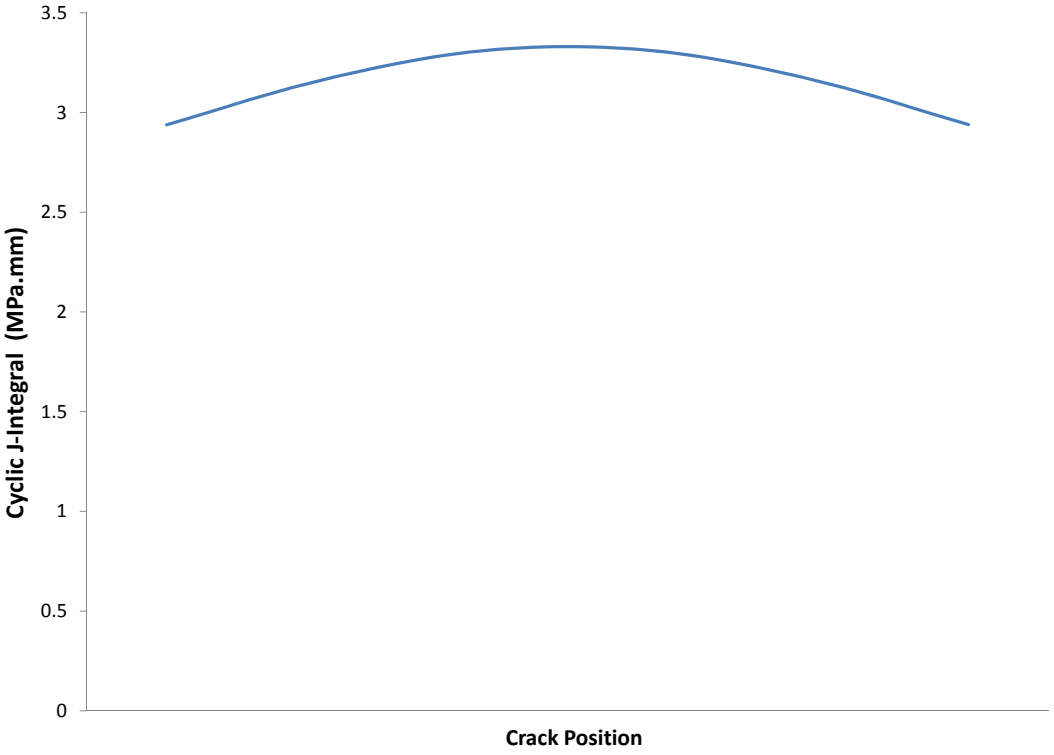

Figure 7.13: ΔJ variation along crack front

7.2.4 Step 4 - Calculate Total Fatigue Life

Once the crack growth parameters are determined, they can be used to determine the crack propagation rate through a suitable law, such as the Paris Law or Dowling & Begley Law. The Dowling & Begley law is used in this investigation using the values of the cyclic J-integral calculated in Step 3. For the material in question, the parameters C' and m' are not available, however, Paris Law constants C and m are known and so the conversion established in Section 6.7 is employed to calculate the appropriate parameters. The Paris law constants for this material are as follows: $C = 5.6 * 10^{-12}$ and $m = 3.25$.

Therefore, from Equations 6.17 and 6.18, converting these parameters to their ΔJ equivalent, m', becomes:

$$m = \frac{3.25}{2} = 1.625 \tag{7.1}$$

and C' becomes:

$$C' = 5.6 * 10^{-12} * (199.753 * 10^3)^{1.625} = 0.002299 \tag{7.2}$$

Once the material constants and the cyclic J-integral have been established, the crack propagation rate can be calculated using the Dowling & Begley law. Two crack propagation analyses will be performed using the average and maximum value of cyclic J-integral and the results of these are summarised in Table 7.4. For the crack average value of ΔJ:

$$\frac{da}{dN} = 0.002299 * \big(3.1402\big)^{1.625} = 0.01475 mm/cycle \tag{7.3}$$

For the maximum value of ΔJ:

$$\frac{da}{dN} = 0.002299 * \big(3.3124\big)^{1.625} = 0.01609 mm/cycle \tag{7.4}$$

Table 7.4: Crack Propagation Rate for average and maximum values of ΔJ

Average ΔJ	0.01475 mm/cycle
Maximum ΔJ	0.01609 mm/cycle

Crack Propagation Fatigue Life

Once the rate has been calculated, the crack propagation fatigue life can be determined. It is important to consider the definition of the point of failure, this could be when the crack propagates throughout the entire specimen or to a critical length. In reality, the crack will reach a critical length, at which point, rapid crack extension will occur throughout the rest of the specimen. Hence, it may not be suitable to assume a linear crack growth rate throughout the entire specimen. Therefore, in order to calculate the total propagation life, the critical crack length needs to be determined. In this case, as is standard for this type of test within Siemens, the critical crack length is assumed to have occurred once the crack has propagated to 50% of the cross-sectional area.

This specimen is a 100mm square plate with a 5mm radius centre hole and so the specimen length is 45mm. The initial crack has been set at 3mm, therefore, the

un-cracked ligament is 42mm. If the critical crack length is assumed to be 50% of the cross-sectional area, due to the three-dimensional symmetry of this specimen, this corresponds to a crack length of 21mm.

Therefore, to calculate the number of cycles required to reach a crack of 21mm:

for the crack average value of ΔJ,

$$dN = \frac{21}{0.01475} = 1422.89 cycles \tag{7.5}$$

for the maximum value of ΔJ,

$$dN = \frac{21}{0.01609} = 1304.66 cycles \tag{7.6}$$

It can be observed that since the value of ΔJ is raised to the power of m in the calculation of the crack propagation rate, any variation in the value of the cyclic J-integral will greatly affect the value of da/dN. This highlights the importance of maintaining the highest level of accuracy during the entire analysis process. The cyclic J-integral offers a measure of the driving force for the crack and so it is believed that it is preferable to use the maximum value of ΔJ for crack growth rate calculations since this incorporates an added level of conservatism in the fatigue life.

Procedure Summary

The proposed procedure has been implemented on a simple geometry specimen in order to demonstrate the techniques. Although a simple specimen, the techniques are directly applicable to any geometry or material and loading conditions and so can also be applied to highly complex industrial applications.

For the geometry and material in question, the procedure has been performed, identifying the key results that are presented in Table 7.5 and 7.6.

Table 7.5: Summary of results obtained using proposed procedure using average value of ΔJ

	EPP	RO
Crack initiation fatigue life (cycles)	275	697
$\Delta J_{average}(MPa.mm)$	3.1402	3.1402
Crack growth rate (mm/cycle)	0.01475	0.01475
Crack propagation fatigue life (cycles)	1422.89	1422.89
Total fatigue life	1697	2119

Table 7.6: Summary of results obtained using proposed procedure using maximum value of ΔJ

	EPP	RO
Crack initiation fatigue life (cycles)	275	697
$\Delta J_{max}(MPa.mm)$	3.3124	3.3124
Crack growth rate (mm/cycle)	0.01609	0.01609
Crack propagation fatigue life (cycles)	1304.66	1304.66
Total fatigue life	1579	2001

7.3 Limitations of the Procedure

Despite the large number of advantages of the proposed technique as discussed in the preceding chapters, there are some limitations which are presented below.

In the calculation of the crack growth rate, it has been assumed that the cyclic load is constant, and therefore the crack propagation rate, da/dN is also constant. This is an unrealistic assumption since in reality, the ΔJ will increase as the crack grows.

Furthermore, this will only increase until $\Delta J = \Delta J_c$, the critical cyclic J-integral, at which point, unstable crack growth will occur, causing the component to fail. Is is therefore unlikely that the crack will be able to grow to the full width of the component.

Since the crack growth rate is not linear as the crack grows, performing a single crack growth rate calculation using a single value of the crack growth parameter could yield inaccurate results. This issue could be addressed by performing additional calculations to model the variation in ΔJ as the crack grows. This could be done by discretising the propagation into a number of smaller increments, thus alleviating the dependence on a single value of ΔJ. This could allow the crack growth rate to be calculated iteratively using a series of small growth steps. The smaller these steps are, the more accurate the crack growth calculation will be, but it will become much more computationally intensive to manually model the growing crack. For this reason, a balance must be met between required accuracy and effort.

A future possibility could lie with the increased use of the XFEM technique, or similar fatigue damage mechanics methods. As has been stated, this technique is currently only capable of modelling contour integrals such as K and J on static cracks, and hence offers no benefit over the standard FEM for the calculation of the crack growth parameters. However, if the XFEM technique were to be developed to permit the calculation of these parameters on a propagating crack, this would provide increased accuracy in crack propagation fatigue life calculations, without the need to employ the labour intensive, incremental crack growth modelling.

Another limitation lies in the definition of failure during the crack propagation. The point at which failure is deemed to have occurred can greatly affect the total calculated fatigue life, and this will depend on the material's ductility. As mentioned above, in reality it is unlikely that the crack will be able to propagate across the entire specimen, since it will become unstable at a critical point. It is therefore unrealistic to calculate the crack propagation fatigue life based on the full specimen width. In this case, the crack was assumed to fail once it reaches 50% of the cross-sectional area, since this approach has previously been used on similar applications within industrial applications. However, the accuracy and validity of this assumption is very difficult to ascertain, since it will vary widely depending on the presence of internal defects

and crystallographic properties across a range of specimens. As suggested, the critical cyclic J-integral or Stress Intensity Factor can also be used to determine the failure condition. However, such data may be unavailable if extensive material testing has not been previously conducted, as was the case in this investigation. This again creates uncertainty in the calculation of the crack propagation rate. The definition of crack failure greatly affects the obtained values of the total fatigue life and so the calculation could potentially yield very inaccurate results. For this reason, this is clearly an area which requires additional investigation in order to assess the definition of the crack failure criterion

The MML concept has only currently been implemented for EPP properties. However, material hardening could have a significant effect on the calculated value of cyclic J-integral. This could cause significant inaccuracies and unrealistic assumptions in the calculation of the crack propagation rate and total fatigue life. In order to ensure that the simulations are as representative as possible of real materials, it is therefore important that more complex material hardening relationships are integrated into the MML concept framework.

The greatest limitation of this procedure is with the limited range of conditions that the techniques can accurately simulate. The investigation described in Chapter 5 only considered pure fatigue loading with no consideration of extended hold times. Creep-fatigue fracture is a prominent failure mechanism in high temperature, high stress environments, such as those experienced in power plant and aerospace applications. For this reason, it is vitally important to be able to simulate the interaction of creep and fatigue during component design. The lack of consideration of creep-fatigue in the proposed procedure is clearly a limitation, and thus an extension to the technique that incorporates the creep-fatigue interaction would greatly enhance its power for use in industrial applications. A method for the extension of this procedure for the inclusion of a creep dwell in the cyclic loading history is presented in the following section and a preliminary analysis is included in Appendix A which could provide a starting point for future work.

This proposed procedure offers a number of valuable techniques for the calculation of crack growth behaviour. These can be used individually or together in the complete

procedure. An advantage of this is that it allows the user to pick and choose different aspects of the procedure that best suit the application in question. However, if the entire process is to be performed in a single procedure, this can become very labour intensive. Although the computational analysis time for each component of the procedure is very small, it can require extensive modelling and remodelling, especially if incremental crack growth modelling is employed, incurring great computational cost for implementation. Therefore, an obvious extension of this work would be to offer some degree of automation, allowing the user to establish the initial geometry and material definition and then run an automated procedure. These areas of weaknesses are further addressed in the Future Works section.

7.4 Procedure for the Calculation of Creep-Fatigue Crack Initiation Damage

The proposed procedure has currently only considered pure fatigue, however, it is possible to also include the evaluation of creep-fatigue damage. This can be performed using the Linear Matching Method Extended Direct Steady Cyclic Analysis (eDSCA). This is an extension to the standard DSCA for pure fatigue loading (described in Chapter 5) which incorporates the presence of high temperature creep dwell to allow the assessment of the creep-fatigue interaction [136]. It permits the calculation of four key parameters: the stress at the start of the creep dwell, the creep strain increment, the related elastic follow up factor and the total strain range during the load cycle, allowing it to be used for the creep crack initiation analysis.

The eDSCA is a numerical method based on solid mechanics concepts and so offers increased accuracy compared to rule based procedures such as R5 and ASME BPVC. The eDSCA method considers the creep-fatigue interaction of cyclic plasticity and creep over the entire load cycle using an iterative approach to represent non-linear behaviour including both plasticity and creep through a series of linear solutions. The loading history is represented by the most extreme load points which reduce the computational time, whilst maintaining high levels of accuracy, making it more efficient than other approximate methods that do not consider the complete creep-fatigue interaction [137,

138].

The eDSCA has been introduced into the LMM framework through an ABAQUS user subroutine to allow the evaluation of the steady state cycle of a structure that is subjected to a cyclic loading history containing a creep dwell. This allows the calculation of the parameters required to construct a stress-strain hysteresis loop; the elastic and plastic strains during loading and unloading, the creep strain and related stress relaxation, the stress at the end of each load instance and the elastic follow up factor (Z), which describes the rate of relaxation of the residual stress.

This representation of the stress-strain response provides invaluable information about the damage mechanism considering the interaction between creep and cyclic plasticity and can be used to assess creep enhanced reversed plasticity, cyclically enhanced creep and creep ratchetting. This assessment is vitally important since the presence of creep can affect the damage mechanism, as for example, a structure which undergoes shakedown when subject to pure fatigue loading, may undergo ratchetting when a creep dwell is introduced.

A typical closed-loop, steady state stress-strain hysteresis loop is shown in Figure 7.14, where point 1 is the end of the load step, point 2 is the end of the hold step, point 3 marks the end of the unloading step, Z is the follow-up factor, ε^{cr} is the creep strain and σ_{cr} is the stress relaxation. This allows the evaluation of the structural response to a cyclic loading history at elevated temperature, considering the accumulation of a residual stress field, cyclic plasticity and its interaction with a creep dwell.

This method allows the solution of a highly complex non-linear problem incorporating the creep fatigue interaction in a very efficient manner through a series of iterative linear elastic solutions, offering considerable advantages over other existing methods.

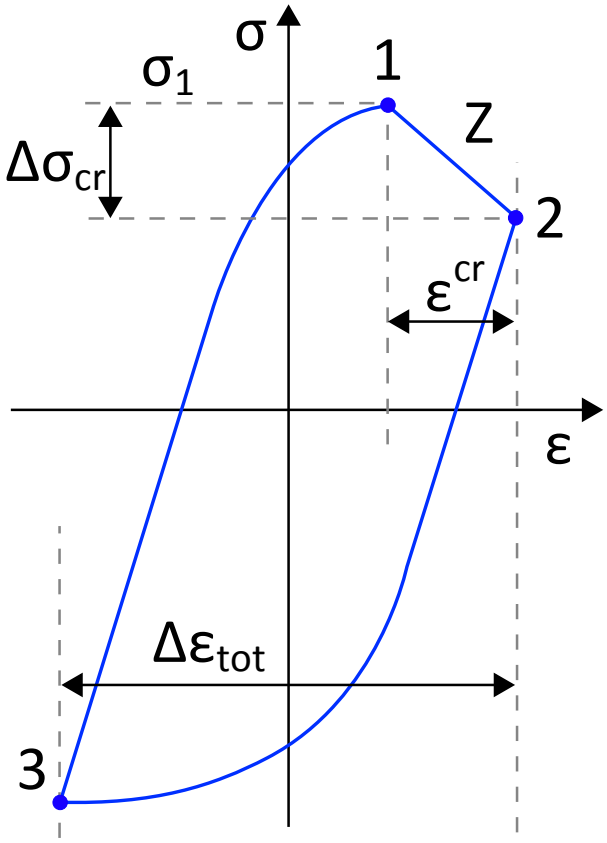

Figure 7.14: Generic steady state cycle stress-strain response with creep dwell

7.4.1 Creep-Fatigue Analysis Case Study

In order to demonstrate the implementation of the eDSCA technique, an extract is presented from a paper published by Barbera and Chen of the SILA Research Group at the University of Strathclyde and Liu of Tsinghua University, entitled "Creep Fatigue Life Assessment of a Pipe Intersection with Dissimilar Material Joint by Linear Matching Method" [138]. All figures and results in this section are taken from this publication, merely to demonstrate the implementation and power of this technique. This example demonstrates a case study which clearly shows significant creep-fatigue interaction including stress relaxation and the accumulation of creep strain.

The pipework example, presented in [130] is further investigated for the inclusion of creep-fatigue loading.

The component comprises a section of pipe with a branch pipe attached via a weld. The main pipe is of radius 120mm with a wall thickness 15mm and is manufactured

from 316LN stainless steel. The branch pipe is of radius 16.5mm with a wall thickness of 3.5mm and manufactured from SA508 structural steel as illustrated in Figure 7.15 [130]. The connecting weld material is INCO182 and is 3.5mm thick with a face angle of 45 ° to the main pipe. Details of the specific material constants are provided in [139] and [140].

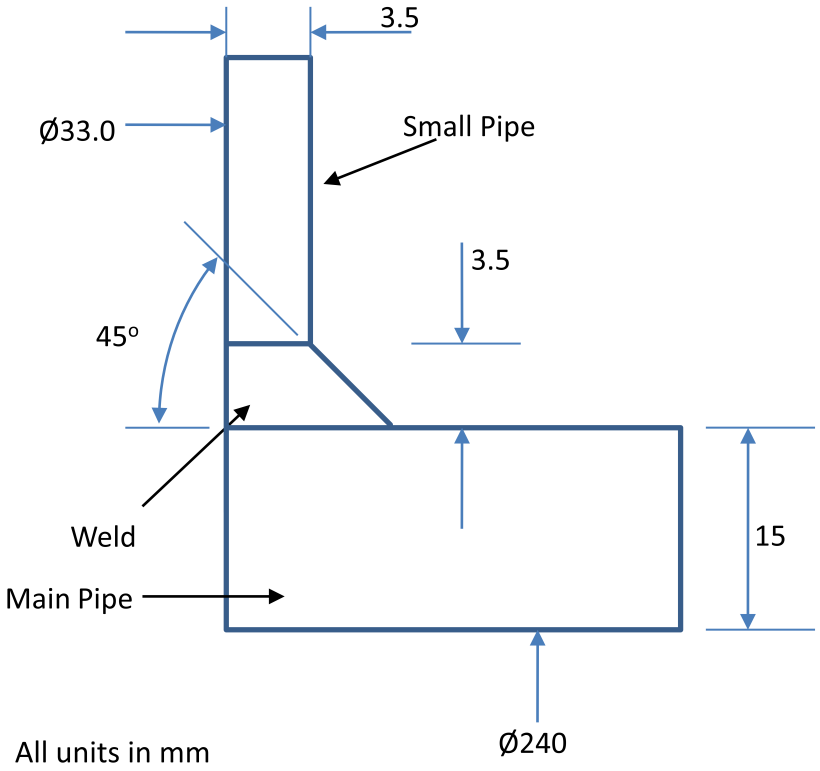

Figure 7.15: Geometry of pipe intersection [130]

For this study, two thermal loading conditions are considered:

1. Cyclic high temperature loading applied to the entire component to assess the impact of thermal stresses arising from the dissimilar materials and coefficients of thermal expansion

2. Thermal gradient cyclic loading considering the effect of transient thermal gradients between the inside and outside of the pipe

For this secondary study, the loading profile comprises 4 steps:

1. Internal temperature is $\theta_0 + \Delta\theta$ and outer temperature is θ_0
2. Component reaches thermal equilibrium and global temperature is $\theta_0 + \Delta\theta$
3. Uniform temperature equilibrium of Step 2 is maintained for extended dwell time
4. Global temperature returns to θ_0

For this loading profile, three different dwell times are considered of 1, 10 and 100 hours to assess the impact of the creep dwell. Due to the symmetry of the component, a quarter model is analysed and the ends of the pipe are constrained to allow in-plane thermal expansion. The finite element mesh is refined in the weld region and this is shown in Figure 7.16 [130].

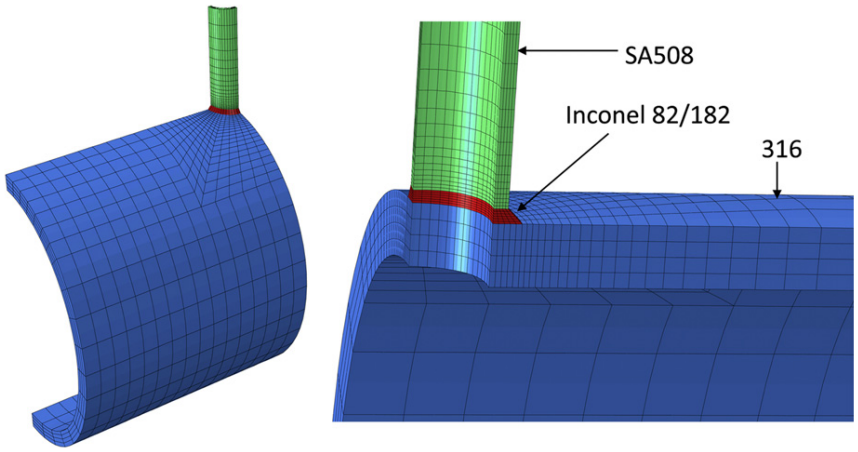

Figure 7.16: One quarter model FE mesh of pipe intersection [130]

Case Study Results

For the first loading scenario of the purely cyclic thermal load, the results are shown in Figure 7.17, where the stress-strain hysteresis loops are plotted for each dwell time. A pure fatigue loop for a case where creep does not occur which operates within the plastic shakedown region is also included for comparative purposes. The major contributing factors to fatigue failure in this case are due to thermal stresses induced by dissimilar metals with different thermal expansion coefficients. It can be observed that stress relaxation occurs when a creep dwell is introduced which increases the reversed plasticity, thus further enhancing the damage. It can also be seen that creep-ratchetting

occurs with longer dwell times, as the reversed plasticity is not fully recovered in each cycle. In this case, the creep-ratchetting is dominated by the accumulation of plastic strain during the unloading phase and the damage occurs in the weld material at the interface to the main pipe.

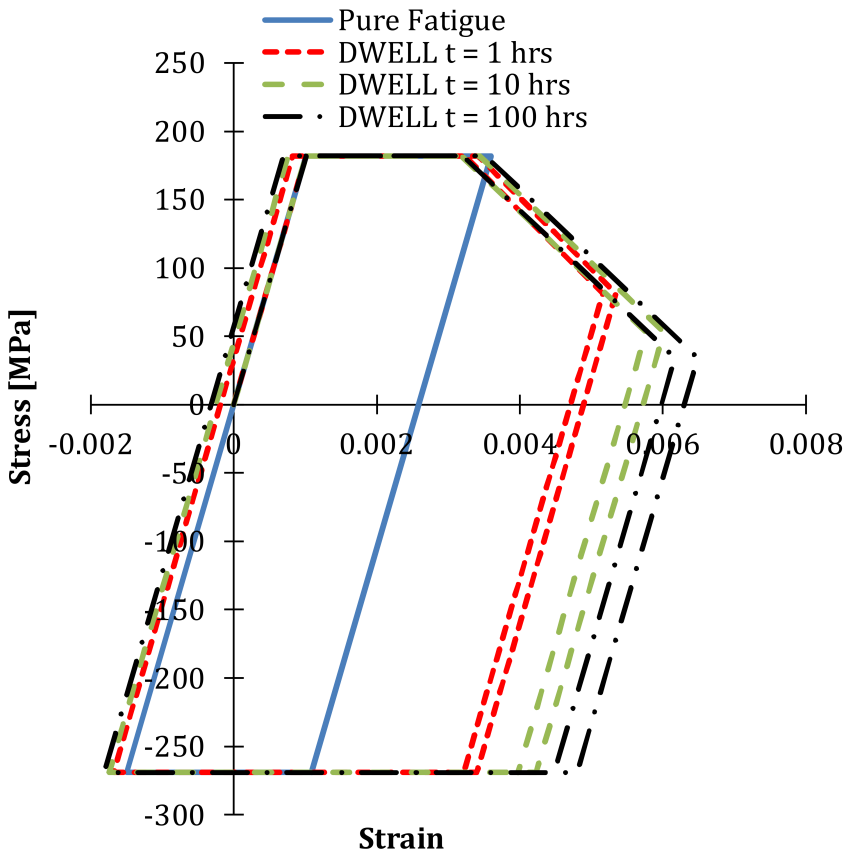

Figure 7.17: Stress-strain hysteresis loops for pure cyclic homogeneous temperature at varying dwell times at the most critical location [138]

For the second loading scenario, the effects are markedly different. The effects of creep can dramatically alter the damage mechanism. The thermal stress relaxation is considerable across the global structure, allowing the stresses to redistribute. The extent of this redistribution as a result of the dwell time can cause the damage location to change.

At a dwell time of 1 hour, the creep strain accumulates at the interface between the branch pipe and the weld material. However, with increasing dwell time, the creep strain begins to extend away from the pipe-weld interface and at a dwell time of 100

hours, significant creep strain accumulates in the main pipe and over a larger area to that of a shorter dwell time. This occurs as a result of the change in the residual stress field as the creep dwell increases. At such long dwell times, creep is a major contributing factor to the failure mechanism and competes with fatigue damage. These observations are shown in Figure 7.18 and Table 7.7. A step-by-step analysis has also been performed as a means of verification to confirm the accuracy of the LMM eDSCA and the results of these are included in Table 7.7.

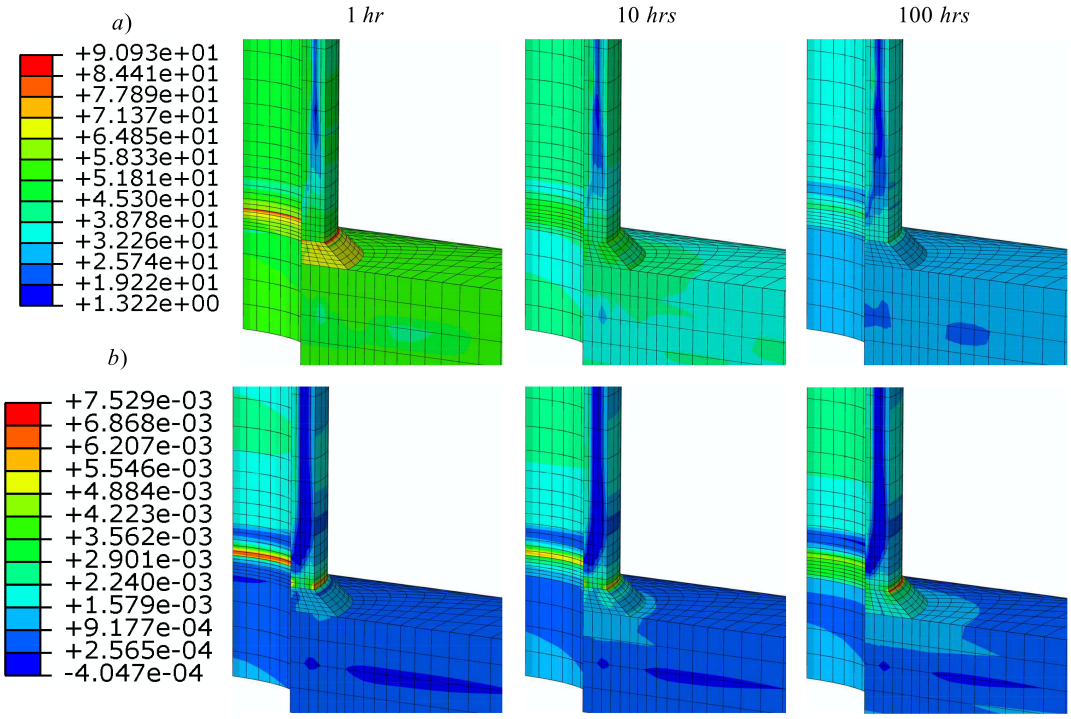

Figure 7.18: (a) von Mises stress at the end of the creep dwell, and b) equivalent creep strain magnitude for cyclic temperature with transient stage for different dwell times [138]

Table 7.7: Comparison of Step by Step analysis and LMM prediction for creep dwell time equal of 1 hour [138]

	Stress thermal transition [MPa]	Stress at high temperature [MPa]	Stress drop due to creep dwell [MPa]	Stress at unloading [MPa]
LMM	477	298.13	94.07	279.1
SBS	472	298	98.03	280.4
	Plastic strain thermal transition	Plastic strain at high temperature	Creep strain	Plastic strain at unloading
LMM	6.144E-02	5.718E-01	5.559E-03	8.557E-03
SBS	6.121E-02	5.733E-02	5.164E-03	8.282E-03

7.4.2 Calculation of Creep Crack Initiation Fatigue Life using eDSCA

Once the complete cyclic response is determined, the creep and fatigue damage can be calculated and the total damage is determined by an interaction of these two components.

For the fatigue damage, Miner's rule is widely used, and this is implemented in both the R5 and ASME BPVC procedures. This law considers cumulative damage modelling for fatigue failure. It states that if there are a value of k different stress levels and the average number of cycles at the i^{th} stress, S_i, is N_i, then the damage fraction, C_D, is given by:

$$\sum_{i=1}^{k} \frac{n_i}{N_i} = C_D \tag{7.7}$$

where n_i is the number of cycles achieved at stress, S_i and N_i is the number of cycles required to reach failure at the i^{th} stress, S_i. As a general case, failure occurs when the

damage fraction equals 1.

However, for the assessment of creep damage, there are three main techniques which are routinely used, the time fraction (TF) rule, creep ductility exhaustion (DE) method [141] and the stress modified ductility exhaustion method and each of these are incorporated into the LMM eDSCA.

Time Fraction Approach

The time fraction method is a creep-stress based method which calculates the creep damage using time to rupture curves according to the time fraction rule, d_c^{TF}, which states:

$$d_c^{TF} = \int_0^{t_h} \frac{dt}{t_f(\sigma, T)} \tag{7.8}$$

where t_h is the hold time, dt is the time increment and t_f is the creep rupture time expressed as a function of stress and temperature and is obtained by experimental creep rupture tests. However, this has been found to be under conservative for small strain ranges and overly conservative for high stress dwell periods [142].

Ductility Exhaustion Approach

The creep ductility exhaustion method uses the creep strain to calculate the creep damage and states that failure will occur at the point when the accumulated strain becomes equal to the available ductility and can be expressed as:

$$d_c^{DE} = \int_0^{t_h} \frac{\dot{\bar{\varepsilon}}_c}{\bar{\varepsilon}_f(\dot{\bar{\varepsilon}}_c, T)} dt \tag{7.9}$$

where t_h is the hold time,$\dot{\bar{\varepsilon}}_c$ is the instantaneous creep strain rate and $\bar{\varepsilon}_f$ is the creep ductility of the material. This method has been found to be more accurate than the time fraction rule, however, it can yield overly conservative results at low levels of initial stress.

Stress Modified Ductility Exhaustion Method

The stress modified ductility exhaustion method was developed by Spindler [143] to address the issue of overly conservative results at low levels of initial stress of the DE method by including the effect of stress. This method considers the ductility as function of both the creep stress and creep strain rate to assess the damage and has been found to offer a better prediction of the creep damage during the load cycle. This modified relationship is given by:

$$d_c^{SM} = \int_0^{t_h} \frac{\dot{\varepsilon_c}}{\varepsilon_f(\dot{\varepsilon_c}, \sigma, T)} dt \tag{7.10}$$

where t_h is the dwell time, $\dot{\varepsilon_c}$ is the instantaneous creep strain rate and $\varepsilon_f(\dot{\varepsilon_c}, \sigma, T)$ is the inelastic strain at failure at the appropriate temperature as a function of the creep strain rate and the stress.

Total Creep and Fatigue Damage

Once each damage component is established, the total damage can then be assessed using a creep-fatigue interaction diagram. This combines the creep and fatigue components to provide the total damage and allows the calculation of the total life. The damage can be given by:

$$\phi_f + \phi_c \leq D \tag{7.11}$$

where ϕ_f and ϕ_c are the accumulated fatigue and creep damage components respectively, and D is a material dependent allowable damage factor. When the sum of the creep and fatigue damage components equals the damage factor, failure occurs.

This interaction between the creep and fatigue components can be plotted on a graph of the fractional creep and fatigue damage to illustrate the point at which rupture will occur. For the case where $\phi_f + \phi_c = 1$ a straight line between $\phi_f = 1$ and $\phi_c = 1$ can be plotted, for points below this line, the component is safe, whilst above this line, rupture will occur. This is a simplified case, however, more complex damage rules exist which produce bilinear or non-linear curve fits where the locus of the curves marks the damage factor. For some materials, these more complex rules can better describe the

creep and fatigue damage components and their interaction. A 45 ° line is also added to highlight the dominant damage mechanism, for points to the left of this line, fatigue is dominant, where as to the right, creep is the dominant damage mechanism. This is illustrated in Figure 7.19.

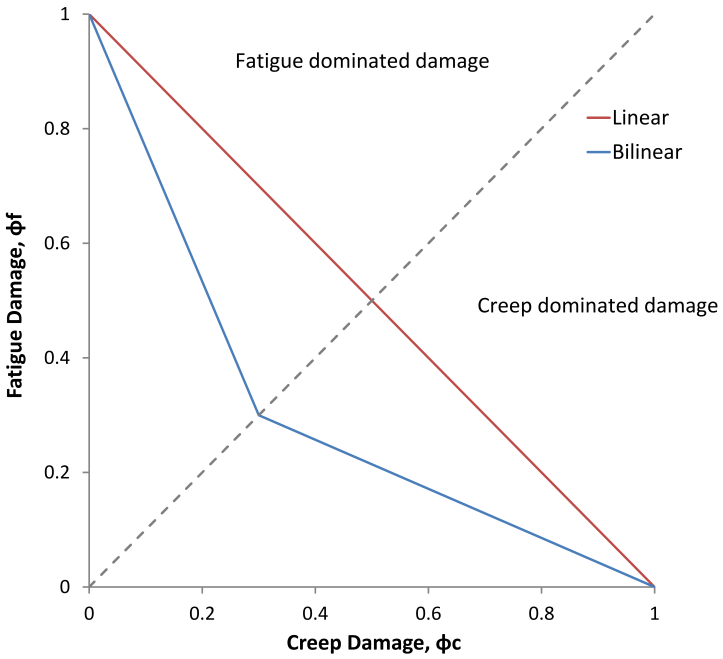

Figure 7.19: Generic creep-fatigue interaction diagram

The components $\phi_f = 1$ and $\phi_c = 1$ provide the total fatigue and creep damage components respectively. However, it is also important to consider the damage per cycle, which is given by ω_f and ω_c for fatigue and creep respectively and are related to the total damage as follows:

$$\phi_f = \omega_f * N_f \tag{7.12}$$

and

$$\phi_c = \omega_c * N_c \tag{7.13}$$

where N_f and N_c are the number of cycles to failure for each damage component.

Once the creep and fatigue damage per cycle are established, the total damage per cycle, ω_T can be obtained as the sum of the two components, such that:

$$\omega_T = \omega_f + \omega_c \tag{7.14}$$

The total life is then given as the reciprocal of the total damage per cycle:

$$N_T = \frac{1}{\omega_T} \tag{7.15}$$

where N_T is the total life.

Case Study Summary

This case study has included the application of the LMM eDSCA to a highly complex industrial specimen of a pipe intersection, clearly demonstrating the power and advantages of the technique. The material response for a range of creep dwell times was determined and plotted for a critical location as a stress-strain hysteresis loop, clearly illustrating the plastic and creep strain, stress relaxation and reversed plasticity. The method also allows the damage locations to be predicted and this example has shown how this can change depending on the creep dwell duration.

The eDSCA has been verified through comparison with a complete step-by-step (SBS) analysis and the obtained results show close agreement, thus confirming their accuracy. However, the SBS analysis took a total CPU time of 14680 seconds to complete, compared to 766 seconds for the LMM analysis. For this reason, and as demonstrated in Chapter 5, SBS analyses do not offer efficient methods for such complex simulations, however, they do offer very valuable methods for verification purposes. Finally, the creep and fatigue damage assessment methods employed by the eDSCA, and how these can be used to calculate the total component life have been described.

This example has demonstrated the great advantages of the LMM compared to full inelastic analysis due to its high level of accuracy and efficiency for the assessment of the steady-state response of structures subjected to a cyclic loading history containing a creep dwell.

7.5 Creep Crack Propagation

The eDSCA technique only considers creep crack initiation and creep crack propagation modelling is not currently supported. Additional future work within the SILA Research Group [144] will attempt to extend the eDSCA to include crack propagation. However, in the current form, for the calculation of creep crack propagation within the LMM framework, the R5 methodologies are implemented which describe the procedures for the assessment of components containing defects under creep and creep-fatigue loading histories.

The R5 methodology for the calculation of creep crack growth utilises the C^* parameter, which characterises the stress and strain rates at the crack tip [4] (pp.4/5.20-29). C^* provides a creep equivalent to the J-integral. This method assesses the early stages of creep crack growth based on the evaluation of this crack tip parameter, together with creep crack experimental data, in a similar manner as K and J are used to describe crack behaviour in linear elastic conditions and plastic conditions. The C^* integral can be calculated using the reference stress methods [145] by:

$$C^* = \sigma_{ref}\dot{\varepsilon}^c_{ref}R' \tag{7.16}$$

where $\dot{\varepsilon}^c_{ref}$ is the creep strain rate at the reference stress, σ_{ref}, calculated for a crack size of a, and $R' = \left(\frac{K}{\sigma_{ref}}\right)^2$ is the characteristic length where K is the stress intensity factor.

LMM and the R5 C^* approach

The R5 C^* can be used in conjunction with the LMM for improved crack growth assessment. Performing the LMM to calculate the shakedown and ratchet limits can allow a more accurate calculation of the reference stress, and thus the C^* parameter, to determine the creep crack growth rate. Hence, the LMM offers a very valuable tool within the R5 procedure for creep fatigue life assessment.

7.5.1 Calculation of Creep Crack Growth Rate

Once the C^* parameter is determined, it can be used to calculate the creep crack growth rate by:

$$\left(\frac{da}{dN}\right)_c = \int_0^{t_h} A_c (C^*)_c^q dt \tag{7.17}$$

where t_h is the dwell period and A_c and q_c are material constants obtained from experimental testing.

Combined Creep and Fatigue Crack Growth Rate

In the presence of combined creep and fatigue, the total crack growth per cycle is split into its fatigue and creep counterparts and the total life can be calculated as the sum of the two, such that:

$$\frac{da}{dN} = \left(\frac{da}{dN}\right)_f + \left(\frac{da}{dN}\right)_c \tag{7.18}$$

where f and c represent the fatigue and creep crack growth rate counterparts.

7.6 Chapter Summary

This chapter has proposed a complete crack growth modelling procedure for fatigue life assessment of complex engineering structures. It does this by identifying the location of crack initiation and the loads and number of cycles required to cause failure, and the calculation of the crack growth rate and the crack propagation fatigue life. The proposed procedure has been applied to a simple geometry to demonstrate its implementation. During the study, the following key results have been obtained:

1. The crack initiation location lies within the centre of the notch
2. For applied loads of 388MPa, the crack will initiate after 275 cycles for EPP properties, and 697 cycles for RO properties
3. The cycle J integral has been calculated at 3.3124MPa.mm
4. The calculated crack growth rate is 0.01609 mm/cycle

5. The number of cycles to reach a critical crack length of 50% of the cross sectional area is 1304 cycles

6. This results in a total fatigue life of 1579 cycles for EPP material properties and 2001 cycles for RO properties

This investigation and its findings clearly demonstrate the power of the techniques presented in this procedure. However, despite its strengths, it has a number of limitations which have been identified and suggested for further investigation. It is suggested in the future works section that these limitations are addressed in order to further enhance the power, efficiency and efficacy of the proposed procedure for use within highly complex industrial applications for crack growth modelling and fatigue assessment.

Finally, the Extended Direct Steady Cyclic Analysis was introduced as a method to calculate the creep crack initiation fatigue life within the LMM framework. A case study has been included which demonstrates the power of this technique for the evaluation of creep-fatigue damage. This method currently only supports creep crack initiation and so the R5 methodology for the assessment of creep crack propagation using the C^* integral, and how this can be used to calculate the total creep-fatigue life, have been described.

Chapter 8

Conclusions & Future Work

8.1 Thesis Summary

The key deliverable of this project and resulting thesis is the development of a complete crack growth assessment procedure combining both crack initiation and propagation analyses. The thesis comprises 2 parts - Part I providing a foundation for the investigation and Part II presenting the core research in the development of the crack assessment procedure.

Chapter 1 provided the rationale behind the project and the requirement for such an investigation. It introduced basic gas turbine theory as this was the industrial focus of the project. The project objectives provided focus for the specific areas of research and these were then presented in Chapters 2 and 3, providing a foundation understanding for the following chapters. Existing fracture mechanics and fatigue methodologies were described, highlighting their weaknesses, thus providing a starting point for the novel techniques developed in this project. Chapter 4 commenced the core research of Part II by describing the design of a representative industrial test specimen which acted as the application for subsequent analyses. Chapter 5 developed a novel technique to design an industrial experimental test programme suitable for causing crack initiation in the previously established test specimen. Chapter 6 extended this to crack propagation analysis with the development of a novel technique for the calculation of the cyclic J-integral to ascertain the crack propagation rate for complex components subjected to plastic deformation. Finally, Chapter 7 combined the previous techniques to establish

a step-by-step procedure for the complete lifetime assessment of a crack, including initiation, propagation rate, path direction and ultimate total fatigue life.

8.2 Conclusions

The major conclusions of this work are presented below:

- Existing fracture mechanics and fatigue methodologies were reviewed and their weaknesses identified to provide focus for the development of an innovative technique
- A representative industrial test specimen was designed and used for the application of the analyses
- Crack initiation was investigated and a novel technique was developed for the calculation of the low cycle fatigue life in complex industrial components
- This technique also offers a method for designing experimental testing programmes suitable for inducing crack initiation
- Crack propagation was investigated and a novel technique for the calculation of the cyclic J-integral was defined
- This technique allows the three-dimensional crack front detail of the cyclic J-integral to be monitored, enabling the identification of the likely points of crack propagation and the subsequent crack growth path
- The technique is cost effective both with respect to time and computational power and can be implemented on complex industrial specimens with great ease offering a viable and preferable method of calculating the cyclic J-integral
- This technique was successfully used in the calculation of the crack propagation rate for complex components subjected to plastic deformation
- A robust, step-by-step procedure was defined comprising the previously established methodologies, allowing the complete assessment of a crack to include

crack initiation life and location, crack propagation rate, crack path direction and ultimate total fatigue life

- The technique is valid for both simple and highly complex structures
- The techniques presented are very flexible and can be used with a range of options allowing the user to select the most appropriate one for the application, thus enhancing its practicality for industrial applications
- This technique has the potential to be invaluable in helping to address current and future engineering challenges within fracture mechanics and fatigue life assessment

8.3 Recommendations for Future Work

The techniques presented in this thesis have been shown to be very powerful and offer valuable analysis tools for use within industry. However, the procedure, in its current form has some limitations, which when addressed, would more greatly enhance the power of the proposed techniques.

The areas that have been identified as requiring further investigation are described below.

- The main limitations with the ergonomics of the procedure lie with the computational implementation. Each step can be run with ease, but performing the entire procedure introduces modelling and meshing issues which can become time consuming to implement for high levels of geometrical complexity. An obvious improvement to the technique would therefore be to automate the procedure. This could be achieved by using a Fortran user-subroutine or Python script to control an ABAQUS FE anaylsis to perform some or all of the components of each step with a level of automation. Utilising the established expertise of the SILA Research Group [144], could allow a robust automated procedure to be developed, which could then be incorporated into the Linear Matching Method Framework and ABAQUS user-subroutine and plugin, thus further enhancing the

ease of implementation for industrial and academic applications for crack growth assessment.

- The definition of component failure is critical when calculating the crack propagation fatigue life. A range of definitions exist which vary widely and can depend on specimen geometry and material. This can give rise to uncertainty in the calculated fatigue life. To this end, in order to gain a realistic understanding of fatigue life, an accurate failure criterion must be established. If fracture toughness data is known, then the critical ΔJ can be calculated. However, without such data, the unambiguous failure criterion cannot be established. For the materials used in this thesis, such data was not available and so an empirical failure criterion was used, based on previous experimental tests. It is therefore recommended that a more thorough investigation into the fracture toughness and failure criteria be performed for these materials. The continued experimental testing that is being performed at Siemens Industrial Turbomachinery, based partly on the findings of this project, should allow advancements to be made in the definition of such failure criteria. The ongoing testing programme involves some very extensive experiments, and as such has been timetabled for the coming years. Unfortunately, at the time of writing, the testing had not been completed and so could not be used to augment the theoretical research contained in this thesis. It is the hope of the author that suitable data will be available in the near future, enabling the continuation of this work.

- During crack propagation, the growth rate may not be linear, instead accelerating as the crack grows. This means that the crack growth calculations based on a single value of ΔJ can become inaccurate. This can be alleviated by discretising the crack growth into a number of steps, where a different value of ΔJ is calculated for the new crack length and repeated iteratively. This would mean that the crack growth rate could be calculated for small increments of crack growth, a, for instance, for $a_1 \geq a \geq a_2$, $a_2 \geq a \geq a_3$ until $a = a_c$, the critical crack length. This could easily be implemented into the MML concept through iterative crack modelling for incrementally increasing crack lengths. This would allow the number of cycles for each stage of the crack growth to be calculated, yielding

more accurate values of total life. It is clear that the accuracy will increase with greater refinement of the crack growth increment, but this would increase the computational effort, however, as above, this could be automated with relative ease through the use of a Python script, controlling an ABAQUS FE analysis to automatically model, mesh and re-mesh the geometry for each increase in crack size.

- As discussed in Chapter 7, a limitation with the current procedure is with the lack consideration of the creep-fatigue interaction. The use of the eDSCA and R5 C^* parameter for modelling a cyclic loading history containing a creep dwell have been described and a case study has been presented which demonstrates their implementation. In addition, a preliminary investigation for the creep-fatigue interaction of the previously used test specimen is included in Appendix A to act as a starting point for the future work to extend the RPDM for creep-fatigue modelling within Siemens.

Appendix A

Preliminary Investigation for Proposed Future Work

A.1 Appendix Overview

This section provides a preliminary investigation and a foundation for the proposed extension of the RPDM method for the inclusion of extended hold times, to accommodate creep-fatigue effects in the analysis.

As explained in Chaper 2, fatigue is a failure mechanism in which gradual damage accumulates as a result of repeated cyclic loading, whereas creep is the progressive damage induced in a material when subjected to a constant load for extended periods of time. This failure mechanism is particularly prominent in high stress and high temperature applications such as gas turbines as well as other applications with similar conditions across the power industry.

Across these industries, extensive investment is made for the development of high performance superalloy materials that are highly creep resistant. Despite this, the loads and temperatures involved mean that creep-fatigue can still be a prominent failure mechanism in these materials which emphasises the importance of gaining a thorough understanding of this mechanism. As a result, continued research in the field of creep involves a large number of researchers in both academia and industry.

This investigation aims to provide a foundation for further works to assist the understanding of creep and the creep-fatigue interaction in complex gas turbine components

by designing an experimental testing programme through an extension of the RPDM.

A.2 Introduction

The inclusion of extended hold times can result in entirely different damage mechanisms to that of pure fatigue and this can have a profound effect on the structural integrity of a component subject to such a load history. A typical creep-fatigue loading profile is illustrated in Figure A.1, where Δt represents the time duration of the applied load.

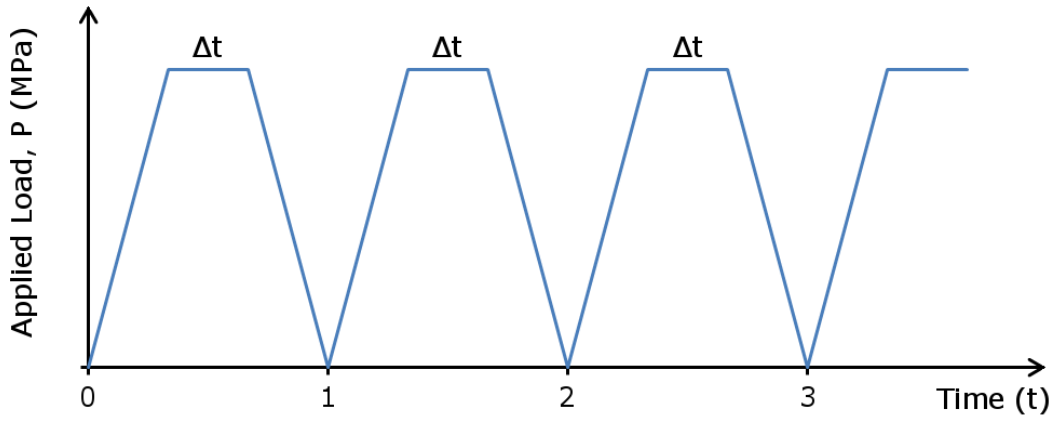

Figure A.1: Generic creep-fatigue load history with extended hold times

This type of loading profile is more representative of real-life applications such as might be experienced in gas turbines where the engines are ramped up, then operated at constant load for a period of time before shutdown, with this cycle being repeated multiple times. In these instances, a pure fatigue LCF analysis may produce overly optimistic and inaccurate results for fatigue life and it is therefore important to consider such loading cycles in the design of complex plant components.

A.2.1 Objectives

This proposed extension would allow a complete creep-fatigue analysis to be performed, and calculation of a component's lifetime for a given operating temperature. This will use the established Linear Matching Method eDSCA Creep-Fatigue subroutine [113] to extend the RPDM technique by incorporating load dwell times, allowing their effect on a component's structural integrity to be ascertained.

A.2.2 Issues of Calculation of Creep-Fatigue

As discussed in Chapter 2, a large number of different constitutive relationships exist that describe creep behaviour. Different materials can exhibit varying behaviour due to this complex damage mechanism and a creep-fatigue law which can accurately model the damage in one material, is unlikely to be applicable to other materials with entirely different relationships.

Computational tools such as bespoke finite element methods may only employ one or some of these laws, which may not match the relationship exhibited by the material in question, in which case, these analysis tools will be inappropriate. As discussed previously, the Linear Matching Method creep-fatigue subroutine currently only supports the Norton-Bailey creep law and this limits the current Linear Matching Method for creep-fatigue analysis. However, the material properties from one creep-fatigue relationship can be reformulated to simulate Norton-Bailey parameters suitable for input to the LMM by using an appropriate approximation method.

In the case of the nickel-based superalloy complex notched specimen in Section 5.3, this issue arises. The material in question exhibits a hyperbolic sine creep-fatigue relationship similar to the Garofalo Law and as such is not compatible with the current LMM creep-fatigue subroutine. The hyperbolic sine law utilises parameters A_g, γ, n_g and m_g which are entirely different to the B_n, n_n and m_n parameters of the Norton-Bailey law. However these hyperbolic sine parameters can be reformulated as Norton-Bailey equivalent parameters using a simple linear interpolation.

A.3 Material Property Analysis

A.3.1 Formulating Hyperbolic Sine parameters for use in the Linear Matching Method

In order to perform a complete creep-fatigue analysis using the Linear Matching Method, an extensive set of material properties are required including Young's Modulus, Poisson's ratio, yield stress and Norton-Bailey creep parameters. Since the only available material creep data for the superalloy follows a hyperbolic sine relationship, these properties must be converted to their Norton-Bailey equivalent form.

A method is given below to convert the parameters for the hyperbolic sine creep law to the equivalent Norton-Bailey parameters which can be used directly in the current LMM framework.

Step 1

The equation for the hyperbolic sine creep law is:

$$\dot{\varepsilon_c} = A_g[\sinh(\gamma\sigma)^{n_g}]t^{m_g} \tag{A.1}$$

Assuming that only secondary creep in considered, $m_g = 0$, and the equation simplifies to:

$$\dot{\varepsilon_c} = A_g[\sinh(\gamma\sigma)^{n_g}] \tag{A.2}$$

Step 2

The creep strain rate is calculated using this equation over a range of stress values and the results plotted in a log-log form as $\log(\dot{\varepsilon_c})$ versus $\log(\sigma)$ as shown in Figure A.2.

Step 3

Over a limited range of $\log(\sigma)$ this curve can be approximated by a linear function,

$$\log(\dot{\varepsilon_c}) = m\log(\sigma) + c \tag{A.3}$$

Step 4

The equation for the Norton-Bailey creep law is:

$$\dot{\varepsilon_c} = B_n\sigma^{n_n}t^{m_n} \tag{A.4}$$

which for secondary creep only, simplifies to:

$$\dot{\varepsilon_c} = B_n\sigma^{n_n} \tag{A.5}$$

Step 5

Taking logs of both sides of this equation:

$$\log(\dot{\varepsilon_c}) = \log(B_n) + \log(\sigma^{n_n}) = n_n \log(\sigma) + \log(B_n) \tag{A.6}$$

Step 6

Equating these two functions

$$\log(\dot{\varepsilon_c}) = n_n \log(\sigma) + \log(B_n) = m \log(\sigma) + c \tag{A.7}$$

Step 7

Therefore, the equivalent Norton-Bailey parameters are given by:

$$n_n = m \tag{A.8}$$

and

$$B_n = 10^c \tag{A.9}$$

where m is the straight line gradient and c is the straight line y-intercept from Figure A.2.

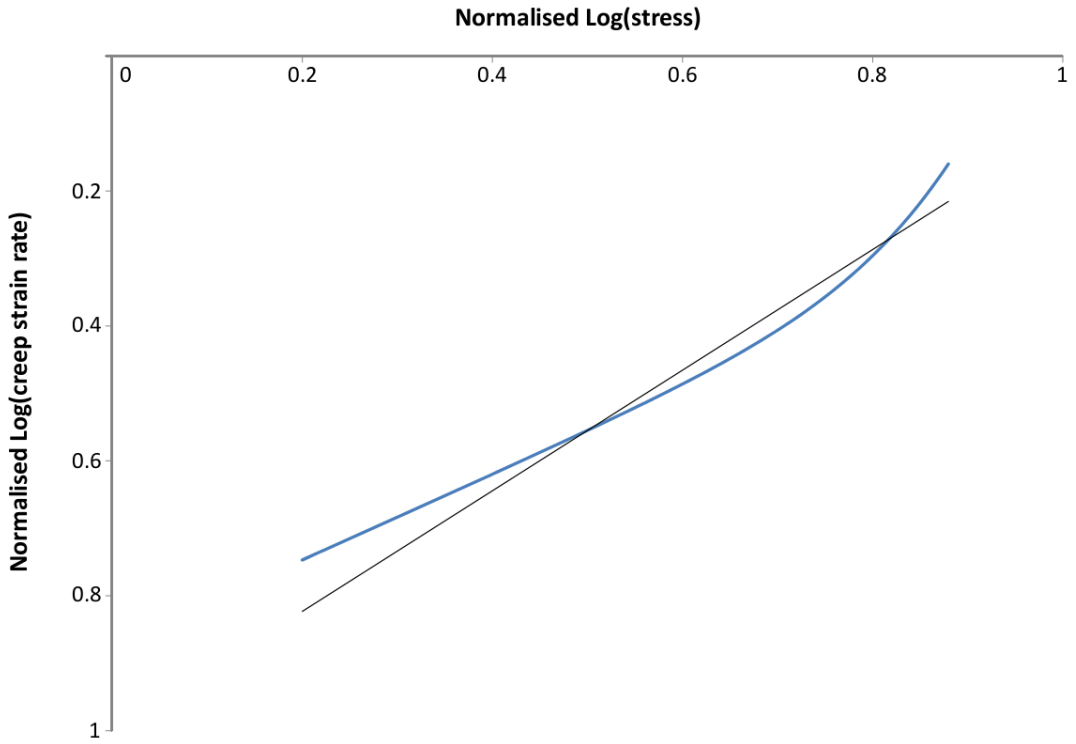

Figure A.2: Graphical linear interpolation to calculate Norton-Bailey parameters

A.3.2 Derivation of Creep Rupture Constants

For implementation in the Linear Matching Method, in addition to the creep parameters, the time to rupture is also required. This is given by the time fraction rule, and appropriate parameters can be derived using a similar linear interpolation as used above.

Step 1

The equation for the time fraction rule is:

$$t^* = B_t \sigma^{-k_t} \tag{A.10}$$

Step 2

Taking logs of both sides of this equation:

$$\log(t^*) = \log(B_t) + \log(\sigma^{-k_t}) \tag{A.11}$$

which can be rearranged as:

$$\log(t^*) = \log(B_t) - k_t \log(\sigma) \tag{A.12}$$

Step 3

The time to rupture is calculated using a range of stress values obtained in experimental testing and the results are plotted in a log-log form as $\log(t^*)$ versus $\log(\sigma)$ as shown in Figure A.3.

Step 4

Over a limited range of $\log(\sigma)$, this curve can be approximated by a linear function:

$$\log(t^*) = m \log(\sigma) + c \tag{A.13}$$

Step 5

Equating these two functions:

$$\log(t^*) = \log(B_t) - k_t \log(\sigma) = m \log(\sigma) + c \tag{A.14}$$

Step 6

Therefore, the time to rupture parameters are given by:

$$k_t = m \tag{A.15}$$

and

$$B_t = 10^c \tag{A.16}$$

where m is the straight line gradient and c is the straight line y-intercept from Figure A.3.

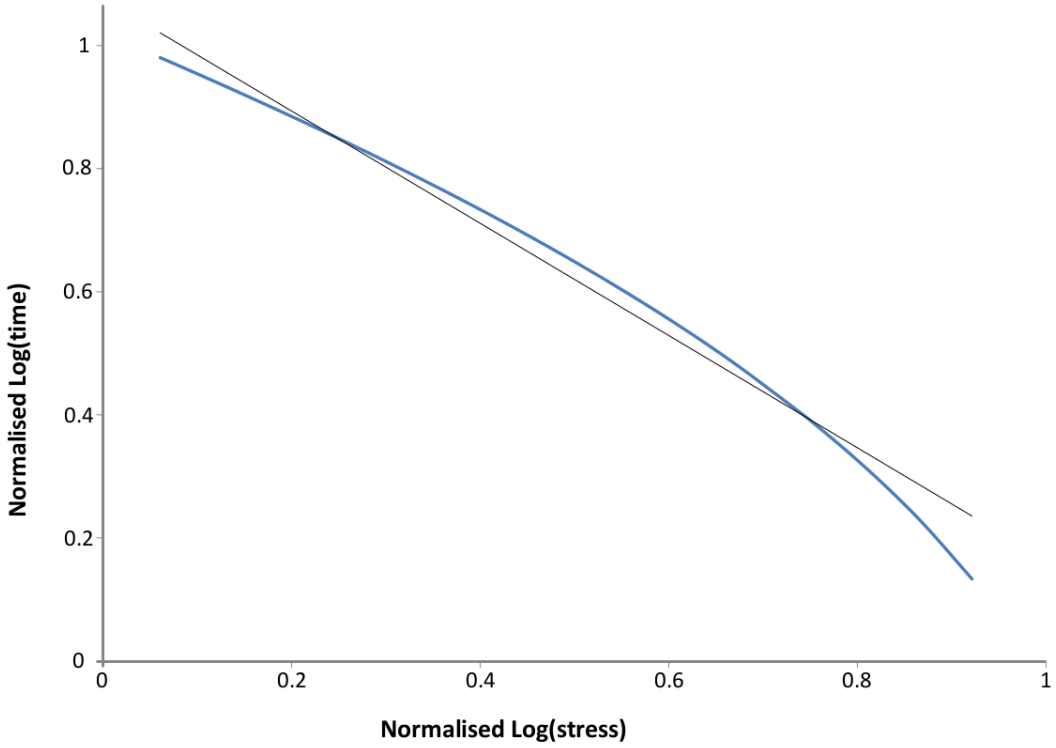

Figure A.3: Graphical linear interpolation to calculate creep rupture parameters

In both cases, the obtained results are entirely dependent on the applied curve fit which can be seen to only be appropriate over a limited stress range and thus the size of this range must be selected to achieve the level of accuracy required.

For the nickel-based superalloy, these calculations shown above allowed the following material properties to be deduced:

Table A.1: Deduced creep material properties

Creep Parameters	B_n	$1.733 * 10^{-17}$
	n_n	4.4705
Creep Rupture	B_t	$8.394 * 10^{20}$
	k_t	6.839

These creep properties can be used in addition to the basic material properties described

in Section 5.3.2, to perform a complete LMM creep-fatigue analysis.

A.4 Creep-Fatigue Analysis

A number of preliminary analyses are performed using the Linear Matching Method Extended Direct Steady Cyclic Analysis (eDSCA) to provide a foundation for the proposed future work. This is implemented in ABAQUS using the LMM creep-fatigue subroutine.

Following on from the previous experimental case where the test was designed for crack initiation only, this extended investigation will only consider creep-fatigue crack initiation. For crack propagation analysis, additional analyses are required to calculate the creep crack growth rate, as discussed in Section 7.5, however, this is outside the scope of this preliminary investigation.

A.4.1 Selection of Operating Temperature

The aim of the experimental test is to induce a level of creep strain that is significant enough to observe its effect, whilst not excessive enough to cause creep rupture in a short dwell time. For the material in question, creep does not become significant until the temperature exceeds 600°C. In order to aid the selection of the most appropriate operating temperature for investigation, an analytical calculation of the induced creep strain in the component under a typical design load of 400MPa was performed. The creep strain was calculated for different dwell times under different ambient temperatures and plotted as shown in Figure A.4.

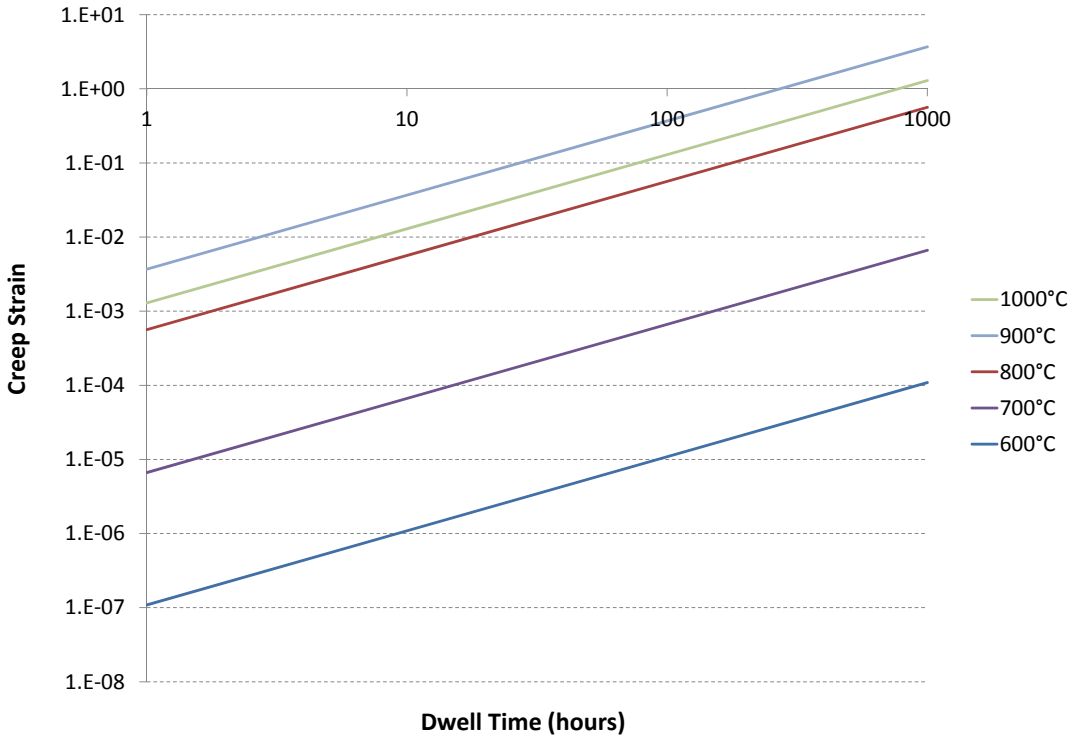

Figure A.4: Chart showing creep strain with increasing temperature

It can be seen that at an operating temperature of 600°C, negligible creep strain is induced, even for a dwell time of 1000 hours. It can also been seen that at a temperature of 1000°C, the creep strain becomes exceedingly large even for short dwell times. It was therefore deemed that the optimal operating temperature for demonstrating the effects of creep-fatigue is 800°C.

A.4.2 Numerical Implementation

The intention of this study is to replicate the conditions experienced by nozzle guide vanes and so simplified loading profiles are established that represent the engine ramp-up, extended operation and shutdown. In an attempt to assess the effect that this type of loading profile has on the structural integrity of the NGVs, creep-fatigue analyses are performed on the representative test specimen as used previously in Chapter 5 and shown in Figure 5.2.

The creep-fatigue analyses are performed at an operating temperature of 800°C and for dwell times of 1, 10 and 100 hours subject to the loading profile illustrated in Figure

A.1 where the applied load is 400MPa.

Under these conditions, and using the established material properties shown in Table A.1, the eDSCA was performed in order to calculate the induced creep strain for each dwell time and to calculate the creep crack initiation fatigue life. The generated hysteresis of these analyses are shown in Figure A.5, clearly showing the increase in creep strain with increasing dwell time.

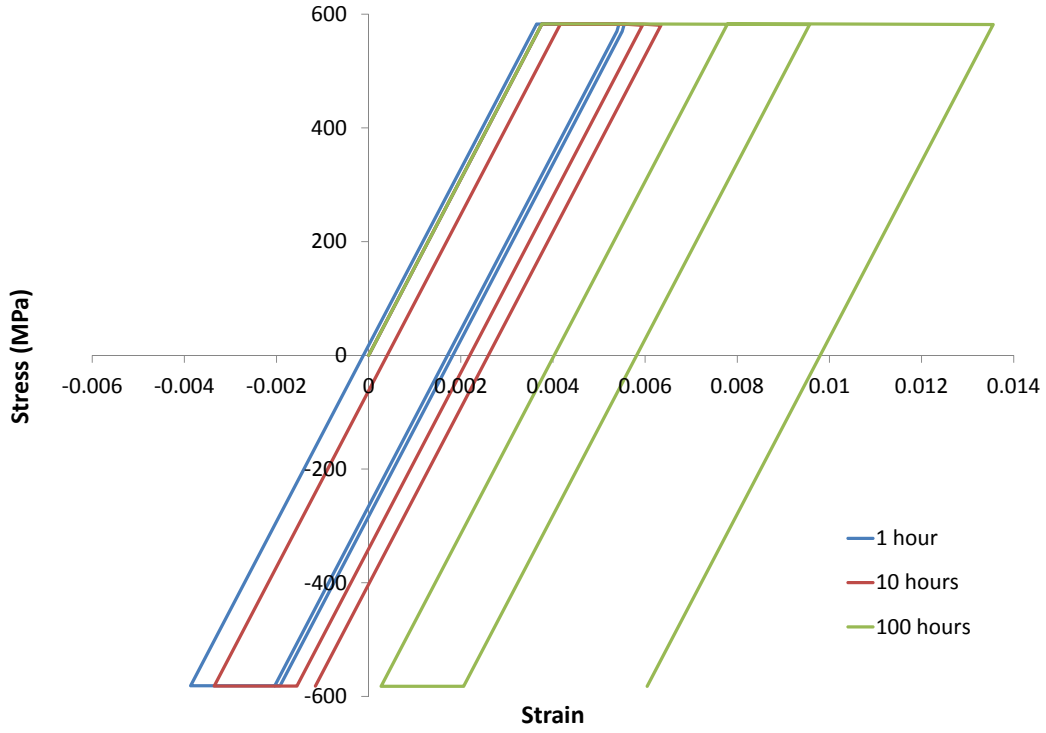

Figure A.5: Hysteresis loops at 800°C at dwell times of 1, 10 and 100 hours

For each temperature, the number of cycles to failure as calculated by the Linear Matching Method Creep-Fatigue subroutine was determined and this is shown in Table A.2 and graphically in Figure A.6.

Table A.2: Creep fatigue life at different temperatures and hold times

Temperature	Dwell Time (hours)	Number of cycles to failure, N_f
600°C	1	3113455.45
	10	311345.55
	100	31134.55
700°C	1	2095.54
	10	209.55
	100	20.96
800°C	1	103.18
	10	10.32
	100	1.03
900°C	1	27.62
	10	2.28
	100	0.52
1000°C	1	16.83
	10	1.68
	100	0.17

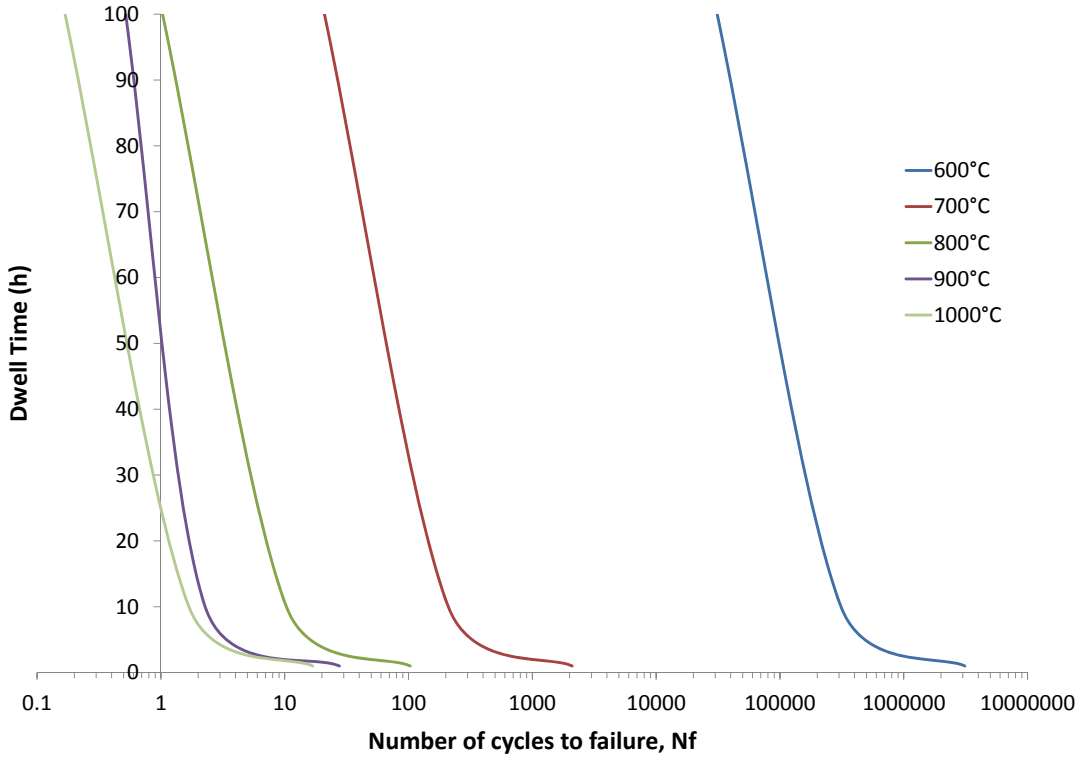

Figure A.6: Graphical representation of creep-fatigue life for increasing temperature

This investigation has been performed for Siemens in their routine structural integrity assessment of gas turbine components and as such the loading conditions were chosen to match their requirements. This has resulted in the lack of any observable relaxation, thus not demonstrating the full power of the LMM creep-fatigue subroutine and the eDSCA. However, for completeness and general interest, a more general case which shows significant creep-fatigue interaction has been included in Section 7.4.

A.5 Investigation Summary

This is only a very brief demonstration of how the Linear Matching Method eDSCA could be used for an industrial creep-fatigue analysis and is intended as a starting point for the proposed future work. A very basic test was performed to demonstrate the implementation of the hyperbolic sine creep law parameters that have been reformulated as Norton-Bailey properties for use within the LMM.

This test was performed under constant load controlled conditions to match test requirements at Siemens and as a result, no stress relaxation was observable. However, this test should be extended to investigate this phenomena and so the next step for this analysis would be to devise a test that incorporates stress relaxation.

Due to the nature of the graphical interpolation that was employed to determine the Norton-Bailey creep parameters from hyperbolic sine properties and the time fraction rule, the accuracy of the obtained results is compromised. This could make this type of conversion impractical for industrial applications where high levels of accuracy are required or a wide stress range is involved.

This also demonstrates a limitation in the current version of the Linear Matching Method creep-fatigue subroutine which only models materials following Norton-Bailey relationships and does not allow other creep relationships. This poses a potential issue for use in industrial applications when material properties may not comply with the LMM framework. However, the LMM is undergoing continued development and this limitation could be addressed in the future.

Despite the limitations of this test due to the issues with material data and specific test conditions, as demonstrated in Chapter 7, this technique has been shown to be very powerful for creep-fatigue assessment in high technology engineering industries

and could become routine in industrial gas turbine applications.

However, in this specific application, further verification and validation of the results would be needed through experimental testing before it could provide useful creep-fatigue information. This would therefore require further investigation and additional support from Siemens or other industrial partners in order to establish this test programme.

A.6 Method Implementation

The creep-fatigue analysis can very simply be incorporated into the Crack Growth Assessment Procedure with some small modifications to the procedure logic, as shown in Figure A.7 and A.8. This then allows the inclusion of creep in the procedure through a modified RPDM method using the eDSCA for extended hold times as well as creep crack propagation analysis using the LMM and R5 procedure for the evaluation of the C^* integral. These additions then allow a complete creep crack initiation and propagation life to be obtained using the proposed procedure.

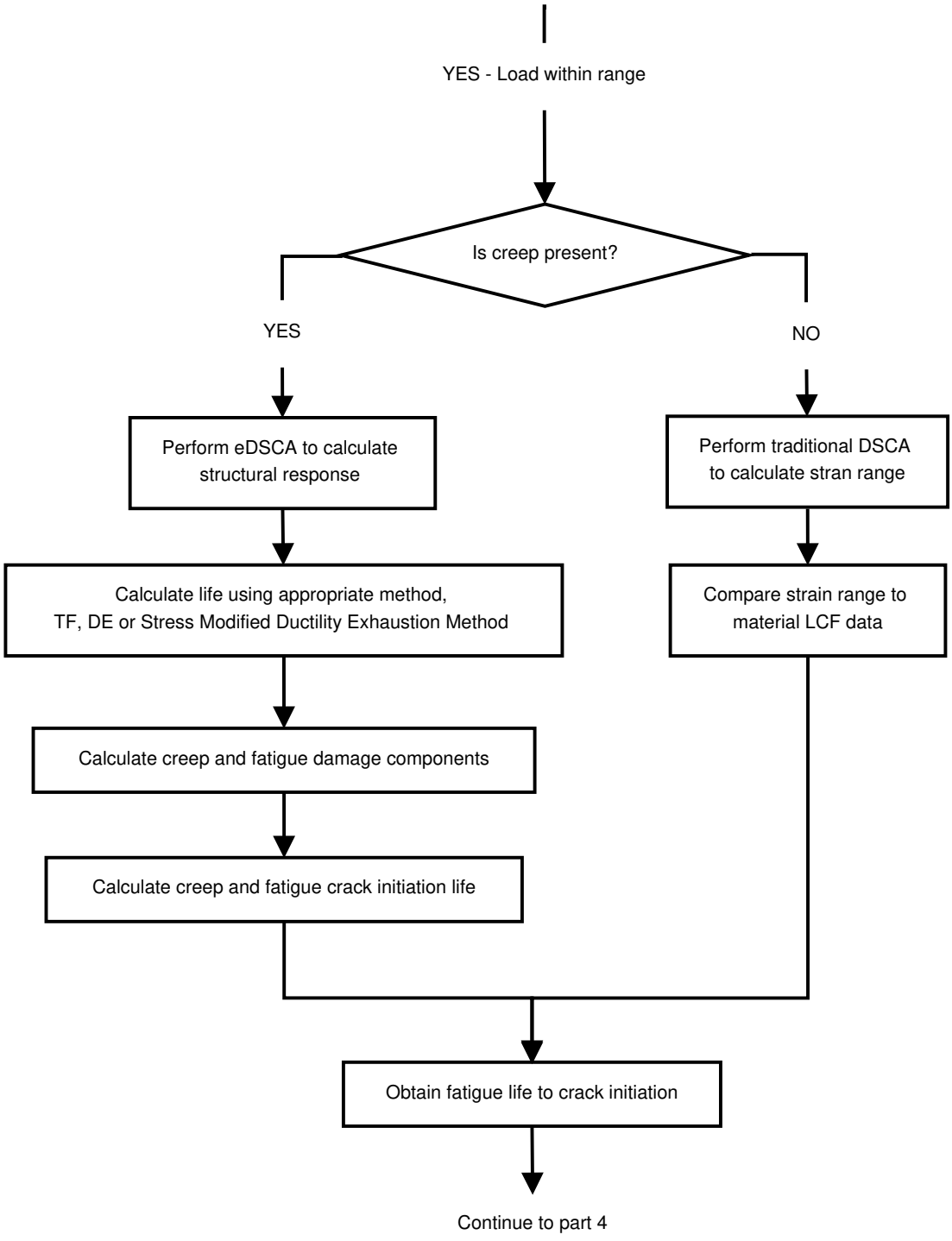

Figure A.7: Crack Assessment Procedure Process Flow - Part 2 (modified to include creep dwell)

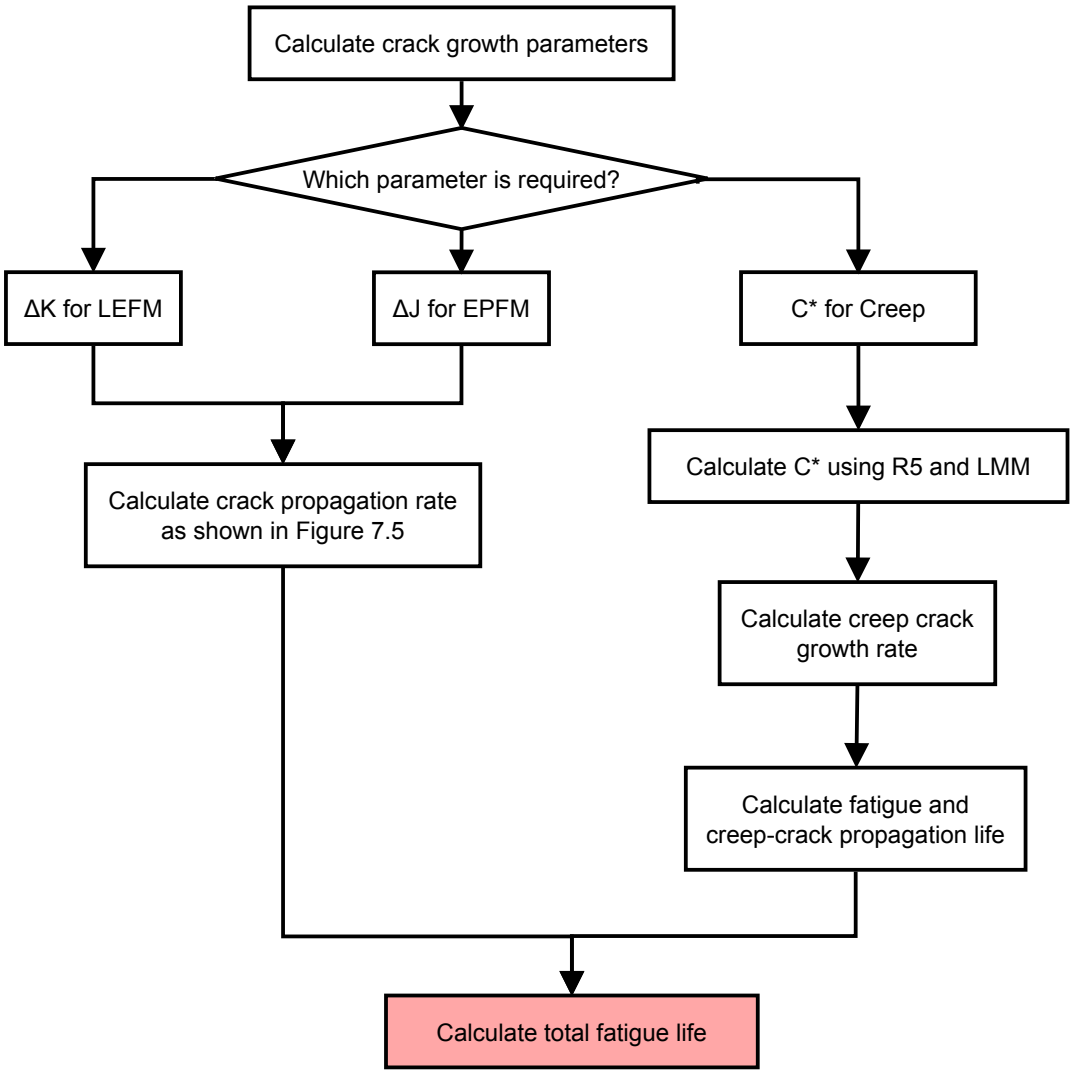

Figure A.8: Crack Assessment Procedure Process Flow - Part 4 (modified to include creep dwell)

A.7 Appendix Conclusions

From this preliminary study, the following conclusions have been made:

- This investigation highlights a necessary development for the Linear Matching Method to include other creep-fatigue laws. This could be implemented through a user definition of the required creep-fatigue law, in a similar manner that material hardening laws are currently defined in the LMM ABAQUS plugin
- The present creep-fatigue implementation in the LMM only considers Norton-Bailey laws and so a method has been developed to reformulate a hyperbolic sine law for application to nickel-based superalloys
- Following a successful conversion of the hyperbolic sine law to a Norton-Bailey formulation, a LMM creep fatigue analysis has been successfully performed
- The procedure logic for the proposed crack growth assessment procedure has been modified to allow for the inclusion of a creep-fatigue analysis including creep crack initiation and propagation life

A.8 Appendix Summary

This appendix has included some preliminary analyses that were performed in an attempt to extend the RPDM method for the inclusion of extended hold times using the eDSCA to investigate the effect of creep-fatigue on the structural integrity of turbine components. The limitations of the technique have been identified which could be addressed with further investigation and industrial support. It is the hope of the author that this preliminary analysis will be of some benefit for the future study and help to pave the way for the continuation of this project.

Once completed, this method could provide a very valuable additional asset to the proposed crack growth modelling procedure, further enhancing its usefulness for industrial structural integrity analysis within Siemens and across other engineering industries.

Glossary

ABAQUS A finite element analysis software package produced by Dassault Systemes. Used for all FE analyses in this thesis.

Advanced Gas-Cooled Reactor A type of nuclear power plant used in the UK that uses carbon dioxide as the coolant and graphite as the moderator.

ASME Boiler & Pressure Vessel Code (BPVC) An American Society of Mechanical Engineers (ASME) assessment procedure for the evaluation of fatigue of nuclear power plant components.

Bree diagram A plot of primary and secondary stress ranges showing the limit load, shakedown, reversed plasticity and ratchetting regions.

Brittle fracture A type of fracture in which little to no deformation occurs before failure.

Computer Numeric Control (CNC) A computerised method of automated operation of machinery.

Contour integral An integral obtained by contour integration along a set path within a structure. Within ABAQUS, this includes the stress intensity factor and J-integral.

Contour plot An image produced using FEA which displays the output variable in a colour coded manner.

Cooling holes Small holes incorporated into turbine components to allow effective cooling.

Crack tip singularity An expression for the stress at a crack tip. When approaching the crack tip, the stress tends to infinity.

Creep The gradual deformation of a material at constant stress and extended time periods.

Creep-Fatigue The combination of creep and fatigue where deformation occurs under repeated cyclic loading with extended load hold times at high temperatures.

Cyclic J-integral The J-integral for a cyclic loading history.

Dielectric fluid An ionised fluid medium that permits an electrical spark to travel between the electrode and workpiece during EDM, whilst also insulating the workpiece from excess electrical current away from the localised spark path.

Direct cyclic analysis (DCA) A computational numerical technique that directly calculates the cyclic response of a structure without the need to model the transition period.

Direct steady cyclic analysis (DSCA) See Direct cyclic analysis.

Dowling and Begley law A relationship for the calculation of crack propagation rate under elastic-plastic conditions which is proportional to the cyclic J-integral.

Ductile fracture A type of fracture in which a large amount of plastic deformation occurs before failure.

Extended direct steady cyclic analysis (eDSCA) An extension to the DSCA for the inclusion of a creep dwell in the loading history.

Elastic Perfectly Plastic (EPP) A simplified relationship which neglects material hardening.

Elastic plastic fracture mechanics (EPFM) The category of fracture mechanics that considers loads above the yield stress, causing plastic deformation.

Electrical discharge machining (EDM) A high precision machining technique which uses electrical sparks to remove material.

eXtended Finite Element Method (XFEM) An extension to the tradition FEM allowing crack propagation modelling.

Fatigue Damage caused as a result of repeated cyclic loading.

Fatigue life assessment A structured technique for calculating the fatigue life of a component.

Finite Element Analysis (FEA) The computational implementation of the finite element method, allowing complex modelling and analysis of engineering structures.

Finite Element Method (FEM) A numerical technique for describing physical conditions by creating and solving a series of equations allowing approximate solutions to be obtained.

Elastic follow-up factor A parameter which describes the rate of relaxation of the residual stress during a creep dwell.

High cycle fatigue (HCF) The category of fatigue in which low levels of stress are applied and the deformation is primarily elastic, with failure occurring in typically more than 10^4 cycles.

J-integral A fracture parameter for conditions when significant plastic deformation occurs.

Leading edge The up-stream side of the turbine blades and NGVs.

Limit load The load at which a component collapses.

Linear Elastic Fracture Mechanics (LEFM) The category of fracture mechanics that considers loads below the yield stress where the material behaviour is elastic and no plastic deformation occurs.

Linear Elastic Material behaviour following LEFM.

Linear Matching Method (LMM) A finite element analysis tool allowing analysis of a cyclic loading history, generating approximate inelastic solutions.

Load displacement curve A plot showing the variation of displacement with increasing load.

Low cycle fatigue (LCF) The category of fatigue in which the applied stress is at or close to the yield stress causing plastic deformation with failure occurring in typically less than 10^4 cycles.

Material hardening See strain hardening.

Mesh A way to separate a geometry into a number of small elements, allowing the implementation of the finite element method.

Non-destructive examination (NDE) A range of techniques for the testing of structures that do not cause any damage.

Nozzle Guide Vane (NGV) A component in the stator part of a turbine that directs hot gases onto the turbine blade.

Paris law A relationship for the calculation of crack propagation rate under linear elastic conditions which is proportional to the stress intensity factor range.

Plain strain conditions A simplified approximation for three dimensional problems that assumes that the strain along the z-direction is zero.

Plane stress conditions A simplified approximation for three dimensional problems that assumes that the stress along the z-direction is zero.

Plasticity/Plastic deformation Non-reversible deformation caused when loads in excess of the yield stress are applied to a structure.

Poisson's ratio The ratio of lateral strain to axial strain for a uniaxial stress state, i.e how the shape of a structure changes in one direction when a load is applied to a normal direction.

R5 A procedure for the assessment of the integrity of structures at high temperature developed by British Energy.

R6 A procedure for the assessment of the integrity of structures containing defects developed by British Energy.

Ramberg Osgood A common law for the description of material hardening.

Ratchet limit The load at which ratchetting occurs.

Ratchetting A damage mechanism in which plastic strain incrementally accumulates during each repeated loading cycle.

Recast layer A side effect of the EDM process which modifies the metallurgical structure of the top layers of the work-piece.

Reference Stress Method (RSM) A range of concepts that offer a means of calculating damage characteristics such as the J-integral. Used in the R5 and R6 procedures.

Reference stress A measure of an averaged stress state across a structure.

Reversed plasticity A damage mechanism in which a small amount of incremental plastic deformation occurs within the first few repeated cycles before reaching a stabilised response.

Seam crack A way to define crack surfaces within ABAQUS which open upon loading during an analysis.

Shakedown limit The load at which shakedown occurs.

Shakedown A damage mechanism in which some initial plastic deformation occurs but then shakes down to an elastic response and no further damage accumulates.

Strain energy release rate The energy released during fracture per unit area of crack surface.

Strain hardening A strengthening of a material caused by plastic deformation.

Stress concentration A location in a structure where the stress is concentrated around features such as cracks, sharp corners or holes.

Stress intensity factor (SIF) The measure of the stress raising capability of a particular feature.

Superalloys A class of alloys that are designed for high performance with excellent mechanical strength, temperature and creep resistance.

Surface Energy The work done per unit area that is required to create a new surface during fracture.

Trailing edge The down-stream side of the turbine blades and NGVs.

Virtual Crack Closure Technique (VCCT) A method to calculate the energy release rate based on the assumption that the energy required to separate a surface is equal to the energy required to close the same surface.

Yield point See yield stress.

Yield stress The stress at which material behaviour changes from elastic to plastic and the onset of deformation occurs.

References

[1] R. Beesley, H. Chen and M. Hughes. A novel simulation for the design of a low cycle fatigue experimental testing programme. *Computers & Structures*, 178: 105–118, 2017.

[2] R. Beesley, H. Chen and M. Hughes. On the modified monotonic loading concept for the calculation of the cyclic j-integral. *Journal of Pressure Vessel Technology*, 137(5), 2015.

[3] R. Beesley, H. Chen and M. Hughes. On the cyclic j-integral of a 3d semi elliptical surface crack. 2014.

[4] R5 Issue 3. *Assessment procedure for the high temperature response of structures.* EDF Energy, 2003.

[5] M. Hughes, O. Riccius, R. Moobola, I. Kuehn and L. Schneider. Cyclic lifetime validation of annular combustor liner segments for heavy duty gas turbines. *ASME Turbo Expo 2007: Power for Land, Sea, and Air*, pages 493–499. American Society of Mechanical Engineers, 2007.

[6] Dassault Systems Simulia Corp. *Version 6.12-3.* 2012.

[7] Zentech International Ltd. *Zencrack.*

[8] Cornell Fracture Group, Cornell University. *Franc3D.*

[9] D. M. Hughes. Nuclear engineering doctorate project proposal form. Unpublished internal document, October 2012.

[10] Siemens. Gas turbine sgt-750. `www.siemens.com/press/photo/EOG201011016-01e`, 2013. [Online; accessed May-2017].

[11] G. R. Irwin. Analysis of stresses and strains near the end of a crack traversing a plate. *Journal of Applied Mechanics*, 24: 361–364, 1957.

[12] A. A. Griffith. The phenomena of rupture and flow in solids. *Philosophical transactions of the royal society of london. Series A, containing papers of a mathematical or physical character*, pages 163–198, 1921.

[13] J. R. Rice. A path independent integral and the approximate analysis of strain concentration by notches and cracks. *Journal of applied mechanics*, 35(2): 379–386, 1968.

[14] A. Wells. Application of fracture mechanics at and beyond general yielding. *British Welding Journal*, 10(11): 563–70, 1963.

[15] D. Broek. *Elementary engineering fracture mechanics*. Springer Science & Business Media, 1982.

[16] T. L. Anderson and T. Anderson. *Fracture mechanics: fundamentals and applications*. CRC press, 2005.

[17] C. E. Inglis. Stresses in a plate due to the presence of cracks and sharp corners. *Spie Milestone series MS*, 137: 3–17, 1997.

[18] A. Rubbra. Alan arnold griffith. 1893-1963. *Biographical Memoirs of Fellows of the Royal Society*, pages 117–136, 1964.

[19] G. Irwin. Onset of fast crack propagation in high strength steel and aluminum. *Proceeding of Second Sagamore Conference*, volume 2, page 289.

[20] H. Westergaard. Bearing pressures and cracks. *Journal of applied mechanics*, 1939.

[21] W. Ramberg and W. R. Osgood. Description of stress-strain curves by three parameters. *National Advisory Committee for Aeronautics*, 1943.

[22] S. Al Laham, S. I. Branch and R. Ainsworth. *Stress intensity factor and limit load handbook*. British Energy Generation Limited, 1998.

[23] R6 Issue 3. *Assessment of the integrity of structures containing defects*. British Energy Generation Ltd, Amendment 10, 1999.

[24] J. Begley and J. Landes. The j-integral as a fracture criterion. *ASTM STP*, 514: 1–20, 1972.

[25] R. Bucci, P. Paris, J. Landes and J. Rice. J integral estimation procedures. *ASTM STP*, 514: 40–69, 1972.

[26] J. Sumpter and C. Turner. Applicability of j to elastic-plastic materials. *International Journal of Fracture*, volume 9, pages 320–321. Kluwer Academic Publishers, Netherlands, 1973.

[27] J. Sumpter and C. Turner. Method for laboratory determination of j c. *Cracks and fracture*. ASTM International, 1976.

[28] C. Shih. J-integral estimates for strain hardening materials in antiplane shear using fully plastic solution. *Mechanics of crack growth*. ASTM International, 1976.

[29] K. Kishimoto, S. Aoki and M. Sakata. On the path independent integral-j. *Engineering Fracture Mechanics*, 13(4): 841–850, 1980.

[30] C. Shih. Relationships between the j-integral and the crack opening displacement for stationary and extending cracks. *Journal of the Mechanics and Physics of Solids*, 29(4): 305–326, 1981.

[31] N. W. Sachs. Practical plant failure analysis: a guide to understanding machinery deterioration and improving equipment reliability. CRC Press, 2006.

[32] P. Withey. Fatigue failure of the de havilland comet i. *Engineering failure analysis*, 4(2): 147–154, 1997.

[33] P. C. Paris, M. P. Gomez and W. E. Anderson. A rational analytic theory of fatigue. *The trend in engineering*, 13(1): 9–14, 1961.

[34] N. E. Dowling. Fatigue failure predictions for complicated stress-strain histories. Technical report, Department of Theoretical and Applied Mechanics, University of Illinois, 1971.

[35] M. Brown and K. Miller. A theory for fatigue failure under multiaxial stress-strain conditions. *Proceedings of the Institution of Mechanical Engineers*, 187(1): 745–755, 1973.

[36] S. Bush. Failure mechanisms in nuclear power plant piping systems. *Journal of pressure vessel technology*, 114(4): 389–395, 1992.

[37] W. Schütz. A history of fatigue. *Engineering fracture mechanics*, 54(2): 263–300, 1996.

[38] S. Farfan, C. Rubio-Gonzalez, T. Cervantes-Hernandez and G. Mesmacque. High cycle fatigue, low cycle fatigue and failure modes of a carburized steel. *International journal of fatigue*, 26(6): 673–678, 2004.

[39] Y. Liu, Y. Li, S. Li, Z. Yang, S. Chen, W. Hui and Y. Weng. Prediction of the s–n curves of high-strength steels in the very high cycle fatigue regime. *International journal of fatigue*, 32(8): 1351–1357, 2010.

[40] K. S. Chan. Roles of microstructure in fatigue crack initiation. *International Journal of Fatigue*, 32(9): 1428–1447, 2010.

[41] T. Morishita and T. Itoh. Evaluation of multiaxial low cycle fatigue life for type 316l stainless steel notched specimen under non-proportional loading. *Theoretical and Applied Fracture Mechanics*, 2016.

[42] K. Shi, L. Cai, S. Qi and C. Bao. A prediction model for fatigue crack growth using effective cyclic plastic zone and low cycle fatigue properties. *Engineering Fracture Mechanics*, 158: 209–219, 2016.

[43] Y. Lin, X.-M. Chen, Z.-H. Liu and J. Chen. Investigation of uniaxial low-cycle fatigue failure behavior of hot-rolled az91 magnesium alloy. *International Journal of Fatigue*, 48: 122–132, 2013.

[44] M. Kamaya. Low-cycle fatigue crack growth prediction by strain intensity factor. *International Journal of Fatigue*, 72: 80–89, 2015.

[45] H. Li, H. Yuan and X. Li. Assessment of low cycle fatigue crack growth under mixed-mode loading conditions by using a cohesive zone model. *International Journal of Fatigue*, 75: 39–50, 2015.

[46] S. Rabbolini, S. Beretta, S. Foletti and M. Cristea. Crack closure effects during low cycle fatigue propagation in line pipe steel: An analysis with digital image correlation. *Engineering Fracture Mechanics*, 148: 441–456, 2015.

[47] G. Chen, Y. Zhang, D. Xu, Y. Lin and X. Chen. Low cycle fatigue and creep-fatigue interaction behavior of nickel-base superalloy gh4169 at elevated temperature of 650 c. *Materials Science and Engineering: A*, 655: 175–182, 2016.

[48] J. Deng, P. Yang, Q. Dong and D. Wang. Research on ctod for low-cycle fatigue analysis of central-through cracked plates considering accumulative plastic strain. *Engineering Fracture Mechanics*, 2015.

[49] Rob Pinell. How the liberty ships of wwii contributed to the study of fracture mechanics. `https://www.linkedin.com/pulse/`

how-liberty-ships-wwii-contributed-study-fracture-mechanics-pinell, 2016. [Online; accessed May-2017].

[50] H. Kobayashi and H. Onoue. Brittle fracture of liberty ships. *Failure Knowledge Database*, 100, 1943.

[51] Science & Society Picture Library Prints. Crashed comet g-alyp, 1954. http://www.ssplprints.com/image/94355/crashed-comet-g-alyp-1954, 1954. [Online; accessed April-2014].

[52] Science & Society Picture Library Prints. Metal fatigue, c 1954. http://www.ssplprints.com/image/119800/metal-fatigue-c-1954, 1954. [Online; accessed April-2014].

[53] Purdue University. Fracture & fatigue lab homepage. https://engineering.purdue.edu/FSLAB/, 2005. [Online; accessed April-2014].

[54] Aloha Airlines. Flight 243, boeing 737-200, n73711, near maui hawaii, april 28, 1988. Technical report, NSTB/AAR-89/03, National Transportation Safety Board, Washington, DC 20594, 1989.

[55] Failure Analysis. Analyzing material fatigue. http://failure-analysis.info/2010/05/analyzing-material-fatigue/, 2010. [Online; accessed 3-December-2015].

[56] L. Coffin Jr. A study of the effect of cyclic thermal stresses on a ductile metal. *American Society of Mechanical Engineers*, 76: 931–950, 1954.

[57] S. S. Manson. *Behavior of materials under conditions of thermal stress*. NACA TN 2933, 1953.

[58] A. Wöhler. *Über die Festigkeits-versuche mit Eisen und Stahl*. 1870.

[59] H. Neuber. Theory of stress concentration for shear-strained prismatical bodies with arbitrary nonlinear stress-strain law. *Journal of Applied Mechanics*, 28(4): 544–550, 1961.

[60] R. Mücke and O. Bernhardi. A constitutive model for anisotropic materials based on neubers rule. *Computer methods in applied mechanics and engineering*, 192(37): 4237–4255, 2003.

[61] M. Zappalorto and P. Lazzarin. A new version of the neuber rule accounting for the influence of the notch opening angle for out-of-plane shear loads. *International Journal of Solids and Structures*, 46(9): 1901–1910, 2009.

[62] M. A. Abbas and S. Sriram. Structural finite element analysis of an electrical lug. *2014 International Conference on Science Engineering and Management Research (ICSEMR)*, pages 1–5. IEEE, 2014.

[63] M. Zappalorto and P. Lazzarin. Some remarks on the neuber rule applied to a control volume surrounding sharp and blunt notch tips. *Fatigue & Fracture of Engineering Materials & Structures*, 37(4): 349–358, 2014.

[64] T. Topper, R. Wetzel and J. Morrow. Neuber's rule applied to fatigue of notched specimens. Technical report, DTIC Document, 1967.

[65] S. M. Tipton. A review of the development and use of neuber's rule for fatigue analysis. Technical report, SAE Technical Paper, 1991.

[66] N. Dowling and J. Begley. Fatigue crack growth during gross plasticity and the j-integral. *ASTM STP*, 590: 82–103, 1976.

[67] J. Sumpter and C. Turner. Method for laboratory determination of jc. *ASTM STP*, 601: 3–18, 1976.

[68] G. Webster and R. A. Ainsworth. *High temperature component life assessment*. Springer Science & Business Media, 2013.

[69] C. Scruby, K. Stacey, D. Buttle, M. Beesley, P. Bentley and W. Daniels. Acoustic emission measurements during hydrotest and cyclic fatigue of a 1/5 scale pwr vessel. *Nuclear Energy*, 29(4): 247–266, 1990.

[70] A. Boiler. *ASME Boiler and Pressure Vessel Code: An International Code*. American Society of Mechanical Engineers, 1998.

[71] J. T. Boyle and J. Spence. *Stress analysis for creep*. Elsevier, 2013.

[72] R. Courant. Variational methods for the solution of problems of equilibrium and vibrations. *Bulletin of the American Mathematical Society*, 49(1): 1–23, 1943.

[73] X.-K. Zhu and J. A. Joyce. Review of fracture toughness (g, k, j, ctod, ctoa) testing and standardization. *Engineering Fracture Mechanics*, 85: 1–46, 2012.

[74] R. Sim. Reference stress concepts in the analysis of structures during creep. *International Journal of Mechanical Sciences*, 12(6): 561–573, 1970.

[75] A. Miller and R. Ainsworth. Consistency of numerical results for power-law hardening materials and the accuracy of the reference stress approximation for j. *Engineering Fracture Mechanics*, 32(2): 233–247, 1989.

[76] M.-H. Military Handbook. 5h: Metallic materials and elements for aerospace vehicle structures. *US Department of Defence, Cancelled May*, 2004.

[77] C. Moosbrugger. Atlas of stress-strain curves. *ASM international, Ohio*, page 299, 2002.

[78] J. Chattopadhyay. Improved j and cod estimation by ge/epri method in elastic to fully plastic transition zone. *Engineering Fracture Mechanics*, 73(14): 1959–1979, 2006.

[79] C. Miehe and E. Gürses. A robust algorithm for configurational-force-driven brittle crack propagation with r-adaptive mesh alignment. *International Journal for Numerical Methods in Engineering*, 72(2): 127–155, 2007.

[80] Z. Zhuang and P. O'Donoghue. The recent development of analysis methodology for rapid crack propagation and arrest in gas pipelines. *International Journal of Fracture*, 101(3): 269–290, 2000.

[81] Z. Zhuang and P. O'Donoghue. Determination of material fracture toughness by a computational/experimental approach for rapid crack propagation in pe pipe. *International Journal of Fracture*, 101(3): 251–268, 2000.

[82] X. Xu and A. Needleman. Numerical simulations of fast crack growth in brittle solids. *Journal of the Mechanics and Physics of Solids*, 42(9): 1397–1434, 1994.

[83] T. Belytschko, J. Fish and B. E. Engelmann. A finite element with embedded localization zones. *Computer methods in applied mechanics and engineering*, 70(1): 59–89, 1988.

[84] T. Belytschko and T. Black. Elastic crack growth in finite elements with minimal remeshing. *International journal for numerical methods in engineering*, 45(5): 601–620, 1999.

[85] N. Moës, J. Dolbow and T. Belytschko. A finite element method for crack growth without remeshing. *International Journal of Numerical Methods in Engineering*, 46(1): 131–150, 1999.

[86] J. M. Melenk and I. Babuška. The partition of unity finite element method: basic theory and applications. *Computer methods in applied mechanics and engineering*, 139(1): 289–314, 1996.

[87] T. Belytschko, W. K. Liu, B. Moran and K. Elkhodary. *Nonlinear finite elements for continua and structures*. John Wiley & Sons, 2013.

[88] M. Stolarska, D. Chopp, N. Moës and T. Belytschko. Modelling crack growth by level sets in the extended finite element method. *International journal for numerical methods in Engineering*, 51(8): 943–960, 2001.

[89] A. Hansbo and P. Hansbo. A finite element method for the simulation of strong and weak discontinuities in solid mechanics. *Computer methods in applied mechanics and engineering*, 193(33): 3523–3540, 2004.

[90] J. Song, P. M. Areias and T. Belytschko. A method for dynamic crack and shear band propagation with phantom nodes. *International Journal for Numerical Methods in Engineering*, 67(6): 868–893, 2006.

[91] H. Yu. *Plasticity and geotechnics*, volume 13, pages 408–410. Springer Science & Business Media, 2007.

[92] H. Chen, W. Chen and J. Ure. A direct method on the evaluation of cyclic behaviour with creep effect. *ASME 2012 Pressure Vessels and Piping Conference*, pages 823–831. American Society of Mechanical Engineers, 2012.

[93] S. Vishnuvardhan, G. Raghava, P. Gandhi, M. Saravanan, S. Goyal, P. Arora, S. K. Gupta and V. Bhasin. Ratcheting failure of pressurised straight pipes and elbows under reversed bending. *International Journal of Pressure Vessels and Piping*, 105: 79–89, 2013.

[94] J. Bree. Elastic-plastic behaviour of thin tubes subjected to internal pressure and intermittent high-heat fluxes with application to fast-nuclear-reactor fuel elements. *The Journal of Strain Analysis for Engineering Design*, 2(3): 226–238, 1967.

[95] D. Moreton and H. Ng. The extension and verification of the bree diagram. *Structural mechanics in reactor technology. Vol. L*. 1981.

[96] H. F. Abdalla, M. M. Megahed and M. Y. Younan. A simplified technique for shakedown limit load determination. *Nuclear Engineering and Design*, 237(12): 1231–1240, 2007.

[97] M. Lytwyn, H. Chen and M. Martin. Comparison of the linear matching method to rolls-royce's hierarchical finite element framework for ratchet limit analysis. *International Journal of Pressure Vessels and Piping*, 125: 13–22, 2015.

[98] M. Staat and M. Heitzer. Lisaa european project for fem-based limit and shakedown analysis. *Nuclear Engineering and Design*, 206(2): 151–166, 2001.

[99] M. Muscat, D. Mackenzie and R. Hamilton. Evaluating shakedown under proportional loading by non-linear static analysis. *Computers & structures*, 81(17): 1727–1737, 2003.

[100] R. Seshadri. The generalized local stress strain (gloss) analysistheory and applications. *Journal of pressure vessel technology*, 113(2): 219–227, 1991.

[101] M. Malena and R. Casciaro. Finite element shakedown analysis of reinforced concrete 3d frames. *Computers & Structures*, 86(11): 1176–1188, 2008.

[102] R. Casciaro and G. Garcea. An iterative method for shakedown analysis. *Computer methods in applied mechanics and engineering*, 191(49): 5761–5792, 2002.

[103] A. R. Ponter and M. Engelhardt. Shakedown limits for a general yield condition: implementation and application for a von mises yield condition. *Inelastic Analysis of Structures under Variable Loads*, pages 11–29. Springer, 2000.

[104] A. R. Ponter. A linear matching method for shakedown analysis. *Inelastic Behaviour of Structures under Variable Repeated Loads*, 432, 2002.

[105] J. Ure, H. Chen and D. Tipping. Verification of the linear matching method for limit and shakedown analysis by comparison with experiments. *Journal of Pressure Vessel Technology*, 137(3): 031003, 2015.

[106] J. Ure. *An Advanced Lower and Upper Bound Shakedown Analysis Method to Enhance The R5 High Temperature Assessment Procedure*. 2013.

[107] H. Chen, A. R. Ponter and R. Ainsworth. The linear matching method applied to the high temperature life integrity of structures. part 1. assessments involving constant residual stress fields. *International Journal of Pressure Vessels and Piping*, 83(2): 123–135, 2006.

[108] H. Chen. Lower and upper bound shakedown analysis of structures with temperature-dependent yield stress. *Journal of Pressure Vessel Technology*, 132(1): 011202, 2010.

[109] H. Chen and A. R. Ponter. A method for the evaluation of a ratchet limit and the amplitude of plastic strain for bodies subjected to cyclic loading. *European Journal of Mechanics-A/Solids*, 20(4): 555–571, 2001.

[110] H. Chen and A. R. Ponter. A direct method on the evaluation of ratchet limit. *Journal of Pressure Vessel Technology*, 132(4): 041202, 2010.

[111] A. R. Ponter and H. Chen. A minimum theorem for cyclic load in excess of shakedown, with application to the evaluation of a ratchet limit. *European Journal of Mechanics-A/Solids*, 20(4): 539–553, 2001.

[112] H. Chen, J. Ure and D. Tipping. Calculation of a lower bound ratchet limit part 1–theory, numerical implementation and verification. *European Journal of Mechanics-A/Solids*, 37: 361–368, 2013.

[113] H. Chen and A. R. Ponter. Linear matching method on the evaluation of plastic and creep behaviours for bodies subjected to cyclic thermal and mechanical loading. *International Journal for Numerical Methods in Engineering*, 68(1): 13–32, 2006.

[114] J. Ure, H. Chen and D. Tipping. Integrated structural analysis tool using the linear matching method part 1–software development. *International Journal of Pressure Vessels and Piping*, 120: 141–151, 2014.

[115] H. Chen, J. Ure and D. Tipping. Integrated structural analysis tool using the linear matching method part 2–application and verification. *International Journal of Pressure Vessels and Piping*, 120: 152–161, 2014.

[116] D. Tipping. The linear matching method: a guide to the abaqus user subroutines. *British Energy Generation, E/REP/BBGB/0017/GEN/07*, 2007.

[117] H. Chen and A. R. Ponter. Integrity assessment of a 3d tubeplate using the linear matching method. part 1. shakedown, reverse plasticity and ratchetting. *International journal of pressure vessels and piping*, 82(2): 85–94, 2005.

[118] H. Chen and A. R. Ponter. Integrity assessment of a 3d tubeplate using the linear matching method. part 2: Creep relaxation and reverse plasticity. *International journal of pressure vessels and piping*, 82(2): 95–104, 2005.

[119] Nickel Institute. High nickel alloys & superalloys. `http://www.nickelinstitute.org/NickelUseInSociety/MaterialsSelectionAndUse/Ni-ContainingMaterialsProperties/HighNickelAlloysAndSuperalloys.aspx`, 2015. [Online; accessed 3-December-2015].

[120] Winbro Group Technologies. Nozzle guide vane. `http://www.winbrogroup.com/applications/ngv/`, 2012. [Online; accessed 3-December-2015].

[121] Trac Components. Nozzle guide vane1. `http://components.trac-group.com/products/aerospace/nozzle-guide-vane/#prettyPhoto[post-104]/0/`, 2015. [Online; accessed 3-December-2015].

[122] E. C. Jameson. *Electrical discharge machining*. Society of Manufacturing Engineers, 2001.

[123] M. Lytwyn, H. Chen and A. Ponter. A generalised method for ratchet analysis of structures undergoing arbitrary thermo-mechanical load histories. *International Journal for Numerical Methods in Engineering*, 104(2): 104–124, 2015.

[124] A. Ponter. The linear matching method for limit loads, shakedown limits and ratchet limits. *Limit States of Materials and Structures*, pages 1–21. Springer, 2009.

[125] W. T. Koiter. *General theorems for elastic-plastic solids*. North-Holland Amsterdam, 1960.

[126] J. Tirosh and S. Peles. Lower and upper shakedown bounds for fatigue limit in two phase materials. *International journal of fracture*, 119(1): 65–81, 2003.

[127] H. Chen and A. R. Ponter. Shakedown and limit analyses for 3-d structures using the linear matching method. *International Journal of Pressure Vessels and Piping*, 78(6): 443–451, 2001.

[128] E. Melan. *Theorie statisch unbestimmter Systeme aus ideal-plastischem Baustoff*. Hölder-Pichler-Tempsky in Komm.:Wien, 1936.

[129] H. Chen, W. Chen, T. Li and J. Ure. On shakedown, ratchet and limit analyses of defective pipeline. *Journal of Pressure Vessel Technology*, 134(1): 011202, 2012.

[130] J. Ure, H. Chen and D. Tipping. Calculation of a lower bound ratchet limit part 2–application to a pipe intersection with dissimilar material join. *European Journal of Mechanics-A/Solids*, 37: 369–378, 2013.

[131] K. Ikeda, M. Yoshimi and C. Miki. Electrical potential drop method for evaluating crack depth. *International Journal of Fracture*, 47(1): 25–38, 1991.

[132] W. Chen and H. Chen. Cyclic j-integral using the linear matching method. *International Journal of Pressure Vessels and Piping*, 108: 72–80, 2013.

[133] K. Tanaka. The cyclic j-integral as a criterion for fatigue crack growth. *International Journal of Fracture*, 22(2): 91–104, 1983.

[134] D. Leidermark, J. Moverare, K. Simonsson and S. Sjöström. A combined critical plane and critical distance approach for predicting fatigue crack initiation in notched single-crystal superalloy components. *International Journal of Fatigue*, 33(10): 1351–1359, 2011.

[135] R. C. McClung, G. Chell, Y. Lee, D. Russell and G. Orient. Development of a practical methodology for elastic-plastic and fully plastic fatigue crack growth. 1999.

[136] H. Chen, W. Chen and J. Ure. A direct method on the evaluation of cyclic steady state of structures with creep effect. *Journal of Pressure Vessel Technology*, 136(6): 061404, 2014.

[137] D. Barbera, H. Chen and Y. Liu. Review and case study of the linear matching method framework for structure integrity assessment. *ASME 2016 Pressure Vessels and Piping Conference*. American Society of Mechanical Engineers, 2016.

[138] D. Barbera, H. F. Chen and Y. H. Liu. Creep fatigue life assessment of a pipe intersection with dissimilar material joint by linear matching method. *Applied Mechanics and Materials*, volume 853, pages 366–371. Trans Tech Publications, 2017.

[139] US Nuclear Regulatory Commission. The battelle integrity of nuclear piping (binp) program-final report. Technical report, NUREG/CR-6837, 2005.

[140] L.-J. Xie, X. Ren, M.-X. Shen and L.-Q. Tu. Parameter correlation of high-temperature creep constitutive equation for rpv metallic materials. *Journal of Nuclear Materials*, 465: 196–203, 2015.

[141] D. Barbera, H. Chen and Y. Liu. On creep fatigue interaction of components at elevated temperature. *Journal of Pressure Vessel Technology*, 138(4): 041403, 2016.

[142] M. Sheridan, D. Knowles and O. Montgomery. Comparison of r5 and asme nh creep-fatigue damage assessment methodologies. *ASME 2013 pressure vessels and piping conference*, pages V01AT01A046–V01AT01A046. American Society of Mechanical Engineers, 2013.

[143] M. Spindler. An improved method for calculation of creep damage during creep–fatigue cycling. *Materials Science and Technology*, 23(12): 1461–1470, 2007.

[144] Structural Integrity and Life Assessment Research Group. Structural integrity and life assessment (sila) research group. `http://http://www.thelmm.co.uk/`, 2016. [Online; accessed 11-January-2016].

[145] A. Baker, M. O'Donnell and D. Dean. Use of the r5 volume 4/5 procedures to assess creep–fatigue crack growth in a 316l (n) cracked plate at 650 c. *International journal of pressure vessels and piping*, 80(7): 481–488, 2003.